

Catalytic Deoxygenation of Fatty Acids to Diesel-range Hydrocarbons over Promoted Platinum Catalysts

**Thesis Submitted to AcSIR
for the Award of the Degree of
Doctor of Philosophy
in
Chemical Sciences**



**By
Janampelli Sagar
(AcSIR Roll No.: 10CC14A26001)**

**Under the Guidance of
Dr. Darbha Srinivas**

**CSIR- National Chemical Laboratory
Pune- 411008, India**

May 2018

May 31, 2018

CERTIFICATE

This is to certify that the work incorporated in the Ph.D. thesis entitled "*Catalytic Deoxygenation of Fatty Acids to Diesel-range Hydrocarbons over Promoted Platinum Catalysts*" submitted by **Mr. Janampelli Sagar** to Academy of Scientific and Innovative Research (AcSIR) in fulfilment of the requirements for the award of the Degree of **Doctor of Philosophy**, embodies original research work under my supervision. I further certify that this work has not been submitted to any other University or Institution in part or full for the award of any degree or diploma. Research material obtained from other sources has been duly acknowledged in the thesis. Any text, illustration, table etc., used in the thesis from other sources, have been duly cited and acknowledged.



Mr. Janampelli Sagar
Research Scholar



Dr. Darbha Srinivas
Research Supervisor

Declaration

I hereby declare that the work presented in the thesis entitled "*Catalytic Deoxygenation of Fatty Acids to Diesel-range Hydrocarbons over Promoted Platinum Catalysts*" submitted for the *Degree of Doctor of Philosophy in Chemical Sciences* to the Academy of Scientific and Innovative Research (AcSIR) New Delhi, has been carried out by me at the Catalysis and Inorganic Chemistry Division, CSIR-National Chemical Laboratory, Pune-411008, India under the supervision of *Dr. Darbha Srinivas*. I further declare that the materials obtained from other sources have been duly acknowledged in this thesis. The work is genuine and has not been submitted in part or full by me for any other degree or diploma to this or any other university.

Date: 31-05-2018

Place: Pune



Mr. Janampelli Sagar

Research Scholar

..... *dedicated to my beloved parents*

Acknowledgement

The work presented in this dissertation becomes a reality with the kind support and help of many individuals. I would like to extend my sincere thanks to all of them.

First of all, it is a great pleasure to acknowledge my deepest thanks and gratitude to my research guide, Dr. Darbha Srinivas, for his constant inspiration, motivation, guidance and constructive criticism which helped me a lot to focus and implement my views in a proper perspective. My deepest personal regards are due for him forever.

My sincere thanks are due to Dr. A. Sudalai, Dr. Paresh Dhepe, Dr. C.P. Vinod, Dr. C.V.V. Satyanarayana, Dr. C.S. Gopinath, Dr. Mrs. S.S. Deshpande, Dr. V.V. Bokade, Dr. Niphadkar, Dr. T. Raja, Dr. Nandini R. Devi, Dr. Subhangi Umbarkar, Mr. R.K. Jha, Mr. P. K. Purushothaman, Ms. Violet Samuel, Mr. Madhu, Mr. Milind and all other scientific and non-scientific staff of the Catalysis Division and NCL for their valuable help and cooperation during my tenure as a research student.

I am also grateful to all my lab-mates Dr. Seemala Bhogeshwararao, Dr. Joby Sebastian, Dr. Mehejabeen Shaikh, Dr. Unnikrishnan P., Dr. Devadutta Nepak, Mr. Ravindra Raut, Mr. Vikram Bankar, Mr. Anthony Devdass, Ms. Navyasree, Mr. Ganesh Giram, Mr. Nagesh Mulik, Ms. Nikitra N. Gupta, Ms. Meera Sebastian, Ms. Haritha C. Nair, Ms. Supriya M. Bodake for their worthy support, love, care and co-operation in completing my work.

I would like to convey my heartfelt thanks to my friends Anu and Harun Baba for their massive love and support in all the problems and personal issues. I am also grateful to my friends V.S.V.S.N. Swamy, Praveen Korra, Prabhakar K., Srikanth D., Venkanna babu, Ekta Sangtani, Narendra P. Reddy., Laxmi Prasad, Chaithanya K., Rami Reddy., Naresh Nalajala., Harsha, Venkatesh, Srikant T., Dhananjay Doke, Shibin and Dheerendra Singh, who helped me in various aspects during my tenure at NCL.

I am extremely indebted to my dear family - my father, mother, brother, sister, brother-in-Law, as well as my M.Sc. faculty who always backed my decisions and provided all kinds of support as well as blessings. I also extend my respect to my school teachers for their blessings throughout. It was their love, care and patience which inspired me to carry out this work.

It is indeed my privilege to thank the Director, NCL, for giving me this opportunity and extending all possible infrastructural facilities at NCL for the research work.

Finally, I thank the University Grants Commission (UGC) for financial assistance.

Mr. Sagar Janampelli

Abbreviations

HDO	Hydrodeoxygenation
DOE	Department of Energy
LVHV	Low Value-High Volume
HVLV	High Value-Low Volume
VO	Vegetable Oils
FFAs	Free Fatty Acids
FAME	Fatty Acid Methyl Ester
HT	Hydrotreatment
ETBE	Ethyl Tertiary Butyl Ether
DCO	Decarboxylation/Decarbonylation
AC	Activated Carbon
TPP	Triphenylphosphine
OA	Oleic Acid
MO _x	Metal Oxide
TEM	Transmission Electron Microscopy
SEM	Scanning Electron Microscopy
TEOS	Tetraethyl orthosilicate
CTAB	Cetyltrimethylammonium bromide
SA	Silica-alumina
BJH	Barrett-Joyner-Halenda
BET	Brunauer, Emmet and Teller
GC	Gas Chromatography
GC-MS	Gas Chromatography-Mass Spectrometry
S _{BET}	Specific Surface Area

Table of Contents

Chapter-1: Introduction	1
1.1. Introduction	2
1.2. Biomass – an alternative to fossil resources	2
1.2.1. Biomass Classification	3
1.2.2. Biorefinery concept – future energy assurance	4
1.2.3. Biogenous feedstocks for renewable fuels and chemicals	5
1.2.4. Upgradation of vegetable oils	5
1.2.5. Biofuels	9
1.2.5.1. First generation biofuels	10
1.2.5.2. Second generation biofuels	10
1.3. Catalytic deoxygenation of vegetable oils/fatty acids producing “green diesel”	11
1.3.1. Deoxygenation pathways for vegetable oils/fatty acids	12
1.3.2. Solid catalysts for deoxygenation of vegetable oils/fatty acids	14
1.3.2.1. Non noble metal based catalysts	14
1.3.2.2. Noble metal based monometallic catalysts	16
1.3.2.3. Noble metal based bimetallic catalysts	18
1.4. Promoter phenomenon	19
1.5. Challenges in deoxygenation of vegetable oils/fatty acids	20
1.5.1. Operation conditions	20
1.5.2. Catalyst stability	20
1.5.3. Hydrogen	20
1.5.4. Capital cost	21
1.6. Scope and objectives of the thesis work	22
1.7. Organization of the thesis	23
1.8. References	25
Chapter-2: Experimental Methods and Characterization Techniques	32
2.1. Introduction	33
2.2. Catalyst preparation	33
2.2.1. Support materials	33
2.2.1.1. AlPO ₄ -5	33
2.2.1.2. Silica-alumina (SA)	34

2.2.1.3. ZrO ₂	34
2.2.1.4. γ -Al ₂ O ₃	34
2.2.2. Supported Pt catalysts	34
2.2.3. Pt supported on reducible oxide modified catalysts	35
2.2.3.1. 4Pt-8WO _x /AlPO ₄ -5	35
2.2.3.2. 4Pt-8WO _x /SA	35
2.2.3.3. 4Pt-8WO _x /ZrO ₂	35
2.2.3.4. 4Pt-8MO _x /Al ₂ O ₃ (M = Mo, Re, W and Sn)	35
2.2.3.5. 4Pt-8MoO _x /ZrO ₂	36
2.3. Characterization techniques and sample preparation	36
2.3.1. X-ray powder diffraction (XRD)	36
2.3.2. Nitrogen physisorption	37
2.3.3. Transmission electron microscopy (TEM)	38
2.3.4. X-ray photoelectron spectroscopy (XPS)	39
2.3.5. NH ₃ -temperature-programmed desorption (NH ₃ -TPD)	39
2.3.6. H ₂ -temperature-programmed reduction (H ₂ -TPR)	40
2.3.7. CO-chemisorption	40
2.3.8. Scanning electron microscopy (SEM)	40
2.4. Reaction procedure	41
2.4.1. Deoxygenation of fatty acids	41
2.4.2. Product analysis	42
2.5. References	43
Chapter-3: Deoxygenation of Oleic Acid over Pt-WO_x/AlPO₄-5	45
3.1. Introduction	46
3.2. Experimental	48
3.2.1. Catalyst preparation	48
3.2.2. Characterization techniques and reaction procedure	48
3.3. Results and discussion	48
3.3.1. Catalyst characterization	48
3.3.1.1. X-ray diffraction	48
3.3.1.2. N ₂ -Physisorption	49
3.3.1.3. NH ₃ -TPD	50
3.3.1.4. H ₂ -TPR	50
3.3.1.5. CO-chemisorption	51

3.3.1.6. Electron microscopic studies (SEM & TEM)	53
3.3.2. Catalytic activity	54
3.3.2.1. Synergistic effect of Pt and promoter	55
3.3.2.2. Effect of Pt and W composition	58
3.3.2.3. Effect of reaction temperature	58
3.3.2.4. Effect of reaction time	59
3.3.2.5. Effect of hydrogen pressure	60
3.3.3. Catalyst recyclability study	60
3.4. Conclusions	64
3.5. References	64
Chapter-4: Deoxygenation of Fatty acids over Reusable Pt-WO_x/Al₂O₃ Catalyst	68
4.1. Introduction	69
4.2. Experimental	71
4.2.1. Catalyst preparation	71
4.2.2. Catalyst characterization and reaction procedure	71
4.3. Results and discussion	71
4.3.1. Catalyst characterization	71
4.3.1.1. X-ray diffraction	71
4.3.1.2. N ₂ -Physisorption	72
4.3.1.3. NH ₃ -TPD	72
4.3.1.4. CO-chemisorption	74
4.3.1.5. TEM	75
4.3.1.6. X-ray photoelectron spectroscopy	76
4.3.2. Catalytic activity	77
4.3.2.1. Influence of WO _x promoter	80
4.3.2.2. Effect of reaction temperature	82
4.3.2.3. Effect of hydrogen pressure	83
4.3.2.4. Substrate scope	83
4.3.3. Catalyst recyclability study and characterization of spent catalyst	83
4.4. Conclusions	88
4.5. References	88
Chapter-5: Effect of Support on the Catalytic Activity of WO_x-promoted Pt in Green Diesel Production	91
5.1. Introduction	92

5.2. Experimental	93
5.2.1. Catalyst preparation	93
5.2.2. Catalyst characterization and reaction procedure	93
5.3. Results and discussion	94
5.3.1. Catalyst characterization	94
5.3.1.1. X-ray diffraction	94
5.3.1.2. N ₂ -physisorption	94
5.3.1.3. NH ₃ -TPD	95
5.3.1.4. TEM	98
5.3.1.5. CO-chemisorption	98
5.3.1.6. X-ray photoelectron spectroscopy	99
5.3.1.7. H ₂ -TPR	103
5.3.2. Catalytic activity	105
5.3.3. Structure-activity correlations	109
5.4. Conclusions	111
5.5. References	111
<hr/>	
Chapter-6: Reducible Oxide Promoted Hydrodeoxygenation Activity of Pt-MO_x/Al₂O₃ in Biofuels Production	115
<hr/>	
6.1. Introduction	116
6.2. Experimental	117
6.2.1. Catalyst preparation	117
6.2.2. Catalyst characterization and reaction procedure	117
6.3. Results and discussion	118
6.3.1. Catalyst characterization	118
6.3.1.1. N ₂ -physisorption	118
6.3.1.2. CO-chemisorption	118
6.3.1.3. X-ray diffraction	118
6.3.1.4. TEM	121
6.3.1.5. NH ₃ -TPD	122
6.3.1.6. H ₂ -TPR	124
6.3.1.7. X-ray photoelectron spectroscopy	125
6.3.2. Catalyst activity	128
6.3.2.1. Effect of promoters	128
6.3.2.2. Effect of reaction parameters	129

6.3.2.3. Catalyst reusability study	135
6.3.2.4. Structure-activity correlation	138
6.4. Conclusions	140
6.5. References	140
Chapter-7: Highly Efficient Pt-MoO_x/ZrO₂ Catalyst for Green Diesel Production	143
7.1. Introduction	144
7.2. Experimental	145
7.2.1. Catalyst preparation	145
7.2.2. Catalyst characterization and reaction procedure	145
7.3. Results and discussion	145
7.3.1. Catalyst characterization	145
7.3.1.1. X-ray diffraction	145
7.3.1.2. N ₂ -physisorption	147
7.3.1.3. CO-chemisorption	148
7.3.1.4. TEM	149
7.3.1.5. NH ₃ -TPD	149
7.3.1.6. H ₂ -TPR	151
7.3.1.7. X-ray photoelectron spectroscopy	152
7.3.2. Catalytic activity	155
7.3.3. Tentative reaction mechanism	164
7.4. Conclusions	166
7.5. References	166
Chapter-8: Summary and Conclusions	169
List of Publications	175

List of Figures

Fig. No.	Figure Caption	Page No.
1.1	Classification of biomass.	3
1.2	Typical structure of triglyceride.	6
1.3	Transesterification of triglyceride with methanol producing biodiesel (FAME).	9
1.4	CO ₂ neutral cycle of biofuels.	9
1.5	Global energy pyramid – comparison of biofuels and fossil fuels.	11
1.6	Upgradation of vegetable oils to biofuels.	12
1.7	Deoxygenation pathways of vegetable oils/fatty acids.	13
1.8	Schematic representation of promoter functioning.	19
1.9	Catalytic systems for deoxygenation.	22
1.10	Scope of the reaction.	23
3.1	XRD profiles of (a) bare AlPO ₄₋₅ and WO _x loaded AlPO ₄₋₅ and (b) reduced 4Pt/AlPO ₄₋₅ and 4Pt-8WO _x /AlPO ₄₋₅ catalysts.	49
3.2	NH ₃ -TPD (experimental and deconvoluted) profiles of (a) AlPO ₄₋₅ (b) 4Pt/AlPO ₄₋₅ and (c) 4Pt-8WO _x /AlPO ₄₋₅ .	50
3.3	H ₂ -TPR of unpromoted (4Pt/AlPO ₄₋₅) and WO _x -promoted (4Pt-8WO _x /AlPO ₄₋₅) catalysts.	51
3.4	SEM images of (a) AlPO ₄₋₅ , (b) 4Pt/AlPO ₄₋₅ and (c) 4Pt-8WO _x /AlPO ₄₋₅ catalysts.	53
3.5	TEM images of reduced Pt/AlPO ₄₋₅ and 4Pt-8WO _x /AlPO ₄₋₅ catalysts and Pt particle size distribution profiles.	54
3.6	¹ H and ¹³ C NMR spectra of oleic acid and products over 4Pt/AlPO ₄₋₅ and 4Pt-8WO _x /AlPO ₄₋₅ .	56
3.7	Effect of WO _x promoter on the catalytic activity of Pt/AlPO ₄₋₅ catalyst	57
3.8	Catalyst recyclability study.	61
3.9	XRD patterns of fresh and spent (a) 4Pt-8WO _x /AlPO ₄₋₅ and (b) 4Pt/AlPO ₄₋₅ catalysts.	62
3.10	TEM histogram profiles of spent Pt/AlPO ₄₋₅ and 4Pt-8WO _x /AlPO ₄₋₅ catalysts.	63
4.1	XRD profiles of (a) reduced 4Pt/Al ₂ O ₃ and 4Pt-8WO _x /Al ₂ O ₃ and (b) “bare”	72

	γ -Al ₂ O ₃ and WO _x loaded Al ₂ O ₃ .	
4.2	NH ₃ -TPD profiles of (a) γ -Al ₂ O ₃ , (b) 4Pt/Al ₂ O ₃ and (c) 4Pt-8WO _x /Al ₂ O ₃ .	74
4.3	TEM images and corresponding Pt particle size histograms of 4Pt/Al ₂ O ₃ (left) and 4Pt-8WO _x /Al ₂ O ₃ (right).	75
4.4	XPS of Pt 4d lines for (a) Pt/Al ₂ O ₃ and (b) Pt-8WO _x /Al ₂ O ₃ and (c) W 4f lines of 4Pt-8WO _x /Al ₂ O ₃ catalysts.	76
4.5	Effect WO _x -promoter on the deoxygenation of OA over Pt/Al ₂ O ₃ .	79
4.6	¹ H NMR spectra of (a) oleic acid (OA), (b) deoxygenation product of OA over 4Pt/Al ₂ O ₃ and (c) deoxygenation product of OA over 4Pt-8WO _x /Al ₂ O ₃ .	79
4.7	Effect of Pt-W composition on the deoxygenation of OA.	80
4.8	Catalytic activities of 4Pt/Al ₂ O ₃ and 4Pt-8WO _x /Al ₂ O ₃ at 280 and 320 °C as a function of reaction time.	81
4.9	Recyclability study of (a) 4Pt-8WO _x /Al ₂ O ₃ and (b) 4Pt/Al ₂ O ₃ .	85
4.10	Comparative XRD profiles of fresh and spent catalysts: (a) 4Pt-8WO _x /Al ₂ O ₃ and (b) 4Pt/Al ₂ O ₃ .	86
4.11	XPS of (a) Pt 4d and (b) W 4f lines of spent 4Pt-8WO _x /Al ₂ O ₃ after 5 recycles.	86
4.12	TEM images of spent catalyst (1 & 2) and Pt particle size histograms (a, b, c and d).	87
5.1	XRD patterns of (a) unpromoted and (b) WO _x -promoted supported Pt catalysts.	95
5.2	(a) N ₂ -physisorption profiles and pore size distribution curves of unpromoted supported Pt catalysts.	97
	(b) N ₂ -physisorption profiles and pore size distribution curves of WO _x -promoted supported Pt catalysts.	98
5.3	NH ₃ -TPD profiles of (a) unpromoted and (b) WO _x -promoted supported Pt catalysts.	99
5.4	(a) TEM images and particle size histograms of unpromoted supported Pt catalysts.	100
	(b) TEM images and particle size histograms of WO _x -promoted supported Pt catalysts.	101
5.5	(a) XPS (Pt 4d lines) of reduced WO _x -promoted supported Pt catalysts.	102
	(b) XPS (Pt 4d lines) of reduced unpromoted supported Pt catalysts.	103

	(c) XPS of W 4f lines of WO _x -promoted supported Pt catalysts.	104
5.6	Effect of Pt dispersion on the catalytic activity of WO _x -promoted supported Pt catalysts.	109
5.7	Effect of Pt electronic nature on the catalytic activity of WO _x -promoted catalysts.	110
5.8	Effect of acidity of WO _x -promoted catalysts on product selectivity.	111
6.1	XRD profiles of Pt-MO _x /Al ₂ O ₃ catalysts.	120
6.2	TEM images of Pt-MO _x /Al ₂ O ₃ (MO _x = MoO _x , WO _x , ReO _x or SnO _x) catalysts.	121
6.3	Pt particle size distribution histograms of Pt-MO _x /Al ₂ O ₃ (MO _x = MoO _x , WO _x , ReO _x or SnO _x) catalysts.	122
6.4	NH ₃ -TPD profiles of (a) 4Pt-8MoO _x /Al ₂ O ₃ , (b) 4Pt-8ReO _x /Al ₂ O ₃ , (c) 4Pt-8WO _x /Al ₂ O ₃ and (d) 4Pt-8SnO _x /Al ₂ O ₃ catalysts.	123
6.5	H ₂ -TPR profiles of reducible oxide-promoted Pt/Al ₂ O ₃ catalysts.	124
6.6	XPS of (a) 4Pt-8MoO _x /Al ₂ O ₃ , (b) 4Pt-8ReO _x /Al ₂ O ₃ , (c) 4Pt-8WO _x /Al ₂ O ₃ and (d) 4Pt-8SnO _x /Al ₂ O ₃ catalysts in Pt 4d region.	126
6.7	XPS of (a) Mo 3d, (b) Re 4f, (c) W 4f and (d) Sn 3d of reducible oxide-promoted Pt/Al ₂ O ₃ catalysts.	127
6.8	Deoxygenation of oleic acid (OA) over reducible oxide-promoted Pt/Al ₂ O ₃ catalysts.	131
6.9	TEM images of spent (at 260 °C; after three reuses) reducible oxide-promoted Pt/Al ₂ O ₃ catalysts.	137
6.10	XRD of fresh and spent (at 260 °C; after three reuses) 4Pt-8MoO _x /Al ₂ O ₃ catalysts.	138
6.11	Correlation of (a) OA conversion with binding energy values of Pt 4d _{3/2} line and (b) octadecane (C ₁₈) selectivity with the ratio of concentration of M ⁿ⁻¹ to M ⁿ ions of promoter metal.	139
7.1	XRD patterns of ZrO ₂ and ZrO ₂ -supported Pt catalysts.	146
7.2	XRD profiles of 2 wt% Pt deposited on varying amounts of MoO _x modified ZrO ₂ .	146
7.3	Nitrogen adsorption-desorption isotherms of ZrO ₂ and ZrO ₂ -supported Pt catalysts.	147
7.4	TEM images and particle size histograms of ZrO ₂ -supported Pt catalysts.	150
7.5	NH ₃ -TPD profiles of ZrO ₂ and ZrO ₂ -supported Pt catalysts.	151

7.6	H ₂ -TPR profiles of ZrO ₂ -supported Pt catalysts.	152
7.7	XPS of 4Pt/ZrO ₂ , 4Pt-8MoO _x /ZrO ₂ and 4Pt-8WO _x /ZrO ₂ in Pt 4f region.	153
7.8	XPS of 4Pt-8MoO _x /ZrO ₂ and 4Pt-8WO _x /ZrO ₂ in Mo 3d and W 4f regions.	154
7.9	XPS of ZrO ₂ -supported Pt catalysts in Zr 3d region.	154
7.10	XRD of spent catalysts.	162
7.11	TEM images and particle size histograms of spent catalysts.	162
7.12	XPS of spent catalysts in Pt 4f region.	163
7.13	XPS of spent catalyst in Mo 3d and W 4f regions.	163
7.14	XPS of spent catalyst in Zr 3d region.	164
7.15	A tentative deoxygenation mechanism of fatty acids over (a) unpromoted Pt and (b) reducible oxide-promoted supported Pt catalysts.	165

List of Schemes

Scheme No.	Scheme Caption	Page No.
5.1	Reaction pathways of fatty acid deoxygenation.	105
6.1	Reduction steps and some intermediates in hydrodeoxygenation of fatty acids.	133

List of Tables

Table No.	Table Heading	Page No.
1.1	List of various edible and inedible vegetable oils.	6
1.2	Major fatty acids with varying chain lengths (saturated/unsaturated).	7
1.3	Non noble metal based catalysts for deoxygenation of vegetable oils/fatty acids.	15
1.4	Noble metal based monometallic catalysts for green diesel production.	17
3.1	Physicochemical properties of the Pt catalysts.	52
3.2	Catalytic activity data: deoxygenation of OA.	55
3.3	Influence of Pt and W composition on the deoxygenation activity.	58
3.4	Effect of reaction parameters on deoxygenation of OA over 4Pt-	59

	8WO _x /AlPO ₄ -5.	
3.5	Recyclability study of 4Pt-8WO _x /AlPO ₄ -5 catalyst.	61
4.1	N ₂ -physisorption, CO-chemisorption and TEM data of Al ₂ O ₃ -supported Pt catalysts.	73
4.2	Acidic properties (NH ₃ -TPD) of Al ₂ O ₃ -supported Pt catalysts.	73
4.3	Influence of Pt and Pt-WO _x composition on the catalytic deoxygenation of OA.	78
4.4	Influence of reaction parameters on deoxygenation of oleic acid over 4Pt-8WO _x /Al ₂ O ₃ .	82
4.5	Deoxygenation of fatty compounds over 4Pt-8WO _x /Al ₂ O ₃ .	83
4.6	Recyclability study of 4Pt-8WO _x /Al ₂ O ₃ and 4Pt/Al ₂ O ₃ catalyst in deoxygenation of oleic acid.	84
5.1	Physicochemical properties of unpromoted and WO _x -promoted supported Pt catalysts.	96
5.2	Deoxygenation of oleic acid over supported Pt catalysts.	107
5.3	Catalytic deoxygenation activity of WO _x -promoted supported Pt catalysts at 280 °C.	108
6.1	Physicochemical characteristics of promoted supported Pt catalysts.	119
6.2	NH ₃ -TPD data of promoted supported Pt catalysts.	123
6.3	Deoxygenation of oleic acid over reducible oxide promoted supported Pt catalysts.	129
6.4	Deoxygenation of oleic acid over reducible oxide-promoted Pt/Al ₂ O ₃ catalysts as a function reaction time.	130
6.5	Deoxygenation of oleic acid over reducible oxide-promoted Pt/Al ₂ O ₃ catalysts as a function reaction temperature.	132
6.6	Effect of catalyst amount and hydrogen pressure on deoxygenation of oleic acid over 4Pt-8MoO _x /Al ₂ O ₃ .	133
6.7	Deoxygenation of fatty compounds over 4Pt-8MoO _x /Al ₂ O ₃ .	134
6.8	Catalyst recyclability study in deoxygenation of oleic acid at 320 °C.	136
6.9	Catalyst recyclability study in deoxygenation of oleic acid at 260 °C.	136
6.10	SEM-EDAX analysis of chemical composition of fresh and spent catalysts (at 260 °C; after three reuses).	137
7.1	Physicochemical characteristics of ZrO ₂ -supported Pt catalysts.	148
7.2	CO-chemisorption data of 2Pt-MoO _x /ZrO ₂ catalysts.	148

7.3	Acidity data of ZrO ₂ -supported Pt catalysts.	149
7.4	Surface chemical composition (atomic ratio) of ZrO ₂ -supported Pt catalysts.	155
7.5	Deoxygenation of oleic acid over 4Pt-8MoO _x /ZrO ₂ and 4Pt-8WO _x /ZrO ₂ catalysts at varying reaction temperature.	156
7.6	Effect of hydrogen pressure on deoxygenation of oleic acid	157
7.7	Influence of reaction time on deoxygenation of OA over 4Pt-8MoO _x /ZrO ₂ catalyst.	158
7.8	Influence of catalyst amount on deoxygenation of oleic acid.	158
7.9	Effect of Mo content on the deoxygenation of OA over 2Pt-xMoO _x /ZrO ₂ (x = 4-16).	159
7.10	Effect of gaseous atmosphere on deoxygenation of oleic acid.	159
7.11	Substrate study over 4Pt-8MoO _x /ZrO ₂ .	160
7.12	Recyclability study of Pt supported on MoO _x /WO _x modified ZrO ₂ catalysts.	161
7.13	Chemical composition (SEM-EDAX) of fresh and spent catalysts	163
8.1	Comparative catalytic activity of Pt supported on reducible oxide modified supports	173

Chapter-1

Introduction

1.1. Introduction

The demand for energy is growing steeply due to urbanization, rising population and improving living standards of human being [1]. Currently, fossil resources (coal, oil and natural gas) are fulfilling the major portion of world's energy requirement. It has been realized that these resources are limited and last for a few more decades only. Transportation sector is the largest user of fossil fuels. In fact, it is the key economic aspect of the development of a country [2]. The evolutionary change in transportation segment is causing severe environment pollution by emitting CO₂, a greenhouse gas along with other effluents. Transport sector contributes about 15% of world's total CO₂ emissions [3]. Due to enormous consumption, consequent depletion of fossil reserves and environment pollution, a need for alternate energy resources has become inevitable.

In 21st century, the terms sustainability and renewability have been gaining tremendous popularity due to the crisis of fossil resource exhaustion. Sustainable development leads to energy assurance and clean environment for future generations. Hence, a substantial attention has been paid to find alternative methods to replace fossils with renewable resources which include solar energy, wind power, hydro power, nuclear power, geothermal power, tidal power and biomass. Considerable research should be dedicated for successful implementation of renewable resources. Biomass is a versatile, sustainable, renewable and promising energy resource that attracted the attention of researchers worldwide.

Catalysis plays an important role providing suitable solutions for societal problems. Catalytic conversion of biomass into renewable transport fuel is an excellent thought to surmount the shortage of fossil fuel resources for future energy assurance and to maintain green environment. Inedible vegetable oils and their constituent fatty acids are the right choice of biomass, having a vast scope of research to produce renewable fuels. Since this biogenous feed is oxygen rich, it must be deoxygenated to exploit its feasible application as hydrocarbon fuel. Thus, catalytic deoxygenation has become the heart of 'biorefinery' where biomass is used as feedstock to produce biofuels and commodity chemicals.

1.2. Biomass – an alternative to fossil resources

Undoubtedly, energy production from renewable resources like biomass is an emerging process technology to fulfill the energy demand and to protect the environment from gases (CO₂, NO_x, CO, etc) produced by burning of petroleum fuels. An adequate research has been devoted to explore efficient technological processes for substitution of

fossil fuels with environmentally benign processes [4, 5]. Among renewable energy resources, biomass contributes more than 50% share to the total renewable energy [6]. Thus, biomass can be referred as solid fuel. It is a spectacular agent that can provide energy potentially while addressing global issues viz., eco-friendliness and sustainability. Currently, the availability of potential biomass worldwide is anticipated to be 6.49 billion tons/year and merely, 2.48 billion tons of biomass is used for energy production which meets 14% of total global energy demand [7]. Many research groups have been working to develop technological solutions for production of commodity chemicals and fuels from biomass. It is being considered to avoid infrastructure modifications of the existing refineries for upgradation of different bio-sources into useful chemicals by aligning the biomass processes with petro refinery due to chemical similarities of these sources of energy [8, 9]. Fatty acids are carboxylic acids with a long hydrocarbon chain (*ca.*, C₈-C₂₄). Removal of acid group is regarded as an important process yielding renewable hydrocarbons and it resembles the hydrotreatment process in a refinery. Thus, deoxygenation of fatty acids or vegetable oils can be aligned with the hydrodeoxygenation process (HDO) of a petro refinery. An integral utilization of biomass in addition with other renewable energy resources would avoid the energy crisis and lead to future energy assurance.

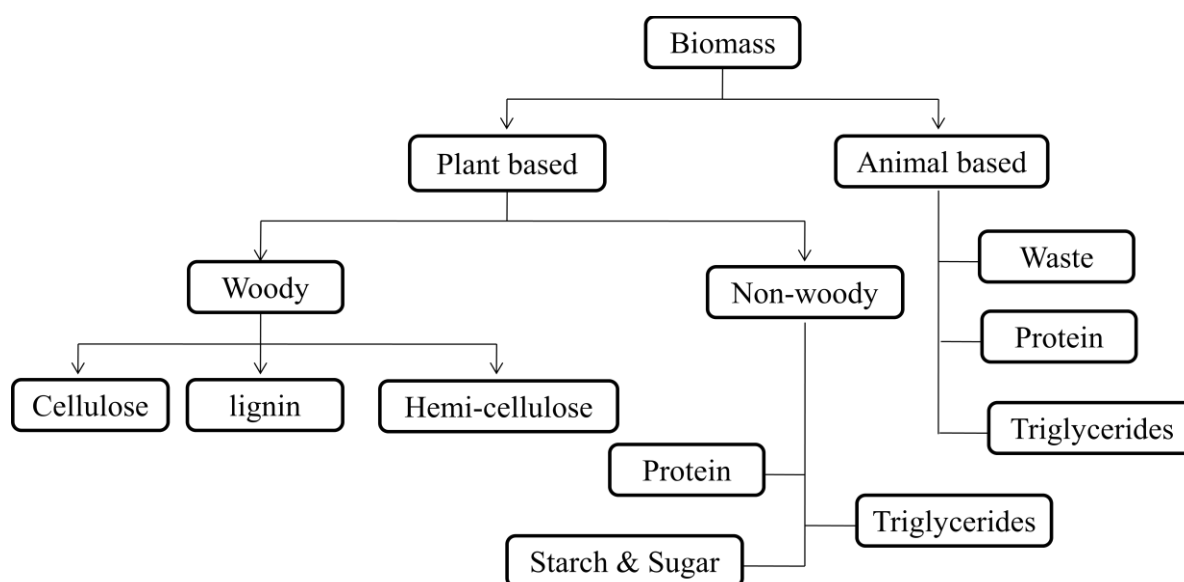


Fig. 1.1. Classification of biomass

1.2.1. Biomass classification

Biomass is an organic matter produced by plants or animals and includes mainly, wood, grains, leaves, flowers, vegetable oils and animal fats. For generalization, biomass can

be classified primarily into two categories based on the source: 1) plant-based biomass and 2) animal-based biomass (Fig. 1.1). The plant biomass is more advantageous over the biomass originated from animals. It is because of the reasons of easy cultivation and abundance. Especially, woody biomass including cellulose, hemi-cellulose and lignin, non-woody biomass including starch, sugar and triglycerides are the promising biogenous feedstocks for renewable chemicals and transport fuels. Animal wastes and fats are not popularized appreciably due to difficulties in their procurement and processing.

1.2.2. Biorefinery concept - future energy assurance

Petro-refinery works on the principle of manufacturing of simple handling and chemically pure defined products. Similar to petroleum, biomass is compositionally complex as it contains compounds of C, H, O, N and S including carbohydrates, lignin, proteins, fats, and to a lesser extent various other chemicals, such as vitamins, dyes, and flavors [10]. Biorefinery is a promising contemporary concept where biomass will be processed into chemicals and fuels and this is analogous to petro-refinery. It can be regarded as a facility which aligns the biomass conversion processes with petro refinery to produce fuels and chemicals from the biomass feedstocks. The goal of a biorefinery is to transform such plentiful biological materials into useful products using a combination of chemical technology and knowledge involved in process intensification. This can be accomplished by removal of hetero-atoms (O and N) from biomass leading to pure hydrocarbons which are well known renewable fuels. The tailoring of this complex bio-feedstock with specific functional groups enables production of commodity chemicals. This process either can be coupled with the petro-refinery processes or performed as standalone process.

According to the US Department of Energy (DOE), a "biorefinery" is an overall concept of a process where plant biomass feedstocks are converted and extracted into a spectrum of valuable products [11]. An integration of biorefinery with well abundant bio raw materials can serve as potential and promising system to fulfil the demand of energy and fine chemicals. However, this requires chemical technology which provides path to make the process simple for defined chemicals. The main goals of biorefinery can be represented in two principles for the production of: 1) low value-high volume (LVHV) and 2) high value-low volume (HVLV) products. These principles are designed to maximize the valued extractibles while reducing the waste streams by converting LVHV platform feedstocks into energy [12]. Herein, the high-value products boost the profitability, whilst the high volume fuels assist to meet the world's energy need. Thus, the biorefinery concept in association with well abundant biogenous platforms enables to achieve sustainability and green environment.

Based on the input feed, flexibility of process and capacity, biorefinery is classified into different phases (phase I, II, and III). Apart from these, green, whole crop, lingo-cellulosic and integrated biorefinery are the further classification based on the process intensifications [13]. However, all of these systems are working on a single line goal for the development of renewable energy based on sustainable feedstock/platform which overcomes the shortage of conventional fossil resources and reduces environment pollution and its consequences.

1.2.3. Biogenous feedstocks for renewable fuels and chemicals

Biorefinery has enough potential to supply sufficient global energy and fine chemicals and hence, it is possible when an appropriate technology is coupled with a specific biomass feedstock. Conversion of biomass feedstocks into fuels and industrially important chemicals creates path for independence from fossil sources. Compared to petro-refinery, chemicals production from biomass feedstocks is benign and attractive. Many chemical conversions have been reported based on developed technology in various fields to produce fine chemicals and fuel type hydrocarbons by implementing different physical and chemical methods [12].

Bio-glycerol is a by-product in biodiesel synthesis process from vegetable oils and methanol. It is produced in surplus amount due to the revolutionary commercialization and bulk scale production of biodiesel. Realizing the importance of this bio-glycerol as C₃-feedstock, processes to produce 1, 2-propanediol, 1, 3-propanediol, ethylene glycol and n-propanol have been considered as green routes for these chemicals production. [14]. On the other hand, furfural, a C₄-feedstock is a potential agent for sustainable production of furans, γ -valerolactone, levulinic acid and 1, 5-pentanediol, etc [15]. Deoxygenation of vegetable oils to renewable hydrocarbons is another emerging technology [16]. Ethanol production by fermentation of woody biomass has attracted enormous attention of researchers [17]. Renewable sugars have been well explored as C₅ and C₆ platform feedstocks that can be converted into many useful chemicals [18].

1.2.4. Upgradation of vegetable oils

In recent years, due to increasing concerns for sustainability and environment protection, industrial application of biomass feedstocks is gaining tremendous interest. Among them, vegetable oils (VO)/free fatty acids (FFA) are one of the potential resources for chemical industry in the near future. Relatively less cost, worldwide availability, and built-in functionality made them attractive to find various applications. Due to similarities between vegetable oils and some of the fractions of petroleum, they can be more susceptible for

chemical transformations producing renewable chemicals and fuels. Therefore, a substantial research has already been focused for the conversion of triglycerides/fats into fuels and industrial chemicals.

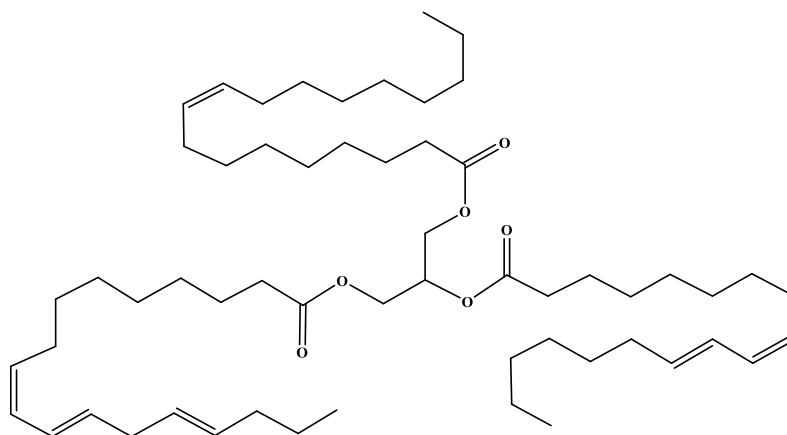


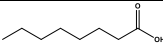
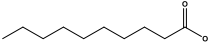
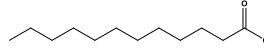
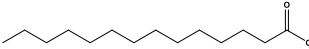
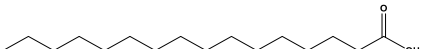
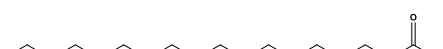
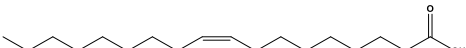
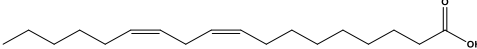
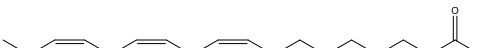
Fig. 1.2. Typical structure of triglyceride.

Table 1.1. List of various edible and inedible vegetable oils

Edible oils	Inedible oils
Sunflower oil	Jatropha oil
Palm oil	Pongamia oil
Mustard oil	Neem oil
Coconut oil	Copaiba oil
Peanut oil	Karanja seeds oil

Chemically, vegetable oils are triglycerides in which three fatty acid are linked to glycerol backbone through ester bonds (Fig. 1.2). Nature of alkyl chain of fatty acid attached to glycerol molecule is different for each vegetable oil. They are mainly classified into two classes: 1) edible and 2) inedible or non-edible vegetable oils (Table 1.1). Inedible oils find many industrial applications without major chemical changes in various fields like paints, lubricants, pharmaceuticals, cosmetics and for other industrial purposes. Vegetable oils have the potential to substitute for a fraction of the petroleum distillates (fuel chemicals) and industrial petrochemicals in the near future. The chain length of fatty acid of a vegetable oil can vary from C₈ (8 carbons atom in fatty acid chain) to C₂₄ (24 carbons in the fatty acid chain). But mostly, C₁₆-C₁₈ fatty acids are major in most of the vegetable oils.

Table 1.2. Major fatty acids with varying chain lengths (saturated/unsaturated)

Fatty acid name	Carbon number	No. of double bonds	Chemical structure
Caprylic acid	8	0	
Capric acid	10	0	
Lauric acid	12	0	
Myristic acid	14	0	
Palmitic acid	16	0	
Stearic acid	18	0	
Oleic acid	18	1	
Linoleic acid	18	2	
Linolenic acid	18	3	

The composition and nature of fatty acid (saturated/unsaturated) is also different for each vegetable oil. Some of the fatty acids are saturated and some are with mono to multi unsaturation. Based on the position of this unsaturation (olefinic bond), the nomenclature of the fatty acid is defined. Table 1.2. presents a list of major fatty acids with varying chain lengths. Palmitic (C_{16:0}) and stearic (C_{18:0}) are common saturated fatty acids, as they are present in most of the vegetable oils as common components. Similarly, oleic (C_{18:1}) and linoleic (C_{18:2}) are the most common unsaturated fatty acids. Some of the oils also contain linolenic acid (C_{18:3}) to a little extent [19]. In United States, soybean is common for biofuels production while palm oil in Malaysia, rapeseed oil in Europe and jatropha oil in India are commonly used for biofuels production. There are mainly three major pathways for upgradation of vegetable oils. These are as follows.

Pyrolysis is generally defined as the thermal decomposition of organic matter in the absence of air or oxygen. This is a well established process to break down larger petroleum hydrocarbon molecules into smaller, more desirable hydrocarbons in the presence of a catalyst and absence of oxygen. Zeolites and mesoporous alluminosilicates are the catalysts used for thermal catalytic cracking [20, 21]. The mimic of pyrolysis can be applied to breakdown the robust vegetable oil moieties [22]. Catalytic cracking of vegetable oils yields hydrocarbons with different chain lengths. However, this process is not atom economical as it forms gaseous products due to random and intensive cracking.

Transesterification of vegetable oils is one of the best methods to valorise them into fuels. In this, alcohols like methanol and ethanol are employed to form fatty acid methyl or ethyl esters (Fig. 1.3). Fatty acid methyl ester (FAME) became more popular worldwide as “biodiesel”. This was anticipated as a promising fuel to substitute petro-diesel. Solid acid and base catalysts were developed for the production of biodiesel from vegetable oils. Unfortunately, the disadvantages including poor stability, poor cold flow properties and low energy content are the main obstacles for its use as fuel [23-25]. However, this can be blended with petero-diesel up to a certain amount (*ca.*, 5-20 %).

Deoxygenation is a versatile, mimicking process of petro-refinery hydrotreating (HT) for the removal of oxygen moieties in vegetable oils producing renewable hydrocarbons. This requires hydrogen pressure which breaks the C-C or C-O bonds via hydrogenolysis [1]. A detailed description on deoxygenation is provided in further sections.

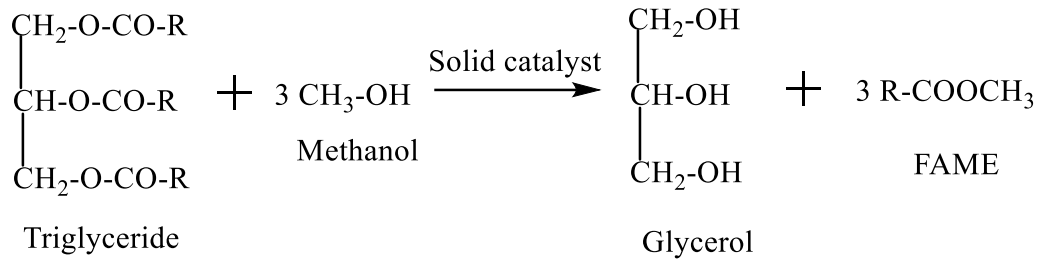


Fig. 1.3. Transesterification of triglyceride with methanol producing biodiesel (FAME).

1.2.5. Biofuels

The energy assurance can be accomplished for future generations due to the potential of biomass for production of renewable chemicals and fuels. The fuels derived from biomass feedstocks are called “biofuels”. They are carbon neutral. As shown in Fig. 1.4, CO₂ emitted by burning of biofuels will be captured back by biomass in the cultivate process. This cycle goes on. Thus, it is anticipated that there will be no net increment in CO₂ amount caused by biofuels consumption. But this estimation is true at a stage where biofuels become predominant over fossil fuels. The sustainability of biofuels versus fossil fuels is depicted in Fig.1.5. Based on the nature of source, biofuels can be classified as follows [27]:

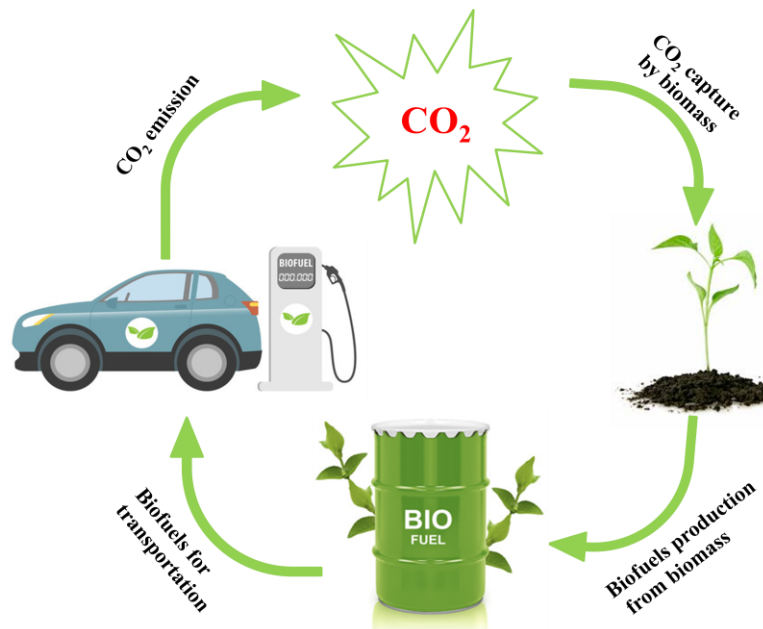


Fig. 1.4. CO₂ neutral cycle of biofuels

1.2.5.1. First generation biofuels

Bioethanol and biodiesel are the examples of 1st generation biofuels as they are manufactured from edible biomass like starch and sugar (for ethanol) and edible oils (for biodiesel). Sugars are directly converted to ethanol by fermentation while starch is depolymerized into monomeric sugars and then, subjected for fermentation by an anaerobic digestion process to produce ethanol using microorganisms (yeast). As per the EU quality standard (EN 228), 5% of bioethanol can be blended with petrol without any engine modification. It may also be used in the form of ethyl tertiary butyl ether (ETBE) to enhance the octane rating of the gasoline. Even higher blends of ethanol can be possible but with a modified engine vehicle manufactured by Ford Company known as “flexible fuel vehicle (FFV). These vehicles are popular in Europe. E85 fuel (85% ethanol and 15% gasoline blend) is used in these vehicles [27].

Biodiesel is fatty acid methyl ester (FAME) obtained by transesterification of triglycerides with methanol. Its use in cold countries is limited due to its high pour point as it can clog filters inside the engine. It is currently recommended that only up to 5–20% of biodiesel could be blended with diesel fuel (B5 - B20) [28-30]. Higher blending ratios are detrimental for its application as fuel due to its high viscosity.

The intention to promote non-petroleum energy sources to avoid dependence on oil imports and to reduce global warming has encouraged the production of biofuels from food crops (edible biomass). Consequently, this led to a debate on “food vs fuel” as crop lands are diverted to produce raw materials for biodiesel and ethanol. This debate resulted in developing second generation biofuels which are made from inedible biomass [31, 32].

1.2.5.2. Second generation biofuels

Food vs fuel controversy changed the research perception to produce biofuels from inedible biomass (woody biomass and inedible vegetable oils) instead of edible biomass as the inedible biomass will not affect the food supply. Agriculture wastes, other organic matter of plants, woody biomass, inedible vegetable oils, waste cooked oils and micro algae oils are the major non-food feedstocks for 2nd generation biofuels.

Lignocellulosic ethanol can be a sustainable route for ethanol economy. But, the conversion of robust lignocellulosic biomass into its monomers and then, fermentation to produce ethanol need sophisticated technology. A mighty challenge is hemicellulose, as it forms pentoses (xylose and arabinose) which are difficult to be fermented. However, genetically, modified yeasts can be applied to overcome this problem [33].

Green diesel is the advanced and emerging concept for substitution of fossil fuels. It is a hydrocarbon mixture produced by deoxygenation of triglycerides/fatty acids of inedible vegetable oils or micro algae oils. Deoxygenation can be carried out over a solid catalyst or by a cracking process [34-36]. Nevertheless, catalytic deoxygenation is the most acceptable process for production of fuel range hydrocarbons. High quality green diesel production is possible by isomerisation done either separately or in a tandem reaction.

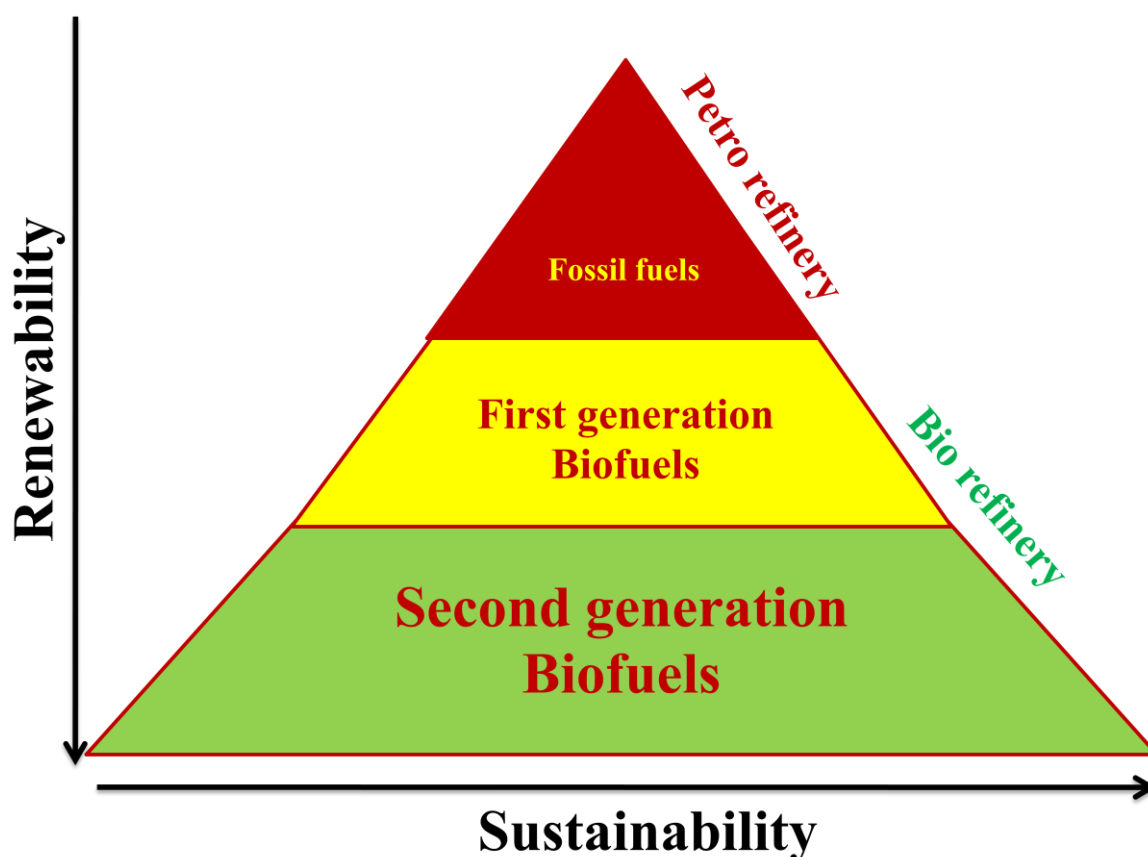


Fig. 1.5. Global energy pyramid – comparison of biofuels and fossil fuels.

1.3. Catalytic deoxygenation of vegetable oils/fatty acids producing “Green Diesel”

Inedible vegetable oils including, jatropha, jojoba, pongamia, etc. are the potential future energy carriers. Vegetable oils are the source of renewable hydrocarbons as they consist of hydrocarbon chain with oxygen moieties in the form of carboxylic acid. Their high viscosity was detrimental for their use as direct fuel without adapting engine modifications. The vegetable oils or constituent fatty acids render tremendous energy storage for future generations in a green and clean approach. Hence, deoxygenation of vegetable oils or fatty acids has been gaining remarkable interest.

As mentioned earlier, the direct use of vegetable oils as diesel fuel is not suitable because of compatibility problems of the existed vehicle engines. Therefore, several

improvement processes have been implemented to produce renewable diesel fuels which are compliant with the vehicle engine infrastructure. Upgradation of oil can happen by cracking, transesterification and deoxygenation (Fig. 1.6) [37, 38]. Cracking involves thermal or catalytic decomposition of triglycerides. The products are lighter alkanes, alkenes, and fatty acids. Formation of lighter alkanes and volatile organic molecules leads to less atom economy [38]. Therefore, cracking is not a favorable upgrading technology of vegetable oils. On the other hand, biodiesel produced by transesterification has proved futile due to its disadvantages.

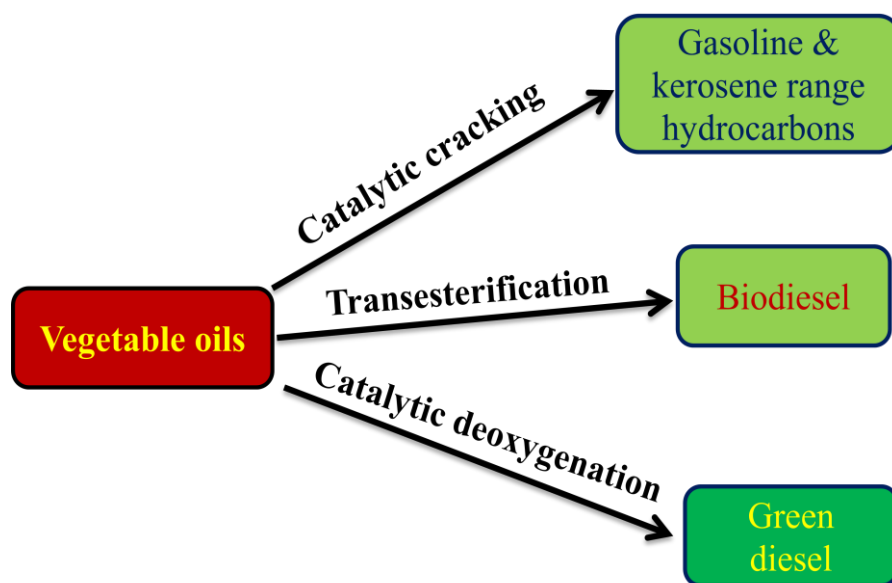


Fig. 1.6. Upgradation of vegetable oils to biofuels.

Catalytic deoxygenation is the promising technology for upgradation of vegetable oils. Removal of oxygen moiety from inedible oils enables production of renewable fuels [16].

1.3.1. Deoxygenation pathways for vegetable oils/fatty acids

For deoxygenation of vegetable oils/fatty acids, two major routes are proposed: 1) decarboxylation/decarbonylation (DCO) and 2) hydrodeoxygenation (HDO).

In decarboxylation/decarbonylation (DCO), oxygen content of the oil is removed in the form of CO_2 or CO . Firstly, triglyceride decomposes into its constituent fatty acids and glycerol (or propane in presence of plenty of H_2). These free fatty acids undergo deoxygenation over solid catalysts to yield hydrocarbons. This process requires less hydrogen pressure. CO_2 elimination leads to form hydrocarbon with one carbon less as compared to the parent fatty acid. CO elimination method is not distinct due to the fact that reverse water gas shift reaction converts CO_2 and H_2 to CO and H_2O . Due to this reason, the mechanistic

investigations are uncertain about the formation of CO in deoxygenation of vegetable oil/fatty acids and it was not considered as a deoxygenation path. The CO₂ generated in this way undergoes many side reactions like methanation and reverse water gas shift reactions based on the catalyst type and reaction conditions [39].

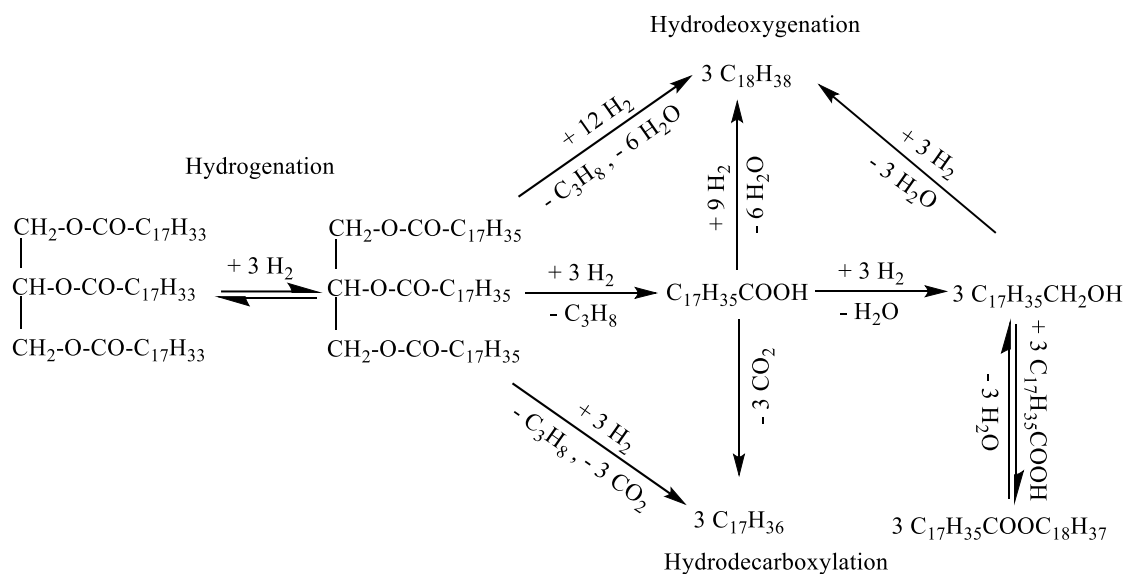


Fig. 1.7. Deoxygenation pathways of vegetable oils/fatty acids.

In hydrodeoxygenation (HDO), oxygen atom in vegetable oil/fatty acid is removed in the presence of hydrogen as water. This process requires moderate to high hydrogen pressure based on the type of the catalyst. Hydrodeoxygenation involves many successive reaction steps. The paraffin formed will have the same number of carbon atoms as in the corresponding fatty acid. Investigation of individual kinetics of HDO of stearic acid and 1-octadecanol intermediate over Ni/HBEA catalyst under similar conditions were performed [40] and the deoxygenation pathway of stearic acid was postulated. According to this study, reduction of carboxylic group to corresponding aldehyde is the rate determining step. Further, the successive hydrogenation of this aldehyde intermediate to alcohol which undergoes sequential dehydration-hydrogenation (catalyzed by acid sites and metal) lead the final alkane. In case of unsaturation, hydrogenation of double bonds is the primary and fast step [41, 42].

1.3.2. Solid catalysts for deoxygenation of vegetable oils/fatty acids

Several catalyst systems have been proposed for deoxygenation of vegetable oils and fatty acids. The catalysts reported till date are grouped into a few categories and discussed below.

1.3.2.1. Non-noble metal based catalysts

Catalytic activity of a supported catalyst depends on many factors including method of preparation, nature of metal precursors and nature of support. Ni or Co supported on alumina in combination with secondary metals like tungsten and molybdenum in sulfided form are well established hydrotreating catalysts [43-47]. The deoxygenation reactions were conducted in the temperature range of 250-360 °C with 7-150 bar of hydrogen. The deoxygenation path relied on the reaction conditions. At high hydrogen pressures, HDO (hydrodeoxygenation) was the predominant pathway, while at high reaction temperatures DCO (decarboxylation/decarbonylation) was the major route. Mono metallic sulfided catalysts showed lower activity than bimetallic catalysts (NiMo > Mo > Ni). To maintain the catalytic activity of these catalysts, sulphur feed had to be supplied continuously to avoid catalyst deactivation [48, 49].

To avoid the problem of product contamination with sulphur significant research has been focused on developing non-noble metal-based sulphur free catalysts. Since, relatively nickel is cheaper and abundant, many Ni-based catalysts were designed and screened for deoxygenation of vegetable oils/fatty acids (Table 1.3). Recently, Loe et al. [50] studied the influence of Cu and Sn to promote the catalytic activity of 20% Ni/Al₂O₃ for deoxygenation of lipids to fuel. In a semi-batch mode operation, deoxygenation of tristearin was performed at 260 °C and the Cu promoted catalyst showed superior activity than the Sn promoted and unpromoted Ni/Al₂O₃ catalyst. The catalytic activity varied in the order: Ni-Cu/Al₂O₃ > Ni-Sn/Al₂O₃ > Ni/Al₂O₃. Hachemi et al. [51] prepared a series of sulphur free Ni catalysts supported on different supports including H-Y, γ -Al₂O₃ and SiO₂. Deoxygenation of stearic acid was performed at 300 °C with 30 bar hydrogen input pressure. Ni/H-Y exhibited higher catalytic activity than the rest of the catalysts.

Xin et al. [52] prepared nickel phosphide catalysts supported on activated carbon (AC) and evaluated for deoxygenation of palmitic acid. It was observed that by varying the Ni/P ratio from 0.5 to 0.8, different nickel phosphide species were formed (Ni₂P and Ni₁₂P₅). It was concluded that the nature of nickel phosphide species and their dispersion are the crucial parameters to control the catalytic activity. In another study, Ni₂P supported on MCM-41 was investigated for deoxygenation of methyl palmitate in a continuous flow

reactor. Ni₂P formed by the direct one-step reduction of P precursor with Ni/P ratio of 0.5, enabled stable activity above 310 °C with 30 bar pressure [53]. Peroni et al. [54] prepared a series of bulk and supported Ni₂P and MoP materials supported on Al₂O₃ and applied them for hydrodeoxygenation of palmitic acid. It was observed that bulk Ni₂P was more active than MoP and Ni₂P/Al₂O₃. It was noted that Ni catalysts followed decarboxylation/decarbonylation route to yield pentadecane while hexadecane was the dominant product over MoP/Al₂O₃. The influence of support on deoxygenation activity of NiMo phases supported on SAPO-11 and Al₂O₃ for jatropha oil was studied by Chen et al. [55]. NiMo/SAPO-11 showed higher deoxygenation activity due to presence of different Mo species and DCO was the major reaction route.

The effect of Ni particle size on deoxygenation of oleic acid to renewable hydrocarbons was reported by Cárdenas et al. [56] over Ni/Al₂O₃ catalyst at 320-340 °C and 16 bar H₂ pressure. A theoretical model to optimize the yield of n-C₁₇ was developed. In a report by Bambang et al. [57], the effect of different supported catalysts on hydrotreatment of soybean oil was investigated. The hydroprocessing activity of the catalysts varied in the order: sulfided NiMo/Al₂O₃ > Pd/Al₂O₃ > sulfided CoMo/Al₂O₃ > Ni/SiO₂-Al₂O₃ > Pt/Al₂O₃ > Ru/Al₂O₃ at a 0.44 catalyst/oil weight ratio. In another study, the non-sulfided NiMoCe/Al₂O₃ catalyst was prepared by wet impregnation method and applied for the hydroprocessing of jatropha oil. Maximum yield for C₁₅-C₁₈ alkanes of 80%, selectivity of 90% and conversion of 89% were obtained at 370 °C, 3.5 MPa and 0.9 h. To optimize the product yield, the influence of reaction temperature (280 - 400 °C) and reaction time (10 - 163 h) were varied. Deoxygenation study revealed that adding of Ce component to NiMo/Al₂O₃ leads to stable catalytic performance, enhanced jatropha oil conversion and C₁₅-C₁₈ product selectivity [58].

Table 1.3. Non noble metal based catalysts for deoxygenation of vegetable oils/fatty acids

S. No	Catalyst	Feedstock	Reaction conditions	Ref. No
1	Ni-Al LDH	Tristearin	T = 260 - 300 °C, P = 40 bar H ₂	[59]
2	MgO/hydrotalcites	Oleic acid	T = 400 °C, t = 3 h	[60]
3	Ni/Al ₂ O ₃	Waste fat	T = 330 °C, P = 50 bar H ₂	[61]
4	NiMo carbides	Soybean oil	T = 400 °C, P = 45 bar	[62]
5	Ni/SAPO-11	Palm oil	T = 280-350 °C, P = 40 bar H ₂	[63]
6	Raney Ni/Al ₂ O ₃	Sunflower oil	T = 280 - 340 °C, P = 21 bar	[64]

7	Ni-H ₃ PW ₁₂ O ₄₀ /HAP	Jatropha oil	T = 360 °C, P = 30 bar	[65]
8	Ni/HBEA	Palm oil	T = 260 °C, P = 40 bar H ₂	[66]
9	Mo/CNT	Palmitic acid	T = 220 °C, P = 40 bar H ₂	[67]
10	Ni, Mo sulfides	Palmitic acid	T = 300 °C, p = 50 bar H ₂	[68]
11	NiP/Supports	Methyl laurate	T = 300 - 340 °C, P = 20 bar H ₂	[69]
12	NiW/Al ₂ O ₃	Biodiesel	T = 200 - 280 °C, P = 100 bar H ₂	[70]
13	NiW/SiO ₂ -Al ₂ O ₃	Fatty acids	T= 300 - 375 °C, P = 20 - 80 bar	[71]
14	W & Mo Carbides	Oleic acid	T = 350 °C, P = 50 bar H ₂	[72]
15	CoMo, NiMo sulfides	Vegetable oils/fatty acids	T = 300 - 350 °C, P = 20 - 50 bar H ₂	[73-75]
16	Mo/ZSM-22	Palmitic acid	T = 260 °C, P = 40 bar H ₂	[76]
17	Co-Fe/Al ₂ O ₃	Biodiesel	T = 400 °C, P = 40 bar H ₂	[77]
18	Fe/MSN	Algae oil	T = 290 °C, P = 30 bar H ₂	[78]
19	Ni-Mg-Al LDH	Triglycerides	T = 350 °C, P = 50 bar	[79]
20	Tungsten catalysts	Stearic acid	T = 350 °C, P = 50 bar H ₂	[80]
21	NiMo/SiO ₂	Vegetable oil	T = 350 °C, P = 40 bar H ₂	[81]
22	Metal nitrides/Al ₂ O ₃	Vegetable oil	T = 380 - 410 °C, P = 75 bar H ₂	[82]
23	F-MoO _x /Zeolite	Oleic acid	T = 360 °C, P = 20 bar H ₂	[83]
24	Zn/ZSM-5	Camelina oil	T = 500 °C, P = 1 bar N ₂	[84]
25	Ni/Al-SBA-15	Biodiesel	T = 300 - 340 °C, P = 30 bar H ₂	[85]

Most of the current investigations focused on development of an efficient and affordable catalyst for sustainable fuel production. As listed in Table 1.3, non-noble metal based catalysts operate at severe conditions. Interestingly, some catalytic systems based on Ni metal were active at low temperature but require high hydrogen pressure.

1.3.2.2. Noble metal based mono metallic catalysts

Noble metals proved to be better catalysts than non-noble metal catalysts. Ford et al. [86] studied the deoxygenation of fatty acids over Pd supported on SiO₂, Al₂O₃ and carbon at 300 °C and 15 bar H₂. It was observed that the initial rates of reaction increased with increasing chain length of fatty acid. Higher adsorption of long chain fatty acids than the smaller ones is responsible for this observation. In another study, Pd supported on mesoporous carbon exhibited complete conversion of oleic acid at 300 °C and 20 bar H₂. Mode of deposition of Pd on the support affected the catalytic activity. Pd deposited in

presence of a stabilizer (PVP or triphenylphosphine; TPP) showed better activity than the naked Pd particles deposited without the stabilizer. By manipulating hydrogen pressure with nitrogen, the significance of hydrogen for the deoxygenation activity was demonstrated [87].

Simakova et al. [88] reported studies on palmitic and stearic acids at 260-300 °C and 17.5 bar H₂ in dodecane solvent over a synthetic carbon-supported Pd catalyst. Different Pd dispersions were achieved by varying the pH while depositing palladium. The particle size effect on the deoxygenation activity was correlated and an optimum dispersion was found. In case of high dispersion, smaller metal particles interacted with the support strongly and changed the nature of active metal phase. On the other hand, too low dispersion with large metal particles led to less active surface and less activity. Hence, an optimum dispersion and particle size of the active metal is necessary. A quantitative oleic acid conversion was achieved at 320 °C with 20 bar of H₂ pressures after 2 h of reaction over Pt supported on zeolite 5A bead catalyst. Microporous ZIF-67 crystalline layer on zeolite beads improved the catalytic activity as well as stability of the catalysts producing heptadecane as the major product even in recycling experiments [89].

Table 1.4. Noble metal based monometallic catalysts for green diesel production

S. No	Catalyst	Feedstock	Reaction conditions	Ref. No
1	Pt/Al ₂ O ₃ -SAPO-11	Vegetable oil	T = 370 °C, P = 30 bar H ₂	[90]
2	Pd/Si-C	Free fatty acids	T = 300 °C, P = 30 bar H ₂	[91]
3	Pt/SAPO-11	Jatropha oil	T = 350 °C, P = 30 bar H ₂	[92]
4	Ru/Montmorillonite	Triglycerides	T = 350 °C, P = 20 bar H ₂	[93]
5	Rh/ZrO ₂	Methyl heptanoate	T = 260-340 °C, P = 80 bar H ₂	[94]
6	Pd/C	Fatty acids	T = 300 °C, P = 20 bar H ₂	[95]
7	Pd/SAB-15	Stearic acid	T = 300 °C, P = 17 bar H ₂	[96]
8	Pt/Al ₂ O ₃	Methyl stearate	T = 330 °C, P = 1 bar H ₂	[97]
9	Pd/SAB-15	Methyl oleate	T = 270 °C, P = 60 bar H ₂	[98]
10	Pt/ZSM-22@SiO ₂	Methyl palmitate	T = 300-360 °C	[99]

Table 1.4 presents some of the catalysts reported in the literature. Most of them followed decarboxylation/decarbonylation path in deoxygenation. Nevertheless, the challenge is to develop an efficient catalyst which works at moderate conditions (low temperature, low H₂ pressure and less catalyst loadings) for production of renewable fuels from biogenous feedstocks. Hence, development of a suitable catalyst remains as challenge task.

1.3.2.3. Noble metal-based bimetallic catalysts

In general, most of the research focused on monometallic catalysts. Only a few reports are available on noble metal-based bimetallic catalysts. These catalysts show distinct catalytic properties than the monometallic catalysts. Synergistic interactions between the two metals alter the catalytic properties. Chen et al. [100] compared the activity of Pt/SAPO-11 and Pt-Sn/SAPO-11 for deoxygenation of methyl palmitate yielding diesel-range hydrocarbons. It was found that the catalytic activity improves by addition of Sn as secondary metal (promoter) to the catalyst. The reaction path got altered from decarboxylation/decarbonylation (in case of monometallic; DCO) to hydrodeoxygenation (in case of bimetallic; HDO). Pt/SAPO-11 was considerably active and selective for C-C bond cleavage (DCO path). On the contrary, the bimetallic Pt-Sn/SAPO-11 was highly active and selective for C=O hydrogenation (HDO path) yielding hexadecane. This was attributed to synergistic interactions between Pt and Sn and partial reduction of SnO₂ to SnO_{2-x}. Catalytic production of renewable hydrocarbons from unsaturated fatty acids without added hydrogen was reported by Vardon et al. [101] over a bimetallic catalyst comprising of Pt and Re supported on carbon. At an elevated temperature of 300 °C, a complete conversion of oleic acid was observed. Hydrogen was supplied by *in situ* generation from aqueous phase reforming of glycerol. Recently, in their report, Johannes et al. [102] revealed the selective hydrogenation of carboxylic acids to produce alcohols or alkanes under mild reaction conditions (140 °C and 20 bar of hydrogen) in n-hexane solvent. This bimetallic catalyst was highly active and selective even for deoxygenation of other aromatic carboxylic acids. However, the main drawback of this work was to use high amount of metal (2 mol% of Pt for 1 mmol of substrate).

The promotional effect of tungsten on Pt/TiO₂ catalyst for deoxygenation of jatropha oil was studied by Choi et al. [103]. A remarkable change in catalytic activity was found after the addition of W to Pt/TiO₂. Proximal contact between W and Pt and the synergy were the cause for superior activity of W promoted catalyst. Ota et al. [104] studied the promotional effect of Pd on Re/CeO₂ catalyst for HDO of vicinal OH groups of biomass feedstocks. The high catalytic performance was assigned to formation of reduced Re⁴⁺ and Re⁺⁵ species in presence of Pd. In another study, the HDO performance of co-loaded Pt-MoO_x/TiO₂ for oxygenated biomass feedstocks was investigated and reported recently [105]. Among the bimetallic catalysts Rh-MoO_x/TiO₂, Ru-MoO_x/TiO₂, Ni-MoO_x/TiO₂, Pd-MoO_x/TiO₂, Cu-MoO_x/TiO₂ and Pt-MoO_x/TiO₂ showed excellent HDO activity. *In situ* IR study of the reaction of adsorbed acetone under H₂ revealed that the high activity of Pt-MoO_x/TiO₂ is

the work load sharing factor of the catalyst. The extent of promotional effect of the promoter depends on the nature of promoter, proximity between primary metal and promoter, nature of support and strength and nature of interactions. Interestingly, the promoter alone cannot catalyze the reaction [108].

1.5. Challenges in deoxygenation of vegetable oils/fatty acids

Although much has been done and many catalyst systems have been reported, there exist technological challenges in the production of renewable fuels. They are the following:

1.5.1. Operation conditions

Ni based catalysts are cheaper than noble metal catalysts, but they operate at high reaction temperatures (*ca.* 300 - 450 °C) and (or) high hydrogen pressures (*ca.* 30 - 100 bar). Hence, development of a deoxygenation catalyst based on a non-noble metal proved futile (Table 1.3). Noble metal-based monometallic catalysts operate at high temperature and with moderate H₂ pressure (Table 1.4). Interestingly, bimetallic (promoted) catalysts based on noble metals work at relatively milder conditions and hence, will be the promising catalytic materials. At present only a few systems are known under this category. Further research needs to be conducted to explore and develop more efficient deoxygenation catalyst which reduces the cost of operation by way of performing at mild conditions and with requirement of less amount of catalyst.

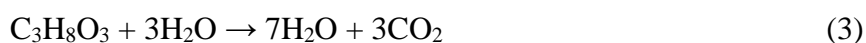
1.5.2. Catalyst stability

Stability is one of the most important parameters for implementing a catalyst in a commercial operation. Sintering or agglomeration of active metal, collapse of structural integrity of the support, leaching of the active ingredients and any structural reformations affect the stability of a catalyst. Deactivation of Pd/C catalyst in decarboxylation of fatty acids (at 300 °C under nitrogen atmosphere) was due to sintering of Pd [109]. Hydrothermal stability of Pt/SAPO-11 for hydrodeoxygenation of vegetable oil was investigated by Rabaev et al. [110]. Leaching of silica due to hydrolysis of Si-O-Al bonds under reaction conditions was the cause for deactivation of the catalyst. In general, the overall stability of a catalyst relies on the extent of metal-support interactions and support hydrothermal stability. The former avoids sintering of the active metal and the latter protects structural integrity of the catalyst.

1.5.3. Hydrogen

Hydrogen is a reactant in hydrodeoxygenation (HDO) reactions. It is usually supplied in excess. Further, it is the cost affecting factor of a process. There have been a few attempts to supply *in situ* generated hydrogen than providing it externally. Hydrogen produced by

decomposition of formic acid was used in the hydroprocessing of crude jatropha oil over Pd/C catalyst yielding C₁₅-C₁₇ hydrocarbons [111]. Fu et al. [112] reported decarboxylation of fatty acids at high temperatures in presence of hydrogen produced *in situ* from water by reforming. Valorisation of waste lipids through hydrothermal catalytic conversion was investigated by Kim et al. [113] over a Pt-Re/C catalyst at a temperature of 300 °C and in presence of water. *In situ* reforming of water produced hydrogen which was then utilized in the deoxygenation reaction. Aqueous phase reforming of glycerol for *in situ* hydrogen generation was studied for the purpose of fatty acid deoxygenation over Pt-Re/C catalyst at 300 °C and 80-110 bar pressure [101]. Glycerol reforms into hydrogen and CO₂ under these conditions (Eqs. 3). This hydrogen, then facilitates hydrogenation of double bonds and decarboxylation/decarbonylation of fatty acid.



These systems partly fulfilled the criteria of omission of external hydrogen supply at high pressures but suffer due to catalyst instability and poisoning. Thus, a catalyst which works efficiently at low hydrogen pressure is beneficial than those mentioned above.

1.5.4. Capital cost

Using conventional hydrotreating catalysts, green diesel production from vegetable oils/fatty acids was commercialized by a few companies including Neste Oil (NExBTL technology), UOP/Eni (Ecofining technology), Petrobras (H-BIO technology) and Tyson-Conoco Phillips [8-10]. The feasibility of the catalytic system for commercialization depends on the efficacy of a catalyst to operate at mild conditions. The order of efficacy of catalysts varies in the order: noble metal-based bimetallic catalysts > noble metal-based monometallic catalysts > non-noble metal-based catalysts. Though Ni catalysts are relatively less expensive, their severe operation conditions and less activity are some drawbacks.

HDO vs DCO: In general, catalyst nature drives the reaction in a selective path. Most of the monometallic catalysts follow DCO path while bimetallic (promoted) catalysts adopt the HDO path. With respect to hydrogen consumption in the reaction, many groups reported that DCO mechanism is viable as it requires less or no H₂ pressure. But, in the absence of hydrogen most of the known catalysts deactivate during the continuous reaction. As the process involves oxygenated feedstocks, strong adsorption of reactant molecules on the active sites poison the catalyst. Moreover, decarboxylation involves loss of one carbon atom as CO₂. On contrary, most of the bimetallic catalysts follow the HDO path in deoxygenation reactions. The amount of hydrogen pressure requirement depends on the catalyst efficiency. It

is a high atom economy process as it doesn't involve loss of carbon. Due to the presence of hydrogen, activity of the catalyst is preserved for a long time. However, the catalyst must be active to work at remarkably low hydrogen pressure from the process economics point of view. Hence, developing a deoxygenation catalyst which works at mild conditions and with good atom economy is still a challenge.

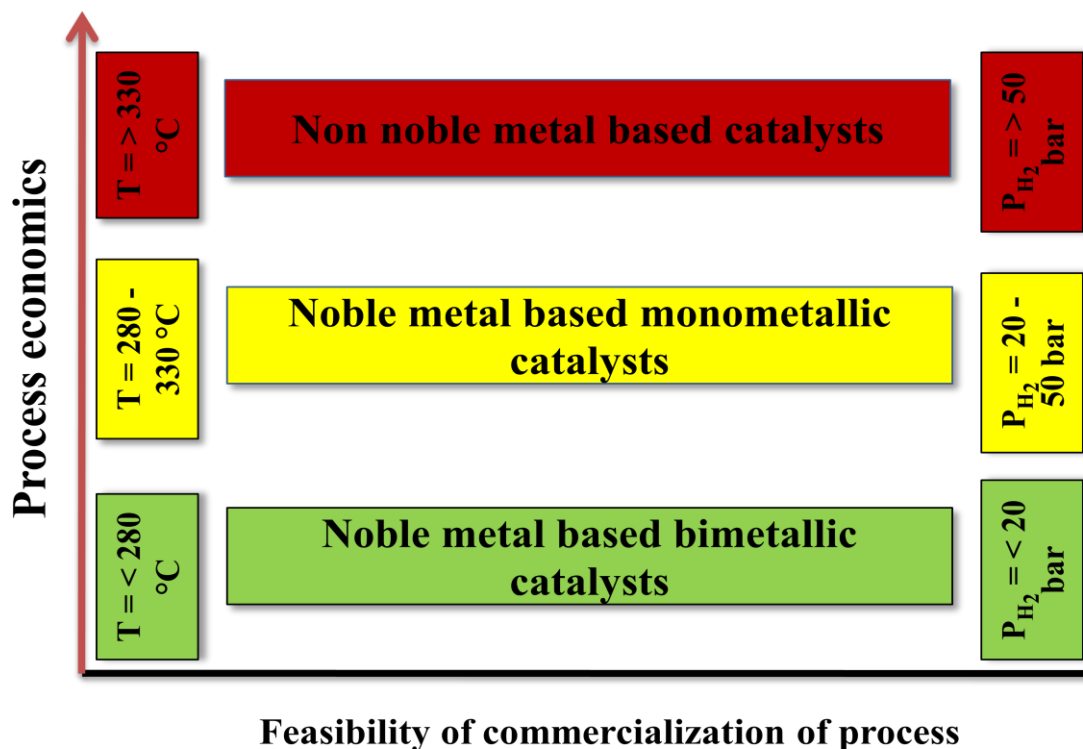


Fig. 1.9. Catalytic systems for deoxygenation

1.6. Scope and objectives of the thesis work

Deoxygenation of inedible vegetable oils or fatty acids is an emerging catalytic technology to produce renewable diesel that fulfils the global energy need (Fig. 1.10). Unlike other biogenous feedstocks, inedible oils are less expensive, less complex, easy to cultivate and do not compete with the food chain. Hence, they form a sustainable feedstock for fuels manufacturing. Catalysts known for deoxygenation have certain drawbacks which include requirement of high amount of catalyst, high reaction temperature and high pressure of hydrogen. Moreover, carbon loss is high and the catalyst is unstable during the reaction. Thus, development of an efficient, reusable catalyst which operates at mild to moderate conditions and with minimal carbon loss is the main objective of this work. Bimetallic catalysts are attractive as they show enhanced activity and selectivity compared to monometallic catalysts. This motivated the design of bimetallic catalysts for atom efficient

and economic operation for renewable diesel production. Different oxide supports are modified with oxides of varying reducibility and then Pt is deposited on it. The electronic contact between reducible promoter oxide and Pt is expected to modify the deoxygenation performance of the catalyst. Reducible oxides used in this study are: WO_x , MoO_x , ReO_x and SnO_x and supports employed are: $\text{AlPO}_4\text{-5}$, $\gamma\text{-Al}_2\text{O}_3$, $\text{SiO}_2\text{-Al}_2\text{O}_3$ and ZrO_2 . By and large, the scope and objective of this work is to develop an efficient catalytic process for renewable (green) diesel production.

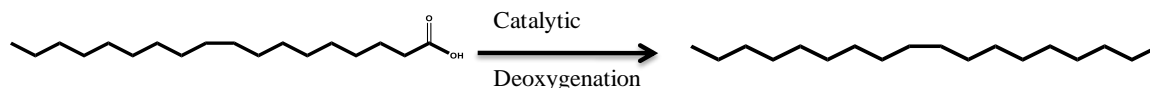


Fig. 1.10. Scope of the reaction

1.7. Organization of the thesis

The thesis is divided into eight chapters. **Chapter-1** provides brief introduction to biomass, biofuels and green diesel. It also presents the scope and objectives of the work. **Chapter-2** presents experimental methodology. Characterization methods, reaction procedure and product analysis are described.

Chapter-3 describes the effect of WO_x promoter on the catalytic performance of Pt- $\text{WO}_x/\text{AlPO}_4\text{-5}$ catalyst for deoxygenation of oleic acid (OA; a representative fatty acid) producing diesel-range hydrocarbons. WO_x -promoted Pt catalyst exhibited enhanced deoxygenation activity than the unpromoted Pt catalyst. A shift in product selectivity from heptadecane (C_{17} ; formed via decarboxylation/decarbonylation (DCO) route) to octadecane (C_{18} ; formed via hydrodeoxygenation (HDO) route) was observed when WO_x was present along with platinum. A catalyst with 1:2 weight ratio of Pt to W (4Pt-8 $\text{WO}_x/\text{AlPO}_4\text{-5}$) was found superior to other compositions. WO_x changed the electronic and structural properties of Pt and enhanced the catalytic activity. However, the stability of the support was a serious issue in the reusability study.

Chapter-4 illustrates studies on Pt- $\text{WO}_x/\text{Al}_2\text{O}_3$ catalysts. Interestingly, 4Pt-8 $\text{WO}_x/\text{Al}_2\text{O}_3$ was highly stable and reusable even after five recycles without any loss of activity. Transmission electron microscopy revealed that Pt sintering is inhibited by the presence of WO_x . Unpromoted Pt/ Al_2O_3 catalyst lost its activity due to Pt sintering. WO_x acted as activity booster as well as stability enhancer of the catalyst. The support stability and promotional effect of WO_x are the key aspects for the superior catalytic activity of Al_2O_3 -supported Pt- WO_x catalyst.

Since support plays a crucial role, different support materials ($\text{AlPO}_4\text{-5}$, Al_2O_3 , ZrO_2 and $\text{SiO}_2\text{-Al}_2\text{O}_3$) with varying acidity are chosen and their influence on the catalytic activity of WO_x -promoted Pt catalysts for the deoxygenation of OA is investigated in **Chapter-5**. Structure-activity correlations reveal that metallic nature of Pt and acidity of the catalyst are the crucial factors determining catalytic performance and product selectivity. Irrespective of support, WO_x enhanced the deoxygenation activity and altered the reaction path of promoted Pt catalysts. Among the catalysts tested, $4\text{Pt-8WO}_x/\text{ZrO}_2$, having adequate metal dispersion and electron rich Pt, reduced WO_x species and less amount of strong acid sites showed highest catalytic deoxygenation performance (complete conversion of OA) with ~90 wt.% of C_{18} selectivity at 260 °C and 20 bar H_2 pressure. This study clearly demonstrates that support plays a crucial role in determining the catalytic performance of WO_x -promoted supported Pt catalysts.

Chapter-6 presents the effect of promoter type (WO_x , MoO_x , SnO_x and ReO_x) on the catalytic deoxygenation of fatty acids over $\text{Pt-MO}_x/\text{Al}_2\text{O}_3$. There exists synergy between Pt and promoter oxide. Initial activity of the catalysts decreases in the order: $4\text{Pt-8MoO}_x/\text{Al}_2\text{O}_3 > 4\text{Pt-8ReO}_x/\text{Al}_2\text{O}_3 > 4\text{Pt-8WO}_x/\text{Al}_2\text{O}_3 > 4\text{Pt-8SnO}_x/\text{Al}_2\text{O}_3$. Structure activity correlations proved that Pt dispersion is affected to a certain extent only. Generation of surface hydroxyl groups by partial reduction of (reducible) promoter oxides shift the reaction path from DCO to HDO by activating OA. The extent of reducibility of these promoter oxides correlated with the C_{18} product selectivity. $4\text{Pt-8MoO}_x/\text{Al}_2\text{O}_3$ with adequate amount of Pt dispersion, e^- rich Pt and acidity shows superior catalytic activity for deoxygenation of fatty acids to hydrocarbons than the other promoted catalysts.

Having discovered that ZrO_2 as a superior support (in Chapter-5) and MoO_x as a superior promoter (in Chapter-6) and Pt to promoter metal weight ratio as 1:2 (in Chapter-4), a catalyst $4\text{Pt-8MoO}_x/\text{ZrO}_2$ is postulated as a candidate catalyst. This is indeed prepared, characterized and tested for deoxygenation activity in **Chapter-7**. This catalyst is found excellent exhibiting C_{18} selectivity of ~95 wt.% at 75 mol% of OA conversion at as low as 200 °C (with 20 bar of H_2 pressure after 5 h). Complete conversion of OA was observed at 240 °C (C_{18} selectivity: ~ 92 wt.%). The performance of this catalyst is much higher than most of the known catalysts for deoxygenation reaction. A tentative mechanism is also proposed based on the results obtained.

Chapter-8 presents overall summary and conclusions of the work.

By and large, this thesis describes new type of highly active, selective and stable reducible oxide promoted-supported Pt catalysts for the deoxygenation of fatty acids

producing green diesel. This work contributes to the area of sustainable energy and renewable fuels.

1.8. References

- [1] A. E. Atabani, A. S. Silitong, H. C. Ong, T. M. I. Mahlia, H. H. Masjuki, I. A. Badruddin, H. Fayaz, *Ren. Sus. Ener. Rev.*, 2013, 18, 211–245.
- [2] <https://webstore.iea.org>. Global energy and CO₂ status report – 2017.
- [3] https://transportgeography.org/?page_id=5717.
- [4] O. O. James, S. Maity, M. A. Mesubi, L. A. Usman, K. O. Ajanaku, T. O. Siyanbola, S. Sahu, R. Chaubey, *Int. J. Energy Res.* 2012, 36, 691–702.
- [5] P. Gallezot, *Chem. Soc. Rev.*, 2012, 41, 1538–1558.
- [6] <https://www.iea.org/Textbase/npsum/renew2017MRSsum.pdf>
- [7] R. B. Gupta, A. Demirbas, *Gasoline, Diesel and Ethanol Biofuels from Grasses and Plants*, New York, Cambridge University Press, 2010.
- [8] D. J. Hayes, *Catal. Today*, 2009, 145, 138–151.
- [9] P. M. Arvela, B. Holmbom, T. Salmi, D. Y. Murzin, *Catal. Rev.*, 2007, 49, 197–340.
- [10] M. Askew, The biorefinery concept. <http://europa.eu.int/comm/research/energy/pdf/renews3.pdf> (August 1, 2005).
- [11] US Department of Energy; <http://www.oit.doe.gov/e3handbook>.
- [12] S. Fernando, S. Adhikari, C. Chandrapal, N. Murali, *ACS Energy & Fuels*, 2006, 20, 1727-1737.
- [13] B. Kamm, M. Kamm, *Principles of biorefinery. Appl. Microbiol. Biotechnol.* 2004, 64, 137-145.
- [14] Y. Nakagawa, M. Tamura, K. Tomishige, *J. Mater. Chem. A*, 2014, 2, 6688.
- [15] R. Mariscal, P. Maireles-Torres, M. Ojeda, I. Sádaba, M. López Granados, *Energy Environ. Sci.*, 2016, 9, 1144-1189.
- [16] R.W. Gosselink, S. A. W. Hollak, S. W. Chang, J. V. Haveren, K. P. de Jong, J. H. Bitter, D. S. van Es, *ChemSusChem*, 2013, 6, 1576 – 1594.

- [17] H. Huang, N. Qureshi, M. H. Chen, W. Liu, V. Singh, *J. Agric. Food Chem.*, 2015, 63 (10), 2760–2766.
- [18] F. H. Isikgor, C. R. Becer, *Polym. Chem.*, 2015, 6, 4497-4559.
- [19] P. Boey, S. Ganesan, G. P. Maniam, M. Khairuddean, *Catal. Today*, 2012, 190, 117-118.
- [20] F. A. Twaiq, N. A. M. Zabidi, S. Bhatia, *Ind. Eng. Chem. Res.*, 1999, 38, 3230–3237.
- [21] F. A. Twaiq, A. R. Mohamed, S. Bhatia, *Micr. Mes. Mater.*, 2003, 64, 95–107.
- [22] J. T. Klopogge, L. V. Duong and R. L. Frost, *Environ. Geol.*, 2005, 47, 967–981.
- [23] D. Srinivas, J. K. Satyarthi, *Catal. Surv. Asia*, 2011, 15, 145–160.
- [24] Y. Chisti, *Biotechnol. Adv.*, 2007, 25, 294–306.
- [25] S. Saka, *Biores. Technol.*, 2010, 101, 7191-7200.
- [26] S. Chen, *Int. J. Clean Coal and Energy*, 2012, 1, 43-55.
- [27] G. W. Festel, *Chem. Eng. Technol.*, 2008, 31, 715–720.
- [28] U. Schuchardta, R. Sercheli, R. M. Vargas, *J. Braz. Chem. Soc.*, 1998, 9, 199-210.
- [29] T. Leng Chew, S. Bhatia, *Biores. Technol.*, 2008, 99, 7911–7922.
- [30] C. N. Hamelinck, A. P. C. Faaij, *Energy Policy*, 2006, 34, 3268–3283.
- [31] <https://www.ncbi.nlm.nih.gov/pmc/articles/PMC2430252/pdf/ehp0116-a00254.pdf>
- [32] B. A. Babcock, June 2011; The Impact of US Biofuel Policies on Agricultural Price Levels and Volatility, ICTSD Programme on Agricultural Trade and Sustainable Development; Issue Paper No. 35; ICTSD International Centre for Trade and Sustainable Development, Geneva, Switzerland. www.ictsd.org.
- [33] R. Wooley, M. Ruth, J. Sheehan, K. Ibsen, *Lignocellulosic Biomass to Ethanol Process Design and Economics Utilizing Co-Current Dilute Acid Prehydrolysis and Enzymatic Hydrolysis Current and Futuristic Scenarios*, National Renewable Energy Laboratory, Golden (Colorado) 1999.
- [34] R.O.M.A. de Souza, L.S.M. Miranda, R. Luque, *Green Chem.* 2014, 16, 2386–2405.
- [35] E. S. Jimenez, M. Crocker, *J. Chem. Technol. Biotechnol.*, 2012, 87, 1041–1050.

- [36] S. N. Naik, V. V. Goud, P. K. Rout, A. K. Dalai, *Ren. Sus. Ener. Rev.*, 2010, 14, 578–597.
- [37] S. Lestari, P. M. Arvela, J. Beltramini, G. Q. M. Lu, D. Y. Murzin, *Chem-SusChem*, 2009, 2, 1109–1119.
- [38] M. S. re, P. M_{ki}-Arvela, I. L. Simakova, J. Myllyoja, D. Y. Murzin, *Russ. J. Phys. Chem. B*, 2009, 3, 1035–1043.
- [39] C. Zhao, T. Brück, J. A. Lercher, *Green Chem.*, 2013, 15, 1720-1739.
- [40] B. Peng, Y. Yao, C. Zhao and J. A. Lercher, *Angew. Chem., Int. Ed.*, 2012, 51, 2072–2075.
- [41] A. Galadima, O. Muraza, *J. Ind. Eng. Chem.*, 2015, 29, 12-23.
- [42] X. Zhao, L. Wei, S. Cheng, J. Julson, *Catalysts*, 2017, 7, 83.
- [43] S. Bezergianni, A. Dimitriadis, G. Meletidis, *Fuel*, 2014, 125, 129–136.
- [44] S. Bezergianni, A. Dimitriadis, D. Karonis, *Fuel*, 2014, 136, 366–373.
- [45] G. W. Huber, P. O’Connor, A. Corma, *Appl. Catal. A*, 2007, 329, 120–129.
- [46] S. Bezergianni, A. Kalogianni, I.A. Vasalos, *Bioresour. Technol.*, 2009, 100, 3036–3042.
- [47] A. Vonortas, N. Papayannakos, *WIREs Energy Environ.*, 2014, 3, 3–23.
- [48] C. Kordulis, K. Bourikas, M. Gousi, E. Kordouli, A. Lycourghiotis, *Appl. Catal. B: Environ.*, 2016, 181, 156–196.
- [49] Z. Huang, S. Ding, Z. Li, H. Lin, F. Li, Lin Li, Z. Zhong, C. Gao, C. Chen, Yue L, *Int. J. Hyd. Energy*, 2016, 41, 16402 -16414.
- [50] R. Loe, E. S. Jimenez, T. Morgan, L. Sewell, Y. Ji, S. Jones, M. A. Isaacs, A. F. Lee, M. Crocker, *Appl. Catal. B: Environ.*, 2016, 191, 147–156.
- [51] I. Hachemi, N. Kumar, P. M. Arvela, J. Roine, M. Peurla, J. Hemming, J. Salonen, D. Y. Murzin, *J. Catal.*, 2017, 347, 205–221.
- [52] H. Xin, K. Guo, D. Li, H. Yang, C. Hu, *Appl. Catal. B: Environ.*, 2016, 187, 375–385.
- [53] Q. Guan, F. Wan, F. Han, Z. Liu, W. Li, *Catal. Today*, 2016, 259, 467–473.

- [54] M. Peroni, G. Mancino, E. Baráth, O. Y. Gutiérrez, J. A. Lercher, *Appl. Catal. B: Environ.*, 2016, 180, 301–311.
- [55] H. Chen, Q. Wang, X. Zhang, L. Wang, *Fuel*, 2015, 159, 430–435.
- [56] M. S. Cárdenas, J. M. Valtierra, S. K. Kamaraj, R. Rafae, M. Ramírez, L. Antonio, S. Olmos, *Catalysts*, 2016, 6, 156-175.
- [57] B. Veriansyah, J. Y. Han, S. K. Kim, S. A. Hong, Y. J. Kim, J. S. Lim, Y. W. Shu, S. G. Oh, J. Kim, *Fuel*, 2012, 94, 578–585.
- [58] J. Liu, K. Fan, W. Tian, C. Liu, L. Rong, *Int. J. Hyd. Energy*, 2012, 37, 17731-17737.
- [59] E. S. Jimenez, T. Morgan, R. Loe, M. Crocker, *Catal. Today*, 2015, 258, 284–293.
- [60] J. G. Na, B. E. Yi, J. N. Kim, K. B. Yi, S. Y. Park, J. Park, J. N. Kim, C. Hyun Ko, *Catal. Today*, 2010, 156, 44–48.
- [61] R. Kaewmeesri, A. Srifa, V. Itthibenchapong, K. Faungnawakij, *Energy Fuels*, 2015, 29, 833–840.
- [62] H. Wang, S. Yan, S. O. Salley, K.Y. Simon Ng, *Fuel*, 2013, 111, 81–87.
- [63] Q. Liu, H. Zuo, T. Wang, L. Ma, Q. Zhang, *Appl. Catal. A: Gen.*, 2013, 468, 68– 74.
- [64] G. Onyestyák, S. Harnos, Á. Szegedi, D. Kalló, *Fuel*, 2012, 102 282–288.
- [65] K. Fan, J. Liu, X. Yang, L. Rong, *Int. J. Hyd. Energy*, 2014, 39, 3690-3697.
- [66] B. Ma, C. Zhao, *Green Chem.*, 2015, 17, 1692–1701.
- [67] R. Ding, Y. Wu, Y. Chen, J. Liang, J. Liu, M. Yang, *Chem. Eng. Sci.*, 2015, 135, 517–525.
- [68] M. F. Wagenhofer, E. Baráth, O. Y. Gutiérrez, J. A. Lercher, *ACS Catal.*, 2017, 7, 1068–1076.
- [69] Y. Yang, J. Chen, H. Shi, *Energy Fuels*, 2013, 27, 3400–3409.
- [70] Z. Zhou, W. Zhang, D. Sun, L. Zhu, J. Jiang, *Int. J. Green Energy*, 2016, 13, 1185–1192.
- [71] Y. Yang, Q. Wang, X. Zhang, L. Wang, G. Li, *Fuel Proc. Technol.*, 2013, 116, 165–174.

- [72] S. A. W. Hollak, R.W. Gosselink, D. S. van Es, J. H. Bitter, *ACS Catal.* 2013, 3, 2837–2844.
- [73] M. R. Nimkarde, P. D. Vaidya, *Energy Fuels*, 2016, 30, 3107–3112.
- [74] D. K. kova, J. Blažek, P. Šimáček, M. Staš, Z. Beňo, *Fuel Proc. Technol.*, 2016, 142,, 319–325.
- [75] H. Y. Wang, T. T. Jiao, Z. Li, C. Li, S. Zhang, J. Zhang, *Fuel Proc. Technol.*, 2015, 139, 91–99.
- [76] Y. Shi, Y. Cao, Y. Duan, H. Chen, Y. Chen, M. Yang, Y.Wu, *Green Chem.*, 2016, 18, 4633–4648.
- [77] T. K. Hari, Z. Yaakob, *Chem. Lett.*, 2015, 44, 1237–1239.
- [78] K. Kandel, J. W. Anderegg, N. C. Nelson, U. Chaudhary, I. I. Slowing, *J. Catal.*, 2014, 314, 142–148.
- [79] T. Morgan, E. S. Jimenez, A. E. H. Ware, Y. Ji, D. Grubb, M. Crocker, *Chem. Eng. J.*, 2012, 189–190, 346– 355.
- [80] R. W. Gosselink, D. R. Stellwagen, J. H. Bitter, *Angew. Chem. Int. Ed.*, 2013, 52, 5089 –5092.
- [81] Y. Liu, R. S. Boyas, K. Murata, T. Minowa, and K. Sakanishi, *Energy Fuels*, 2011, 25, 4675–4685.
- [82] J. Monniera, H. Sulimma, A. Dalai, G. Caravaggio, J. Monnier, *Appl. Catal. A: Gen.*, 2010, 382, 176–180.
- [83] O. B. Ayodele, H. U. Farouk, J. Mohammed ,Y . Uemurad, W.M.A.W. Daud, J. Taiwan Inst. Chem. Eng., 2015, 50, 142-152.
- [84] X. Zhao, L. Wei, J. Julson, Z. Gu, and Y. Cao, *Korean J. Chem. Eng.*, DOI: 10.1007/s11814-015-0028-8.
- [85] C. O. Hernández, Y. Yang, P. Pizarro, V. A. P. O’Shea, J. M. Coronado, D. P. Serrano, *Catal. Today*, 2013, 210, 81– 88.
- [86] J. P. Ford, J. G. Immer, H. H. Lamb, *Top. Catal.*, 2012, 55, 175–184.

- [87] A. Dragu, S. Kinayyigit, E. J. García-Suárez, M. Florea, E. Stepan, S. Velea, L. Tanaseg, V. Collière, K. Philippot, P. Granger, V. I. Parvulescu, *Appl. Catal. A: Gen.*, 2015, 504, 81–91.
- [88] I. Simakova, O. Simakova, P. M. Arvela, A. Simakov, M. Estrada, D. Y. Murzin, *Appl. Catal. A: Gen.*, 2009, 355, 100–108.
- [89] L. Yang, K. L. Tate, J. B. Jasinski, and M. A. Carreon, *ACS Catal.* 2015, 5, 6497–6502.
- [90] M. Rabaev, M. V. Landau, R. V. Nehemya, V. Koukouliev, R. Zarchin, M. Herskowitz, *Fuel*, 2015, 161, 287–294.
- [91] E. Sari, M. Kim, S. O. Salley, K.Y. Simon Ng, *Appl. Catal. A: Gen.*, 2013, 467, 261–269.
- [92] N. Chen, S. Gong, H. Shirai, T. Watanabe, E. W. Qian, *Appl. Catal. A: Gen.*, 2013, 466, 105–115.
- [93] Y. Liu, R. Sotelo-Boyás, K. Murata, T. Minowa, K. Sakanishi, *Catalysts*, 2012, 2, 171-190.
- [94] Y. Bie, A. Gutierrez, T. R. Viljava, J. M. Kanervo, and J. Lehtonen, *Ind. Eng. Chem. Res.*, 2013, 52, 11544–11551.
- [95] B. Rozmyszowicz, P. M. Arvela, A. Tokarev, A. R. Leino, K. Eranen, D. Y. Murzin, *Ind. Eng. Chem. Res.*, 2012, 51, 8922–8927.
- [96] S. Lestari, P. Maki-Arvela, K. Eranen, J. Beltramini, G. Q. M. Lu, D. Y. Murzin, *Catal Lett.*, 2010, 134, 250–257.
- [97] P. T. Do, M. Chiappero, L. L. Lobban, D. E. Resasco, *Catal. Lett.*, 2009, 130, 9–18.
- [98] S. P. Lee, A. Ramli, *Chem. Cent. J.*, 2013, 7, 149.
- [99] N. Chen, N. Wang, Y. Ren, H. Tominaga, E. W. Qian, *J. Catal.*, 2017, 345, 124–134.
- [100] N. Chen, Y. Ren, E. W. Qian, *J. Catal.*, 2016, 334, 79–88.
- [101] D. R. Vardon, B. K. Sharma, H. Jaramillo, D. Kim, J. K. Choe, P. N. Ciesielski, T. J. Strathmann, *Green Chem.*, 2014, 16, 1507–1520.
- [102] J. Ullrich, B. Breit, *ACS Catal.* 2018, 8, 785–789.

- [103] I. Choi, J. S. Lee, C. U. Kim, T. W. Kim, K. Y. Lee, K. R. Hwang, *Fuel*, 2018, 215, 675–685.
- [104] N. Ota, M. Tamura, Y. Nakagawa, K. Okumura, K. Tomishige, *Angew. Chem. Int. Ed.*, 2015, 54, 1897–1900.
- [105] K. Kon, T. Toyao, W. Onodera, S. M. A. H. Siddiki, Kenichi, Shimizu, *ChemCatChem.*, 2017, 9, 2822–2827.
- [106] <http://eng.thesaurus.rusnano.com/wiki/article14001>.
- [107] Boswell, Bayley: *J. Phys. Chem.*, 1925, 29, 11-19.
- [108] <https://www.emedicalprep.com/study-material/chemistry/surface-chemistry/catalytic-promoters>
- [109] E. W. Ping, J. Pierson, R. Wallace, J. T. Miller, T. F. Fuller, C. W. Jones, *Appl. Catal. A: Gen.*, 2011, 396, 85–90.
- [110] M. Rabaeva, M. V. Landau, R. V. Nehemya, A. Goldbourt, M. Herskowitz, *J. Catal.*, 2015, 332, 164–176.
- [111] K. R. Hwang, I. Choi, H. Y. Choi, J. S. Han, K. H. Lee, J. S. Lee, *Fuel*, 2016, 174, 107–113.
- [112] J. Fu, X. Lu, P. E. Savage, *ChemSusChem.*, 2011, 4, 481 – 486.
- [113] D. Kim, D. R. Vardon, D. Murali, B. K. Sharma, T. J. Strathmann, *ACS Sus. Chem. Eng.*, 2016, 4, 1775–1784.
- [114] <http://www.nesteoil.com>.
- [115] <http://www.uop.com/pr/releases/PR.EniEcofiningFacility.pdf>.
- [116] <http://www2.petrobras.com.br/tecnologia/ing/hbio.asp>.
- [117] <http://www.tyson.com/RenewableEnergy/Initiative/Conoco/Default.aspx>.

Chapter-2
Experimental Methods and Characterization Techniques

2.1. Introduction

This chapter presents the synthesis procedures of catalysts studied this work. It also describes the techniques employed for characterisation of the catalyst, reaction procedure for catalytic activity tests and methods of product analysis. The supports $\text{AlPO}_4\text{-5}$, silica-alumina (SA; $\text{SiO}_2\text{-Al}_2\text{O}_3$) and ZrO_2 were prepared by following the procedures reported elsewhere. The required quantity of metals (Pt, W, Mo, Re and Sn) was deposited on the solid supports by using wet-impregnation method. The following are the catalysts prepared, characterised and used in this study.

Pt/ $\text{AlPO}_4\text{-5}$, Pt- WO_x / $\text{AlPO}_4\text{-5}$, Pt/ Al_2O_3 , Pt- WO_x / Al_2O_3 ,
Pt- MoO_x / Al_2O_3 , Pt- ReO_x / Al_2O_3 , Pt- SnO_x / Al_2O_3 , Pt/ ZrO_2 ,
Pt- WO_x / ZrO_2 , Pt- MoO_x / ZrO_2 , Pt/SA, Pt- WO_x /SA

The catalysts were characterised by powder X-ray diffraction (XRD), nitrogen-physorption, scanning electron microscopy (SEM), transmission electron microscopy (TEM), inductively coupled plasma-optical emission spectroscopy (ICP-OES), energy dispersive X-ray analysis (EDAX), X-ray photoelectron spectroscopy (XPS), scanning electron microscopy (SEM), CO-chemisorption, NH_3 -temperature-programmed desorption (NH_3 -TPD), H_2 -temperature-programmed reduction (H_2 -TPR) techniques. The deoxygenation activity of these catalysts was tested for oleic acid (a representative fatty acid) producing diesel-range hydrocarbons (green diesel).

2.2. Catalyst preparation

2.2.1. Support materials

2.2.1.1. $\text{AlPO}_4\text{-5}$

The $\text{AlPO}_4\text{-5}$ material was prepared using a molar gel composition of Al_2O_3 : 1.3 P_2O_5 : 1.6 TEA : 1.3 HF : 425 H_2O [1]. Initially, phosphoric acid solution was prepared by dissolving 14.84 g of orthophosphoric acid (88%, Merck Co.) in 28 g of Milli-Q water. To it, 8.28 g of TEA (triethylamine, 99%, Alfa aesar) was added drop-wise while stirring at 25 °C. The solution was cooled to 0 °C and aluminum isopropoxide (20.92 g, Kemphasol) was added in small amounts while stirring. The gel formed was brought back to 25 °C and stirred for 2 h. Then, HF solution (3.32 g of 40% HF, Thomas baker in 356.8 g of water) was added drop-wise to the above gel, stirred for another 2 h and transferred into a Teflon-lined stainless-steel autoclave (300 ml). It was allowed for crystallization at 180 °C for 6 h (without agitation) in an electric oven. The solid formed was separated, washed with copious amounts of distilled water and dried at 110 °C for 12 h. Finally, it was calcined at 600 °C for 6 h to get white $\text{AlPO}_4\text{-5}$ powder (yield = 15.6 g).

2.2.1.2. Silica-alumina (SA)

This support was prepared by co-precipitation method (Si/Al = 80). In its preparation [2], 18.6 g of tetraethyl orthosilicate (TEOS, Sigma-Aldrich Co., 99%) was added drop-wise to 0.422 g of aluminum nitrate nonahydrate (extra pure, Merck) dissolved in 20 ml of Milli-Q water. The mixture was stirred for 30 min at 25 °C. Then, 25% ammonia solution (Thomas Baker) was added till the pH of the suspension was 11 and then, it was allowed to stir for another 15 min. The precipitate formed was filtered, washed thoroughly with copious amount of distilled water (500 ml), dried at 110 °C for 12 h and calcined in a muffle furnace at 550 °C for 2 h.

2.2.1.3. ZrO₂

Support zirconia was prepared hydrothermally by following a method reported elsewhere [3]. In a typical synthesis, solution A was prepared by dissolving 30 g of cetyltrimethylammonium bromide (CTAB, Spectro Chem.) in 250 ml of Milli-Q water at 50 °C. Solution B was prepared by dissolving 16.85 g of zirconyl nitrate (Thomas Baker) in 100 ml of water at 50 °C. Solution B was added drop-wise to solution A and stirred vigorously at 25 °C for 15 min. After that, 100 ml of 12.5% ammonia solution was added very slowly and the suspension was stirred for 30 min. The gel was transferred into a Teflon-lined stainless steel autoclave (300 ml), which then was kept at 140 °C for 6 h in the pre-heated oven. The autoclave was cooled to 25 °C. The solid formed was collected, washed with plenty of water as well as with ethanol solution to remove residual unreacted chemicals, dried at 100 °C for 12 h and calcined at 650 °C for 6 h in a muffle furnace.

2.2.1.4. Al₂O₃

γ -Al₂O₃ was a commercial sample procured from Süd-Chemie India Pvt. Ltd.

2.2.2. Supported Pt catalysts

For a 4 wt% of Pt loading on supports (AlPO₄-5, γ -Al₂O₃, SA and ZrO₂), 0.0794 g of tetraammineplatinum(II) nitrate (99.99%, Sigma-Aldrich Co.) was dissolved in 10 ml of Milli-Q water and then, added to 1 g of support material taken in a 100 ml glass, round bottom flask. The suspension was stirred for 4 h at 40 °C and then, the water was removed over a rotary evaporator. The solid formed was dried at 110 °C for 12 h and calcined at 450 °C (at a ramp rate of 2 °C/min) for 4 h. Then, it was reduced at 350 °C for 2.5 h in a flow of dry hydrogen (20 ml/min). Catalysts with 1 and 2 wt% Pt were prepared in similar manner employing appropriate amount of Pt source. Color: dark gray.

2.2.3. Pt supported on reducible oxide modified catalysts

2.2.3.1. 4Pt-8WO_x/AlPO₄₋₅

These catalysts were prepared in two steps.

Step 1: Varying amounts of tungsten (W = 2, 4, 8, 12, 16 wt%) were deposited on AlPO₄₋₅ by a wet-impregnation method. The prepared material was labeled as xWO_x/AlPO₄₋₅, where x refers to the weight percentage of W. In a typical preparation of 8WO_x/AlPO₄₋₅, ammonium metatungstate (0.1066 g, (NH₄)₆W₁₂O₃₉.xH₂O, 99.9%, Alfa Aesar) was dissolved in 10 ml of Milli-Q water. It was added to 1 g of AlPO₄₋₅ taken in a glass, round-bottom flask (100 ml), stirred for 16 h at 40 °C and then, water was evaporated over a rotary evaporator. The solid formed was dried at 110 °C for 12 h and calcined at 450 °C (ramp rate = 2°C/min) for 4 h.

Step 2: Various amounts of platinum (1, 2 and 4 wt%) were loaded on xWO_x/AlPO₄₋₅ by a wet-impregnation method. The formed material was designated as yPt-xWO_x/AlPO₄₋₅. In the preparation of 4Pt-8WO_x/AlPO₄₋₅, tetraammineplatinum(II) nitrate (0.0794 g) was dissolved in Milli-Q water (10 ml) and added to 8WO_x/AlPO₄₋₅ (1 g) taken in a glass round-bottom flask (100 ml). The suspension was stirred for 4 h at 40 °C and water was removed over a rotary evaporator. The solid formed was dried at 110 °C for 12 h and calcined at 450 °C (at a ramp rate of 2 °C/min) for 4 h. Then, it was reduced at 350 °C for 2.5 h in a flow of dry hydrogen (20 ml/min).

2.2.3.2. 4Pt-8WO_x/SA

4 wt% of platinum and 8 wt% of tungsten were loaded on SA (silica-alumina) support by following the procedure as described in section 2.2.3.1.

2.2.3.3. 4Pt-8WO_x/ZrO₂

4 wt% of platinum and 8 wt% of tungsten were impregnated on ZrO₂ support by following wet-impregnation method as described in section 2.2.3.1.

2.2.3.4. 4Pt-8MO_x/Al₂O₃ (M = Mo, Re, W and Sn)

A series of reducible oxide modified Al₂O₃ catalysts (4Pt-8MoO_x/Al₂O₃, 4Pt-8ReO_x/Al₂O₃, 4Pt-8WO_x/Al₂O₃ and 4Pt-8SnO_x/Al₂O₃) were prepared in two steps. In the first step, reducible oxide (8 wt% of metal (M)) was deposited on γ-Al₂O₃ and then, in the second step, 4 wt% of Pt was deposited on it further. The depositions were done by wet-impregnation method.

In a typical procedure, ammonium metatungstate (0.1066 g; as W source), ammonium molybdate (0.147 g; $(\text{NH}_4)_6\text{Mo}_7\text{O}_{24}\cdot 4\text{H}_2\text{O}$, 99%, Thomas Baker, as Mo source), ammonium perrhenate (0.1152 g; NH_4ReO_4 , 99%, Sigma-Alrich Co., as Re source) or stannic chloride (0.236 g; $\text{SnCl}_4\cdot 5\text{H}_2\text{O}$, Thomas Baker, as Sn source) was dissolved in 10 ml of Milli-Q water. Then, 1 g of $\gamma\text{-Al}_2\text{O}_3$ powder was added. It was stirred for 16 h at 40 °C. Later, water in it was removed over a rotary evaporator (at 65 °C). The white solid formed was dried for 12 h at 110 °C, ground and calcined for 4 h at 450 °C (ramp rate = 2 °C/min). The material, thus prepared, was denoted as $8\text{MO}_x/\text{Al}_2\text{O}_3$. Then, 0.0794 g of tetraammineplatinum(II) nitrate was dissolved in 10 ml of Milli-Q water. $8\text{MO}_x/\text{Al}_2\text{O}_3$ (1 g) was added and the suspension was stirred for 4 h at 40 °C. After that, water in it was removed over a rotary evaporator. The solid formed was dried and calcined as described above. Then, it was reduced in a flow of hydrogen (flow rate = 20 ml/min) at 350 °C for 2.5 h. The catalyst, thus obtained, was named as 4Pt- $8\text{MO}_x/\text{Al}_2\text{O}_3$.

2.2.3.5. 4Pt- $8\text{MoO}_x/\text{ZrO}_2$

Step 1: Firstly, various amounts (4, 8, 12 and 16) of Mo were deposited on ZrO_2 support by wet-impregnation method. In a typical procedure, for $8\text{MoO}_x/\text{ZrO}_2$, 0.147 g of ammonium molybdate was dissolved in 10 ml of Milli-Q water. Then, 1 g of ZrO_2 powder was added. It was stirred for 16 h at 40 °C. The water in it was removed over a rotary evaporator. The white solid formed was dried for 12 h at 110 °C, ground and calcined for 4 h at 450 °C (ramp rate = 2 °C/min).

Step 2: In the second step, for 4 wt% of Pt, 0.0794 g of tetraammineplatinum(II) nitrate was dissolved in 10 ml of Milli-Q water. $8\text{MoO}_x/\text{ZrO}_2$ (1 g) was added and the suspension was stirred for 4 h at 40 °C. Then, the water in it was removed over a rotary evaporator. The solid formed was dried and calcined as described above. Then, it was reduced in a flow of hydrogen (flow rate = 20 ml/min) at 350 °C for 2.5 h.

2.3. Characterization techniques and sample preparation

2.3.1. X-ray powder diffraction (XRD)

XRD is a basic and imperative characterization technique to elucidate the crystallinity, phase purity, crystal structure, and crystallite size of crystalline solid catalysts. X-ray diffraction pattern of solid material is the result of an interaction between the incident monochromatized X-rays (CuK_α or MoK_α) and the atoms of a periodic lattice. Bragg's equation: $n\lambda = 2d\sin\theta$ describes the constructive interference of diffracted X-rays by the atoms of an ordered lattice. Here, λ is the wavelength of X-rays, d is the distance between two lattice planes (i.e. interplanar distance), θ is the angle between incoming X-rays and normal to the reflecting lattice plane and n is an integer known as the order of reflection [4, 5]. Powder

samples were pressed as thin layer on a glass plate having sample holding pit and powder XRD patterns were recorded in the 2θ range of $5 - 90^\circ$ at a scan rate of $2^\circ/\text{min}$ on an X'pert Pro Philips diffractometer equipped with Ni-filtered CuK_α radiation (40 kV, 30 mA).

Analyses of the position, area and shape of diffraction peaks allows identification of lattice parameters, type and composition of phase present, percentage crystallinity and crystallite size of the sample. Average crystallite size can be estimated using the Scherrer equation (Eq. 2.1),

$$\tau = K\lambda/\beta\cos\theta \quad (2.1)$$

where τ is the mean size of the ordered (crystalline) domain (which may be smaller or equal to the grain size), K is a dimensionless shape factor, with a value close to unity, but varies with the actual shape of the crystallite, λ is the X-ray wavelength and β is the line width at half the maximum intensity (FWHM). Generally, heterogeneous catalysts exist as polycrystalline powders. Sharp diffraction pattern is observed only when the sample possesses a sufficiently long range order.

2.3.2. Nitrogen physisorption

Surface aspects of the catalyst samples were examined by using BET (Brunauer, Emmet and Teller) method which is a versatile technique based on the theory considering a multilayer adsorption of a gas on the solid surface. The outcome of this theory is well known in the form of BET equation which can be represented as:

$$P/V(P_0-P) = 1/cV_m + [(c-1)/cV_m] (P/P_0) \quad (2.2)$$

where P is adsorption equilibrium pressure, P_0 is saturation vapour pressure of the adsorbate at the experimental temperature, V is volume of N_2 adsorbed at a pressure P , V_m is volume of adsorbate required for monolayer coverage, and c , a constant that is related to the heat of adsorption and liquefaction [6-8]. The linear relationship between $P/V(P_0-P)$ and P/P_0 is necessary to estimate the quantity of adsorbed nitrogen. The monolayer volume (V_m) is given by $1/(S+I)$, where S is the slope which is equal to $(c-1)/cV_m$ and I is the intercept equal to $1/cV_m$. The surface area of the material (S_{BET}) is related to V_m , by the equation:

$$S_{\text{BET}} = (V_m/22414)N_a\sigma \quad (2.3)$$

where, N_a is Avogadro number and σ is mean cross sectional area covered by one adsorbate molecule. The accepted σ value for N_2 is 0.162 nm^2 . To derive pore size distribution from physisorption isotherms, several computational procedures were reported. Most popular and

accepted among them is Barrett-Joyner-Halenda (BJH) model, which is based on speculative emptying of the pores by a step-wise reduction of P/P_0 . Allowance is made for the contraction of the multilayer in those pores already emptied by the condensate [6]. The pore size distribution is generally expressed as a plot of $\Delta V_p/\Delta r_p$ versus r_p , here V_p is pore volume and r_p is pore radius.

At low pressure (10^{-4} Torr) and liquefaction temperature of N_2 (-196 °C), the amount of adsorbed nitrogen can be estimated by BET equation which is the standard method to determine surface area, pore volume and pore size distribution of nanoporous materials. All these measurements were performed on a Quadrasorb SI, Quanta Chrome instrument. Specific surface area was determined by total surface area of the sample by sample weight. About 100 mg of catalyst sample was taken in a quartz cell and evacuated at 200 °C for 3 h. Then, the quartz cell was dipped in a liquid nitrogen container up to the sample level and started passing nitrogen through it. Adsorption and desorption of nitrogen was measured in the P/P_0 range of 0 to 0.99.

2.3.3. Transmission electron microscopy (TEM)

Transmission electron microscopy (TEM) is an advanced technique for microstructural and compositional analysis of the solid materials. The TEM images of the solid sample (finely dispersed as thin layer) provide information of particle size distribution, metal dispersion and chemical composition of the supported metal. This technique involves: (i) irradiation of a very thin sample by a high-energy electron beam, which is diffracted by the lattices of a crystalline or semi-crystalline material and propagated along different directions, (ii) imaging and angular distribution analysis of the forward scattered electrons (unlike scanning electron microscopy where backscattered electrons are detected) and (ii) energy analysis of the emitted X-rays [9].

In general, a primary electron beam of high energy and high intensity passes through a condenser to produce parallel rays, which impinge on the sample. As the attenuation of the beam depends on the density and thickness, the transmitted electrons form a 2D projection of the sample mass. Further, this will be magnified by the electron optics to construct the so-called bright field image. Whereas, the diffracted electron beams produce dark image, which are slightly off angle from the transmitted beam. Typical conditions involved in TEM instrument operation are: 100-200 keV electrons, 10^{-6} mbar vacuum, 5 nm resolutions and magnification of about 3×10^5 (or) 10^6 . The topographic information can be utilized for structural characterization and phase identification in the atomic vicinity [10]. It also provides

a real space image on the atomic distribution in the bulk and surface of a crystalline material. TEM images of the catalysts were recorded on a Technai-G2 T20 super twin instrument fitted with a 200 kV field emission gun. 0.001-0.005 g of the sample was taken into a beaker containing 5 ml of isopropanol solvent. Then it was sonicated for 0.5 h at room temperature. After that, a single drop was placed on a copper grid (200 mesh, ICON Analytical), allowed it for drying overnight and subjected to analysis.

2.3.4. X-ray photoelectron spectroscopy (XPS)

X-ray photoelectron spectroscopy also known as Electron Spectroscopy for Chemical Analysis (ESCA) is a well known technique in material chemistry to elucidate the nature, oxidation state, dispersion of the surface species of a solid material [14]. XPS spectra were obtained by irradiating the material with a beam of X-rays and simultaneously measuring the kinetic energy and number of electrons that escape from the top of the surface composition being analyzed. XPS analysis of pre-reduced catalyst samples was performed on a Thermo Fisher Scientific Instruments, UK (Model: K-Alpha+) equipment using Al-K α anode (1486.6 eV) in transmission lens mode and equipped with multi channel plate (MCP) detector. Peaks were referenced to C_{1s} appeared at 284.8 eV. The percentage concentration of the metal and sensitivity factor of an element can be estimated using the following equations.

$$S = f \sigma D \lambda \quad (2.4)$$

Where f = X-ray flux, σ = photoelectron cross section, D = detector efficiency and λ = electron mean free path, and

$$C_X = (A_i S_i) / \Sigma (A_i S_i) \quad (2.5)$$

Where C = concentration of element X, I = area of metal photo emission peak and S = sensitivity factor of a particular element.

The XPS spectra lines were deconvoluted into different peaks to fit their corresponding spin-orbit doublets. For this, XPS peak41 and/or CasaXPS software was used. The samples were pelletized, reduced under the flow of hydrogen and subjected to analysis.

2.3.5. NH₃-temperature-programmed desorption (NH₃-TPD)

Temperature-programmed desorption is one of the most widely used and flexible techniques to estimate the total acidity/basicity of the solid samples [15]. In this study, the total acidity of the catalysts was quantified using temperature-programmed desorption measurements conducted on a Micromeritics Auto Chem 2910 instrument using NH₃ as probe molecule (NH₃-TPD). In a typical experiment, 0.1 g of the catalyst was taken in a U-shaped

quartz sample tube. Prior to measurements, the catalyst was pre-treated in He (30 ml/min) at 200 °C for 1 h. It was then cooled to 100 °C and a mixture of NH₃ in He (10 vol%) was fed to the sample (30 ml/min) for 1 h. Then, the sample was flushed with He (30 ml/min) at 100 °C for 1 h. Before starting the desorption analysis, baseline was checked for stability. TPD measurements were done in the temperature range of 100-500 °C (for SA and ZrO₂ based catalysts), 100-550 °C (for AlPO₄-5 based catalysts) and 80-550 °C (for Al₂O₃ based catalysts). The NH₃ desorption profiles were broad and could be deconvoluted into different peaks to calculate approximately the distribution of acid sites of the catalysts. Based on the desorption temperature (T_{\max}), the acid sites were classified into weak ($T_{\max} = 100-200$ or 250 °C), medium ($T_{\max} = 200$ or 250 °C to 350 °C) and strong sites ($T_{\max} = < 350$ °C).

2.3.6. H₂-temperature-programmed reduction (H₂-TPR)

Hydrogen-temperature-programmed reduction (H₂-TPR) is a best technique to find the efficient reduction conditions of a metal. In this, an oxidized catalyst sample is subjected to a programmed temperature raise while passing hydrogen through it. The H₂-TPR measurements of the catalysts used in this thesis were done on a Micromeritics Auto Chem 2910 instrument. In this experiment, 0.1 g of the sample was taken in a U-shaped quartz tube, heated at 200 °C for 1 h and passed He (30 ml/min) for 1 h. Then, it was allowed to cool down to 50 °C. The TPR pattern was recorded in the flow of 5% H₂ in Ar in the temperature range of 50-800/900 °C [16, 17]. The amount of hydrogen consumption was estimated to compare the feasibility of the reduction. A standard CuO powder was used to calibrate the amount of H₂ consumption.

2.3.7. CO-chemisorption

Percentage metal dispersion (D%), active metal surface area, average crystallite size were determined by CO-chemisorption studies performed on a Quanta Chrome Autosorb iQ instrument. In a typical chemisorption experiment, about 0.2 g of the catalyst was taken in U-shaped quartz tube. It was first degassed at 200 °C (heating rate = 20 °C/min) under a flow of He (20 ml/min) for 120 min and reduced with H₂ (20 ml/min) at 350 °C (heating rate = 20 °C/min) for 150 min followed by evacuating the sample at 350 °C for 120 min. Temperature of the sample was lowered down to 40 °C (in 1 min) under vacuum. CO (carbon monoxide) was introduced and chemisorption measurements were started (equilibrium tolerance = 0, equilibrium time = 3 min, adsorption points = 80, 160, 240, 320, 400, 480 and 560 mmHg, analysis temperature = 40 °C, thermal equilibrium time = 10 min, leak test = 1 min).

2.3.7. Scanning electron microscopy

Morphological properties of the materials were examined by scanning electron microscopy (SEM). SEM scans over a sample surface with a probe of electrons (5- 50 eV) and detects the yield of either secondary or back-scattered electrons as a function of the position of the primary beam. Contrast is generally caused by the orientation of the sample towards detector. Parts of the surface facing the detector appear brighter than the surface pointing away from the detector. The interaction between the electron beam and the sample generates different kinds of signals providing detailed information about the surface structure and morphology of the sample. When an electron from the beam encounters a nucleus in the sample, the resultant Coulombic attraction leads to a deflection in the electron's path, known as Rutherford elastic scattering. A fraction of these electrons will be completely backscattered, re-emerging from the incident surface of the sample. Since the scattering angle depends on the atomic number of the nucleus, the primary electrons arriving at a given detector position can be used to produce images containing topological and compositional information. SEM is also proficient for carrying out analysis of selected point regions on the sample, which is particularly important in qualitatively or semi-quantitatively determination of chemical composition by using energy dispersive X-ray analysis (EDAX). The composition of the material is resolved by measuring the characteristic X-rays that are generated by the contact of the electrons with matter. Samples were dispersed in isopropanol solvent by sonication for 30 min and drop casted on silicon wafer, allowed for drying at room temperature for 12 h and subjected to analysis. The images were recorded using an ESEM Quanta-200 3D instrument operating at 20 kV. The chemical composition of the catalysts was also estimated from SEM-EDAX by probing the samples at different random places.

2.4. Reaction procedure

Fatty acid deoxygenation reactions were performed in a 300 ml (controller model: 4848) or 100 ml (controller model: 4871) capacity stainless-steel batch autoclave supplied by Parr Instruments Co., USA. The reactor was equipped with a heating arrangement, overhead stirrer, thermo well, internal cooling coil, gas inlet and outlet, liquid sampling valve, safety rupture disc, pressure gauge and a transducer for digital pressure display.

2.4.1. Deoxygenation of fatty acid

Prior to the reaction (deoxygenation of fatty acid), the catalysts were reduced at 350 °C for 2.5 h under a flow of hydrogen (20 ml/min). The colour of the catalysts was turned from dark grey to black after the reduction. The temperature of the catalyst was brought down to 25 °C and carefully, without exposing to atmosphere, 0.2 g of reduced catalyst was

transferred into a Parr stainless-steel batch autoclave containing oleic acid (OA; a typical fatty acid, Sigma-Aldrich Co., 2 g), n-heptane (solvent, Merck Co., 30 g). Then the reactor was initially flushed with nitrogen and later with hydrogen. Finally, the reactor was pressurized with hydrogen to a desired value (3 - 40 bar). In some experiments instead of hydrogen, the reactor was charged with 20 bar of nitrogen or carbon dioxide to understand the effect of gaseous atmosphere. Later, the reaction was conducted for specific durations (0 - 5 h) in the temperature range of 180 - 320 °C. The set temperature was established within 1 h. Reaching the point of desired temperature was considered as 0 (zero) min run and taken as starting point. The agitation was kept constant at 600 revolutions per minute. After the reaction, the reactor was cooled down to 25 °C and depressurized. The liquid portion was separated from the catalyst by centrifugation/filtration. Solvent was removed over a rotary evaporator and the product isolated was subjected for analysis.

2.4.2. Product analysis

OA conversion was determined from the acid values of the product and reactants (Eqs. 2.6 and 2.7). For determination of acid value, about 0.1 g of the sample was weighed in a conical flask and dissolved in 10 ml of solvent mixture containing equal amounts of diethyl ether and ethanol (50:50 v/v%); 2-3 drops of phenolphthalein indicator was added and titrated against a 0.1 N standardized NaOH solution until an end point (colorless to pink) was observed. The acid value of the sample was calculated by the formula:

$$\text{Acid Value} = \frac{V_{\text{NaOH}} \times N_{\text{NaOH}} \times 56.1}{W_{\text{Sample}}} \quad (2.6)$$

where, 56.1 is the molecular weight of KOH (as acid value is always reported as mg of KOH per gram of the sample). N_{NaOH} is the normality of NaOH, V_{NaOH} is the volume of NaOH consumed and W_{Sample} is the weight of the sample taken for titration.

$$\text{Fatty acid conversion (mol\%)} = \frac{\text{Initial acid value} - \text{Final acid value}}{\text{Initial acid value}} \times 100 \quad (2.7)$$

All the products and reactants were analyzed by gas chromatography (GC). The sample was derivatized with N, O-bis(trimethylsilyl)trifluoroacetamide (BSTFA; Sigma-Aldrich Co.). A known quantity of the sample was dissolved in an equal amount of pyridine and 100 wt% excess of BSTFA was added to it. The mixture was heated to 70 °C for 45 min and injected in the GC (Varian 450 GC; SelectTM biodiesel column of dimensions: 15 m (length) x 0.32 mm (diameter) x 0.10 μm (film thickness). Helium was the carrier gas. In the analysis: injector and detector temperatures were set at 300 °C and split ratio was set at 1:50.

The following temperature program was used: 80 °C (start) - 280 °C (at 20 °C/min) - hold (10 min). Products were identified by GC-mass spectrometry (GC-MS, Agilent Technology 7890B; HP-5 column, 30 m (long) x 0.25 mm (i.d.)). Products were analyzed also by nuclear magnetic resonance spectroscopy (^1H and ^{13}C NMR; Bruker 200 MHz).

2.5. References

- [1] <http://www.iza-online.org/synthesis/default.htm>.
- [2] Atsushi Ishihara, Hirotaka Negura, Tadanori Hashimoto, Hiroyuki Nasu, *Applied Catalysis A: General*, 2010, 388, 68–76.
- [3] M. Mokhtar, S.N. Basahel, T.T. Ali, *J. Mater. Sci.* 2013, 48, 2705.
- [4] W. H. Bragg, W. L. Bragg, *The crystalline state*, Vol. 1, Mcmillan, New York (1949).
- [5] G. Bargeret, in: *handbook of Hetrogenous Catalysis*, Vol. 2, EDS: G. Ertl, H. Knozinger, J. Weitkamp, Wiley-VCH, Weinheim, 1997, 464.
- [6] S. Brunauer, P. H. Emmet, E. Teller, *J. Am. Chem. Soc.* 1938, 60, 309.
- [7] E. P. Barrett, L. G. Joyner, P. P. Halenda, *J. Am. Chem. Soc.*, 1951, 73, 373.
- [8] G. Ertl, H. Knozinger, F. Schuth, J. Weitkamp, *handbook of Heterogeneous Catalysis*, Vol 2 (2008), Wiley-VCH, Weinheim.
- [9] J. R. Fryer, *Chemical Applications of Transmission Electron Microscopy*, Academic Press, San Diego (1979).
- [10] J. M. Thomas, O. Terasaki, P. L. Gai, W. Zhou, J. Gonzalez-Calbet, *Acc. Chem. Res.*, 2001, 34, 583.
- [11] B. E. Sundquist, *acta Metall*, 1964, 12, 67.
- [12] J. R. Anderson, *Structure of metallic catalysts*, Academic press, London, 1975, p. 296.
- [13] J. F. Scholten, in *preparation of catalysts II: Scientific Bases for the Preparation of Heterogeneous Catalyst*, B. Delmon, P. Grange, P. Jacobs, G. Poncelet, (Eds), Elsevier, Amsterdam, 1979, p.685.
- [14] K. Seigbahn, C. Nordling, A. Fahlmann, R. Nordberg, K. Hamrin, J. Hedman, G. Johansson, t. Bergmark, S. E. Karlsson, I. Lindgern, B. Lindberg, *ESCA – Stomic*

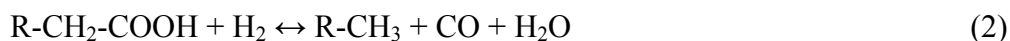
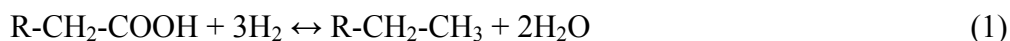
Molecular and Solid State Structure Studied by Means of Electron Spectroscopy, Almquist and Wicksell, Uppsala, 1967.

- [15] J. Shen, R. D. Cortright, Y. Chen, J. a. Dumesic, Catal. Lett., 1994, 26, 247.
- [16] S. D. Robertson, B. D. McNicol, J. H. de. Bass, S. C. kloet, J.W. Jenkins, J. Catal., 1975, 37, 424-431.
- [17] A. Jones, B. D. McNicol, Temperature Programmed Reduction for Solid Material Characterization, Marcel Dekker, new York, 1986.

Chapter-3
Deoxygenation of Oleic Acid over Pt-WO_x/AlPO₄-5

3.1. Introduction

Deoxygenation is an attractive approach for producing renewable transport fuels (green diesel) from inedible vegetable oils [1-7]. While addressing the issues related to global warming, implementation of these carbon-neutral, hydrocarbon-based biofuels can possibly extend the life span of conventional (fossil) resources even to the next generations and at the same time, meet the global energy demands. Green diesel is advantageous over biodiesel (fatty acid methyl ester (FAME); produced by transesterification of vegetable oils with short chain alcohols like methanol) due to its higher cetane number (75-90), lower pour point and higher oxidation stability [8]. It can be fueled directly in the conventional engines without modification. It can also be blended in any proportion with the fossil diesel and used (as the component hydrocarbons of green diesel are similar to those present in the conventional diesel). Moreover, the problematic and limiting filter plugging and cold flow properties of biodiesel in the temperate parts of the world could be minimized by using green diesel. There are three reaction pathways (Eqs. 1 – 3) for the removal of oxygen from vegetable oils or fatty acids [9, 10]. In Eq. (1), the deoxygenation occurs through formation of water along with a hydrocarbon having the same carbon number as that of the parent fatty acid. This reaction is known as hydrodeoxygenation or hydrodehydrogenation (HDO). In Eqs. (2) and (3), it follows decarbonylation and decarboxylation (DCO) paths resulting in CO and CO₂, respectively, along with a hydrocarbon having one carbon lesser (C_{n-1}) than the original fatty acid (C_n). The advantage of the DCO route is that it requires lesser or little hydrogen but, at the loss of one carbon as CO/CO₂. Water-gas shift (CO + H₂O ↔ CO₂ + H₂) and methanation (CO + 3H₂ ↔ CH₄ + H₂O and CO₂ + 4H₂ ↔ CH₄ + 2H₂O) are the side reactions that might occur during the hydrotreating process of vegetable oil/fatty acid.



The conventional hydrotreating catalysts (sulfided NiMo/Al₂O₃ and CoMo/Al₂O₃) are effective also for HDO of vegetable oil/fatty acid [11-21]. Neste Oil (NExBTL technology), [22, 23] UOP//Eni (Ecofining technology) [24-26], Petrobras (H-BIO technology) [27] and Tyson-Conoco Phillips [28] announced their pilot/commercial scale production of green diesel based on these catalyst systems and HDO route. Linear paraffins produced by HDO are isomerized in a second step to produce high quality (low cloud point) biofuel. Supported noble metals lead to decarbonylation/decarboxylation (Eqs. (2) and (3)) [29-35]. Murzin and co-workers [36] used a commercial Pd/C catalyst for decarboxylation of stearic acid, ethyl

stearate and tristearine in a semi-batch reactor. Pd/C was found superior to Pt, Rh, Ni, Os and Ir/C. Resasco and co-workers [37] reported the use of Pt/Al₂O₃ for conversion of methyl stearate. However, the yield of hydrocarbons was not satisfactory (about 60% at 6.9 bar and 325 °C). Several studies reported the use of microporous zeolite (SAPO-11, SAPO-31, SAPO-34, ZSM-11, ZSM-22, etc.)-supported Pt catalysts, wherein the product, a mixture of iso- and n-paraffins, having better cold flow characteristics, is produced in one-step [38–45]. In those catalysts, metal component facilitated decarbonylation/decarboxylation and the acidic support enabled hydroisomerization of the n-paraffins formed through the metal-catalyzed reaction. However, zeolite lost its structural integrity during the hydrotreatment of vegetable oils due to hydrolysis of Si-O-Al or Si-(PO₄)-Al bonds and thereby, the loss in acidity [46]. There have been efforts to improve the stability of zeolite catalysts [47].

Bimetallic catalysts have been reported for the deoxygenation reactions. Tsodikov et al. [48] studied deoxygenation of individual fatty esters and fatty acid triglycerides from vegetable oils and lipid extracts from microalgae in the presence of Pt-Sn/Al₂O₃ catalysts prepared by deposition method. Co-deposition of Sn changed the activity and selectivity of Pt in the deoxygenation reaction. The hydrocarbon products contained a considerable portion of alkenes. The alkene content increased with increasing Sn fraction in the catalyst. Kim et al. [49] reported the valorization of waste lipids through hydrothermal catalytic conversion and *in situ* hydrogen production using Pt-Re/C (5 wt% of each metal) catalyst. Murata et al. [50] reported that rhenium modified Pt/H-ZSM-5 yields higher amount of C₁₅-C₁₈ alkanes compared to "neat" Pt/H-ZSM-5 in the hydrotreatment of jatropha oil. Metallic Pt and Re were independently present on the ZSM-5 surface, but there existed synergism of these two metals enhancing the catalytic activity. Asano et al. [51] found that the activity and selectivity for hydrodeoxygenation of 2-furancarboxylic acid to valeric acid was higher over metal oxide-supported Pt-MoO_x than on monometallic Pt catalyst. Bimetallic catalysts (Pt-Re, Pt-Ir, etc.) compared to classical hydrocarbon reforming catalysts (Pt/Al₂O₃) showed better stability and greater activity/selectivity in skeletal rearrangement of hydrocarbons [52]. This chapter describes the influence of tungsten oxide on the fatty acid deoxygenation activity of Pt in Pt-WO_x/AlPO₄-5 catalysts. While supported Pt-WO_x catalysts have been known for high catalytic performance in selective hydrogenolysis of glycerol to 1, 3-propanediol [52-57], their activity in green diesel production from vegetable oils or its components is not explored till date. The work also explores the stability of AlPO₄-5 support under the conditions of fatty acid deoxygenation.

3.2. Experimental

3.2.1. Catalyst preparation

Aluminum isopropoxide (Al source) and orthophosphoric acid (P source; 88%, GR) were procured from Kemphasol and Merck Co., respectively. Tetraammineplatinum(II) nitrate (Pt source, 99.99%) and ammonium metatungstate [(NH₄)₆W₁₂O₃₉.xH₂O, WO_x source, 99.9%] were obtained from Sigma-Aldrich and Alfa Aesar, respectively. Triethylamine (TEA, template used in the synthesis, 99%) and hydrofluoric acid (HF, 40%) were purchased from Alfa Aesar and Thomas Baker, respectively. All the solvents (AR grade) were procured from Merck and the reagents were obtained from Sigma-Aldrich.

AlPO₄-5 used in this work was prepared as described in Chapter-2 [58]. Pt/AlPO₄-5 and Pt-WO_x/AlPO₄-5 catalysts were prepared by wet impregnating Pt on AlPO₄-5 (Chapter-2).

3.2.2. Characterization techniques and reaction procedure

The catalysts were characterized by XRD, N₂-physisorption, NH₃-TPD, H₂-TPR, CO-chemisorption, SEM and TEM techniques. Details on the methods of catalyst characterization, reaction procedure and product analysis are presented in Chapter-2.

3.3. Results and discussion

3.3.1. Catalysts characterization

3.3.1.1. X-ray diffraction

AlPO₄-5 belongs to the class of microporous aluminophosphates. It has AFI structure possessing one-dimensional 12-membered channel oriented parallel to the crystallographic c-axis and surrounded by 4 and 6-membered rings. It is built from alternating vertex-sharing of AlO₄⁻ and PO₄⁺ tetrahedra. Guo et al. [59] assigned the structure of the as-synthesized form (with template molecules in it) to a hexagonal lattice described by space group of P6cc. The crystal structure of its calcined form (without template) was assigned by Mora et al. [60] to an orthorhombic lattice with a space group of Pcc2. AlPO₄-5 used in the present study was synthesized using triethylamine (TEA) as template and a synthesis gel having a molar composition of 1Al₂O₃ : 1.3P₂O₅ : 1.6TEA : 425H₂O : 6*iso*-PrOH : 1.3HF. The platinum and tungsten containing catalysts were prepared by wet-impregnation method (Chapter-2). Representative X-ray powder diffraction (XRD) patterns of AlPO₄-5 and WO_x/AlPO₄-5, reduced 4Pt/AlPO₄-5 and 4Pt-8WO_x/AlPO₄-5 (herein the numbers 4 and 8 represent the weight percentages of metallic Pt and W in the catalyst, respectively) are shown in Fig. 3.1. Structure formation, crystallinity and purity of AlPO₄-5 were confirmed by observing the

characteristic peaks at 7.4, 12.8, 14.9, 19.8, 21.8, 22.5, 25.9, 28.3, 29.1, 30.1, 31.1, 34.5 and 35.98°. As the tungsten loading increased (from 4 to 16 wt%), the intensity of the peaks corresponding to WO_x (at 2θ = 23.2 and 33.4°) increased [Figure 3.1.(a)]. However, the intensity of the support (AlPO₄-5) peaks decreased when tungsten oxide was present on it. This could be due to some damage of the structure or blockage of the pores of AlPO₄-5 by tungsten oxide. In case of 4Pt/AlPO₄-5 and 4Pt-8WO_x/AlPO₄-5 catalysts, the XRD patterns revealed the presence of metallic Pt in a cubic closed-packed structure with a space group Fm $\bar{3}$ m (JCPDS No. 65–2868) showing peaks at 39.8, 46.3, 67.7, 81.3 and 86.2°. These peaks of Pt⁰ could be assigned to (111), (200), (220), (311) and (322) crystal planes, respectively [Figure 3.1.(b)]. 4Pt-8WO_x/AlPO₄-5 showed additionally, peaks at 23.2 and 33.4° confirming the presence of a WO₃ phase.

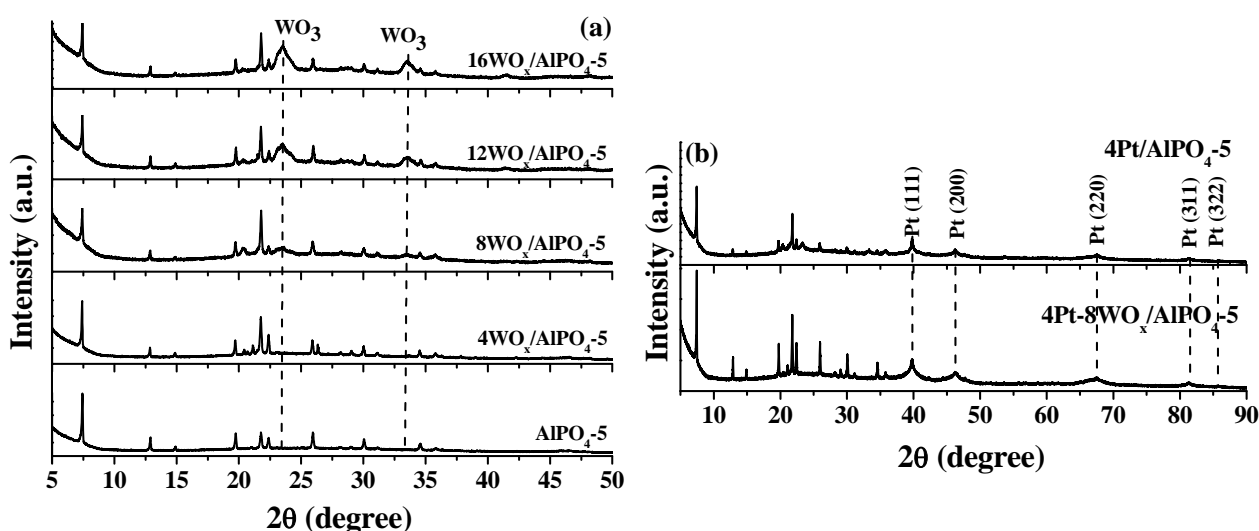


Fig. 3.1. XRD profiles of (a) bare AlPO₄-5 and WO_x loaded AlPO₄-5 and (b) reduced 4Pt/AlPO₄-5 and 4Pt-8WO_x/AlPO₄-5 catalysts. Peaks due to WO_x and Pt⁰ are marked.

The peaks due to Pt⁰ in 4Pt/AlPO₄-5 were broader compared to those in 4Pt-8WO_x/AlPO₄-5 indicating that Pt⁰ crystallites were smaller in size in the case of the former than in the latter. The average crystallite size of Pt⁰ estimated using Debye–Scherrer formula and the most intense (111) reflection was found to be 6.7 and 16 nm for 4Pt/AlPO₄-5 and 4Pt-8WO_x/AlPO₄-5, respectively. In other words, WO_x addition led to larger Pt crystallites.

3.3.1.2. N₂-Physisorption

Nitrogen-physisorption studies revealed that upon metal loading, the specific surface area (*S*_{BET}) of AlPO₄-5 decreased from 144 (for AlPO₄-5) to 129 (for 4Pt/AlPO₄-5) and 102 m²/g (for 4Pt-8WO_x/AlPO₄-5). The average pore volume (PV) decreased from 0.23 to 0.19

cc/g (Table 3.1). This decrease is due to blockage of pore mouths of AlPO₄-5 by Pt and WO_x particles.

3.3.1.3. NH₃-TPD

Acidity of the catalysts was determined with NH₃ as probe molecule. The NH₃ desorption profiles of AlPO₄-5 and the catalysts (Fig. 3.2) were broad and manifest acidic sites of different strength. They could be deconvoluted into four to five peaks. Acidic sites were categorized into weak (desorption maximum below 200 °C), medium (200 - 300 °C) and strong (300 - 500 °C) (Table 3.1). Marked effects were noticed in the temperature-programmed desorption (NH₃-TPD) profile when WO_x was also present on the catalyst surface. Metal addition enhanced the catalyst acidity. The overall acidity of the catalyst increased from 0.792 (for AlPO₄-5) to 0.867 (for 4Pt/AlPO₄-5) and 0.945 mmol/g (for 4Pt-8WO_x/AlPO₄-5). While addition of Pt enhanced the weak (from 0.168 to 0.214 mmol/g) as well as strong (from 0.160 to 0.248 mmol/g) acid sites, inclusion of WO_x enhanced mainly the strong acid sites (from 0.160 to 0.504 mmol/g) at the expense of weak and medium acid sites.

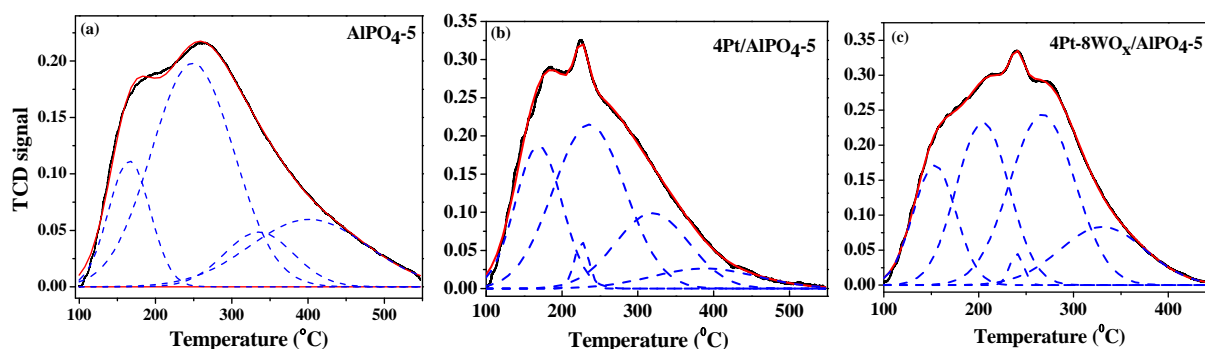


Fig. 3.2. NH₃-TPD (experimental and deconvoluted) profiles of (a) AlPO₄-5 (b) 4Pt/AlPO₄-5 and (c) 4Pt-8WO_x/AlPO₄-5.

3.3.1.4. H₂-TPR

Temperature-programmed reduction with hydrogen (H₂-TPR) of 4Pt/AlPO₄-5 showed a sharp peak at 74 °C due to reduction of platinum from +2 to metallic (zero) state (Fig. 3.3). It also showed some reduction behavior above 700 °C which is due to reduction of support structural phosphate ions to phosphite ions. On the other hand, 4Pt-8WO_x/AlPO₄-5 showed two additional broad peaks at around 325 and 600 °C, respectively. These peaks are attributed to step-wise reduction of WO₃ (from +6 to +5 and +4 states) on the surface. Usually, WO₃ reduces above 700 °C. However, in presence of Pt, its reducibility has been enhanced and started reducing at 325 °C itself. Similarly, the reduction of Pt²⁺ shifted to

lower temperatures (from 74 to 69 °C) and the amount of hydrogen consumed (in Pt reduction) was increased by 14.8 %, in spite of larger Pt crystallites in this case. This facile and enhanced reducibility could be attributed to the synergy between Pt and WO_x. Hydrogen spillover occurs from Pt to WO_x and partly reducing its surface. Such facile redox behavior was observed also by Zhu et al. [61] for Pt-W/ZSM-5 catalysts and Benson et al. [62] for WO₃ and platinum black mixtures. Thus, WO_x modifies the structure and electronic properties of Pt due to synergistic effect.

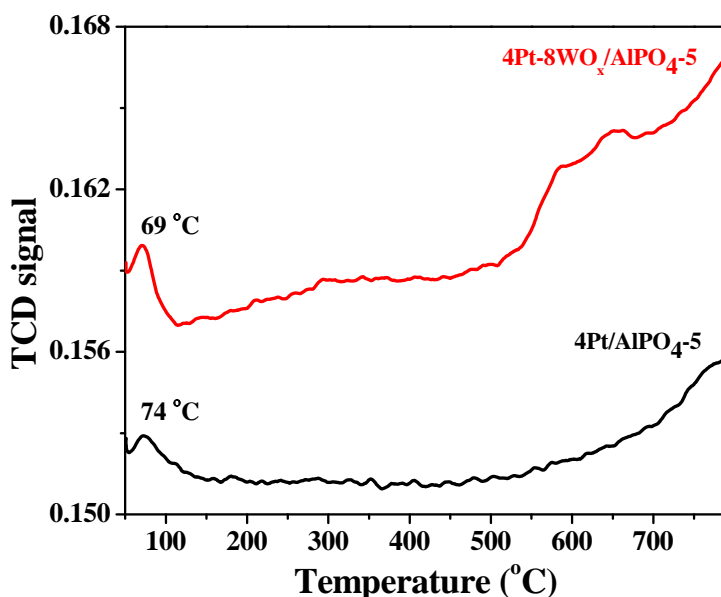


Fig. 3.3. H₂-TPR of unpromoted (4Pt/AlPO₄-5) and WO_x-promoted (4Pt-8WO_x/AlPO₄-5) catalysts.

3.3.1.5. CO-chemisorption

These studies pointed out that Pt active metal surface area decreases from 45 to 16 m²/g and Pt dispersion decreases from 18 to 6% when tungsten was also present on the catalyst. The reduction in the dispersion can be attributed to the facts of synergistic effect between Pt and W and the hindrance of tungsten domains on the surface for free Pt dispersion. As a consequence, large crystallite size of Pt was observed in 4Pt-8WO_x/AlPO₄-5 (17.9 nm) than in 4Pt/AlPO₄-5 (6.3 nm) (Table 3.1). It is gratifying to note that these values are also in concurrence with the crystallite size values of Pt determined from XRD. Thus, it reveals that the presence of WO_x alters the morphological characteristics of platinum supported on AlPO₄-5.

Table 3.1. Physicochemical properties of the Pt catalysts

Sample	N ₂ -Physisorption		NH ₃ -TPD				CO-chemisorption				Pt crystallite size (XRD; nm)
	S _{BET} (m ² /g)	Pore volume (cc/g)	Total acidity (mmol NH ₃ /g)	Acid strength distribution			% Pt dispersion (D %)	CO uptake (μmol/g)	Pt surface area (m ² /g)	Pt avg. crystallite size (nm)	
				Weak (<200 °C)	Medium (200-300°C)	Strong (>300 °C)					
AlPO ₄ -5	144	0.23	0.792	0.168	0.463	0.160	-	-	-	-	-
4Pt/AlPO ₄ -5	129	0.23	0.867	0.214	0.405	0.248	18	37	45	6.3	6.7
4Pt-8WO _x /AlPO ₄ -5	102	0.19	0.945	0.160	0.282	0.504	6	13	16	17.9	16.0

3.3.1.6. Electron microscopic studies (SEM & TEM)

The morphological characteristics of the catalysts were determined using scanning electron microscopy (SEM) and transmission electron microscopy (TEM). Two types of AlPO₄-5 morphologies (rods and no-definite shape) were detected by SEM (Fig. 3.4(a)). It was also observed that there is no change in the morphology of the support even after impregnation with tungsten and Pt, respectively (Fig. 3.4 (b and c)). TEM images of reduced samples revealed the presence of a non-uniform distribution of platinum nano particles on AlPO₄-5 surface. The average particle size of Pt was found higher in 4Pt-8WO_x/AlPO₄-5 than in 4Pt/AlPO₄-5 (Fig. 3.5) which values are in good agreement with the results obtained from XRD. Tungsten addition showed a marked affect on the dispersion of Pt and thereby altered crystallite size. However, the Pt particle size by TEM for 4Pt-8WO_x/AlPO₄-5 is much smaller than those obtained by XRD and CO-chemisorption, while that for 4Pt/AlPO₄-5 is similar. This difference is because TEM focuses on a certain region only while XRD and CO-chemisorption provide the bulk values.

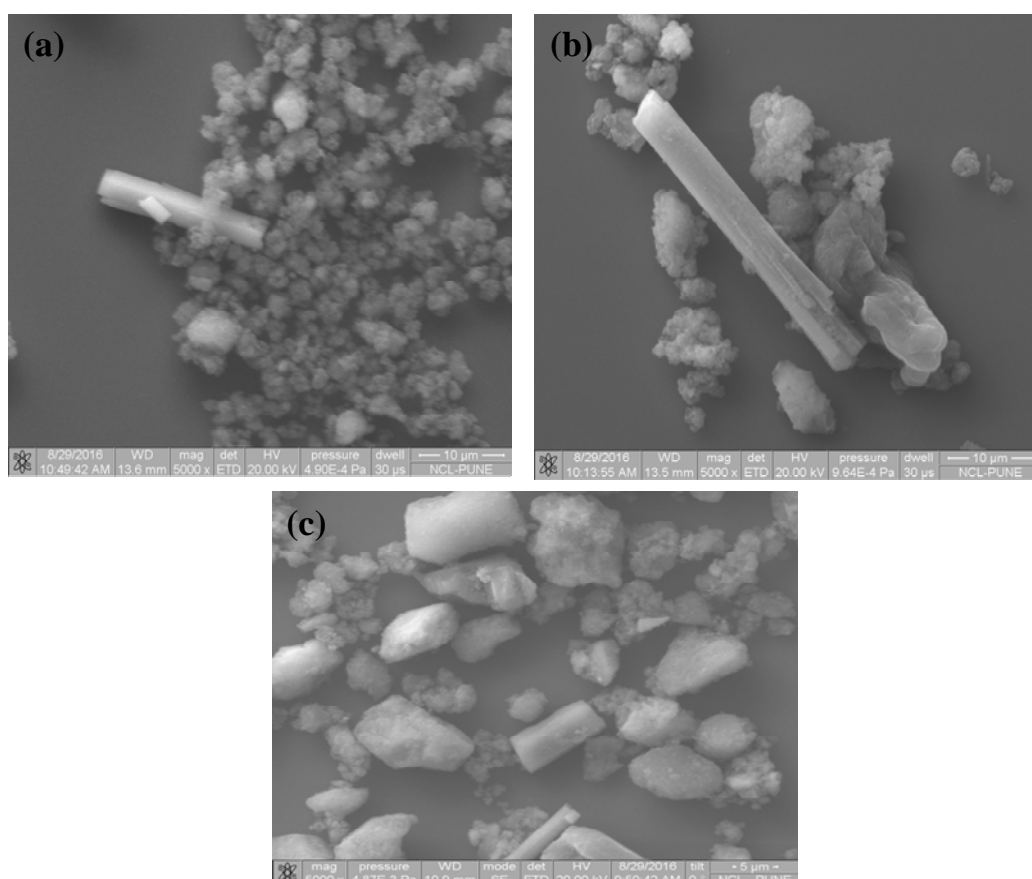


Fig. 3.4. SEM images of (a) AlPO₄-5, (b) 4Pt/AlPO₄-5 and (c) 4Pt-8WO_x/AlPO₄-5.

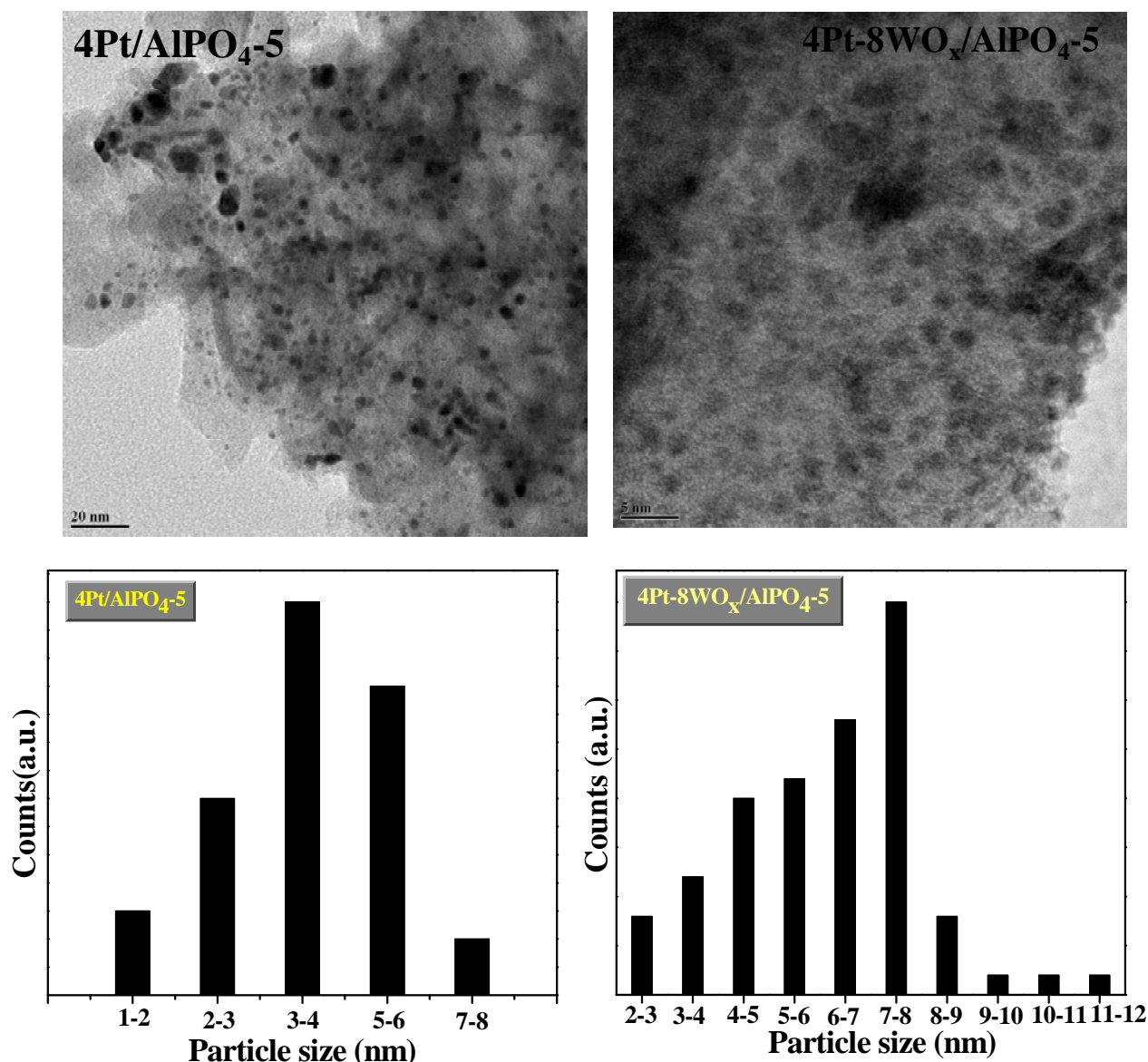


Fig. 3.5. TEM images of reduced Pt/AlPO₄-5 and 4Pt-8WO_x/AlPO₄-5 catalysts and Pt particle size distribution profiles.

3.3.2. Catalytic activity

Oleic acid (OA) was taken as a representative fatty acid as it is a component of a large number of vegetable oils. It is an unsaturated fatty acid with a double bond between 9th and 10th carbon atoms of OA. In the hydrotreating reaction, C=C hydrogenation (transforming oleic acid - OA into stearic acid - SA) is the fastest step than hydrodeoxygenation. The hydrotreating reactions were conducted in a batch reactor at 260 – 320 °C and 0 – 20 bar hydrogen for 0.5 to 5 hrs. Controlled experiment in the absence of a catalyst (at 320 °C, 20 bar H₂ and 5 h) revealed only 1 mol% of acid conversion (to hydrocarbons and oxygenates like octadecanol and octadecanal). In other words, thermal cracking of OA is almost negligible at these reaction conditions. Bare AlPO₄-5 and 8WO_x/AlPO₄-5 were also not very active (acid

conversion = 5.0 and 6.0 mol%, respectively). Heptadecane (C₁₇) and corresponding aldehyde and alcohol (hereafter named as others) were the major products of the converted acid over AlPO₄-5. Over 8WO_x/AlPO₄-5, C₁₇ hydrocarbons formed (via decarboxylation) at a selectivity of 73.4%. Selectivity of this product for bare AlPO₄-5 was 56.6% only (Table 3.2). A significant enhancement in acid conversion to 90 mol% was observed over 4Pt/AlPO₄-5; C₁₇ (formed through decarbonylation/ decarboxylation; DCO) was the major product (with a selectivity of 61.7%) and C₁₈ (formed through hydrodeoxygenation; HDO) has a selectivity of 30.6% (Table 3.2). When 4Pt-8WO_x/AlPO₄-5 was used as catalyst, complete conversion of OA to hydrocarbons was observed. Interestingly, the selectivity of C₁₈ was higher (66.5%) than C₁₇ (26.3%) (Table 3.2). A representative ¹³C DEPT NMR spectra of OA and the product obtained over 4Pt-8WO_x/AlPO₄-5 confirmed the complete conversion of OA to hydrocarbons. Absence of a peak at 28.1 ppm in the ¹³C NMR spectra revealed that the product was a linear alkane and even if any hydroisomerized product formed (by acid catalysis) that was below the detection limit of ¹³C NMR (Fig. 3.6). Even the GC analysis did not reveal the presence of isomerized hydrocarbons.

Table 3.2. Catalytic activity data: deoxygenation of OA

Catalyst	Acid conversion (mol %) ^a	Product selectivity (Wt. %) ^b			
		Octadecane (C ₁₈)	Heptadecane (C ₁₇)	Other HCs (C ₁₀ -C ₁₆)	Others ^c
No catalyst (blank)	1.0	1.6	13.2	5.6	79.6
AlPO ₄ -5	5.0	4.6	56.6	12.0	26.8
8WO _x /AlPO ₄ -5	6.0	8.9	73.4	8.1	9.6
4Pt/AlPO ₄ -5	90.0	30.6	61.7	6.8	0.9
4Pt-8WO _x /AlPO ₄ -5	100.0	66.5	26.3	6.9	0.3

Reaction conditions: OA = 2 g, catalyst = 10 wt. % of OA, solvent = 30 g of n-heptane, pressure = 20 bar of H₂, temperature = 320 °C, time = 5h, reactor = 300 ml Parr batch autoclave, RPM = 600. ^aDetermined by titration against NaOH, ^bQuantified by GC, ^cOthers include oxygenates like aldehyde, alcohol and esters.

3.3.2.1. Synergistic effect of Pt and promoter

The influence of WO_x as promoter on the catalytic deoxygenation activity of supported Pt catalyst with respect to time is depicted in Fig. 3.7. It is clear that Pt-8WO_x/AlPO₄-5 is more active (97 mol% acid conversion was observed even in a 30 min run at 320 °C and 20 bar H₂) than Pt/AlPO₄-5 catalyst (which showed only 58 mol%

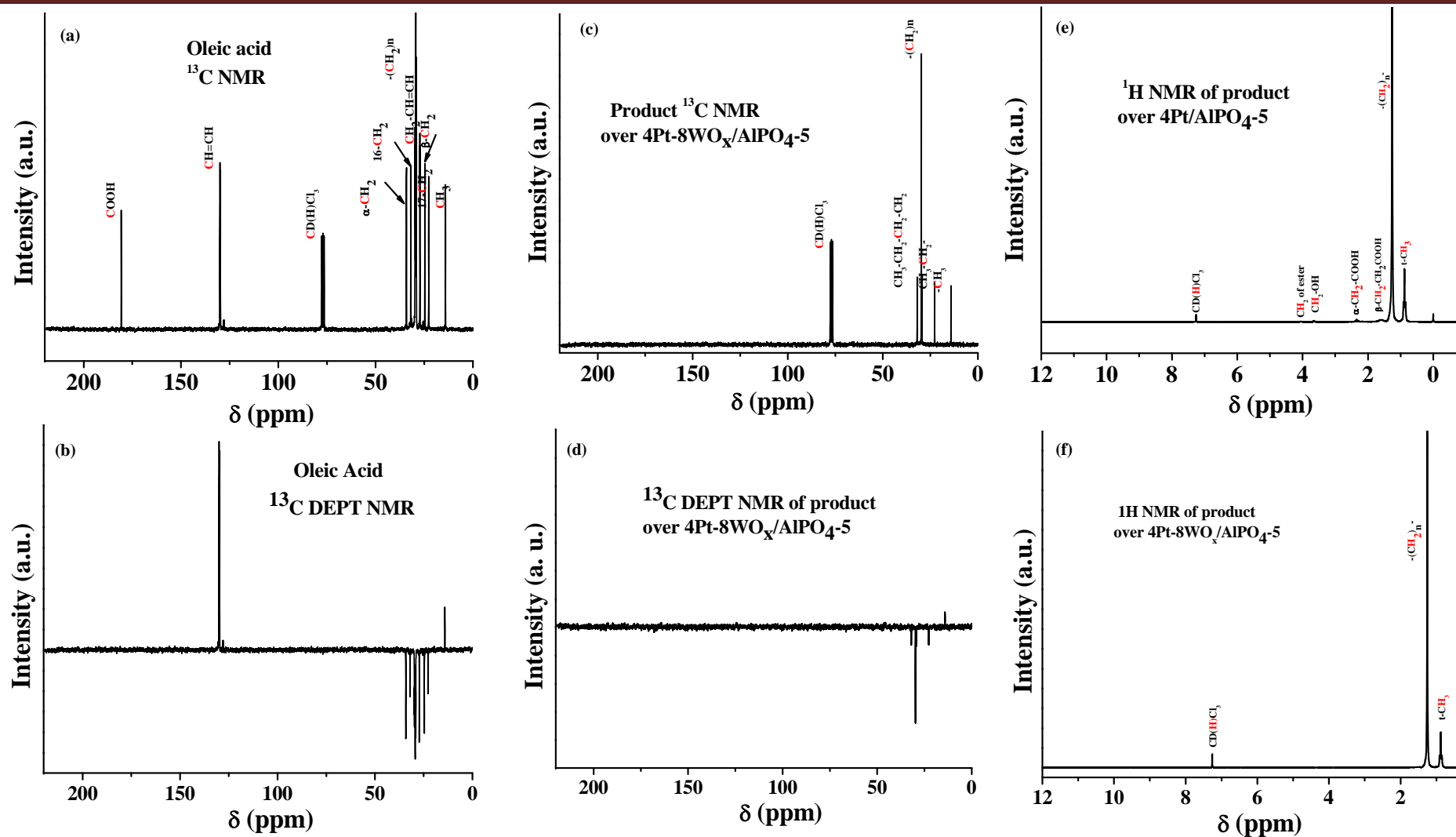


Fig. 3.6. ¹H and ¹³C NMR spectra of oleic acid and products over 4Pt/AlPO₄-5 and 4Pt-8WO_x/AlPO₄-5. Reaction conditions: same as in Table 3.2

of acid conversion). However, when the run was conducted for longer hours (5 h), this gap in acid conversion between these two catalysts decreased (to 10%; Fig. 3.7(a)). In other words, to achieve same conversion, the Pt catalyst without WO_x requires longer reaction time (> 5 h). This clearly reveals that WO_x enhances the catalytic activity of Pt. Interestingly, a switch over in the mechanism of deoxygenation from DCO to HDO (yielding more amount of C₁₈ product than C₁₇) occurred when WO_x was present along with Pt on AlPO₄-5 surface (Table 3.2; Fig. 3.7(b)). The reducibility of Pt is greatly enhanced by the addition of WO_x. This has led to an excellent H₂-spillover efficiency of Pt and thereby showed a remarkable catalytic activity even at less contact time (30 min). On the other hand, WO_x also showed partial reduction (Fig. 3.3) in presence of Pt, generating new active sites (probably surface hydroxyl groups by the partial reduction of WO_x). Thus, may in turn contribute to the activity enhancement and shifting the reaction mechanism (from DCO to HDO; Table 3.2). All of these changes are due to synergistic interactions between Pt and W. These observations revealed the crucial role of WO_x as promoter in determining the deoxygenation activity of supported Pt as well as product selectivity. The theoretical yield of the hydrocarbon product recovered after solvent removal by evaporation was more than 95%. Hence, even if some lighter products were formed they must have been in smaller amount only.

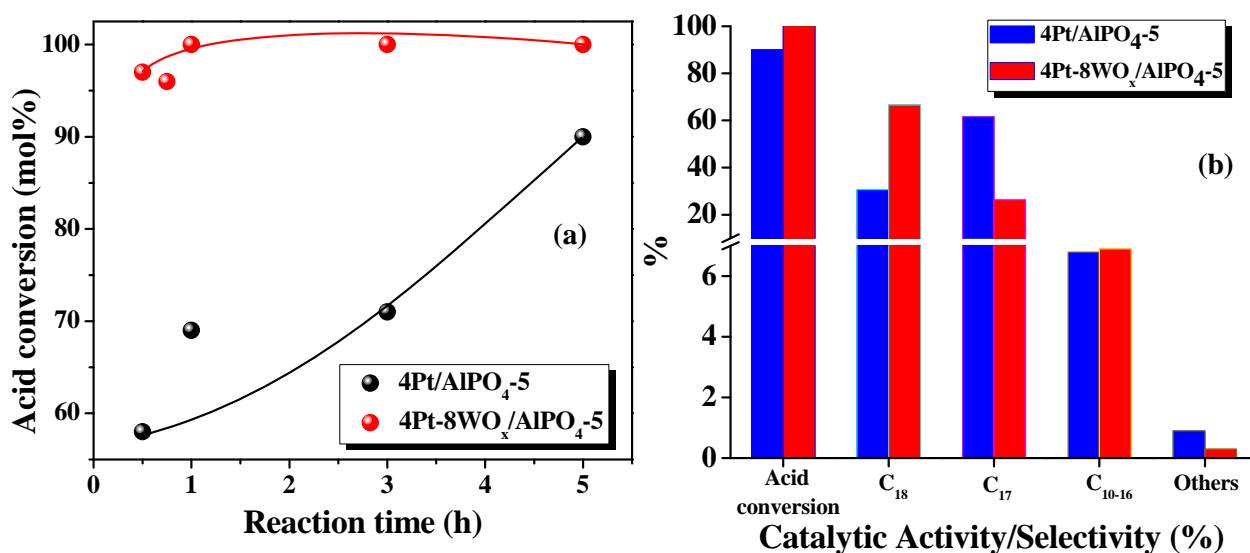


Fig. 3.7. Effect of WO_x promoter on the catalytic activity of Pt/AlPO₄-5 catalyst. *Reaction conditions:* OA = 2 g, catalyst = 10 wt. % of OA, solvent = 30 g of n-heptane, pressure = 20 bar H₂, temperature = 320 °C, reaction time = 0.5 - 5h (for a) and 5 h (for b), reactor = 300 ml Parr batch autoclave, revolutions per minute (RPM) = 600.

3.3.2.2. Effect of Pt and W composition

With a view to understand the influence of Pt and W composition, catalysts having varying amounts of Pt and W were prepared and tested for deoxygenation of OA at 320 °C and 20 bar H₂ for 5 h (Table 3.3). Catalytic activity decreased (from 100% to 35%) with increasing amount of W relative to Pt. The catalyst with Pt to W ratio of 1 : 2 showed complete conversion of OA and high selectivity for C₁₈ (78.3 %). A catalyst with 2 wt. % of Pt and 4 wt. % of W was found superior to others (Table 3.3; run no. 2). In other words, the ratio of Pt to W is crucial in designing promoted catalysts for superior catalytic activity and selectivity. As showed in Table 3.3, high W amount is detrimental to the catalytic activity as well as for the C₁₈ product selectivity. This is due to the fact that at higher W loadings the bulkier tungsten domains may be masking the Pt particles thereby hindering the exposure of Pt particles on the surface. This detrimental effect of high W loadings can also be attributed to low Pt dispersions in presence of bulky tungsten realms. However, from these observations, it was understood that a good synergistic interaction would be established with a certain ratio of Pt and W loadings only.

Table 3.3. Influence of Pt and W composition on the deoxygenation activity

Run No.	Catalyst	Acid conversion (mol %)	Product selectivity (Wt.%)			
			C ₁₈	C ₁₇	C ₁₀₋₁₆	Others
1	1Pt-2WO _x /AlPO ₄ -5	84.0	75.8	22.4	0.9	0.9
2	2Pt-4WO _x /AlPO ₄ -5	100	78.3	20.8	0.8	0.1
3	4Pt-8WO _x /AlPO ₄ -5	100	66.5	26.3	6.9	0.3
4	2Pt-8WO _x /AlPO ₄ -5	53.0	54.6	25.0	7.1	13.3
5	2Pt-12WO _x /AlPO ₄ -5	55.0	66.2	23.6	8.3	1.9
6	2Pt-16WO _x /AlPO ₄ -5	35.0	67.0	21.5	7.7	3.8

Reaction conditions: same as mentioned at Table 3.2

3.3.2.3. Effect of reaction temperature

A controlled deoxygenation study in the temperature range 260 to 320 °C (Table 3.4; run nos. 1 - 4) was performed with 4Pt-8WO_x/AlPO₄-5 catalyst. These results pointed out that 4Pt-8WO_x/AlPO₄-5 is highly active even at a temperature as low as 280 °C exhibiting 100% OA conversion to hydrocarbons and C₁₈ was the major product with a selectivity of 81.7%.

Meanwhile, higher temperatures led to some cracking of the hydrocarbon product (C₁₀ - 16 selectivity increases from 0.7 to 6.9%; Table 3.4, run no. 4). OA conversion of 93 mol% even at 260 °C reveals notable deoxygenation activity of the catalyst (with ~80 wt.% of C₁₈ selectivity) and the effect of WO_x promoter on Pt.

Table 3.4. Effect of reaction parameters on deoxygenation of OA over 4Pt-8WO_x/AlPO₄-5

Run No.	Parameter	Acid conversion (mol %)	Product selectivity (wt. %)			
			C ₁₈	C ₁₇	C ₁₀₋₁₆	Others ^d
<i>Effect of reaction temperature (°C)^a</i>						
1	260	93.0	80.8	18.3	0.9	0
2	280	100	81.7	17.6	0.7	0
3	300	100	75.0	23.8	0.7	0.5
4	320	100	66.5	26.3	6.9	0.3
<i>Effect of reaction time (h)^b</i>						
5	0.5	97.0	71.2	27.9	0.8	0.1
6	0.75	96.0	70.8	28.3	1.6	0.1
7	1.0	100	75.4	23.9	0.6	0.1
8	3.0	100	75.0	24.0	0.7	0.3
9	5.0	100	66.5	26.3	6.9	0.3
<i>Effect of hydrogen pressure (bar)^c</i>						
10	0	43.0	3.6	93.0	2.3	1.1
11	5	88.0	23.4	69.2	6.9	0.5
12	10	97.0	53.2	39.2	7.1	0.5
13	20	100	66.6	26.3	6.9	0.3

Reaction conditions: OA = 2 g, catalyst = 10 wt. % of OA, solvent = 30 g of n-heptane, reactor = 300 ml Parr batch autoclave, RPM = 600. *For a:* pressure = 20 bar H₂, time = 5 h, temperature = 260 - 320 °C. *For b:* pressure = 20 bar H₂, time = 0.5 - 5h, temperature = 320 °C, *For c:* pressure = 0 - 20 bar H₂ (in case of entry no. 10, the reactor was charged with 20 bar of N₂), time = 5h, temperature = 320 °C. ^dOthers include oxygenates like aldehyde, alcohol and esters.

3.3.2.4. Effect of reaction time

Even at 30 min of reaction time (at 320 °C and 20 bar of H₂), near complete conversion of OA (97.0 mol%) with 71.2 wt.% of C₁₈ selectivity was obtained over 4Pt-8WO_x/AlPO₄-5. At longer times (beyond 3 h) cracking of hydrocarbon and a consequent mild

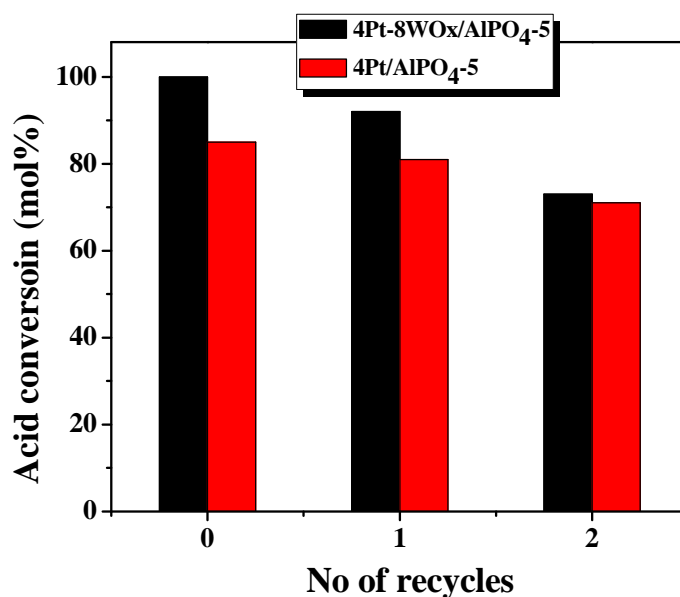
drop in C₁₈ selectivity (to 66.6 wt%) was observed (Table 3.4, run nos. 5-9). These data indicate that the WO_x-promoted catalyst is highly active even at short contact times.

3.3.2.5. Effect of hydrogen pressure

Hydrogen pressure was varied from 5 to 20 bar to understand its effect on the deoxygenation of OA over Pt-8WO_x/AlPO₄-5 catalyst. It is worthy to note that acid conversion increased from 88 to 100 mol% as the hydrogen pressure was changed from 5 – 20 bar. In addition to that, the HDO product selectivity increased from 23.4 to 66.5 % and DCO product selectivity decreased from 69.2 to 26.3 % indicating that high hydrogen pressure favors the HDO path (Table 3.4, run nos. 11-13). Deoxygenation occurs even in the absence of hydrogen and an acid conversion of 43 % was obtained with C₁₇ being the main product (selectivity = 93%) (Table 3.4, run no. 10). These observations point out that the catalyst of the study is active even in the absence of hydrogen but higher conversions and higher HDO selectivity could be obtained in the pressure of hydrogen.

3.3.3. Catalyst recyclability study

Fig. 3.8 illustrates the recyclability of unpromoted and WO_x-promoted Pt catalysts. Table 3.5 presents the recyclability data of 4Pt-8WO_x/AlPO₄-5 in deoxygenation of oleic acid and methyl oleate at 280 or 320 °C. In this study, at the end of each run, the catalyst was separated, washed with acetone and dried in an oven at 110 °C for 12 h. It was reduced in hydrogen (at 350 °C for 2.5 h) prior to use in the next recycle. It was observed that both of these catalysts lost their catalytic activity in recycling experiments. OA conversion dropped from 100 to 73 mol% for 4Pt-8WO_x/AlPO₄-5 and from 85 to 71 mol% for 4Pt/AlPO₄-5 after 2 recycles. To know the causes for the loss in activity, the spent catalysts were subjected to analysis by XRD (Fig. 3.9) and TEM (Fig. 3.10). TEM revealed that the average particle size of metallic platinum increased after reusing the catalyst. This increase was more (by 6 nm) for 4Pt/AlPO₄-5 than for 4Pt-8WO_x/AlPO₄-5 (by 1 nm). On the other hand, XRD confirmed the presence of Pt and WO_x in the spent catalysts. However, the crystallite size of Pt increased from 6.7 to 20 nm for 4Pt/AlPO₄-5 and from 16 to 23 nm for 4Pt-8WO_x/AlPO₄-5. Thus, tungsten oxide controlled the sintering of Pt particles. The notable feature in case of 4Pt-8WO_x/AlPO₄-5 was that the intensity of support peaks decreased suggesting loss in support crystallinity (Fig. 3.9). This is due to structure collapse which was observed only in case of WO_x-promoted Pt catalyst rather than unpromoted catalyst since promoted catalyst follows HDO mechanism where water is a byproduct. In presence of water, the hydrolysis of Al-O-P bonds causes loss in structural integrity of AlPO₄-5 support. This effect was not found in case

Fig. 3.8. Catalyst recyclability study. *Reaction conditions:* as mentioned in Table 3.5Table 3.5. Recyclability study of 4Pt-8WO_x/AlPO₄-5 catalyst

Recycle Number	Acid or ester conversion (mol %)	Product selectivity (wt. %)			
		C ₁₈	C ₁₇	C ₁₀₋₁₆	Others
<i>Reaction conditions:</i> oleic acid (OA) = 6 g, catalyst = 10 wt% of OA, n-heptane = 40 g, H ₂ pressure = 25 bar, reaction temperature = 320 °C, reaction time = 5 h, others include octadecanal and octadecanol.					
0 (Fresh)	100	80.0	19.0	0.8	0.2
1 st	92.0	85.1	13.0	1.6	0.3
2 nd	73.0	88.2	9.7	1.0	1.1
<i>Reaction conditions:</i> Methyl oleate (MO) = 6 g, catalyst = 10 wt% of MO, n-heptane = 40 g, H ₂ pressure = 25 bar, reaction temperature = 320 °C, reaction time = 5 h, others include oleic acid, stearic acid, octadecanal and octadecanol.					
0 (Fresh)	100	69.9	14.0	12.8	3.3
1 st	87.0	72.4	7.8	17.0	2.8
2 nd	48.0	44.7	6.9	30.0	18.4
<i>Reaction conditions:</i> Oleic acid (OA) = 6 g, catalyst = 10 wt% of OA, n-heptane = 40 g, H ₂ pressure = 25 bar, reaction temperature = 280 °C, reaction time = 5 h, others include octadecanal and octadecanol.					
0 (Fresh)	96.0	84.2	14.9	0.9	0
1 st	78.0	85.4	13.3	0.8	0.5
2 nd	60.0	67.2	16.2	0.6	16.0

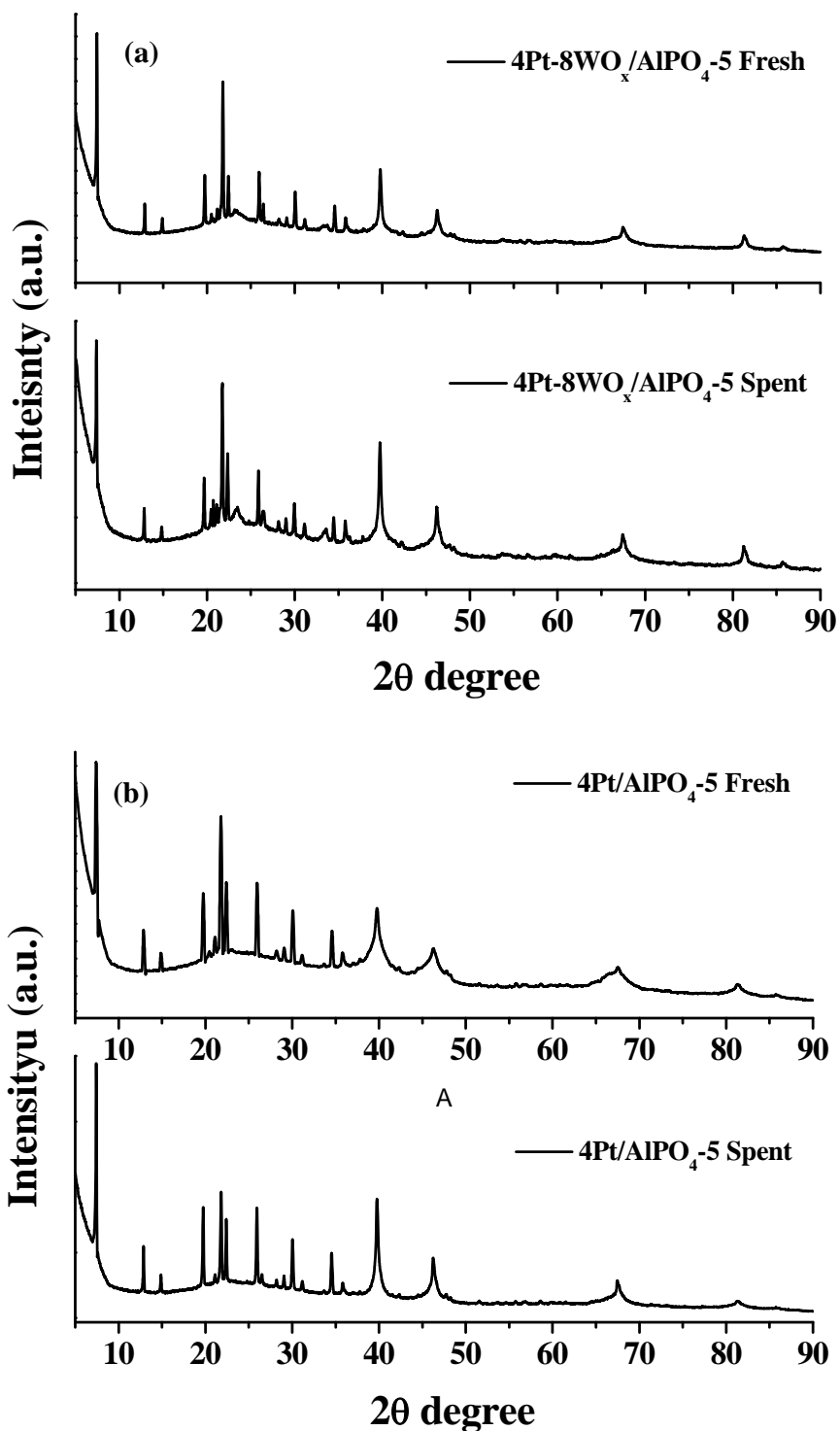


Fig. 3.9. XRD patterns of fresh and spent (a) 4Pt-8WO_x/AlPO₄-5 and (b) 4Pt/AlPO₄-5 catalysts. Reaction conditions: oleic acid (OA) = 6 g, catalyst = 10 wt% of OA, n-heptane = 40 g, H₂ pressure = 25 bar, reaction temperature = 320 °C, reaction time = 5 h.

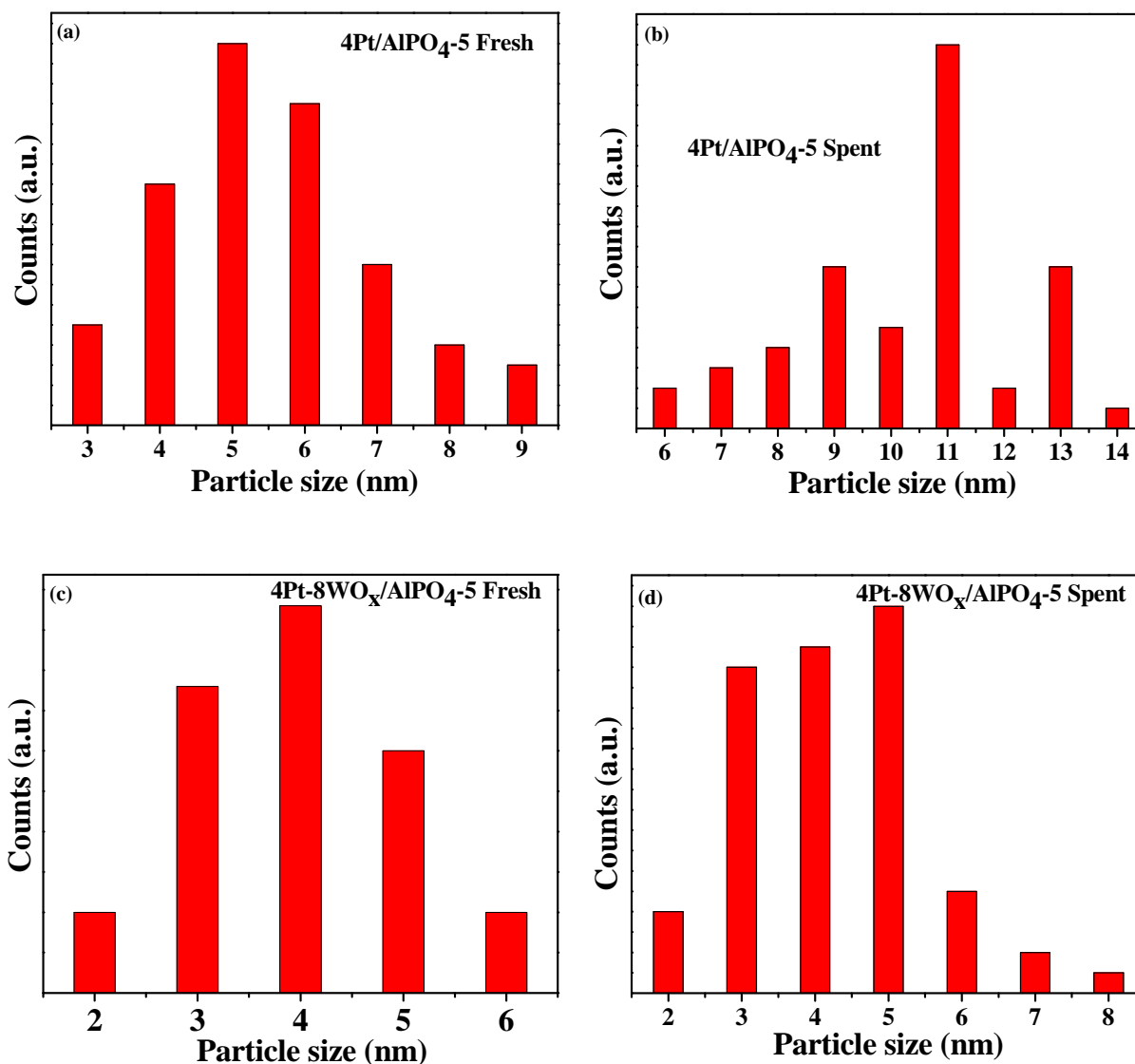


Fig. 3.10. TEM histogram profiles of spent Pt/AlPO₄-5 and 4Pt-8WO_x/AlPO₄-5 catalysts. Reaction conditions: same as mentioned in at Fig. 3.9.

4Pt/AlPO₄-5 catalyst as it followed DCO mechanism and the structure of support was intact (Fig. 3.9).

Such hydrothermal instability was observed also for SAPO-11 catalysts [47] and hydrolysis of Si-O(PO₃)-Al bonds and leaching of silica was reported in those catalysts. Therefore, the loss in AlPO₄-5 crystallinity (in case of 4Pt-8WO_x/AlPO₄-5) and sintering of Pt particles (in case of 4Pt/AlPO₄-5) are the causes of activity loss in recycling studies. Recycling studies were conducted also at 280 °C and by using methyl oleate instead of oleic acid. Even in those studies loss in catalytic activity was observed (Table 3.5). The present study reveals that even the Al-O(PO₃)-Al bond undergoes hydrolysis and structure collapses

at the reaction conditions. Thus further studies are needed to improve the stability of these catalysts to exploit their potential applications in biofuels manufacturing.

3.4. Conclusions

Tungsten oxide promoted Pt/AlPO₄-5 exhibits high catalytic activity even at 280 °C for deoxygenation of oleic acid (a representative fatty acid). These catalysts were superior to the unpromoted Pt/AlPO₄-5 catalyst. WO_x modified the structure (crystallite/particle size) and electronic (redox) properties of Pt. Interestingly, it switched over the deoxygenation mechanism from DCO to HDO path. The enhanced H₂-spillover (by 14.8 %; H₂-TPR) and presence of strong acid sites (300 - 500 °C; NH₃- TPD) are the cause for the high activity of Pt-WO_x/AlPO₄-5 catalysts even at lower temperatures. Catalysts with Pt to W weight ratio of 1:2 were found better than the rest of the ratio. TEM confirmed that Pt sintering was restricted by WO_x. On the other hand, Pt/AlPO₄-5 showed sintering of Pt to a greater extent. However, both of these catalysts lost their catalytic activity upon reuse. The loss in structural integrity due to hydrolysis of Al-O-P bonds (in case of 4Pt-8WO_x/AlPO₄-5) and considerable Pt sintering (in case of 4Pt/AlPO₄-5) are the main reasons for their loss in activity in recycling experiments. This study revealed the influence of promoter (WO_x) on the catalytic activity of Pt and hydrothermal stability of the AlPO₄-5 support for deoxygenation of vegetable oils/fatty acids producing fuel hydrocarbons.

3.5. References

- [1] D. C. Elliott, *Energy Fuels* 2007, 21, 1792–1815.
- [2] T. V. Choudhary, C. B. Phillips, *Appl. Catal A: Gen.* 2011, 397, 1–12.
- [3] P. M. Mortensen, J. D. Greenwaldt, P. A. Jensen, K. G. Knudsen, A. D. Jensen, *Appl. Catal. A: Gen.* 2011, 407, 1–19.
- [4] C. Zhao, T. Bruck, J. A. Lercher, *Green Chem.* 2013, 15, 1720–1739.
- [5] J. Satyarthi, T. Chiranjeevi, D. T. Gokak, P. S. Viswanathan, *Catal. Sci. Tech.* 2013, 3, 70–80.
- [6] E. Furimsky, *Catal. Today* 2013, 217, 13–56.
- [7] E. Santillan, -Jimenez, M. Crocker, *J. Chem. Tech. Biotechnol.* 2012, 85, 1041–1050.
- [8] *Hand Book of Biofuels: Process and Technologies*, (Eds.: R. Luque, J. Campelo, J. Clark), Woodhead Publishing Ltd., 2011.
- [9] R. W. Gosselink, S. A. W. Hollak, S.-W. Chang, J. van Haveren, K. P. de Jong, J. H.

- Bitter, D. S. van Es, *ChemSusChem* 2013, 6, 1576–1594.
- [10] M. Sna^ore, I. Kubic^ˇkova, P. M_{ki}-Arvela, K. Er_{nen}, D. Y. Murzin, *Ind. Eng. Chem. Res.* 2006, 45, 5708–5715.
- [11] B. Donnis, R. G. Egeberg, P. Blom, K. G. Knudsen, *Top. Catal.* 2009, 52, 229–240.
- [12] W. Kiatkittipong, S. Phimsen, K. Kiatkittipong, S. Wongsakulphasatch, N. Laosiripojana, S. Assabumrungrat, *Fuel Process. Technol.* 2013, 116, 16–26.
- [13] L. Boda, G. Onyesty_k, H. Solt, F. L_{nyi}, J. Valyon, A. Thernesz, *Appl. Catal. A: Gen.* 2010, 374, 158–169.
- [14] J. Hancs_k, Z. Eller, G. P_çlczmman, Z. Varga, A. Holl_g, G. Varga, *Clean Techn. Environ. Policy*, 2014, 16, 1445–1454.
- [15] B. Veriansyah, J. Y. Hau, S. K. Kim, S.-A. Hong, Y. J. Kim, J. S. Lim, Y.-W. Shu, S.-G. Oh, J. Kim, *Fuel* 2012, 94, 578–585.
- [16] T. M. Sankaranarayanan, M. Banu, A. Pandurangan, S. Sivasanker, *Bioresource Tech.* 2011, 102, 10717–10723.
- [17] J. K. Satyarthi, D. Srinivas, *Energy Fuels*, 2011, 25, 3318–3322.
- [18] US Patent No. 8,558,042 B2 (2013) - Syntroleum Corporation, US.
- [19] US Patent Appl. No. 2004/0230085 A1 (2004) - Birch Stewart Kolasch & Birch, US.
- [20] B. Peng, Y. Yao, C. Zhao, J. A. Lercher, *Angew. Chem. Int. Ed.* 2012, 51, 2072–2075.
- [21] B. Peng, X. Yuan, C. Zhao, J. A. Lercher, *J. Am. Chem. Soc.* 2012, 134, 9400–9405.
- [22] B. Peng, C. Zhao, S. Kasakov, S. Foraita, J. A. Lercher, *Chem. Eur. J.* 2013, 19, 4732–4741.
- [23] <http://www.nesteoil.com>.
- [24] US Patent No. 7,511,181 B2 (2009) - UOP LLC, US.
- [25] US 8,003,836 B2 (2011) - UOP LLC, US.
- [26] <http://www.uop.com/pr/releases/PR.EniEcofiningFacility.pdf>.
- [27] <http://www.petrobras.com.br/tecnologia/ing/hbio.asp>.
- [28] <http://www.tyson.com/RenewableEnergy/Initiative/Conoco/Default.aspx>.
- [29] R. Raut, V. V. Banakar, D. Srinivas, *J. Mol. Catal. A: Chem.* 2016, 417, 126–134.
- [30] US Patent No. 8,142,527 B2 (2012) - Ben-Furion University of the Negev Research and Development Authority, US.
- [31] US Patent No. 8,388,829 B2 (2013) - Battelle Memorial Institute, US.
- [32] J. Fu, F. Shi, L. T. Thomson Jr., X. Lu, P. L. Savage, *ACS Catal.* 2011, 1, 227–231.
- [33] E. W. Ping, J. Pierson, R. Wallace, J. T. Miller, T. F. Fuller, C. W. Jones, *Appl. Catal. A: Gen.* 2011, 396, 85–90.

- [34] H. G. Manyar, C. Paun, R. Pilus, D. W. Rooney, J. M. Thompson, C. Hardacre, *Chem. Commun.* 2010, 46, 6279–6281.
- [35] J. A. Lopez-Ruiz, R. J. Davis, *Green Chem.* 2014, 16, 683–694; g) A. T. Madsen, E. H. Ahmed, C. H. Christensen, R. Fehrmann, A. Riisager, *Fuel*, 2011, 90, 3433–3438.
- [36] S. Lestari, P. M_{ki}-Arvela, H. Bernas, O. Simakova, R. Sjöholm, J. Beltramini, G. Q. Max Lu, J. Myllyoja, I. Simakova, D. Y. Murzin, *Energy Fuels* 2009, 23, 3842–3845
- [37] P. T. Do, M. Chiappero, L. L. Lobban, D. E. Resasco, *Catal. Lett.* 2009, 130, 9–18.
- [38] M. Ahmadi, E. E. Macias, J. B. Jasinski, P. Ratnasamy, M. A. Carreon, *J. Mol. Catal. A: Chem.* 2014, 386, 14–19.
- [39] M. Ahmadi, A. Nambo, J. B. Jasinski, P. Ratnasamy, M. A. Carreon, *Catal. Sci. Tech.* 2015, 5, 380–388.
- [40] L. Yang, K. L. Tate, J. B. Jasinski, M. A. Carreon, *ACS Catal.* 2015, 5, 6497–6502.
- [41] M. Herskowitz, M. V. Landau, Y. Reizner, D. Berger, *Fuel* 2013, 111, 157–164.
- [42] M. Rabaev, M. V. Landau, R. Vidruk-Nehemya, V. Koukouliev, R. Zarchin, M. Herskowitz, *Fuel* 2015, 161, 287–294.
- [43] N. Chen, N. Wang, Y. Ren, H. Tominaga, E. W. Qian, *J. Catal.* 2017, 345, 124–134.
- [44] C. Wang, Z. Tian, L. Wang, R. Xu, Q. Liu, W. Qu, H. Ma, B. Wang, *ChemSusChem* 2012, 5, 1974–1983.
- [45] C. Wang, Q. Liu, X. Liu, L. Yan, C. Luo, L. Wang, B. Wang, Z. Tian, *Chinese J. Catal.* 2013, 34, 1128–1138.
- [46] W. Lutz, R. Kurzhals, S. Sauerbeck, H. Toufar, J.-C. Buhl, T. Gesing, W. Altenburg, C. Jäger, *Micropor. Mesopor. Mater.* 2010, 132, 31–36.
- [47] M. Rabaev, M. V. Landau, R. Vidruk-Nehemya, A. Goldbourn, M. Herskowitz, *J. Catal.* 2015, 332, 164–176.
- [48] M. V. Tsodikov, A. V. Chistyakov, M. A. Gubanov, P. A. Zharova, S. S. Shapovalov, A. A. Pasynskii, V. V. Kriventsov, I. I. Moiseev, *Rus. Chem. Bull. Int. Ed.* 2015, 64, 2062–2068.
- [49] D. Kim, D. R. Vardon, D. Murali, B. K. Sharma, T. J. Strathmann, *ACS Sustainable Chem. Eng.* 2016, 4, 1775–1784.
- [50] K. Maruta, Y. Liu, M. Inaba, I. Takahara, *Energy Fuels* 2010, 24, 2404–2409.
- [51] T. Asano, M. Tamura, Y. Nakagawa, K. Tomishige, *ACS Sustainable Chem. Eng.* 2016, 4, 6253–6257.
- [52] J. S. M'Boungou, J. L. Schmitt, G. Maire, F. Garin, *Catal. Lett.* 1991, 10, 391–400.
- [53] S. Zhu, X. Gao, Y. Zhu, G. Cui, H. Zheng, Y. Li, *Appl. Catal. B: Env.* 2014, 158–159,
-

- 391–399.
- [54] S. Zhu, X. Gao, Y. Zhu, Y. Li, *J. Mol. Catal. A: Chem.* 2015, 398, 391–398.
- [55] C. Liu, C. Zhang, S. Sun, K. Liu, S. Hao, J. Xu, Y. Zhu, Y. Li, *ACS Catal.* 2015, 5, 4612–4623.
- [56] S. Garc_a-Fernandez, I. Gandarias, J. Requies, M. B. G_emez, s. Bennici, A. Auroux, P. L. Arias, *J. Catal.* 2015, 323, 65–75.
- [57] J. Wang, N. Le, C. Yang, Y. Su, X. Zhao, A. Wang, *Chinese J. Catal.* 2016, 37, 1513–1519.
- [58] <http://www.iza-online.org/synthesis/default.htm>.
- [59] Z. Guo, C. Guo, Q. Jin, B. Li, D. Ding, *J. Porous Mater.* 2005, 12, 29–33.
- [60] A. J. Mora, A. N. Fitch, M. Cole, R. Goyal, R. H. Jones, H. Jobic, S. W. Carr, *J. Mater. Chem.* 1996, 6, 1831–1835.
- [61] Z. Zhu, G. Lu, Y. Guo, Y. Guo, Z. Zhang, Y. Wang, X.-Q. Gong, *ChemCatChem* 2013, 5, 2495–2503.
- [62] J. E. Benson, H. W. Kohn, M. Boudart, *J. Catal.* 1966, 5, 307–313.

Chapter-4
Deoxygenation of Fatty Acids over Reusable
Pt-WO_x/Al₂O₃ Catalyst

4.1. Introduction

Hydrodeoxygenation of sustainable feedstock like inedible oils / fatty acids is promising approach for producing diesel-range hydrocarbons [1-4]. These renewable, carbon-neutral biofuels could be used in conventional diesel engines as standalone fuels or as blends with the petro-diesel. Moreover, the hydrodeoxygenation process suits for large scale integration with petroleum refining. Neste oil (NExBTL) [5] and UOP-Eni (Ecofining) [6-8] have commercialized this process of iso-paraffin-rich diesel fuel substitute (green diesel). Mo and W promoted hydrotreating catalysts (Ni-Mo/Al₂O₃, Ni-W/Al₂O₃, Co-Mo/Al₂O₃ and Co-W/Al₂O₃) are used in the reaction [9-12]. However, drawbacks of this process are requirement of high hydrogen pressure (*ca.*, 50 - 80 bar) and high reaction temperature (*ca.*, 325 - 360 °C), making the process expensive.

Supported noble metals (Pd and Pt) are highly active even at low hydrogen pressures (*ca.*, 5 - 20 bar). They operate through decarbonylation / decarboxylation (DCO) route than hydrodeoxygenation / hydrodehydrogenation (HDO) mechanism resulting in paraffins having one carbon atom lesser than the feedstock [13-15]. Murzin and co-workers [16-20] made seminal contributions on deoxygenation of fatty acids and their derivatives using supported metal and noble metal catalysts, among which the Pd/C was found superior to Pt, Rh, Ni, Os and Ir/C. Do et al. [21] investigated the use of 1 wt.% Pt/Al₂O₃ for deoxygenation of methyl stearate with heptadecane (C₁₇) as the major product. After 5 h, the conversion of methyl stearate at 325 °C and 6.9 bar under H₂ flow was about 64% where as under helium flow it was 42%. The deactivation of the catalyst was observed in time-on-stream studies due to site blocking by oligomerization of unsaturated hydrocarbons and heavy compounds (*ca.*, symmetrical ketones) that lead to coke. Madsen et al. [22] accounted a study of hydrotreatment of oleic acid (OA) and tripalmitin mixture (in a molar ratio of 1:3) with 20 bar H₂ in a stirred batch autoclave using 5 wt.% Pt/γ-Al₂O₃ catalyst and found that the conversion of OA increased from 6 to 100% when the temperature was increased from 250 to 325 °C. Vonortas and Papayannakos [23] studied the effect of a refined palm oil on the hydrodesulphurization (HDS) of heavy atmospheric gasoil and vegetable oil mixtures with a Pt/γ-Al₂O₃ catalyst. Ahmadi et al. [24], employing bifunctional Pt/SAPO-11 and Pt/chloride Al₂O₃ catalysts, combined the steps of decarboxylation and further isomerization/aromatization of the resultant product of oleic and palmitic acids to gasoline/diesel-range hydrocarbons. The degree of decarboxylation decreased in recycling experiments due to formation of carbonaceous matter on the catalyst surface. Yang et al. [25, 26] reported the application of

metal organic framework-supported Pt catalysts for decarboxylation of oleic acid. Octadecane and heptadecane with product distribution of 55.1 and 21.53%, respectively, in the liquid product, at an oleic acid conversion of 92%, were obtained by using Pt/Ga-MOF catalyst at 320 °C, 20 bar hydrogen pressure and after a reaction time of 2 h [25]. By using Pt/ZIF-67 membrane/zeolite 5A bead catalyst, these authors obtained heptadecane with a selectivity of 91% in presence of CO₂ [26].

Tsodikov et al. [27] investigated deoxygenation of individual fatty esters and fatty acid triglycerides from vegetable oils and lipid extracts from microalgae in the presence of Pt-Sn/Al₂O₃ catalysts prepared by deposition method. Co-deposition of Sn altered the activity and selectivity of Pt in the deoxygenation reaction and the alkene amount in hydrocarbon products mixture increased with increasing Sn fraction in the catalyst. Chistyakov et al. [28] presented the use of Pt-Sn/Al₂O₃ for reductive deoxygenation of rapeseed oil. Rabaev et al., [29, 30] probed hydrodeoxygenation, isomerization and aromatization of vegetable oils over Pt/SAPO-11 and Pt/Al₂O₃/SAPO-11 catalysts. Addition of amine surfactant (hexadecylamine) to SAPO-11 crystallization gel increased the hydrothermal stability of SAPO-11. A stable operation with >99% deoxygenation and liquid organic product containing 15% mono-aromatics and with cloud point less than -35 °C was achieved.

γ -Al₂O₃ is a versatile material not only in the area catalysis as catalyst or catalyst support but also in various fields like gas purifications, abrasive materials, paints, glass, cosmetics etc. γ -Al₂O₃ is one of the transition forms of aluminum oxide. Its structure is assigned traditionally to defect cubic spinel (space group of Fd $\bar{3}$ m) with vacancies on Al(III) positions. The unit cell consists of 32 oxygen and 64/3 Al(III) to fulfill stoichiometry [31]. However, Al (III) ions can occupy both the tetrahedral and octahedral positions but the precise Al occupancy is still a matter of debate.

In general, to make the deoxygenation process cost effective the following conditions needs to be satisfied: (1) operation at lower temperature (< 300 °C) and pressure (\leq 20 bar H₂), (2) minimal carbon loss or enhanced C₁₈/C₁₇ selectivity and (3) catalyst stability and reusability. Chapter 3 revealed the influence of WO_x as promoter on the deoxygenation activity of Pt supported on AlPO₄-5. Though the catalyst was proved excellent agent for green diesel production from oleic acid, it was found that the hydrothermal stability of the support at reaction conditions was the main issue. Thus, it is important to develop a stable promoted Pt based catalyst for deoxygenation. In view of the above objectives, it is reported here, for the first time, the application of Pt-WO_x/Al₂O₃ for deoxygenation of fatty acids and their methyl esters at 260 - 320 °C and 0 - 20 bar H₂ pressure producing green diesel.

Recently, Al₂O₃ and ZrO₂-supported Pt-WO_x catalysts have been examined for selective hydrogenolysis of glycerol to 1, 3-propanediol [32-34]. Their application in green diesel production has not been reported. Herein, WO_x could act as structural and electronic modifier of Pt and influence its catalyst performance.

4.2. Experimental

4.2.1. Catalyst Preparation

A commercial γ -Al₂O₃ (supplied by Süd-Chemie India Pvt. Ltd., New Delhi) was used as support in this study. The WO_x and Pt were loaded on γ -Al₂O₃ by wet impregnation method. A detailed procedure for the preparation of these catalysts is given in Chapter-2.

4.2.2. Catalyst Characterization and reaction procedure

The physicochemical properties of the catalysts used in this study were probed by various characterization techniques as described in Chapter-2. The deoxygenation reaction and product analysis methods are same as mentioned in Chapter-2.

4.3. Results and discussion

4.3.1. Catalyst characterization

4.3.1.1. X-ray diffraction

Platinum (1–4 wt.%) and tungsten (2–16 wt.%) were deposited on γ -Al₂O₃ by wet impregnation method. 4Pt/Al₂O₃ (reduced at 350 °C in hydrogen atmosphere) showed characteristic X-ray powder diffraction (XRD) peaks at 39.7, 46.2, 67.3, 81.3 and 85.6° arising from (111), (200), (220), (311) and (322) planes of metallic Pt in a cubic closed-packed structure with a space group of Fm $\bar{3}$ m (JCPDS No. 65-2868) [Fig. 4.1(a)]. The first three and the fifth peaks of Pt⁰ overlapped with the XRD peaks of the support, γ -Al₂O₃. Reduced 4Pt-8WO_x/Al₂O₃ exhibited a marginal shift in Pt⁰ peak positions (to 39.8, 46.3, 67.5, 81.3 and 85.9°) pointing out the influence of tungsten on platinum structure. No additional peaks (at 23.6 and 33.5°) due to crystalline monoclinic tungsten oxide [35] were detected until the tungsten content was 16 wt% [Fig. 4.1(b)]. Thus at a W concentration of <16 wt.%, WO_x is homogeneously dispersed on the support surface. Zhu et al. [33] reported similar observations. In other words, in the present catalyst (4Pt-8WO_x/Al₂O₃), tungsten is in the dispersion threshold (or sub-monolayer coverage). In Chapter-3, it was found that X-ray detectable crystalline WO_x forms even at 8 wt.% loading when deposited on AlPO₄-5.

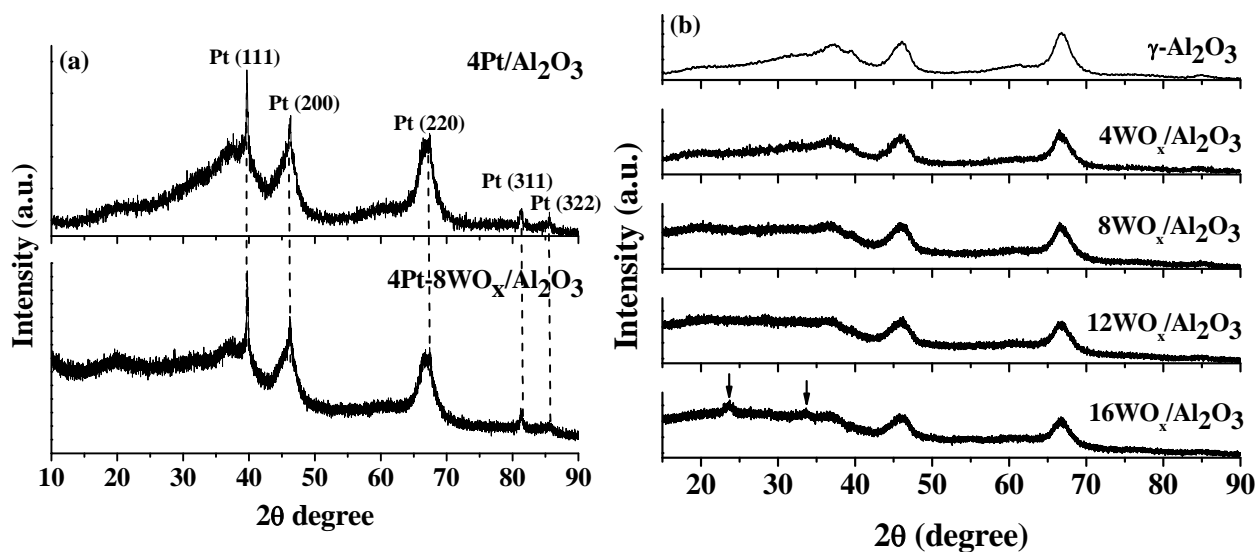


Fig. 4.1. XRD profiles of (a) reduced 4Pt/Al₂O₃ and 4Pt-8WO_x/Al₂O₃ and (b) "bare" γ -Al₂O₃ and WO_x loaded Al₂O₃.

4.3.1.2. N₂-Physisorption

N₂-physisorption experiments reveals that upon Pt and W loading, the specific surface area (S_{BET}) of γ -Al₂O₃ decreases from 352 m²/g to 292 m²/g (for 4Pt/Al₂O₃) and 266 m²/g (for 4Pt-8WO_x/Al₂O₃) (Table 4.1). Pore volume decreased from 0.68 to 0.67 and 0.57 cc/g, respectively, due to occlusion of Pt and WO_x in the pores and pore mouths of γ -Al₂O₃. However, an increase in average pore size from 3.9 nm (for γ -Al₂O₃) to 4.5 nm (for 4Pt/Al₂O₃) and 4.3 nm (for 4Pt-8WO_x/Al₂O₃) was observed (Table 4.1). It is likely that a small portion of impregnated Pt/W also gets into the lattice of γ -Al₂O₃ and thereby altering the pore size.

4.3.1.3. NH₃-TPD

Acidic properties of the catalysts were determined by temperature-programmed desorption of ammonia (NH₃-TPD) method (Table 4.2). The desorption profile of γ -Al₂O₃ contained two broad peaks with temperature maxima at 157 and 336 °C which are attributed to acid sites of weak and strong strength, respectively (Fig. 4.2). 4Pt/Al₂O₃ showed a similar NH₃ desorption profile but with higher intensity of the high temperature peak, implying a larger number of stronger acid sites when Pt was impregnated on γ -Al₂O₃. 4Pt-8WO_x/Al₂O₃ on the other hand, showed an additional desorption peak at 249 °C corresponding to acid sites of WO_x (Fig. 4.2). Also, the peak at 336 °C was more intense than in 4Pt/Al₂O₃. The amount of NH₃ desorbed from these catalysts in the temperature range (200–550 °C) increased in the order: γ -Al₂O₃ (0.586 mmol/g) < 4Pt/Al₂O₃ (0.707 mmol/g) < 4Pt-8WO_x/Al₂O₃ (0.881 mmol/g). Thus, WO_x enhances the acidity of the catalysts. The spread of the high temperature

Table 4.1. N₂-physisorption, CO-chemisorption and TEM data of Al₂O₃-supported Pt catalysts

Catalyst	N ₂ -Physisorption			CO-chemisorption				Pt average particle size (nm; TEM)
	S _{BET} (m ² /g)	Pore volume (cc/g)	Avg. pore size (nm)	Pt metal dispersion (%)	Average crystallite size (nm)	Monolayer uptake of CO (μmol/g)	Pt metal surface area (m ² /g)	
γ-Al ₂ O ₃	352	0.68	3.9	-	-	-	-	-
4Pt/Al ₂ O ₃	292	0.67	4.5	98	1.2	100	242	2.5
4Pt-8WO _x /Al ₂ O ₃	266	0.57	4.3	84	1.4	86	207	3.0
4Pt-8WO _x /Al ₂ O ₃ spent	212	0.40	3.8	23	4.9	24	57	5.0

Table 4.2. Acidic properties (NH₃-TPD) of Al₂O₃-supported Pt catalysts

Catalyst	Total acidity (mmol NH ₃ /g)	Acid strength distribution		
		Weak (<200 °C)	Medium (200-300 °C)	Strong (>300 °C)
γ-Al ₂ O ₃	0.99	0.403	0.213	0.373
4WO _x /Al ₂ O ₃	1.15	0.483	0.404	0.261
8WO _x /Al ₂ O ₃	1.24	0.545	0.431	0.263
12WO _x /Al ₂ O ₃	1.28	0.63	0.468	0.174
16WO _x /Al ₂ O ₃	1.30	0.530	0.616	0.154
4Pt/Al ₂ O ₃	1.27	0.562	0.633	0.074
4Pt-8WO _x /Al ₂ O ₃	1.41	0.380	0.556	0.325

peak up to 500 °C do not rule out the possibility of some Brønsted acid sites in these catalyst samples. An enhancement in total acidity and the acidity of weak and moderate sites was observed with increasing tungsten content on γ -Al₂O₃ (Table 4.2).

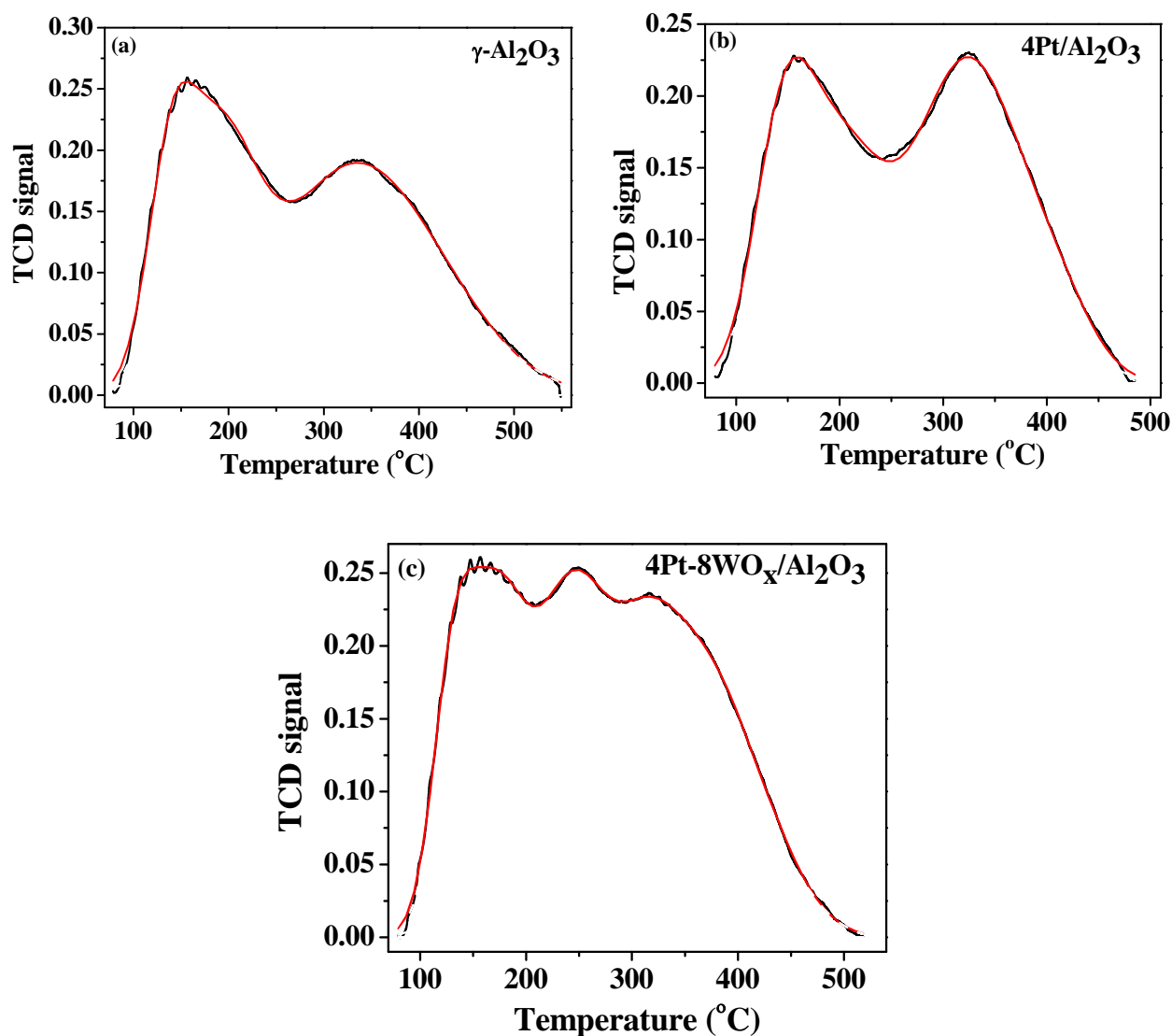


Fig. 4.2. NH₃-TPD profiles of (a) γ -Al₂O₃, (b) 4Pt/Al₂O₃ and (c) 4Pt-8WO_x/Al₂O₃.

4.3.1.4. CO-chemisorption

Tungsten had a marked effect on the CO-uptake of the catalyst (Table 4.1). The chemisorption studies revealed a decrease in monolayer CO uptake from 100 μ mol/g (for 4Pt/Al₂O₃) to 86 μ mol/g (for 4Pt-8WO_x/Al₂O₃). This corresponds to an increase in average metal crystallite size from 1.2 nm (for 4Pt/Al₂O₃) to 1.4 nm (for 4Pt-8WO_x/Al₂O₃) and decrease in metal dispersion from 98 to 84%. Pt surface area decreases from 242 (for 4Pt/Al₂O₃) to 207 m²/g (for 4Pt-8WO_x/Al₂O₃). In other words, tungsten deposition leads to

larger crystallites of Pt. A similar effect of tungsten on Pt was observed also for Pt-WO_x/AlPO₄₋₅ catalysts (Chapter-3).

4.3.1.5. TEM

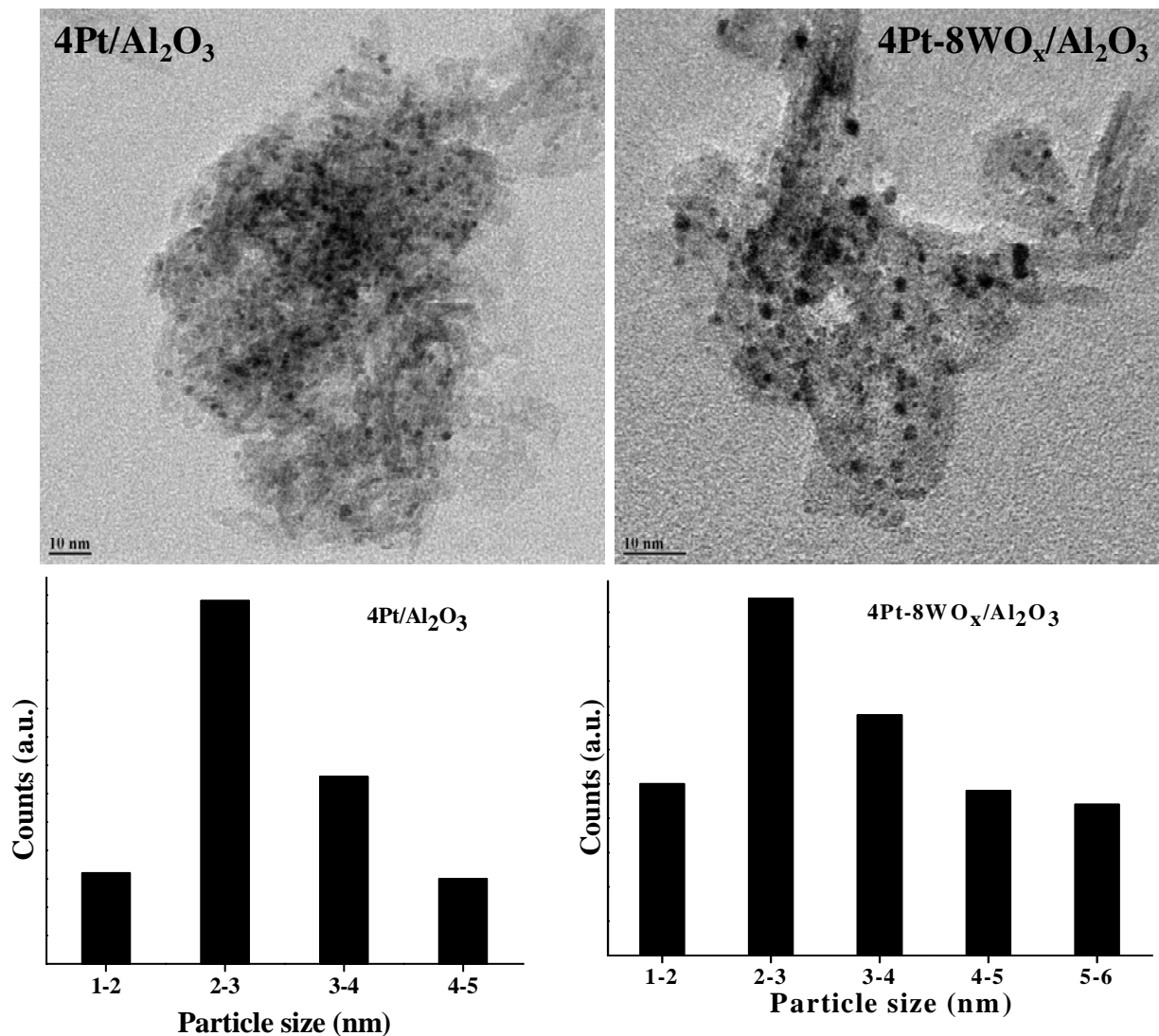


Fig. 4.3. TEM images and corresponding Pt particle size histograms of 4Pt/Al₂O₃ (left) and 4Pt-8WO_x/Al₂O₃ (right).

According to TEM analysis, Pt particles in 4Pt/Al₂O₃ and 4Pt-8WO_x/Al₂O₃ are in the range of 1–6 nm. TEM images and particle size distribution curves (Fig. 4.3) infer that tungsten increases marginally the mean particle size of Pt from 2.5 to 3 nm as well as the spread of particle size distribution of Pt. This trend in TEM agrees well with the CO-chemisorption data.

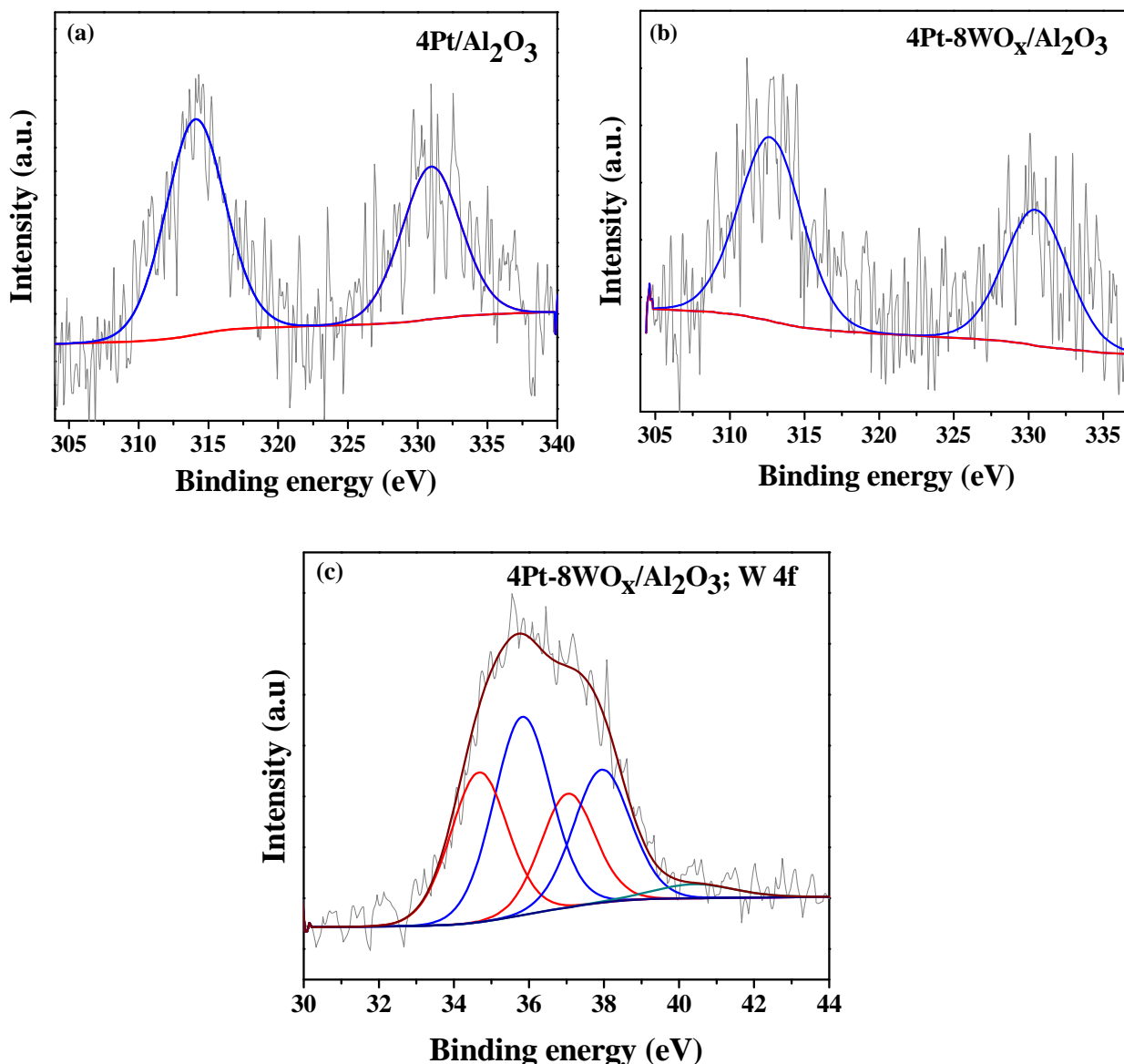


Fig. 4.4. XPS of Pt 4d lines for (a) Pt/Al₂O₃ and (b) Pt-8WO_x/Al₂O₃ and (c) W 4f lines of 4Pt-8WO_x/Al₂O₃ catalysts

4.3.1.6. X-ray photoelectron spectroscopy

The surface chemical species of the reduced catalysts were probed by XPS. 4Pt/Al₂O₃ showed two peaks at 314.2 and 331.0 eV ascribed to Pt 4d_{5/2} and Pt 4d_{3/2} of metallic Pt, respectively (Fig. 4.4). XPS provided clear evidence for the complete reduction of platinum to its metallic state [35]. The absence of platinum oxide peaks in XRD also confirms the complete reduction of platinum. The Pt 4d lines were followed instead of the most intense Pt 4f lines due to their overlap with the strong Al 2p peaks [37]. For 4Pt-8WO_x/Al₂O₃, the peaks due to Pt 4d_{5/2} and Pt 4d_{3/2} shifted to lower binding energy (312.6 and 330.4 eV, respectively). This shift in peaks positions is an indication of the electronic effect of tungsten

oxide. Platinum in 4Pt-8WO_x/Al₂O₃ is richer in electron density than in 4Pt/Al₂O₃. On the other hand, in W 4f region, peaks corresponding to both +6 and +5 oxidation states of tungsten were observed (Fig. 4.4). W⁶⁺ showed peaks at 35.8 and 38.0 eV due to W 4f_{7/2} and W 4f_{5/2} lines. The spin-orbit components for W⁵⁺ species appeared at 34.7 and 37.1 eV, respectively [33, 38]. Surface W⁶⁺ and W⁵⁺ species are in the proportion of 56% and 44%, respectively. The hydrogen atoms from dissociatively adsorbed hydrogen molecule on Pt surface would spillover onto WO_x surface and lead to its reduction from W⁶⁺ to W⁵⁺ state [39]. Accordingly, electron donor-acceptor interaction between Pt⁰ and WO_x would probably take place on γ-Al₂O₃ surface. The peak due to W 2p was observed at 40.6 eV. From these observations, it is understood that addition of WO_x enhances the reducibility of Pt (making it electron rich) due to enduring synergistic effect between Pt and WO_x. This may, in turn enhance the H₂ splitting and thereby, facilitate deoxygenation activity. In a similar manner, the presence of nascent H species (H⁺ and H⁻) generated by H₂ splitting over Pt particles, could perform partial reduction of WO_x forming surface hydroxyl groups. Partial reduction of WO_x is well evidenced by XPS. Hence, the surface hydroxyl groups on the WO_x domains may act as new and potential active sites for activation of fatty acids differing from the way of the fatty acid activation happens directly on the support and they by change the reaction path in deoxygenation.

4.3.2. Catalytic activity

Deoxygenation of fatty acids occurs by different reaction pathways. In the hydrodeoxygenation / hydrodehydration (HDO) route, oxygen in the fatty acid is removed as water while forming a hydrocarbon with same number of carbon atoms as that of parent fatty acid (Eq. (1)). In the decarbonylation and decarboxylation (DCO) routes, the oxygen in the fatty acid is removed as CO and CO₂, respectively, while forming a hydrocarbon having one carbon atom lesser than the parent fatty acid [Eqs. (2) and (3)]. The extents of HDO and DCO reactions depend on the nature of the catalyst and reaction conditions. Supported noble metal catalysts often follow the DCO pathway in fatty acid deoxygenation.

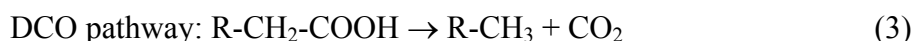
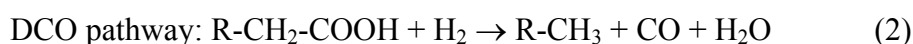


Table 4.3 presents comparative catalytic activity data of different Al₂O₃-supported Pt catalysts in deoxygenation of oleic acid (OA). Control experiments (Table 4.2, Run No. 1) pointed out that this reaction doesn't proceed in the absence of a catalyst at the chosen

experimental conditions (320 °C, 20 bar H₂, 5 h). Neat γ -Al₂O₃ enabled OA conversion of 17 mol%. Octadecane (C₁₈) and heptadecane (C₁₇) formed in 40.6 and 44.0% selectivity, respectively. A large amount (12.7%) of other products (which include octadecanal and octadecanol) was formed. In presence of 8WO_x/Al₂O₃, OA conversion was nearly the same (18 mol%) as in case of Al₂O₃ but then, C₁₈ (formed through HDO mechanism) is the major product (74% selectivity). A significant amount (22.1%) of other products was also detected. Over Pt/Al₂O₃, conversion of OA boosted to 74–76% (Table 4.3, Run Nos. 4 and 5), C₁₇ (formed through DCO mechanism) is the major product (selectivity 79–83.7%). Interestingly, over Pt-WO_x/Al₂O₃ catalysts (Table 4.3, Run Nos. 7–11) complete conversion of OA and high selectivity for C₁₈ was observed. Other products were negligible. Thus, this study reveals a synergistic enhancement in catalytic activity (OA conversion) and reversal in product selectivity from C₁₇ (for Pt/Al₂O₃) to C₁₈ (for Pt-WO_x/Al₂O₃) when both Pt and WO_x were present in the catalyst composition (Fig. 4.5).

Table 4.3. Influence of Pt and Pt-WO_x composition on the catalytic deoxygenation of OA

Run No.	Catalyst	Acid conversion (mol%) ^a	Product selectivity (wt.%) ^b			
			C ₁₈	C ₁₇	C ₁₀₋₁₆	Others ^c
1	-	1.0	1.6	13.2	5.6	79.6
2	γ -Al ₂ O ₃	17.0	40.6	44.0	2.7	12.7
3	8WO _x /Al ₂ O ₃	18.0	74.3	2.2	1.4	22.1
4	2Pt/Al ₂ O ₃	74.0	15.2	83.7	0.9	0.2
5	4Pt/Al ₂ O ₃	76.0	19.0	79.0	1.6	0.4
6	1Pt-2WO _x /Al ₂ O ₃	72.0	36.1	61.4	1.8	0.7
7	2Pt-4WO _x /Al ₂ O ₃	98.0	52.0	47.0	1.0	0
8	4Pt-8WO _x /Al ₂ O ₃	100	67.1	31.6	1.3	0
9	2Pt-8WO _x /Al ₂ O ₃	100	63.0	36.0	1.0	0
10	2Pt-12WO _x /Al ₂ O ₃	100	67.6	31.6	0.8	0
11	2Pt-16WO _x /Al ₂ O ₃	100	73.6	25.6	0.8	0

Reaction conditions: OA = 2 g, catalyst = 10 wt. % of OA, solvent = 30 g of n-heptane, pressure = 20 bar of H₂, temperature = 320 °C, time = 5h, reactor = 300 ml Parr batch autoclave, RPM = 600. ^aDetermined by titration against NaOH, ^bQuantified by GC, ^cOthers include oxygenates like aldehyde, alcohol and esters.

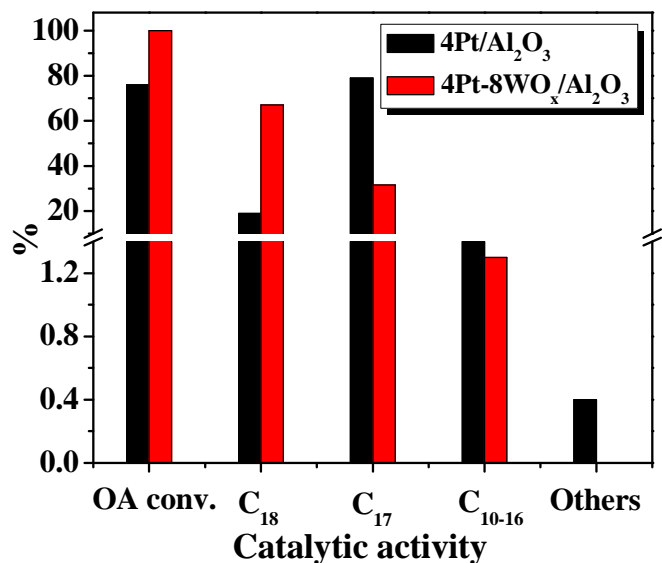


Fig. 4.5. Effect WO_x-promoter on the deoxygenation of OA over Pt/Al₂O₃. Reaction conditions: same as in Table 4.3.

Confirmation for C₁₇ and C₁₈ paraffin formation was obtained from ¹H NMR (Fig. 4.6) and GC-MS. As found in Chapter-3, even in this study, WO_x promoter showed as marked effect deoxygenation activity/selectivity of Pt/Al₂O₃.

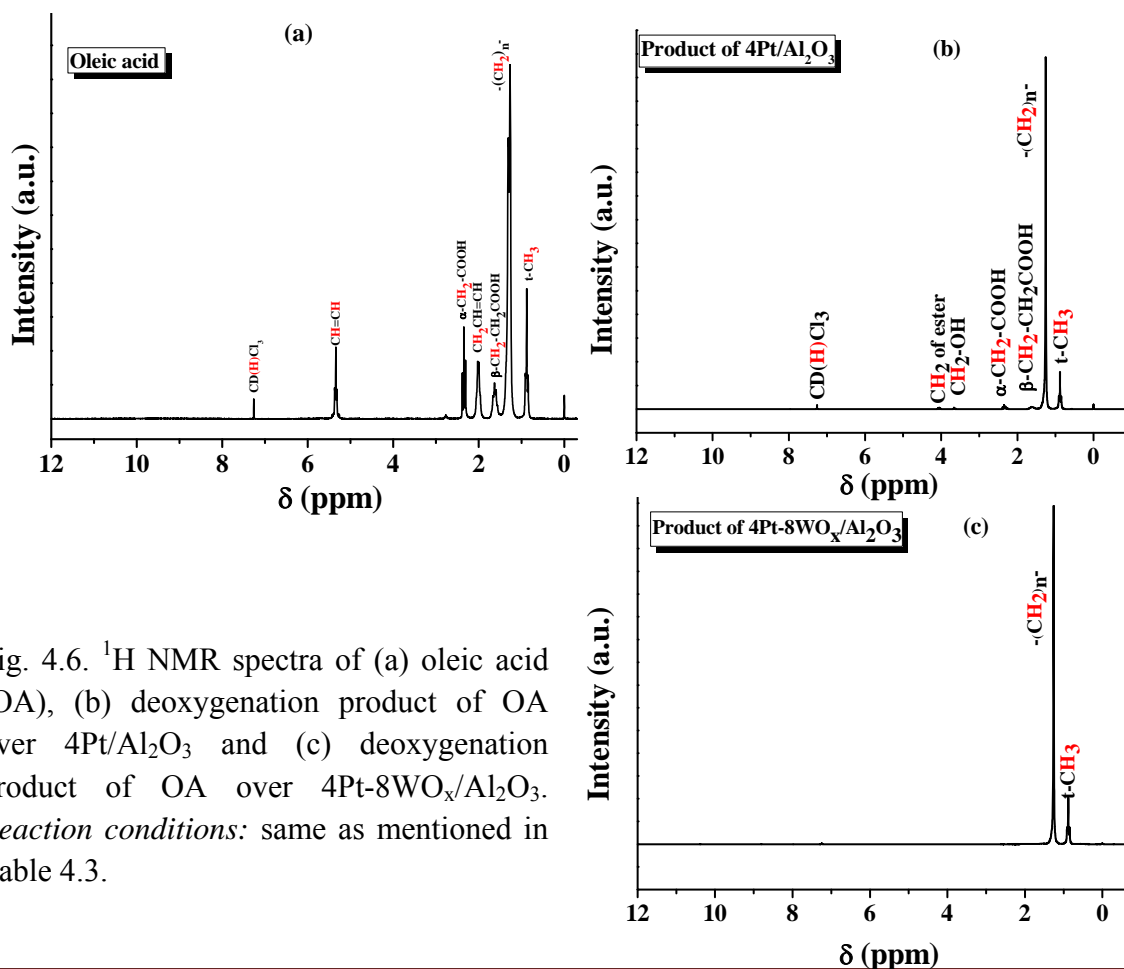


Fig. 4.6. ¹H NMR spectra of (a) oleic acid (OA), (b) deoxygenation product of OA over 4Pt/Al₂O₃ and (c) deoxygenation product of OA over 4Pt-8WO_x/Al₂O₃. Reaction conditions: same as mentioned in Table 4.3.

4.3.2.1. Influence of WO_x promoter

As shown in Chapter-3, WO_x has a marked effect on the activity and selectivity of Al₂O₃-supported Pt catalyst. WO_x-promoted Pt/Al₂O₃ was significantly more active than the unpromoted Pt/Al₂O₃ in converting fatty acids to renewable fuel hydrocarbons (Fig. 4.5). A considerable shift in the product selectivity (from DCO to HDO) occurred when WO_x was also present on the catalyst along with Pt. The Pt and W composition had also a definite effect (Table 4.3, compare Run Nos. 7, 9, 10 and 11) on catalytic activity. C₁₈ product selectivity increased with increasing W content. A composition with 8 wt% W was found optimum. Note that at this composition tungsten is in the limits of dispersion threshold (XRD) [32, 33]. While maintaining Pt to W weight ratio at 1:2, the content of Pt was increased from 1 to 2 and 4 wt.%. An increase in OA conversion from 72 to 100 mol% and C₁₈ selectivity from 36.1 to 67.1% and decrease in C₁₇ selectivity from 61.4 to 31.6% was observed. 2Pt-4WO_x/Al₂O₃ exhibited OA conversion of 98 mol% under similar conditions, but C₁₈ selectivity was 52% and C₁₇ was 47% (Table 4.3, Run No.7). A plot between OA conversion and Pt content (Fig. 4.7) reveals that the catalyst, 4Pt-8WO_x/Al₂O₃ demonstrates optimum catalytic activity in the deoxygenation reaction.

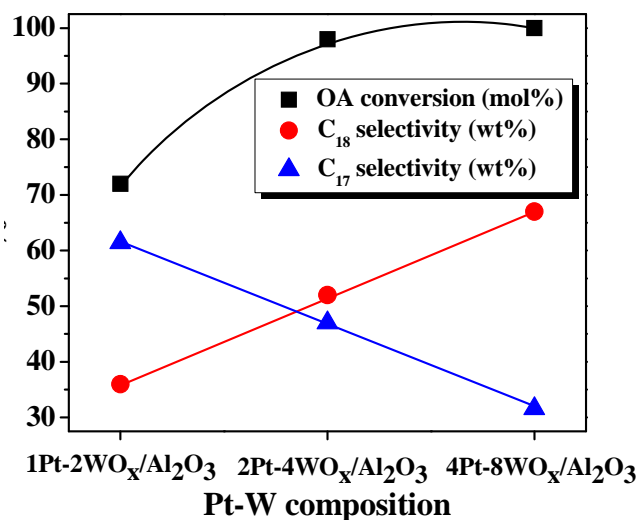


Fig. 4.7. Effect of Pt-W composition on the deoxygenation of OA. *Reaction conditions:* same as mentioned in Table 4.3.

Fig. 4.8 depicts catalytic activity of 4Pt/Al₂O₃ and 4Pt-8WO_x/Al₂O₃ as a function of reaction time at 280 and 320 °C. It took about 1 h for the reactor to attain the steady temperature of 280 °C. Even at the start of reaction at 280 °C, 4Pt-8WO_x/Al₂O₃ showed OA to paraffins conversion of 63 mol% which increased with reaction time to 85 mol% at the end

of 1 h and to 98% after 5 h. 4Pt/Al₂O₃ catalyst, on the other hand, showed only 23 mol% conversion of OA at the beginning of the reaction (at 280 °C) which increased to 40 mol% after 1 h of reaction (Fig. 4.8(a)). OA conversion without any catalyst at 280 °C was 6 mol%. Over 4Pt/Al₂O₃, at 320 °C, OA conversion increased with increasing reaction time and attained a maximum of 74 mol% after 5 h. Under similar conditions 4Pt-8WO_x/Al₂O₃ exhibited complete conversion of OA within 0.5 h itself (Fig. 4.8(b)). All these results point out that the bimetallic catalyst exhibits higher activity than 4Pt/Al₂O₃. Irrespective of OA conversion, product selectivity was nearly the same throughout the run (Table 4.4; Run Nos. 11-14). In other words, the tungsten promoted Pt catalyst was selective for the hydrodeoxygenation product (C₁₈; 65–71%) while the unpromoted Pt catalyst was selective for the decarboxylation product (C₁₇; 68–74%). Based on conversions at 15 min, turnover frequency (TOF; moles of OA to paraffins conversion per mole of exposed surface Pt atoms determined from CO chemisorption per hour) for 4Pt/Al₂O₃ and 4Pt-8WO_x/Al₂O₃ were determined to be 1.8 and 6.0 h⁻¹, respectively.

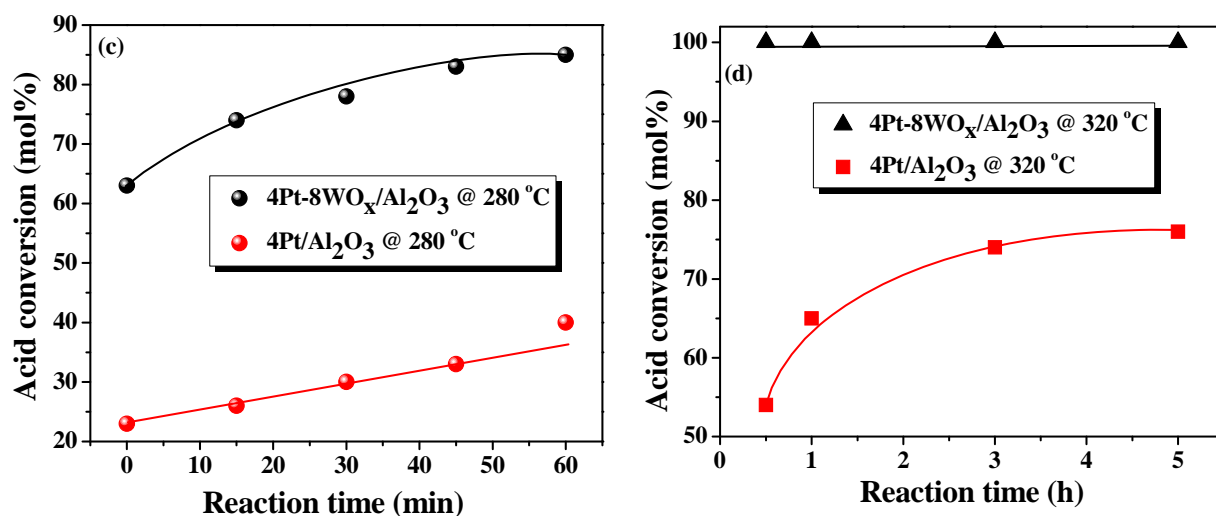


Fig. 4.8. Catalytic activities of 4Pt/Al₂O₃ and 4Pt-8WO_x/Al₂O₃ at 280 and 320 °C as a function of reaction time. *Reaction conditions*: for (a): OA = 2 g, catalyst = 10 wt. % of OA, solvent = 30 g of n-heptane, pressure = 20 bar of H₂, temperature = 280 °C, time = 0 – 60 min, reactor = 300 ml Parr batch autoclave, RPM = 600 and for (d): temperature = 320 °C, time = 0.5 - 5 h, rest of the conditions are same as for (a).

Table 4.4. Influence of reaction parameters on deoxygenation of oleic acid over 4Pt-8WO_x/Al₂O₃

Run No.	Reaction Parameter	OA conversion (mol%) ^a	Product selectivity (wt.%) ^b			
			C ₁₈	C ₁₇	C ₁₀₋₁₆	Others ^c
<i>Effect of reaction temperature (°C):^d</i>						
1	260	86.0	75.3	21.8	1.7	1.3
2	280	98.0	69.2	30.1	0.7	0
3	300	100	66.4	32.8	0.8	0
4	320	100	67.1	31.6	1.3	0
<i>Effect of hydrogen pressure (bar):^e</i>						
5	0	56.0	8.6	87.8	2.6	1.0
6	1	96.4	11.5	87.1	1.4	0
7	2	98.0	23.2	75.6	1.2	0
8	5	100	33.4	64.8	1.0	0.8
9	10	100	50.0	48.3	0.8	0.9
10	20	100	67.1	31.6	1.3	0
<i>Effect of reaction time (h):^f</i>						
11	0.5	78.0	65.4	33.5	0.9	0.2
12	1	83.0	66.5	32.1	1.2	0.2
13	3	94.0	71.3	27.3	0.7	0.7
14	5	98.0	69.2	30.1	0.7	0

^aDetermined from titration with NaOH. ^bDetermined from GC analysis. ^cOthers include octadecanal, octadecanol and esters. ^dReaction conditions: catalyst = 0.2 g, oleic acid (OA) = 2 g, n-heptane (solvent) = 30 g, pressure = 20 bar H₂, reaction temperature = 260 - 320 °C, reaction time = 5 h. ^eReaction conditions: catalyst = 0.2 g, oleic acid (OA) = 2 g, n-heptane (solvent) = 30 g, pressure = 0 - 20 bar H₂ (incase of 0 bar H₂, the reactor was charged with 20 bar of N₂), reaction temperature = 260 - 320 °C, reaction time = 5 h. ^fReaction conditions: catalyst = 0.2 g, oleic acid (OA) = 2 g, n-heptane (solvent) = 30 g, pressure = 20 bar H₂, reaction temperature = 280 °C, reaction time = 0.5 - 5 h

4.3.2.2. Effect of reaction temperature

The effect of reaction parameters on deoxygenation of OA over 4Pt-8WO_x/Al₂O₃ is presented in Table 4.4. The bimetallic catalyst of the present study is highly active even at

260 °C (Table 4.4, Run No. 1). OA conversion of 86 mol% and C₁₈ paraffin product selectivity of 75.3 wt.% were obtained. Selectivity of C₁₈ decreased from 75.3 to 66.4 wt.% as the temperature increased above 260 °C (Run Nos. 1–4) due to enhanced DCO activity over HDO activity at higher temperatures.

4.3.2.3. Effect of hydrogen pressure

Hydrogen had a marked effect on the activity and product selectivity. Reaction occurred (OA conversion = 56 mol%) even in the absence of hydrogen (Table 4.3, Run No. 5). Near complete conversion of OA was noted even at 1–2 bar H₂. But with increasing hydrogen pressure, HDO product selectivity had increased (compare Run Nos. 5–10). The corresponding OA conversion at zero hydrogen pressure for 4Pt-8WO_x/AlPO₄-5 was 43 mol% only. Comparatively under similar conditions, this catalyst showed better catalytic performance than 4Pt-8WO_x/AlPO₄-5 reported in Chapter-3.

4.3.2.4. Substrate scope

With a view to examine the scope of reaction, the experiments were also conducted taking palmitic acid (C_{16,0}), oleic acid (C_{18,1}) and methyl oleate (biodiesel) at 300 °C and 20 bar H₂ (Table 4.5). In all those experiments, complete conversion of substrate was observed. Irrespective of the fatty component, HDO (C₁₆ or C₁₈ product) was the selective deoxygenation pathway.

Table 4.5. Deoxygenation of fatty compounds over 4Pt-8WO_x/Al₂O₃

Run No.	Substrate	Conversion (mol%)	Product selectivity (wt. %)					
			C ₁₈	C ₁₇	C ₁₆	C ₁₅	C ₁₀₋₁₄	Others
1	Palmitic acid (C _{16,0})	100	0	0	64.3	32.8	0.4	2.5
2	Oleic acid (C _{18,1})	100	66.4	32.8	0.6	0.2	0	0
3	Methyl oleate (biodiesel)	100	65.8	17.9	7.4	2.3	3.9	2.7

Reaction conditions: Catalyst = 0.2 g, substrate = 2 g, n-heptane (solvent) = 30 g, pressure = 20 bar H₂, reaction temperature = 300 °C, reaction time = 5 h.

4.3.3. Catalyst recyclability study and characterization of spent catalyst

The reusability of the catalyst was tested in five recycling experiments conducted at 320 °C and 25 bar H₂ using OA as substrate. 4Pt-8WO_x/Al₂O₃ was found reusable (Table 4.6); 100% conversion of OA was observed in all the recycling studies. Interestingly, C₁₈ product selectivity increased from 67.1 to 80.8 wt.% upon reuse, while C₁₇ product selectivity

decreased from 31.6 to 18.5 wt.% (Fig. 4.9(a)). Unlike Pt-WO_x on AlPO₄₋₅ (Chapter-3), WO_x-promoted Pt of this study (4Pt-8WO_x/Al₂O₃) is quite stable and reusable. ICP analysis of spent catalyst showed no loss in Pt or W contents. On the other hand, 4Pt/Al₂O₃ showed a marginal loss in OA conversion from 78 to 64 mol% (Table 4.5; Fig. 4.9(b)). The selectivity of C₁₇ (heptadecane) over 4Pt/Al₂O₃ decreased from 83 to 68.7 wt.% and C₁₈ (octadecane) increased from 15.9 – 18.0 wt.%. The amount of other products increased from 0.3 to 12.5 wt.% (Fig. 4.9(b)). This is perhaps due to the blockage of active sites by the deposition of carbonaceous products on the catalyst surface.

Table 4.6. Recyclability study of 4Pt-8WO_x/Al₂O₃ and 4Pt/Al₂O₃ catalyst in deoxygenation of oleic acid.^a

Number of recycle.	OA conversion (mol %) ^b	Product selectivity (wt.%) ^c			
		C ₁₈	C ₁₇	C ₁₀₋₁₆	Others ^d
<i>Recyclability of 4Pt-8WO_x/Al₂O₃</i>					
0 (Fresh)	100	67.1	31.6	1.3	0
1	100	75.7	23.5	0.8	0
2	100	75.8	23.0	1.2	0
3	100	76.7	22.6	0.7	0
4	100	78.8	20.4	0.8	0
5	100	80.8	18.5	0.7	0
<i>Recyclability of 4Pt/Al₂O₃</i>					
0 (Fresh)	78	15.9	83.0	0.8	0.3
1	74	19.0	77.6	1.0	2.4
2	71	21.3	74.2	0.8	3.7
3	70	18.5	75.0	0.8	5.7
4	64	18.0	68.7	0.8	12.5

^aReaction conditions: Catalyst = 0.6 g, oleic acid (OA) = 6 g, n-heptane (solvent) = 40 g, pressure = 25 bar H₂, reaction temperature = 320 °C, reaction time = 5 h. ^bDetermined from titration with NaOH. ^cDetermined from GC analysis. ^dOthers include octadecanal, octadecanol and esters

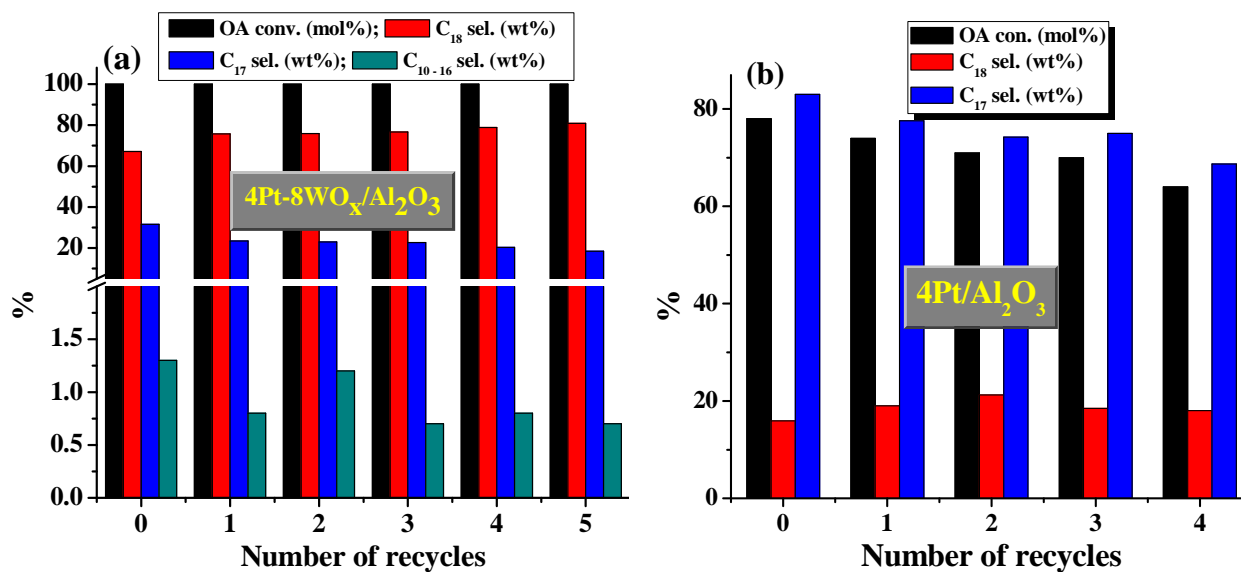


Fig. 4.9. Recyclability study of (a) 4Pt-8WO_x/Al₂O₃ and (b) 4Pt/Al₂O₃. Reaction conditions: same as mentioned at Table 4.6.

XRD of spent 4Pt-8WO_x/Al₂O₃ catalyst (after five cycles) was comparable to that of the fresh catalyst (Fig. 4.10(a)) and confirms structural integrity due to its hydrothermal stability. In contrast, the spent 4Pt/Al₂O₃ catalyst showed moderately broadened X-ray diffractions of Pt (Fig. 4.10(b)). N₂-physisorption studies of 4Pt-8WO_x/Al₂O₃ revealed a marginal decrease in S_{BET} (from 266 to 212 m²/g), total pore volume (from 0.57 to 0.40 cc/g) and average pore size (from 4.3 to 3.8 nm; Table 4.1). CO-chemisorption (in agreement with TEM results) points out sintering of Pt. As shown in the Table 4.1, metal dispersion decreased from 84 to 24% and Pt crystallite size increased from 1.4 to 4.9 nm in spent 4Pt-8WO_x/Al₂O₃ (Table 4.1). In spite of these structural changes, 4Pt-8WO_x/Al₂O₃ showed stable reusable deoxygenation activity.

XPS of the spent catalyst showed a marginal shift in Pt 4d_{5/2} and 4d_{3/2} peaks to 312.8 and 330.3 eV, respectively in conformity with a change in particle size of Pt (Fig. 4.11(a)). Recall that the corresponding peaks for the fresh catalyst were observed at 312.6 and 330.4 eV, respectively. The spent catalyst in W 4f spectral region showed peaks at 35.9 and 38.0 eV corresponding to +6 tungsten species and at 34.7 and 37.1 eV attributable to +5 tungsten species (Fig.4.11(b)). Surface tungsten +6 and +5 species in the spent catalyst were in the proportion of 68 and 32%, respectively.

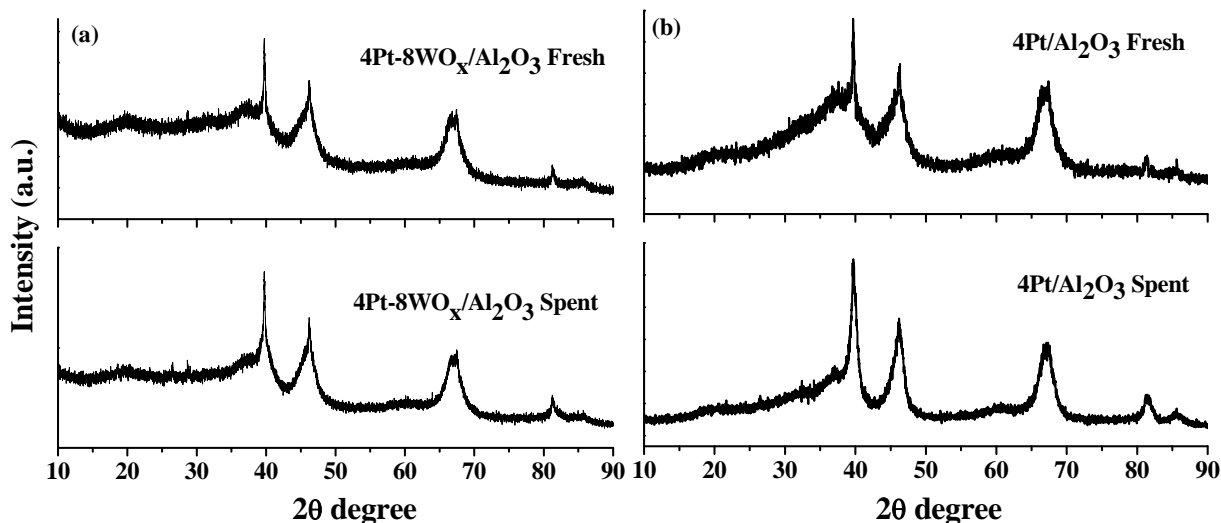


Fig. 4.10. Comparative XRD profiles of fresh and spent catalysts: (a) 4Pt-8WO_x/Al₂O₃ and (b) 4Pt/Al₂O₃. Reaction conditions: same as mentioned at Table 4.6.

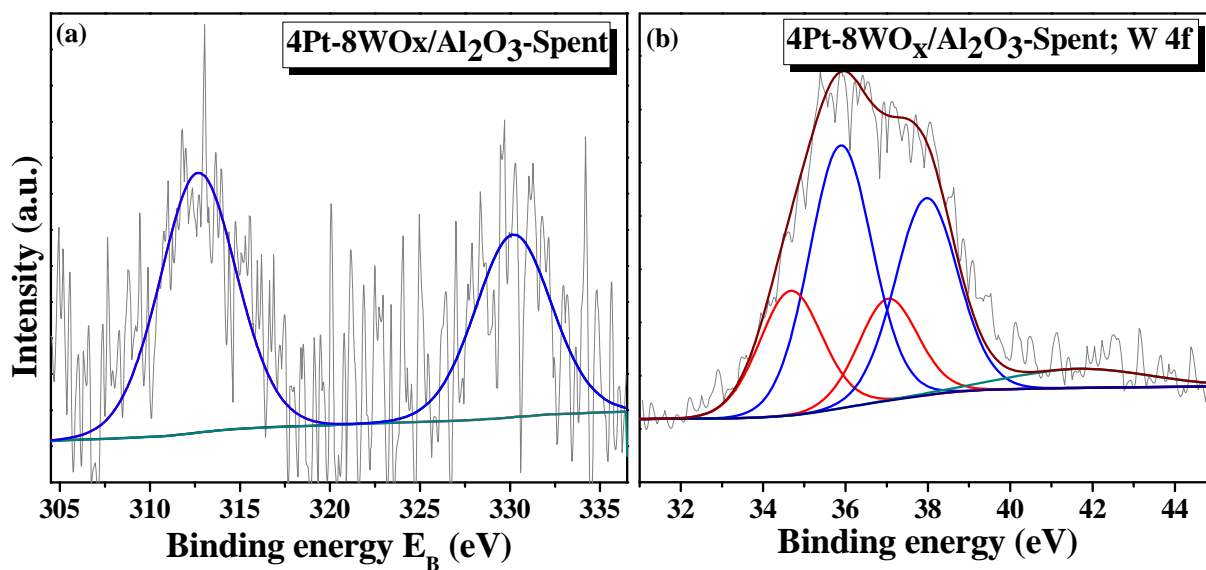


Fig. 4.11. XPS of (a) Pt 4d and (b) W 4f lines of spent 4Pt-8WO_x/Al₂O₃ after 5 cycles.

The TEM images and particle size histograms of the spent 4Pt/Al₂O₃ and 4Pt-8WO_x/Al₂O₃ catalysts are presented in Fig. 4.12. These images infer sintering of Pt in spent catalysts. However, this increase in particle size is lesser in the case of 4Pt-8WO_x/Al₂O₃ (particle size increase is from 2.5 nm (in fresh catalyst) to 5 nm (in spent catalyst)) than for 4Pt/Al₂O₃ (increase is from 2.5 to 14 nm). Thus, WO_x limited the sintering of Pt on reuse. The WO_x domains present on the surface hold the Pt particles with synergy thereby hinder the lateral re-dispersion of Pt by obstruction. As result of this, 4Pt-8WO_x/Al₂O₃ exhibited

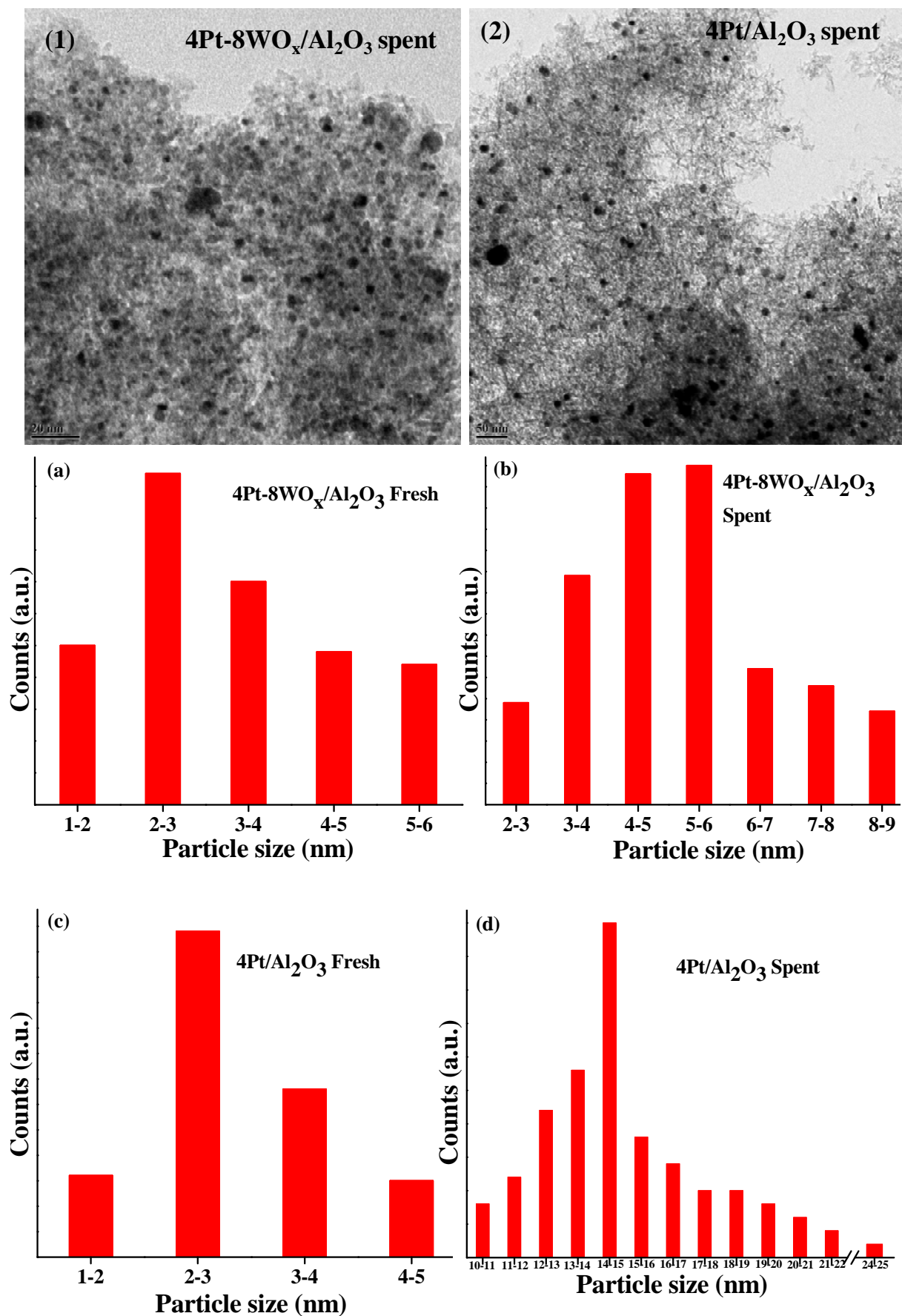


Fig. 4.12. TEM images of spent catalyst (1 & 2) and Pt particle size histograms (a, b, c and d)

excellent stability and activity even after 5 recycles while the unpromoted Pt/Al₂O₃ catalyst proved to be unstable. WO_x promoter not only enhanced the activity but changed the selectivity while providing high stability. Thus, WO_x acted as activity booster and stability enhancer.

4.4. Conclusions

Bimetallic Pt-WO_x supported on γ -Al₂O₃ exhibits high catalytic activity for deoxygenation of fatty acids and their esters. WO_x promoted the catalytic activity and HDO selectivity of Pt/Al₂O₃. A catalyst with 4 wt% Pt and 8 wt% tungsten showed optimum catalytic performance. Interestingly, these catalysts are reusable and exhibit structural and chemical integrity at reaction conditions. The synergy existed between Pt and W facilitated the reducibility of Pt. Partial reduction of WO_x in presence of Pt led to form W⁺⁵ species which in turn may serve as new active sites probably responsible for the shift in reaction mechanism from DCO to HDO. Tungsten altered the structural (electronic and particle size) and acidic properties of Pt/Al₂O₃, and thereby, promoted its catalytic activity and selectivity. Moreover, TEM images of spent catalysts revealed that WO_x prohibited the sintering of Pt. Hence, WO_x acted as activity booster as well as stability enhancer of this catalyst.

4.5. References

- [1] T. V. Choudhary, C.B. Phillips, *Appl. Catal. A: Gen.* 397 (2011) 1.
- [2] P. M. Mortensen, J.-D. Greenwaldt, P.A. Jensen, K.G. Knudsen, A.D. Jensen, *Appl. Catal. A: Gen.* 407 (2011) 1.
- [3] C. Zhao, T. Bruck, J.A. Lercher, *Green Chem.* 15 (2013) 1720.
- [4] B. lama, *Hand Book of Biofuels: Process and Technologies*, in: R. Luque, J. Campelo, J. Clark (Eds.), Woodhead Publishing Ltd., 2011.
- [5] <http://www.nesteoil.com>.
- [6] US Patent No. 7,511,181 B2 (2009) – UOP LLC, US.
- [7] US Patent No. 8,003,836 B2 (2011) – UOP LLC, US.
- [8] <http://www.uop.com/pr/release/PR.EniEcofiningFacility.pdf>.
- [9] B. Donnis, R.G. Egeberg, P. Blom, K.G. Knudsen, *Top. Catal.* 52 (2009) 229.
- [10] T. M. Sankaranarayanan, M. Banu, A. Pandurangan, S. Sivasanker, *Bioresour. Technol.* 102 (2011) 10717.

- [11] J. K. Satyarthi, D. Srinivas, *Energy Fuels* 25 (2011) 3318.
- [12] M. Gousi, C. Andriopoulou, K. Bourikas, S. Ladas, M. Sotiriou, C. Kordulis, A. Lycourghiotis, *Appl. Catal. A: Gen.* 536 (2017) 45.
- [13] (a) J. Fu, F. Shi, L.T. Thomson Jr., X. Lu, P.L. Savage, *ACS Catal.* 1 (2011) 227; (b) L. Yang, K.L. Tate, J.B. Jasinski, M.A. Carreon, *ACS Catal.* 5 (2015) 6497.
- [14] M. Ahmadi, A. Nambo, J.B. Jasinski, P. Ratnasamy, M.A. Carreon, *Catal. Sci. Technol.* 5 (2015) 380.
- [15] R. Raut, V.V. Banakar, D. Srinivas, *J. Mol. Catal. A: Chem.* 417 (2016) 126.
- [16] S. Lestari, P. Mäki-Arvela, H. Bernas, O. Simakova, R. Sjöholm, J. Beltramini, G.Q. Max Lu, J. Myllyoja, I. Simakova, D.Y. Murzin, *Energy Fuels* 23 (2009) 3842.
- [17] I. Simakova, O. Simakova, P. Mäki-Arvela, D.Y. Murzin, *Catal. Today* 150 (2010) 28.
- [18] I. Kubičkova, M. Snåre, K. Eränen, P. Mäki-Arvela, D.Y. Murzin, *Catal. Today* 106 (2005) 197.
- [19] I. Simakova, O. Simakova, P. Mäki-Arvela, A. Simakova, M. Estrada, D.Y. Murzin, *Appl. Catal. A: Gen.* 355 (2009) 100.
- [20] P. Mäki-Arvela, I. Kubickova, M. Snåre, K. Eränen, D.Y. Murzin, *Energy Fuels* 21 (2007) 30.
- [21] P.T. Do, M. Chiappero, L.L. Lobban, D.E. Resasco, *Catal. Lett.* 130 (2009) 9.
- [22] A.T. Madsen, E.H. Ahmed, C.H. Christensen, R. Fehrmann, A. Riisager, *Fuel* 90 (2011) 3433.
- [23] A. Vonortas, N. Papayannakos, *Fuel Proc. Technol.* 150 (2016) 126.
- [24] M. Ahmadi, E.E. Macias, J.B. Jasinski, P. Ratnasamy, M.A. Carreon, *J. Mol. Catal. A: Chem.* 386 (2014) 14.
- [25] L. Yang, G.L. Ruess, M.A. Carreon, *Catal. Sci. Technol.* 5 (2015) 2777.
- [26] L. Yang, M.A. Carreon, *J. Chem. Technol. Biotechnol.* 92 (2017) 52.
- [27] M.V. Tsodikov, A.V. Chistyakov, M.A. Gubanov, P.A. Zharova, S.S. Shapovalov,

- A.A. Pasynskii, V.V. Kriventsov, I.I. Moiseev, *Rus. Chem. Bull. Int. Ed.* 64 (2015) 2062.
- [28] A.V. Chistyakov, V.V. Kriventsov, A.V. Naumkin, A.Y. Pereyaslavtsev, P.A. Zharova, M.V. Tsodikov, *Pet. Chem.* 56 (2016) 607.
- [29] M. Rabaev, M.V. Landau, R. Vidruk-Nehemya, A. Goldbourt, M. Herskowitz, *J. Catal.* 332 (2015) 164.
- [30] M. Rabaev, M.V. Landau, R. Vidruk-Nehemya, V. Koukouliev, R. Zarchin, M. Herskowitz, *Fuel* 161 (2015) 287.
- [31] Louise Samain, Aleksander Jaworski, Mattias Edén, Danielle M. Ladd, Dong-Kyun Seo, F. Javier Garcia-Garcia, Ulrich Häussermann, *Journal of Solid State Chemistry*, 217 (2014) 1.
- [32] S. García-Fernández, I. Gandarias, J. Requies, M.B. Guemez, S. Bennici, A. Auroux, P. L. Arias, *J. Catal.* 323 (2015) 65.
- [33] S. Zhu, X. Gao, Y. Zhu, Y. Li, *J. Mol. Catal. A: Chem.* 398 (2015) 391.
- [34] S. Zhu, X. Gao, Y. Zhu, J. Cui, H. Zheng, Y. Li, *Appl. Catal. B: Env.* 158–159 (2014) 391.
- [35] K. Song, H. Zhang, Y. Zhang, Y. Tang, K. Tang, *J. Catal.* 299 (2013) 119.
- [36] J. Chaminand, L. Djakovitch, P. Gallezot, P. Marion, C. Pinel, C. Rosier, *Green Chem.* 6 (2004) 359.
- [37] T. Deng, H. Liu, *Green Chem.* 15 (2013) 116.
- [38] T.Y. Kim, D.S. Park, Y. Choi, J. Baek, J.R. Park, J. Yi, *J. Mater. Chem.* 22 (2012) 10021.
- [39] S. Kuba, M. Che, R.K. Grasselli, H. Knözinger, *J. Phys. Chem. B* 107 (2003) 3459.

Chapter-5
Effect of Support on the Catalytic Activity of Pt-WO_x in
Green Diesel Production

5.1. Introduction

Biofuels derived from biomass are renewable and carbon neutral [1]. Their use can lead to energy independence and sustainable environment (by way of reduced greenhouse gas emissions). They can also improve savings on oil import bill, rural revitalization and employment creation. The integration of agro-energy crops and biorefinery technologies will lead to a new manufacturing paradigm in coming years towards achieving sustainable development. Vegetable oils (in particular, non-edible oils) are an important source of biomass to produce biodiesel [2–4]. While transesterification of vegetable oils with methanol enables fatty acid methyl esters (FAME; the 1st generation biodiesel), deoxygenation processes lead to diesel-range hydrocarbons (green diesel; the 2nd generation biodiesel). The latter category has an advantage over the former in terms of its thermal and oxidation stability. Moreover, it can be blended in any amount with the petro-diesel or used as a standalone fuel in conventional diesel engines without subjecting the engine to any modifications.

Deoxygenation can be achieved by two mechanisms viz., hydrodeoxygenation (HDO, wherein oxygen in presence of hydrogen is taken out as water) and decarbonylation/decarboxylation (DCO, wherein oxygen is removed as CO/CO₂). In the former case, the hydrocarbons produced will have the same number of carbon atoms as in the feedstock. Whereas in the latter case, they have one carbon less compared to the feedstock. A few companies have commercialized the HDO process of green diesel production [5–9] by using conventional hydrotreating catalysts viz., Ni-Mo(W)/Al₂O and Co/Mo(W)/Al₂O₃. These operations require high hydrogen pressure (50 – 80 bar) and high reaction temperatures (320 - 350 °C) [10–15]. Supported noble metal catalysts (ca., Pt(Pd)/zeolite, Pt(Pd)/SAPO-11/34, Pd/C, etc) assume the DCO mechanism [16–22]. However, the stability of catalyst during the reaction is still an issue. Process economics, operation at moderate conditions (250–280 °C, ≤20 bar H₂), catalyst stability, minimum or negligible carbon loss, high hydrocarbon yield and high product selectivity are still issues in green diesel production.

Chapters-3 and 4 revealed that when Pt is promoted with WO_x, the catalytic activity and HDO product selectivity (in deoxygenation of fatty acid) increases significantly. These types of bimetallic catalysts have been reported for deoxygenation reactions [23, 24] and found that the second metal acts as a spacer or structure modifier to the active phase (primary metal). Tsodikov et al. [25] studied the deoxygenation of fatty acid triglycerides in vegetable oils and lipid extracts

from microalgae in presence of Pt-Sn/Al₂O₃ and reported the influence of Sn on the catalytic activity and product selectivity of the catalyst. Chen et al. [26], reported hydrodeoxygenation of methyl palmitate over Pt-Sn/SAPO-11. They found that the occurrence of reduced tin oxide (SnO_{2-x}) species is crucial for the HDO pathway and the presence of Pt-Sn alloy is important for high isomerization activity. Kim et al. [27], valorized waste lipids through hydrothermal catalytic conversion and *in situ* hydrogen production using Pt-Re/C catalyst. Murata et al. [28] reported rhenium modified Pt/H-ZSM-5 for hydrotreatment of jatropha oil. They found synergy between Pt and Re enhancing the catalytic activity. Hydrodeoxygenation of stearic acid was effectively catalyzed by Pd-Ni/H-ZSM-5 [29]. The acidity of H-ZSM-5 influenced the performance of Pd-Ni bimetallic catalyst. The alloyed Pd-Ni enhanced the internal H-atom transfer between the two metals and thereby increased the reaction rate. Dwiatmoko et al. [30] reported hydrodeoxygenation of guaiacol on tungstated zirconia supported Ru catalysts. The acidic supports manipulate the HDO reaction pathway and product distribution. The study in this chapter explores the effect of support on the catalytic performance of WO_x-promoted Pt in deoxygenation of oleic acid (OA, a representative fatty acid). Al₂O₃, SiO₂-Al₂O₃, AlPO₄-5 and ZrO₂ supports with varying acidity were chosen for the study. Factors influencing the catalytic activity (OA conversion) and hydrocarbon product selectivity are probed.

5.2. Experimental

5.2.1. Catalyst preparation

The supports (except γ -Al₂O₃ which was supplied by Süd-Chemie India Pvt. Ltd., New Delhi) - ZrO₂, AlPO₄-5, silica-alumina (SA) were synthesized as described in Chapter-2. Wet impregnation method was used to load tungsten as well as platinum on these supports (see Chapter-2).

5.2.2. Catalyst characterization and reaction procedure

The catalysts used in this study were characterized by various characterization techniques as described in Chapter-2. The deoxygenation reaction and product analysis methods are the same as mentioned in Chapter-2.

5.3. Results and discussion

5.3.1. Catalyst characterization

5.3.1.1. X-ray diffraction

An optimized amount of platinum (4 wt%) was deposited on different supports (unpromoted and 8 wt.% WO_x-promoted SA, Al₂O₃, ZrO₂ and AlPO₄-5) by wet impregnation method and reduced in a flow of hydrogen at 350 °C for 2.5 h prior to investigations. The XRD profiles of different supported Pt and Pt-WO_x catalysts (Fig. 5.1(a and b)) confirm the presence of metallic Pt in cubic closed-packed structure with a space group of Fm-3m (JCPDS No. 65-2868) showing characteristic peaks at 39.7, 45.2, 67.3, 81.3 and 85.6° arising from (111), (200), (220), (311) and (322) planes of Pt crystallites. Except for 4Pt-8WO_x/Al₂O₃, the other WO_x-promoted catalysts showed additional, weak peaks at 23.6 and 33.5° due to presence of crystalline monoclinic tungsten oxide (WO₃) species (Fig. 5.1(b)). Absence of these peaks for 4Pt-8WO_x/Al₂O₃ infers that WO_x (up to a loading of 8 wt %) is below its monolayer coverage on the Al₂O₃ surface and hence, could not be detected by XRD. All these peaks (both of Pt and WO₃) overlapped with the XRD peaks of the supports. Silica-alumina (SA) and Al₂O₃ supports showed broad, diffused reflections. ZrO₂, on the other hand, showed intense characteristic reflections at 2θ values of 24.2 (m), 28.5 (m), 30.4 (t), 31.5 (m), 34.4 (m, t), 35.6 (m), 40.9 (m), 50.7 (m, t), and 60.2° (t) confirming its presence of tetragonal (t) and monoclinic (m) crystalline phases (Fig. 5.1(a and b)). AlPO₄-5 exhibited sharp XRD peaks at 7.4, 12.8, 14.9, 19.8, 21.8, 22.5, 25.9, 28.3, 29.1, 30.1, 31.1, 34.5 and 35.9° validating its orthorhombic lattice with a space group of Pcc2 (Fig. 5.1(a and b)) [32]. Determination of average crystallite size of Pt (from XRD) was not attempted as the Pt peaks overlapped with the peaks of the support. The intensity/area of Pt peaks in unpromoted catalysts was lower than in promoted catalysts inferring that promotion with WO_x influenced the percentage crystallinity of Pt. Supported Pt-WO_x catalysts have higher percentage crystallinity than the unpromoted supported Pt catalysts.

5.3.1.2. N₂-Physisorption

Surface aspects (specific surface area (S_{BET}), average pore size, total pore volume) of the catalysts were determined from N₂-physisorption studies (Table 5.1). The S_{BET} values of the WO_x promoted supported Pt catalysts were lower than those of the unpromoted Pt catalysts (Table 5.1). This decrease is significant with SA than with other supports. In general, S_{BET} of catalysts with different supports varied in the order: Al₂O₃ > SA > AlPO₄-5 > ZrO₂. Fig. 5.2(a

and b) presents isotherms of unpromoted and WO_x-promoted supported Pt catalyst and pore size distribution profiles.

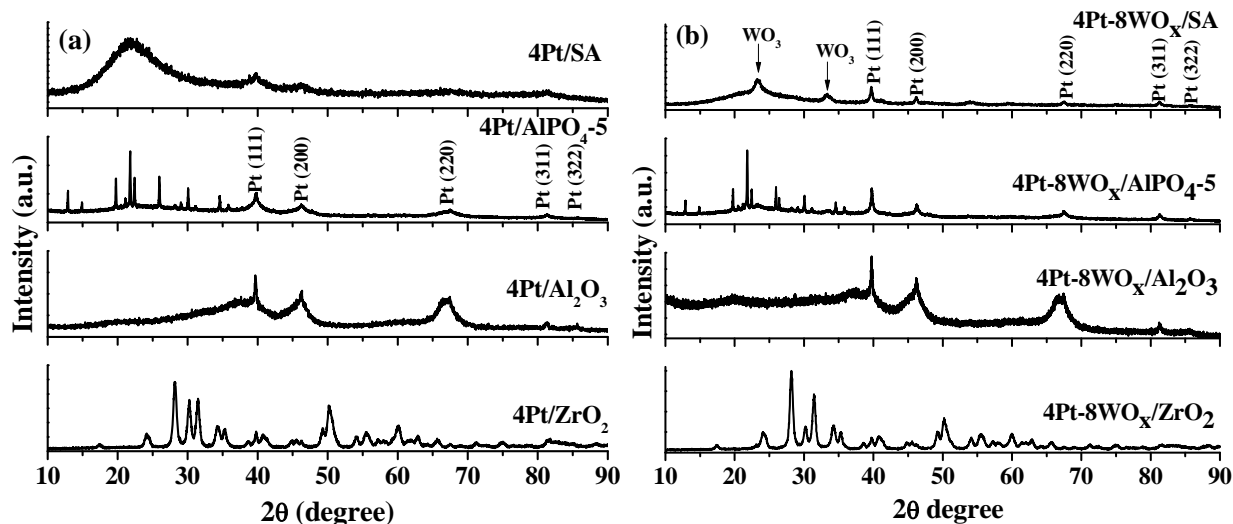


Fig. 5.1. XRD patterns of unpromoted Pt (a) and WO_x-promoted Pt supported catalysts

5.3.1.3. NH₃-TPD

Total acidity of both the series of the catalysts (unpromoted and WO_x-promoted supported Pt) was estimated by temperature-programmed desorption of ammonia (NH₃-TPD). These studies revealed that the acidity of the catalyst with different supports decreases as follows: Al₂O₃ > AlPO₄-5 > SA > ZrO₂ (Table 5.1). Among the two series of the catalysts, ZrO₂ catalyst possessed lesser total acidity than the rest of the catalysts in the series. Except for ZrO₂, an increase in an overall acidity was found when WO_x was also present in the catalyst (Table 5.1). NH₃-TPD profiles of unpromoted supported Pt catalysts showed two overlapping NH₃ desorption peaks in the temperature ranges of 150–215 °C and 330–385 °C attributable to weak and strong acid sites, respectively (Fig. 5.3(a)). The WO_x-promoted Pt catalysts showed an additional NH₃ desorption peak in the temperature range of 245–265 °C due to acid sites of moderate strength arising from tungsten oxide. The weak and strong acid sites in these samples showed desorption peaks at 150–180 °C and 315–350 °C, respectively (Fig. 5.3(b)). Thus, these measurements reveal that addition of WO_x enhances the acidity (in particular the moderate and strong acid sites) of the catalyst.

Table 5.1. Physicochemical properties of unpromoted and WO_x-promoted supported Pt catalysts

Catalyst	S _{BET} (m ² /g)	Total acidity (mmol NH ₃ /g)	CO-chemisorption			
			Monolayer CO uptake (μmol/g)	Active Pt surface area (m ² /g)	Average crystallite size of Pt (nm)	Pt dispersion (%)
4Pt/SA	261	0.410	55.0	65	4.3	27
4Pt/AlPO ₄₋₅	129	0.867	37.1	44	6.2	18
4Pt/ZrO ₂	42	0.260	44.0	53	5.3	21
4Pt/Al ₂ O ₃	292	1.270	100.0	242	1.2	49
4Pt-8WO _x /SA	123	0.470 (0.348)	11.0 (1.1)	13 (1.3)	21.0 (105.0)	5 (0.5)
4Pt-8WO _x /AlPO ₄₋₅	102	0.945 (1.130)	13.0 (0.5)	15 (0.6)	21.0 (245.0)	6 (0.2)
4Pt-8WO _x /ZrO ₂	40	0.240 (0.244)	30.0 (19.2)	37 (23)	7.6 (12.1)	15 (9.4)
4Pt-8WO _x /Al ₂ O ₃	266	1.410 (1.423)	86.0 (15.0)	103 (18)	2.7 (15.8)	42 (7.2)

Values in parentheses are for the spent catalysts evaluated at 260 °C for 5 h in deoxygenation of OA using 20 bar H₂.

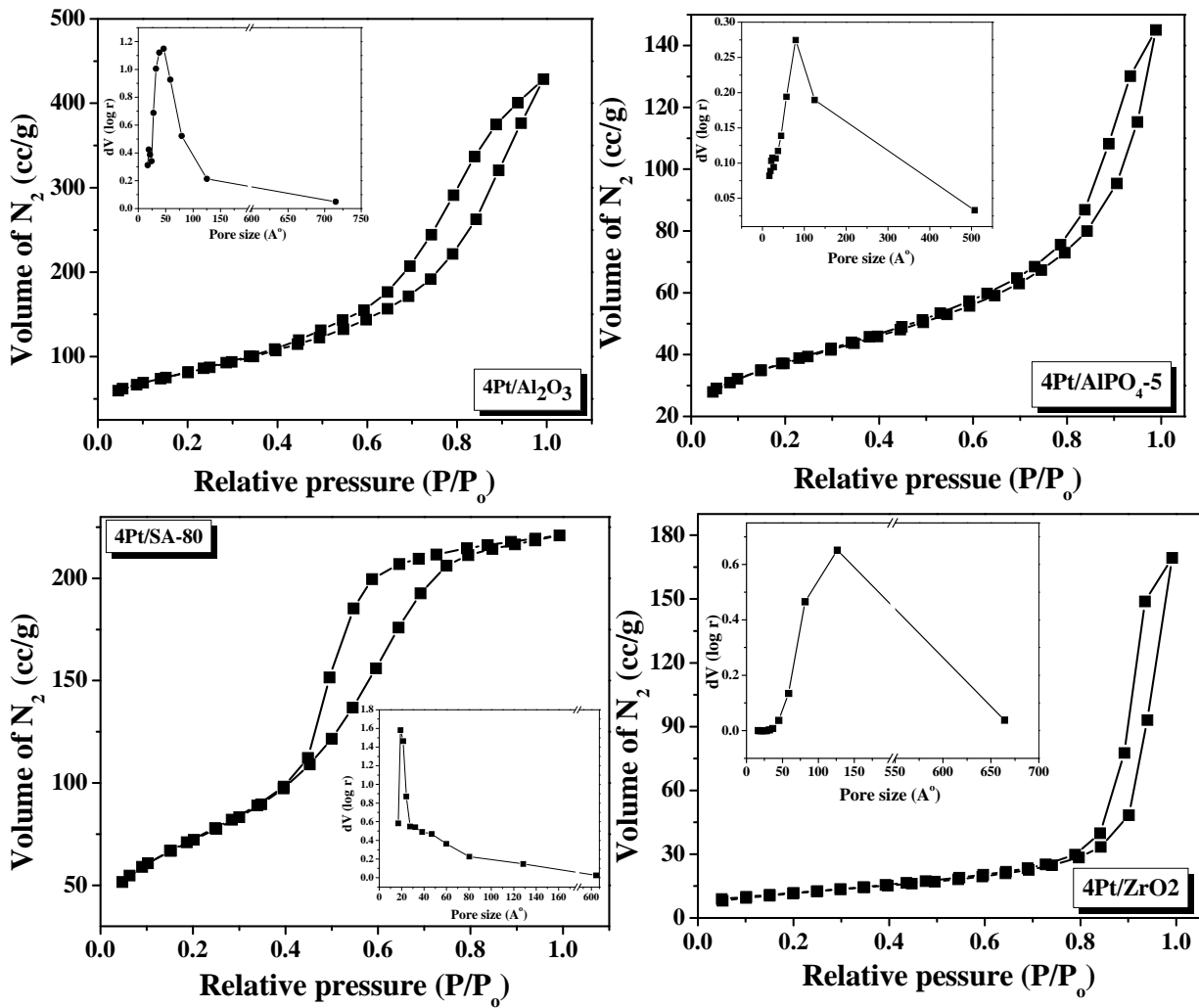
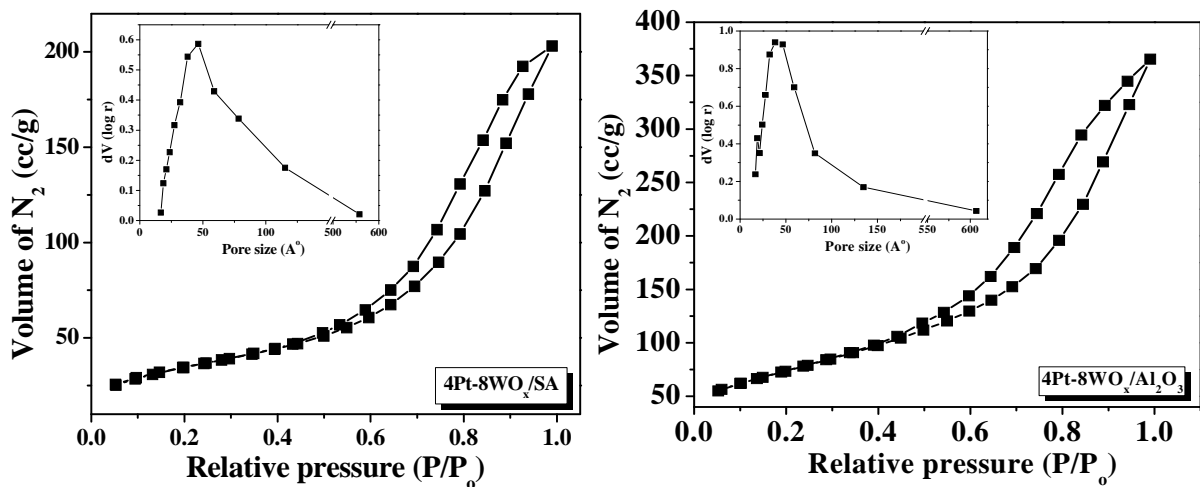


Fig. 5.2(a). N₂-physorption profiles and pore size distribution curves of unpromoted supported Pt catalysts.



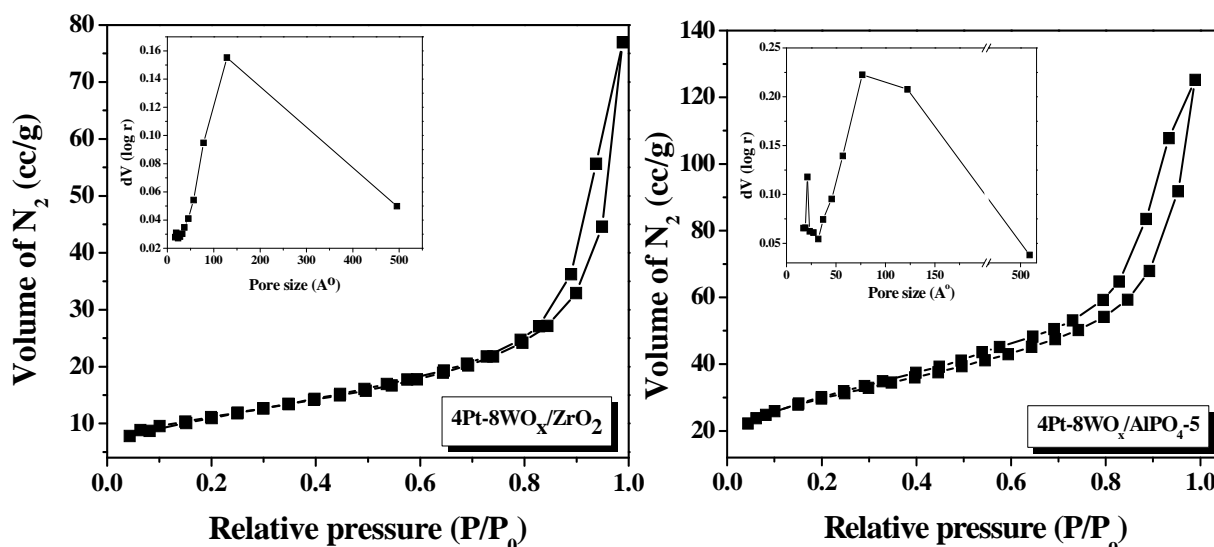


Fig. 5.2(b). N₂-physorption profiles and pore size distribution curves of WO_x-promoted supported Pt catalysts.

5.3.1.4. TEM

TEM images of the catalysts confirmed the presence of dispersed Pt particles on catalyst surfaces (Fig. 5.4). Particle size histograms (constructed observing about 100 random Pt particles) point out that the size distribution is somewhat broader and the average particle size of Pt is higher for supported Pt-WO_x than for supported Pt catalysts. On promotion with WO_x, the average particle size of Pt increased from 2.5 to 3 nm (on Al₂O₃), 4 to 4.5 nm (on ZrO₂), 3.8 to 12 nm (on SA) and 4 to 7 nm (on AlPO₄₋₅). Thus, WO_x led to increased Pt crystallites. This increment varied with support, it is being minimum for Al₂O₃ and ZrO₂ and maximum for AlPO₄₋₅ and SA.

5.3.1.5. CO-chemisorption

Active surface area, average crystallite size and dispersion of Pt metal were determined from CO-chemisorption studies (Table 5.1). In unpromoted catalysts, the crystallite size was in the range of 4–5 nm for Pt supported on SA, AlPO₄₋₅ and ZrO₂, while it was 1.2 nm for Pt on Al₂O₃. Percentage metal dispersion for different unpromoted catalysts decreased in the order: 4Pt/Al₂O₃ (49%) > 4Pt/SA (27%) > 4Pt/ZrO₂ (21%) > 4Pt/AlPO₄₋₅ (18%). Upon promotion with WO_x, the average crystallite size of Pt increased markedly (Table 5.1). Percentage Pt dispersion decreased over different promoted Pt catalysts in the order: 4Pt-8WO_x/Al₂O₃ (42%) > 4Pt-

8WO_x/ZrO₂ (15%) > 4Pt-8WO_x/AlPO₄-5 (6%) > 4Pt-8WO_x/SA (5%). These observations are in line with the results derived from TEM. Any differences observed are due to the fact that TEM focuses only on a certain region while CO-chemisorption provides the bulk value information.

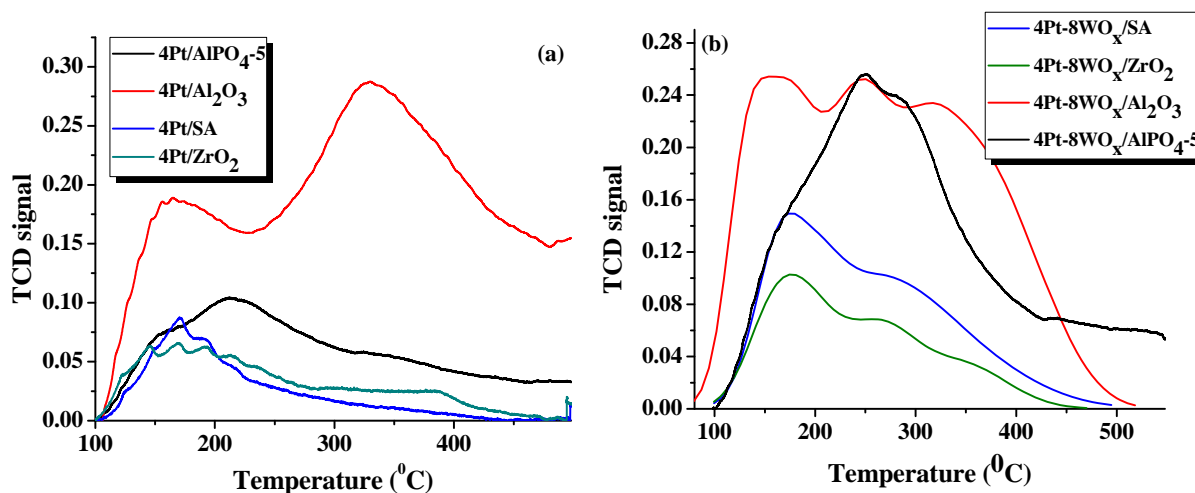


Fig. 5.3. NH₃-TPD profiles of (a) unpromoted and (b) WO_x-promoted supported Pt catalysts.

5.3.1.6. X-ray photoelectron spectroscopy

The surface structure of reduced catalysts was probed by X-ray photoelectron spectroscopy (XPS). All the WO_x-promoted catalysts showed two X-ray photoelectron spectral peaks at 313.9–314.4 and 331.2–331.8 eV attributable to Pt 4d_{5/2} and 4d_{3/2}, respectively (Fig. 5.5(a)). Absence of peaks due to Pt²⁺ points out complete reduction of platinum to its metallic state [33]. Absence of platinum oxide peaks in XRD also confirms complete reduction of platinum in these catalysts. The Pt 4d lines were followed in the present study instead of the most intense 4f lines due to their overlap with the strong Al 2p peaks [34] of SA, Al₂O₃ and AlPO₄-5-based catalysts. Compared to unpromoted Pt catalysts, the Pt 4d peaks of WO_x-promoted catalysts shifted to lower binding energy (B.E.) (Fig. 5.5(b)). This shift in Pt 4d peaks position to lower B.E. reveals change in electronic structure of Pt (metallicity) due to presence of tungsten oxide. The 4d_{3/2} spectral line was found more sensitive to these electronic changes. Metallic nature of Pt (electron-rich Pt) in different promoted catalysts decreased (as the Pt 4d_{3/2} line shifted to lower B.E.) as follows: 4Pt-8WO_x/ZrO₂ (331.2 eV) > 4Pt-8WO_x/AlPO₄-5 (331.3 eV) > 4Pt-8WO_x/Al₂O₃ (331.5 eV) > 4Pt-8WO_x/SA (331.8 eV). In W 4f region, XPS lines corresponding to +6 and +5 oxidation states of tungsten were observed (Fig. 5.5(c)). W⁶⁺ showed peaks at 35.0–35.7 and 37.3–37.9 eV due to W 4f_{7/2} and 4f_{5/2} transitions. These spin-orbit

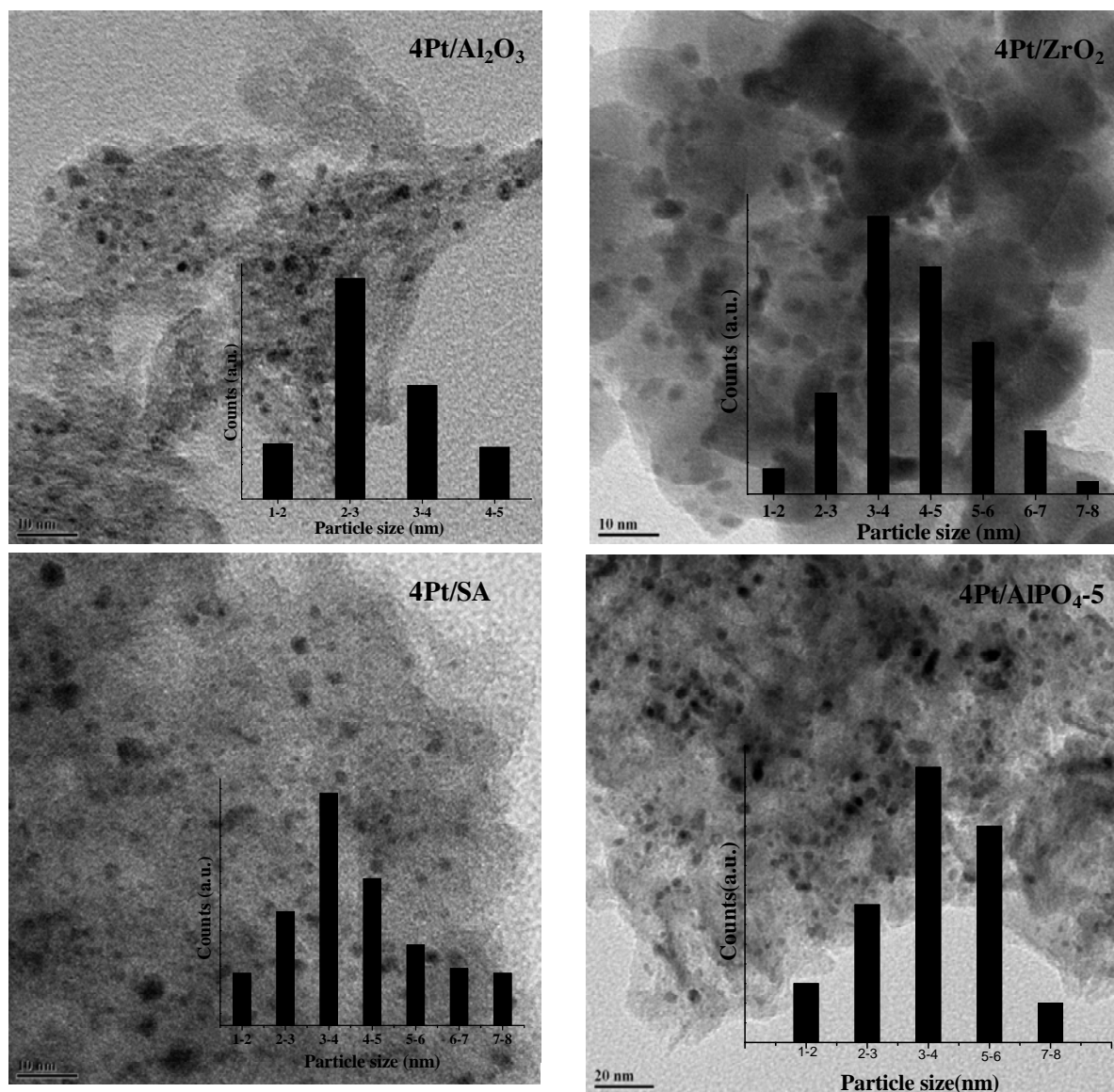


Fig. 5.4 (a). TEM images and particle size histograms of unpromoted supported Pt catalysts.

components of W⁵⁺ species appeared at 34.3–34.8 and 36.3–36.7 eV, respectively [35, 36]. The B.E. values of W (+5 and +6) species varied in the similar manner as of the Pt peaks. These W peaks were deconvoluted, integrated and surface W⁵⁺/W⁶⁺ concentrations were estimated. For different catalysts the values are as follows: 4Pt-8WO_x/Al₂O₃ (65.9/34.1), 4Pt-8WO_x/ZrO₂ (55.1/44.9), 4Pt-8WO_x/AlPO₄-5 (48.4/51.6) and 4Pt-8WO_x/SA (38.7/61.3). The hydrogen atoms

from dissociatively adsorbed hydrogen molecule on Pt surfaces would spillover onto WO_x surface and lead to its reduction from +6 to +5 state [37]. This efficiency of hydrogen atom spill over is more for more metallic 4Pt-8WO_x/ZrO₂ than for 4Pt-8WO_x/AlPO₄₋₅, 4Pt-8WO_x/Al₂O₃ and 4Pt-8WO_x/SA. Accordingly, electron donor-acceptor interaction between Pt⁰ and WO_x would probably take place.

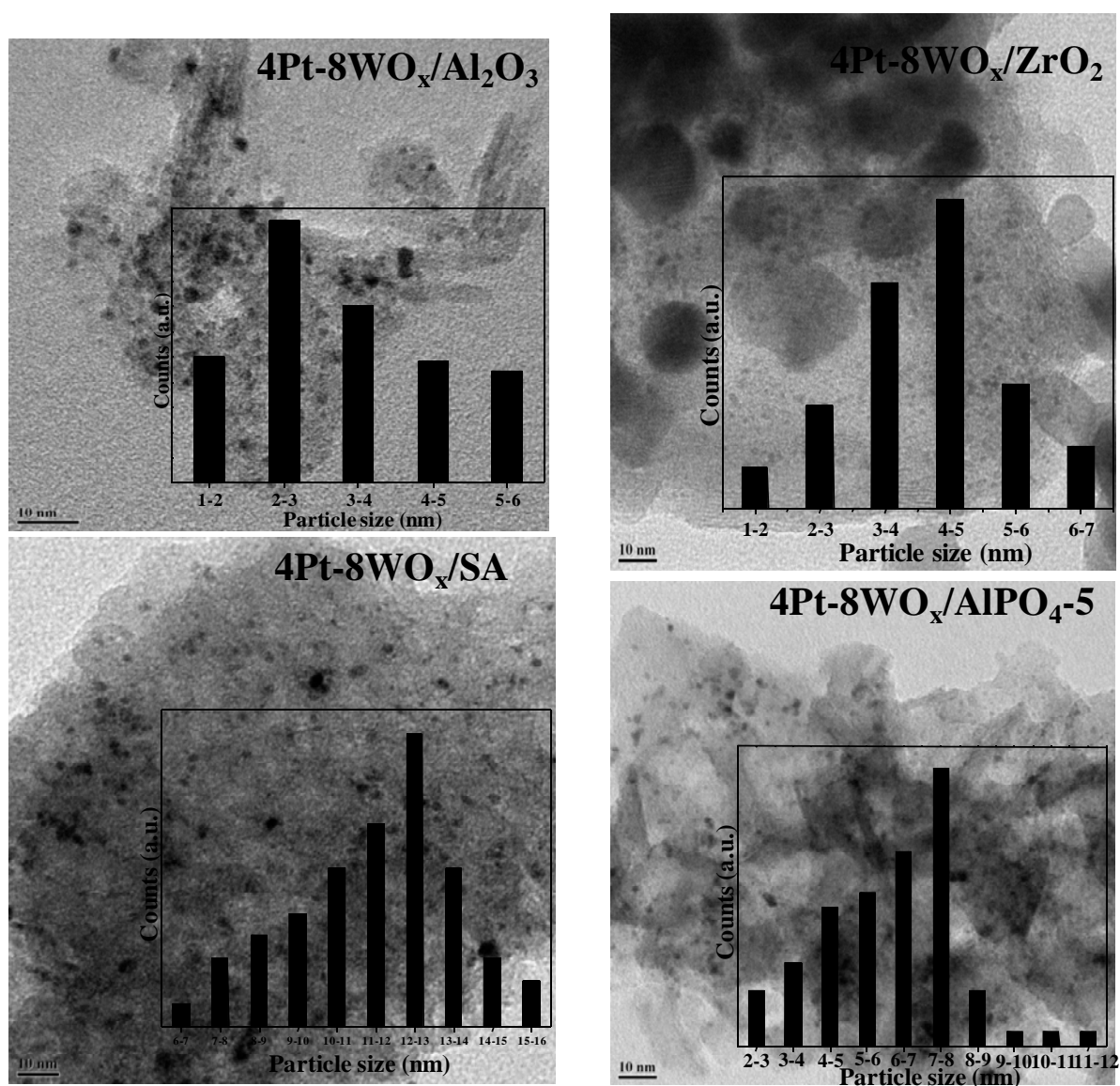


Fig. 5.4(b). TEM images and particle size histograms of WO_x-promoted supported Pt catalysts.

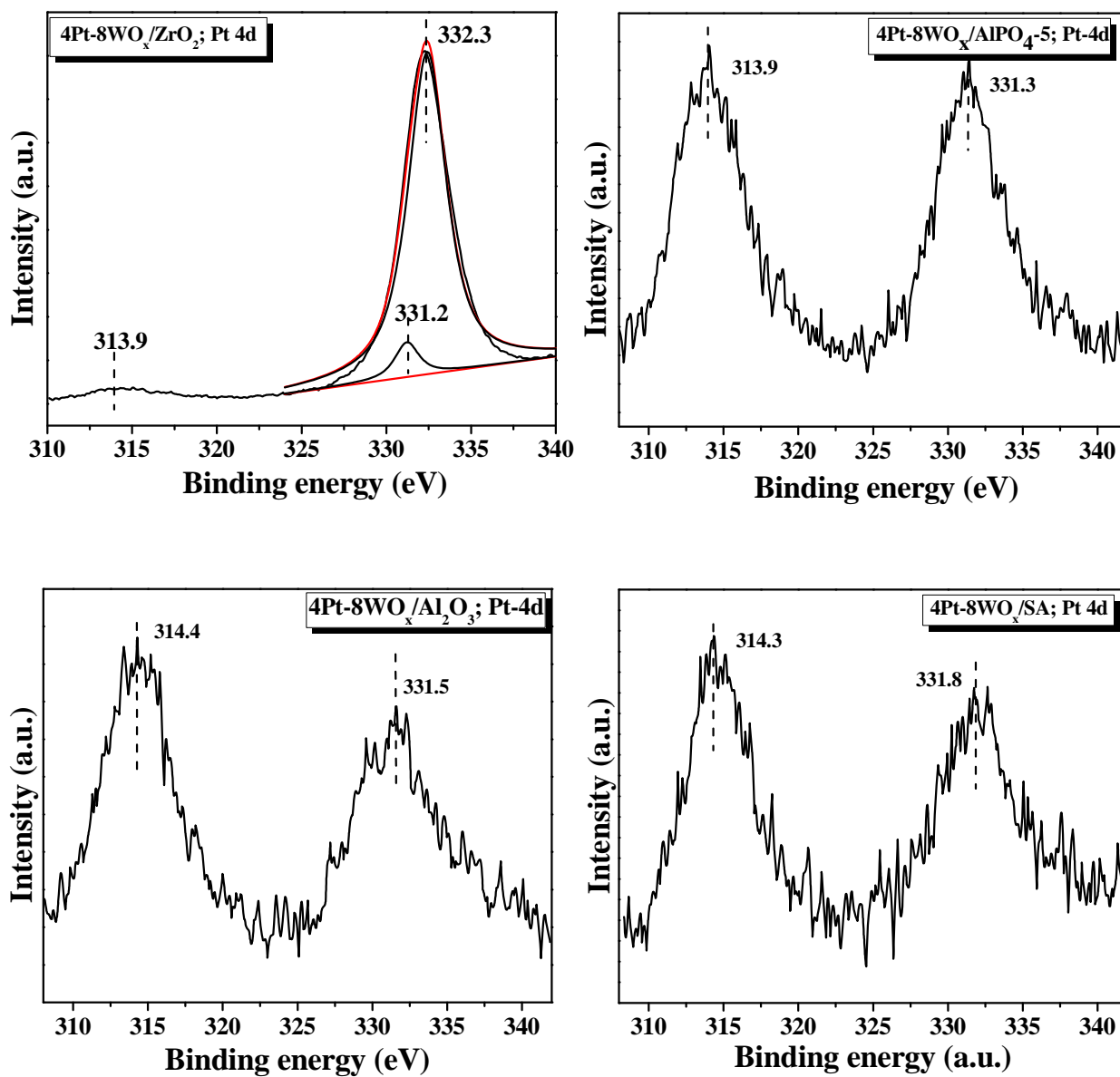


Fig. 5.5(a). XPS (Pt 4d lines) of reduced WO_x-promoted supported Pt catalysts.

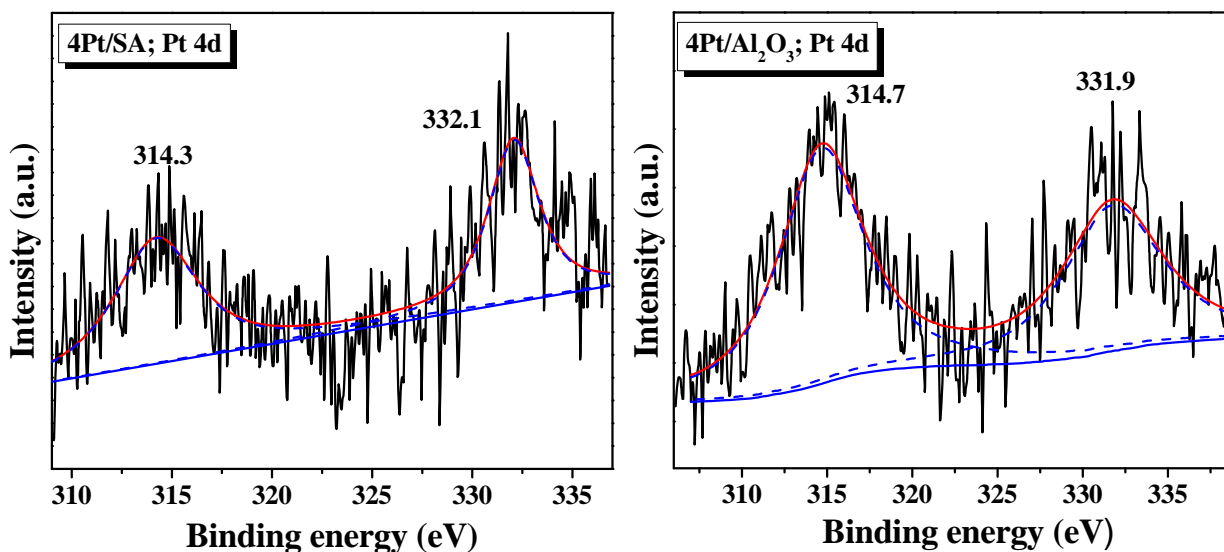


Fig. 5.5(b). XPS (Pt 4d lines) of reduced unpromoted supported Pt catalysts.

5.3.1.7. H₂-TPR

Temperature-programmed reduction with hydrogen (H₂-TPR) of unreduced promoted Pt catalysts showed a sharp peak at 59–75 °C due to reduction of platinum from +2 to zero state. It also showed two broad reduction peaks at 310–384 and 590–680 °C attributed to step-wise reduction of WO₃ (from +6 to +5/4) on the surface. Usually, WO₃ reduces above 700 °C. However, in presence of Pt, its reducibility started at 310 °C itself. Based on TPR peak positions the reducibility of Pt and W in 4Pt-8WO_x/ZrO₂ (Pt: 67 °C, W:310 and 590 °C) was found higher than in the other catalysts. This facile and enhanced reducibility could be attributed to the synergy between Pt and WO_x and support interaction. Hydrogen spillover occurs from Pt to WO_x, partly reducing its surface. Such facile redox behavior was observed also by Zhu et al. [38] for Pt-W/ZSM-5 catalysts and Benson et al. [39] for WO₃ and platinum black mixtures. Thus, WO_x modifies the structure and electronic properties of Pt and support influences the acidity, reducibility, metallic nature and dispersion.

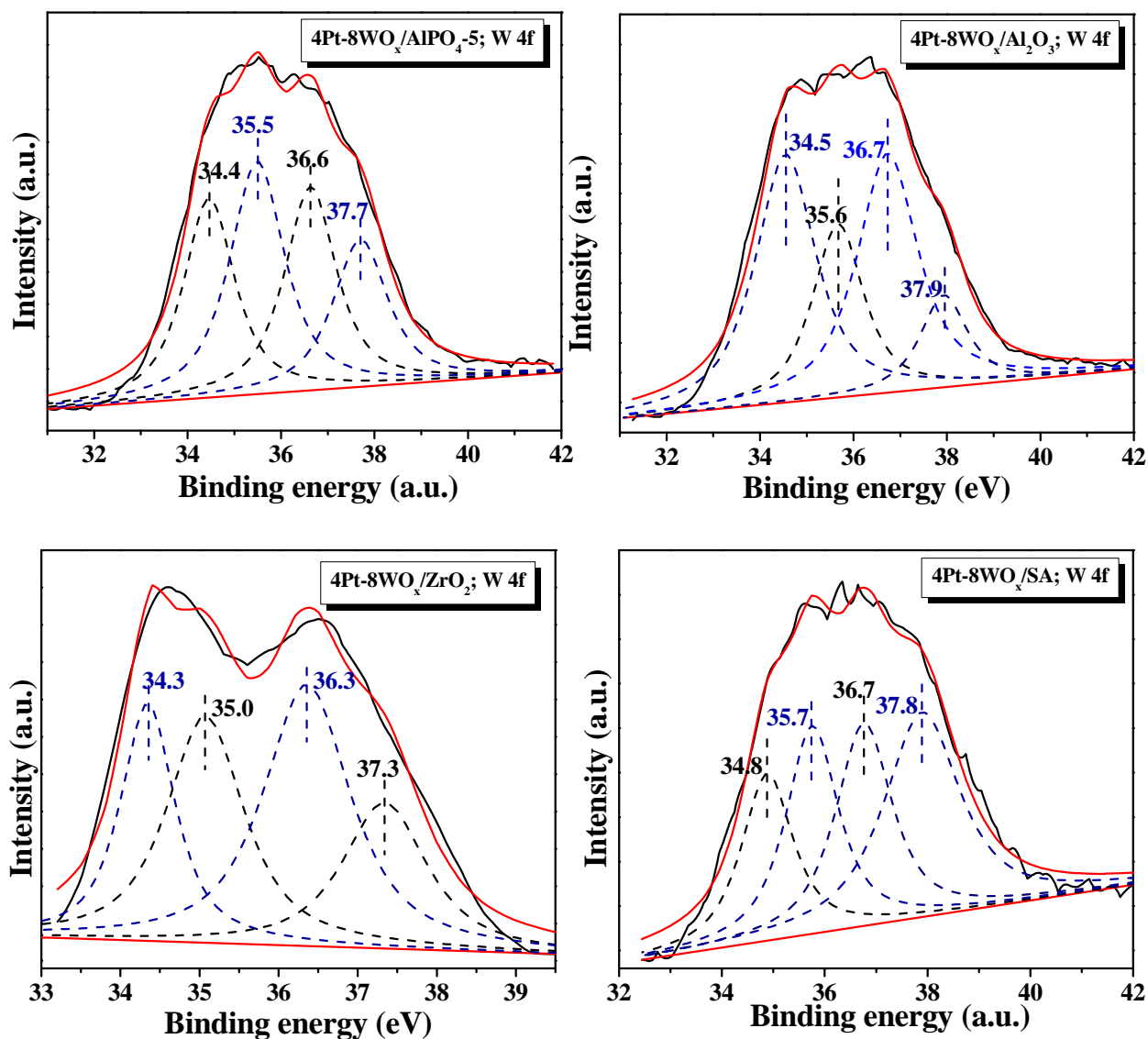
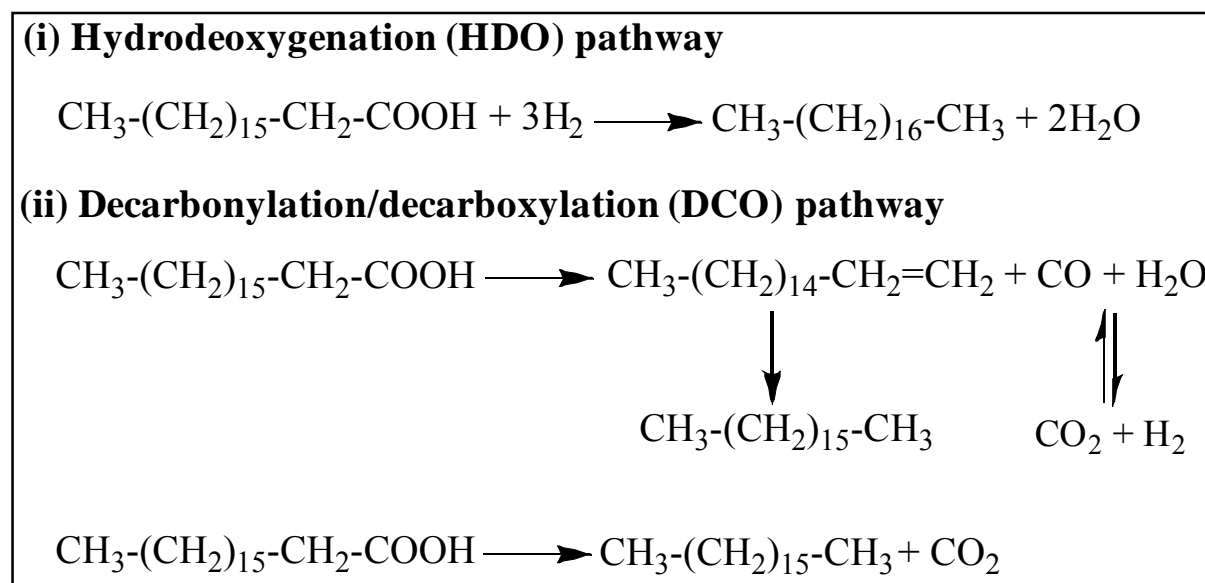


Fig. 5.5(c). XPS W 4f lines of WO_x-promoted supported Pt catalysts.

5.3.2. Catalytic activity

Catalytic activity data for deoxygenation of oleic acid (OA) over unpromoted and WO_x-promoted supported Pt catalysts are reported in Table 5.2. These catalysts were highly active for the deoxygenation reaction even at 260 °C. Significant conversion of OA was observed within 15 min itself. As stated before, deoxygenation can occur through two different reaction pathways: (1) hydrodeoxygenation (HDO) and (2) decarbonylation/decarboxylation (DCO) (Scheme 5.1). The HDO path results in octadecane (C₁₈) as final hydrocarbon product with alcohols and aldehydes (other products) being intermediates in hydrogenation. Water is the byproduct of the reaction. Through DCO pathway, heptadecane (C₁₇) is the final hydrocarbon product with CO + H₂O/CO₂ being the byproducts. C₁₈ and C₁₇ alkenes would also be formed as intermediates. However, at chosen reaction conditions (20 bar H₂), alkanes are the major products with aldehyde/alcohols (others) being the minor products.



Scheme 5.1. Reaction pathways of fatty acid deoxygenation.

Control experiments at 260 °C and 20 bar H₂ pressure revealed that the deoxygenation reaction of OA in the absence of a catalyst was insignificant at these conditions (Table 5.2; OA conversion at the end of 15 min and 5 h was 3 mol% and 5 mol%, respectively). Hence, this temperature was chosen in other experiments to monitor the effect of catalyst support on the deoxygenation activity. Support has a marked effect on the catalytic activity (OA conversion). The catalytic activity of unpromoted Pt on different supports at the end of 15 min varied in the

order: 4Pt/ZrO₂ (40 mol%) > 4Pt/AlPO₄₋₅ (39 mol%) > 4Pt/SA (36 mol%) > 4Pt/Al₂O₃ (12 mol%) and the same at the end of 5 h decreased in the order: 4Pt/SA (69 mol%) > 4Pt/ZrO₂ (55 mol%) > 4Pt/AlPO₄₋₅ (48 mol%) > 4Pt/Al₂O₃ (36 mol%). In general, C₁₇ is the major product (than C₁₈) at both 15 min and 5 h, conforming the preference of DCO mechanism over unpromoted Pt catalysts. At longer times (5 h), 4Pt/AlPO₄₋₅ and 4Pt/Al₂O₃ showed formation of significant quantities of other products. This changed order in activity and selectivity could be due to difference in the stability of these catalysts during the run.

The WO_x-promoted supported Pt catalysts exhibited a significant increase in catalytic activity (compared to their unpromoted Pt analogues) which varied at the end of 15 min in the order: 4Pt-8WO_x/ZrO₂ (62 mol%) > 4Pt-8WO_x/SA (52 mol%) > 4Pt-8WO_x/AlPO₄₋₅ (48 mol%) > 4Pt-8WO_x/Al₂O₃ (39 mol%) and at the end of 5 h in the order: 4Pt-8WO_x/ZrO₂ (100 mol%) > 4Pt-8WO_x/AlPO₄₋₅ (93 mol%) > 4Pt-8WO_x/Al₂O₃ (86 mol%) > 4Pt-8WO_x/SA (82 mol%) (Table 5.2). Irrespective of the support, the promoted Pt catalysts exhibited significantly higher selectivity for C₁₈ (71–91%) than for C₁₇ (8.2–21.8%) hydrocarbon product confirming that HDO is the prominent mechanism of deoxygenation over these WO_x-promoted Pt catalysts. The content of other products with WO_x-promoted Pt was very less compared to that with corresponding unpromoted Pt catalysts. 4Pt-8WO_x/ZrO₂ exhibited complete conversion and near 90% selectivity for C₁₈ (HDO) product. These observations clearly point out that WO_x enhances the catalytic activity and HDO selectivity of Pt. Catalytic activity increased with increasing reaction temperature but the C₁₈ selectivity was lower (Table 5.3). At higher temperatures elimination of CO/CO₂ from OA through DCO competes with the catalytic HDO reaction and thereby lowers the selectivity of C₁₈ product.

The catalyst, 4Pt-8WO_x/Al₂O₃ was reused in five recycling experiments conducted at 320 °C and 25 bar H₂ pressure; 100% conversion of OA was achieved in all the recycling studies; interestingly, C₁₈ product selectivity increased from 67.1 to 80.8% on reuse, while C₁₇ selectivity decreased from 31.6 to 18.5%. In these experiments, at the end of each run, the catalyst was separated, washed with acetone and dried at 110 °C for 12 h. It was reduced in hydrogen at 350 °C for 2.5 h prior to use in the next recycle. For 4Pt-8WO_x/AlPO₄₋₅, decrease in catalytic activity upon reuse in two recycling experiments was observed. No Pt or W loss was detected in

Table 5.2. Deoxygenation of oleic acid over supported Pt catalysts^a

Catalyst	Reaction time = 15 min					Reaction time = 5 h				
	OA conversion (mol%) ^b	Product selectivity (wt. %) ^c				OA conversion (mol%) ^b	Product selectivity (wt. %) ^c			
		C ₁₈	C ₁₇	C ₁₀₋₁₆	Others ^d		C ₁₈	C ₁₇	C ₁₀₋₁₆	Others ^d
No catalyst	3.0	2.0	0.2	4.7	98.0	5.0	5.7	4.2	0.0	90.0
<i>A: Unpromoted Pt catalysts</i>										
4Pt/SiO ₂ -Al ₂ O ₃	36.0	36.3	60.0	0.7	2.0	69.0	37.4	61.1	0.7	0.7
4Pt/AlPO ₄ -5	39.0	15.0	82.6	0.4	1.9	48.0	13.8	74.9	0.7	10.5
4Pt/Al ₂ O ₃	12.0	28.5	63.6	1.3	6.6	36.0	22.0	64.0	0.9	13.0
4Pt/ZrO ₂	40.0	43.0	40.0	0.0	17.0	55.0	37.1	58.2	0.8	3.9
<i>B: WO_x promoted Pt catalysts</i>										
4Pt-8WO _x /SiO ₂ -Al ₂ O ₃	52.0	88.2	10.9	0.6	0.2	82.0	88.0	11.3	0.4	0.4
4Pt-8WO _x /AlPO ₄ -5	48.0	82.6	15.0	0.4	1.9	93.0	80.8	18.3	0.8	0.0
4Pt-8WO _x /Al ₂ O ₃	39.0	71.3	21.7	0.6	6.5	86.0	75.3	21.8	1.6	1.3
4Pt-8WO _x /ZrO ₂	62.0	91.4	8.2	0.5	0.4	100.0	89.4	10.0	0.6	0.0

^aReaction conditions: Catalyst = 0.2 g, oleic acid (OA) = 2 g, n-heptane (solvent) = 30 g, pressure = 20 bar H₂, reaction temperature = 260 °C, ^bDetermined from titration with NaOH, ^cDetermined from GC analysis, ^dOthers include octadecanal and octadecanol.

the spent catalyst (ICP-OES analysis). XRD of the spent 4Pt-8WO_x/Al₂O₃ catalyst (after 5 recycles) was the same as that of the fresh catalyst. Only a marginal decrease in S_{BET} from 266 to 212 m²/g was observed (Chapter-4). However, TEM of the spent catalyst inferred a marginal increase in Pt particle size from 3 to 5 nm. In case of 4Pt-8WO_x/AlPO₄-5, the particle size of Pt (after two recycles) increased by 1 nm. However, the crystallinity of the support AlPO₄-5 decreased on reuse (Chapter-3).

NH₃-TPD and CO-chemisorption studies of the spent catalysts in the experiments conducted at 260 °C, 20 bar H₂ pressure and 5 h run time revealed that except for 4Pt-8WO_x/SA the acidity of the catalyst increased marginally (from 0.945 to 1.130 mmol/g for 4Pt-8WO_x/AlPO₄-5, 0.240 to 0.244 mmol/g for 4Pt-8WO_x/ZrO₂ and 1.410 to 1.423 mmol/g for 4Pt-8WO_x/Al₂O₃) (Table 5.1). This could be because of wetting of catalyst surface with OA. Particle size of Pt increased drastically for 4Pt-8WO_x/Al₂O₃ (from 2.7 to 15.8 nm), 4Pt-8WO_x/SA (21 to 105 nm) and 4Pt-8WO_x/AlPO₄-5 (21 to 245 nm) in low temperature (260 °C) reactions. However, this increase in Pt particle size was lower for 4Pt-8WO_x/ZrO₂ (7.6 to 12.1 nm). In other words, the support while influencing the catalytic activity, it also affected the sintering of Pt and overall stability of the catalyst in recycle experiments. Thus the choice of support is crucial.

Table 5.3. Catalytic deoxygenation activity of WO_x-promoted supported Pt catalysts at 280 °C^a

Catalyst	OA conversion (mol%) ^b	Product selectivity (wt.%) ^c			
		C ₁₈	C ₁₇	C ₁₀₋₁₆	Others ^d
4Pt-8WO _x /SiO ₂ -Al ₂ O ₃	90.0	84.0	15.0	0.6	0.4
4Pt-8WO _x /AlPO ₄ -5	100.0	81.7	17.6	0.7	0
4Pt-8WO _x /Al ₂ O ₃	98.0	69.2	30.1	0.7	0
4Pt-8WO _x /ZrO ₂	100.0	85.1	14.3	0.6	0

^aReaction conditions: Catalyst = 0.2 g, oleic acid (OA) = 2 g, n-heptane (solvent) = 30 g, pressure = 20 bar H₂, reaction temperature = 280 °C, reaction time = 5 h, ^bDetermined from titration with NaOH, ^cDetermined from GC analysis, ^dOthers include octadecanal and octadecanol.

5.3.3. Structure-activity correlations

A plot of Pt dispersion (for WO_x-promoted catalysts) versus catalytic activity reveals that OA conversion increases with increasing metal dispersion (on SA, AlPO₄-5 and ZrO₂ supports), but then, beyond a certain dispersion value it started decreasing (Fig. 5.6). The 4Pt-8WO_x/ZrO₂ seems to have optimum dispersion of metal for higher catalytic activity. On the other hand, 4Pt-8WO_x/SA having percentage metal dispersion of 5 and 4Pt-8WO_x/Al₂O₃ having dispersion of 42 exhibited more or less the same OA conversion (82 and 86 mol%, respectively). Thus, Fig. 5.6 reveals that metal dispersion is important but not the primary factor determining the catalytic deoxygenation activity.

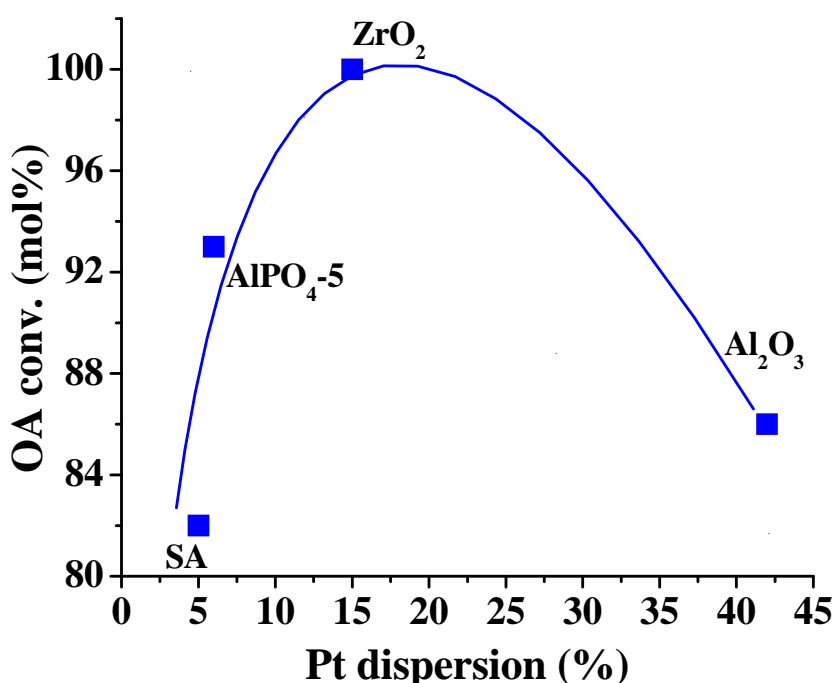


Fig. 5.6. Effect of Pt dispersion on the catalytic activity of WO_x-promoted supported Pt catalysts.

An inverse correlation was observed between binding energy of Pt (4d_{3/2}) and OA conversion (Fig. 5.7). OA conversion increased with decreasing value of binding energy that is with increasing metallic nature of platinum (electron rich platinum). This is because higher the metallicity higher will be the dissociative splitting and spillover of adsorbed hydrogen and thereby, higher will be the catalytic activity. 4Pt-8WO_x/ZrO₂ having lowest Pt 4d_{3/2} binding

energy showed the highest catalytic activity, while 4Pt-8WO_x/SA having highest value of binding energy showed the lowest catalytic performance.

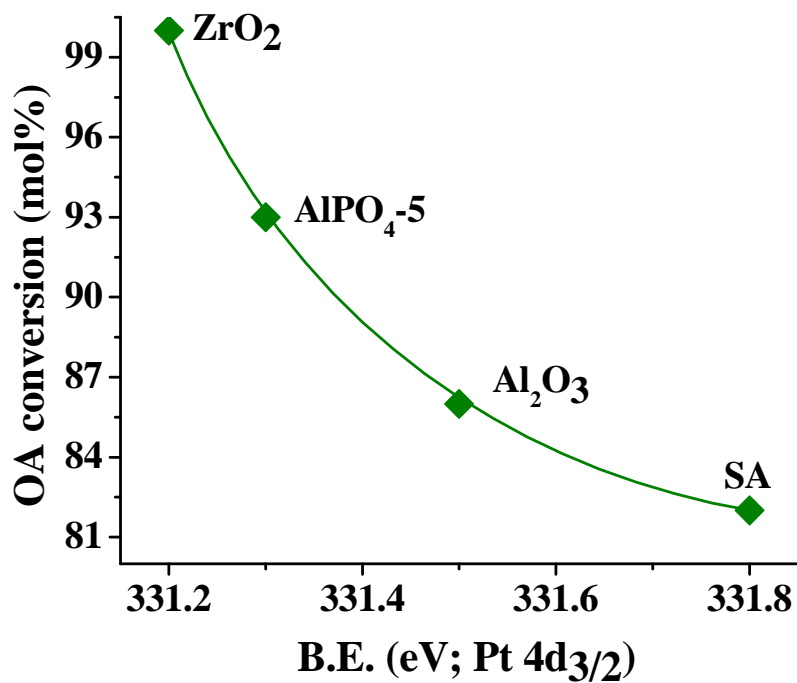


Fig. 5.7. Effect of Pt electronic nature on the catalytic activity of WO_x-promoted catalysts

It was observed that acidity (medium + strong acid sites, NH₃ desorption in the temperature range of 200–550 °C) and C₁₈ (HDO) product selectivity were found to have inverse linear relation (Fig. 5.8). Higher the acidity higher would be the cracking activity and hence, lower would be C₁₈ selectivity. Among the catalysts tested, 4Pt-8WO_x/Al₂O₃ having higher amount and strength of strong acid sites (Fig. 5.3) showed lower selectivity for C₁₈, while 4Pt-8WO_x/ZrO₂ having lower acidity showed higher selectivity for C₁₈ product. Metallic or electron rich Pt is crucial for high activation and splitting of hydrogen and thereby, the deoxygenation reaction. Dispersion and surface area of Pt are important but electron rich metal (which is also determined by the acidity of the support) is a more important parameter in hydrodeoxygenation of vegetable oils. Because of this reason, some catalysts in spite of having high surface area and metal dispersion could not perform well.

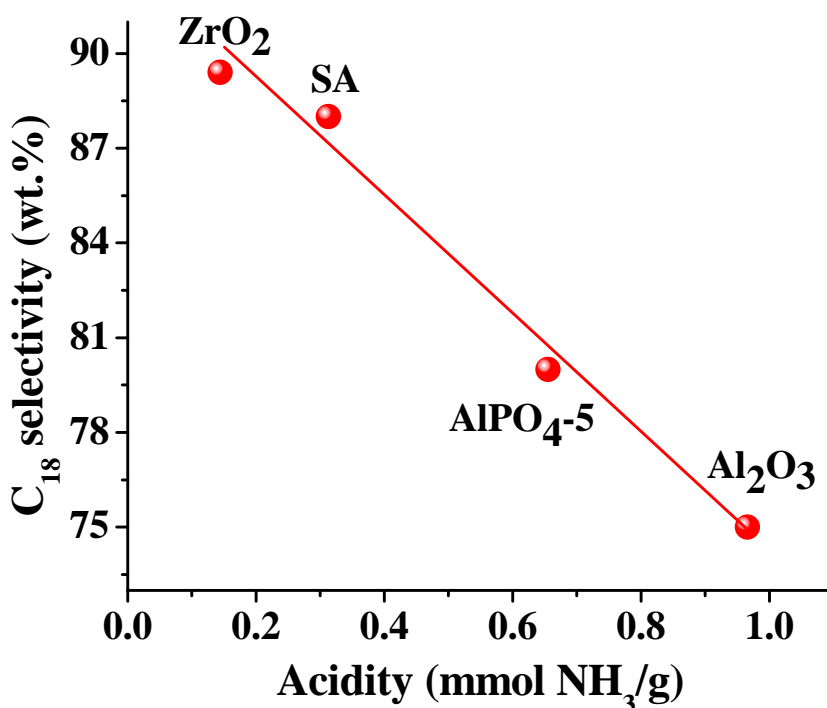


Fig. 5.8. Effect of acidity of WO_x-promoted catalysts on product selectivity.

5.4. Conclusions

Deoxygenation of OA forming diesel-range hydrocarbons (green diesel) was investigated over unpromoted and WO_x-promoted Pt catalysts supported on SA, Al₂O₃, AlPO₄₋₅ and ZrO₂. Promotion with WO_x and support affected the structure and electronic properties of platinum. WO_x promoted the catalytic activity and HDO selectivity of platinum. Supports through their varying acidity influenced metal dispersion and electron density at platinum. These catalysts were highly active for deoxygenation of OA even at 260 °C. WO_x-promoted Pt supported on ZrO₂ showed superior performance to the other catalysts, due to adequate metal dispersion, high electron density at metal (enhancing hydrogen dissociation activity), high amount of W⁵⁺ species in its composition (enhancing OA activation) and less amount of strong acid sites. This study reveals that choice of support is crucial in designing an efficient deoxygenation catalyst.

5.5. References

- [1] B. Iama, in: R. Luque, J. Campelo, J. Clark (Eds.), *Hand Book of Biofuels: Process and Technologies*, Woodhead Publishing Ltd., 2011.
- [2] T.V. Choudhary, C.B. Phillips, *Appl. Catal. A: Gen.* 397 (2011) 1-12.

- [3] P.M. Mortensen, J.-D. Greenwaldt, P.A. Jensen, K.G. Knudsen, A.D. Jensen, *Appl. Catal. A: Gen.* 407 (2011) 1-19.
- [4] C. Zhao, T. Bruck, J.A. Lercher, *Green Chem.* 15 (2013) 1720-1739.
- [5] <http://www.nesteoil.com>.
- [6] US Patent No. 7,511,181 B2 (2009) -UOP LLC, US.
- [7] US Patent No. 8,003,836 B2 (2011) - UOP LLC, US.
- [8] <http://www.uop.com/pr/release/PR.EniEcofiningFacility.pdf>.
- [9] <http://www.tyson.com/RenewableEnergy/Initiative/Conoco/Default.aspx>.
- [10] B. Donnis, R.G. Egeberg, P. Blom, K.G. Knudsen, *Top. Catal.* 52 (2009) 229-240.
- [11] T.M. Sankaranarayanan, M. Banu, A. Pandurangan, S. Sivasanker, *Bioresour. Technol.* 102 (2011) 10717-10723.
- [12] J. K. Satyarthi, D. Srinivas, *Energy Fuels*, 25 (2011) 3318-3322.
- [13] M. Gousi, C. Andriopoulou, K. Bourikas, S. Ladas, M. Sotiriou, C. Kordulis, A. Lycourghiotis, *Appl. Catal. A: Gen.* 536 (2017) 45-56.
- [14] A. N. Varakin, V. A. Salnikov, M. S. Nikulshina, K. I. Maslakov, A. V. Mozhaev, *Catal. Today*, 292 (2017) 110-120.
- [15] N. Arun, J. Maley, N. Chen, R. Sammynaiken, Y. Hu, A.K. Dalai, *Catal. Today*, 291 (2017) 153-159.
- [16] L. Yang, K.L. Tate, J.B. Jasinski, M.A. Carreon, *ACS Catal.* 5 (2015) 6497-6502.
- [17] M. Ahmadi, A. Nambo, J.B. Jasinski, P. Ratnasamy, M.A. Carreon, *Catal. Sci. Technol.* 5 (2015) 380-388.
- [18] S. Lestari, P. Mäki-Arvela, H. Bernas, O. Simakova, R. Sjöholm, J. Beltramini, G.Q. Max Lu, J. Myllyoja, I. Simakova, D.Y. Murzin, *Energy Fuels*, 23 (2009) 3842-3845.
- [19] I. Simakova, O. Simakova, P. Mäki-Arvela, A. Simakova, M. Estrada, D.Y. Murzin, *Appl. Catal. A: Gen.* 355 (2009) 100-108.

- [20] P.T. Do, M. Chiappero, L.L. Lobban, D.E. Resasco, *Catal. Lett.* 130 (2009) 9-18.
- [21] M.Y. Kim, J.-K. Kim, M.-E. Lee, S. Lee, M. Choi, *ACS Catal.* 7 (2017) 6256-6267.
- [22] M. Sánchez-Cárdenas, J. Medina-Valtierra, S.-K. Kamaraj, F. Trejo-Zárraga, L.A.Sánchez-Olmos, *Environ. Prog. Sustain. Energy* (2017), <http://dx.doi.org/10.1002/ep.12563>.
- [23] Nicolás A. Grosso-Giordano, Todd R. Eaton, Zhenyu Bo, Sara Yacob, Chieh-Chao Yang, Justin M. Notestein, *Appl. Catal. B: Environ.*, 192 (2016) 93–100.
- [24] Ryan Loe, Eduardo Santillan-Jimenez, Tonya Morgan, Lilia Sewell, Yaying Ji, Samantha Jones, Mark A. Isaacs, Adam F. Lee, Mark Crocker, *Appl. Catal. B: Environ.*, 191 (2016) 147–156.
- [25] M. V. Tsodikov, A. V. Chistyakov, M. A. Gubanov, P. A. Zharova, S. S. Shapovalov, A. A. Pasynskii, V.V. Kriventsov, I.I. Moiseev, *Rus. Chem. Bull. Int. Ed.* 64 (2015) 2062-2068.
- [26] N. Chen, Y. Ren, E.W. Qian, *J. Catal.* 334 (2016) 79-88.
- [27] D. Kim, D.R. Vardon, D. Murali, B.K. Sharma, T.J. Strathmann, *ACS Sustain.Chem. Eng.* 4 (2016) 1775-1784.
- [28] K. Maruta, Y. Liu, M. Inaba, I. Takahara, *Energy Fuels* 24 (2010) 2404-2409.
- [29] J. Zhang, C. Zhao, *ACS Catal.* 6 (2016) 4512-4525.
- [30] A. A. Dwiatmoko, I. Kim, L. Zhou, J.-W. Choi, D.J. Suh, J. Jae, J.-M. Ha, *Appl. Catal. A: Gen.* 543 (2017) 10-16.
- [31] M. Mokhtar, S.N. Basahel, T.T. Ali, *J. Mater. Sci.* 48 (2013) 2705-2713.
- [32] A.J. Mora, A.N. Fitch, M. Cole, R. Goyal, R.H. Jones, H. Jobic, S.W. Carr, *J. Mater.Chem.* 6 (1996) 1831-1835.
- [33] J. Chaminand, L. Djakovitch, P. Gallezot, P. Marion, C. Pinel, C. Rosier, *Green Chem.* 6 (2004) 359-361.

- [34] T. Deng, H. Liu, *Green Chem.* 15 (2013) 116-124.
- [35] S. Zhu, X. Gao, Y. Zhu, Y. Li, *J. Mol. Catal. A: Chem.* 398 (2015) 391-398.
- [36] T.Y. Kim, D.S. Park, Y. Choi, J. Baek, J.R. Park, J. Yi, *J. Mater. Chem.* 22 (2012) 10021-10028.
- [37] S. Kuba, M. Che, R.K. Grasselli, H. Knözinger, *J. Phys. Chem. B* 107 (2003) 3459-3463.
- [38] Z. Zhu, G. Lu, Y. Guo, Y. Guo, Z. Zhang, Y. Wang, X.-Q. Gong, *ChemCatChem* 5(2013) 2495-2503.
- [39] J.E. Benson, H.W. Kohn, M. Boudart, *J. Catal.* 5 (1966) 307-313.

Chapter-6
Reducible Oxide Promoted Hydrodeoxygenation Activity
of Pt-MO_x/Al₂O₃ in Biofuels Production

6.1. Introduction

At present most of the world energy needs are met from fossil resources. These energy resources are limited and at the current rate of consumption they last for a few more decades only. Further, their use has adversely affected the environment. Renewable energy has been becoming important in the 21st century towards achieving the goal of sustainable development. Biofuels derived from inedible biomass are a suitable source of renewable energy for transportation [1]. These fuels are carbon neutral. They lead to reduced greenhouse gas (GHG) emissions. Their use could render to reduced oil import bill for a nation not rich in fossil resources. Deoxygenation is an important reaction in biorefinery [2]. It is an attractive approach for producing renewable, diesel-range hydrocarbons (namely "*green diesel*") from inedible oils which could be used as stand-alone fuel or as blend with the conventional diesel for application in IC engines [3, 4]. Green diesel comes with an added advantage of high cetane number, low cloud point and high oxidation stability. Further, the green diesel process could be integrated with the petroleum refining processes.

Oxygen in vegetable oils can be removed by two ways: decarbonylation/decarboxylation (hereafter referred as DCO) and hydrodeoxygenation/hydrodehydrogenation (hereafter referred as HDO). The extent of each reaction depends on the catalyst and process conditions. Neste Oil, UOP/Eni (EcofiningTM), Honeywell (Green Jet Fuel Technology), ConocoPhillips - Tyson Foods have commercialized the green diesel production through the HDO route [5-7]. Conventional hydrotreating catalysts *viz.*, Ni-Mo(W)/Al₂O₃ and Co/Mo(W)/Al₂O₃ are used. But they require high temperature (325 - 380 °C) and hydrogen pressure (50 - 80 bar) [8, 9]. Supported noble metal catalysts (*ca.*, Pt(Pd)/zeolite, Pt(Pd)/SAPO-11/34, Pd/C, etc.) adopt the DCO pathway [10-15]. However, stability of these catalysts during the reaction is still an issue. For deoxygenation process to be economical, the catalyst should be highly active even at low temperatures (200 - 260 °C) and pressure (5 - 20 bar hydrogen) with little or minimum carbon loss and high product selectivity and yield. Development of such a catalytic hydrodeoxygenation process is highly desirable.

Promoters alter the electronic and structural factors of the active phases in the catalyst. These changes in the catalyst structure bring in drastic change in reaction rates and reaction path. Promoter is the work load sharing factor of the active phase. The modification of the catalyst nature by promoter/additives was well studied and reported by many research groups for glycerol hydrogenolysis as well as deoxygenation of biomass (fatty acids and vegetable oils) [16-18]. Tsodikov et al. [19] disclosed that co-deposition of Sn changes the activity and

selectivity of Pt in deoxygenation of fatty acid triglycerides derived from vegetable oils and micro algae. Choi et al. [20] reported that $\text{WO}_x/\text{Pt}/\text{TiO}_2$ is a more efficient catalyst than Pt/TiO_2 , WO_x/TiO_2 and Pd/AC for deoxygenation of stearic acid and jatropha fatty acids enabling conversions of 86% at 300-410 °C. Kon et al. [21] presented high efficiency of $\text{Pt}-\text{MoO}_x/\text{TiO}_2$ for hydrodeoxygenation of fatty acids and triglycerides at 230 °C and 50 bar H_2 with a product yield of 89 - 99% in 48 h at high Pt loading (0.1 mol%).

In the hydrogenolysis of glycerol over $\text{Pt}/\text{WO}_x/\text{Al}_2\text{O}_3$ catalyst, García-Fernández et al. [22] and Zhu et al. [23] found that highly dispersed polytungstate species, improved electronic interaction between Pt and tungsten oxide and hydrogen spillover are the factors responsible for high 1,3-propanediol selectivity. Robinson et al. [24] reported that Mo in Pt-Mo bimetallic catalyst was in a reduced state under the reaction conditions of hydrodeoxygenation of m-cresol. Mo sites in contact with Pt surface enable increased interaction with the oxygen of m-cresol and dramatically lower the barrier for m-cresol tautomerization followed by deoxygenation. Yang et al. [25] demonstrated that Pd promotes the reduction of iron species and the generation of Pd-Fe alloy and both these effects lead to higher activity of $\text{Pd}-\text{FeO}_x/\text{SiO}_2$ than Pd/SiO_2 catalyst for HDO of furans. Thus, reducibility of promoter oxide and contact between metal-promoter oxide are crucial in deoxygenation reactions. To establish this further and to develop a still more efficient catalyst, in this work, a series of reducible oxide (MO_x ; M = Mo, Re, W and Sn)-promoted $\text{Pt}/\text{Al}_2\text{O}_3$ catalysts for deoxygenation reaction are investigated. The relative redox potentials of metals in these oxides (with respect to Pt) are different and thereby, affect differently the deoxygenation activity/selectivity of fatty acids producing green diesel.

6.2. Experimental

6.2.1. Catalyst preparation

In this study, a commercial $\gamma\text{-Al}_2\text{O}_3$ (supplied by Süd-Chemie India Pvt. Ltd., New Delhi) was used as support without any further modifications. A known quantity (8 wt%) of different metal oxides (WO_x , MoO_x , ReO_x and SnO_x) and Pt (4 wt%) were loaded on $\gamma\text{-Al}_2\text{O}_3$ by using wet-impregnation method. The details of procedures involved in catalyst preparation are mentioned in Chapter-2.

6.2.2. Catalyst characterization and reaction procedure

For characterization of the catalysts, various techniques (X-ray powder diffraction (XRD), N_2 -physisorption, CO-chemisorption, NH_3 -Temperature-programmed desorption (NH_3 -TPD), H_2 -Temperature-programmed reduction (H_2 -TPR), X-ray photoelectron spectroscopy (XPS) and transmission electron microscopy (TEM)) were used and a detailed

illustration of characterization techniques, reaction procedure and product analysis methods are presented in Chapter-2.

6.3. Results and discussion

6.3.1. Catalyst characterization

6.3.1.1. N_2 -Physisorption

γ - Al_2O_3 used in this study has a specific surface area (S_{BET}) of 352 m^2/g , pore volume of 0.68 cc/g and average pore size of 3.9 nm. On loading Pt, S_{BET} of the sample (4Pt/ Al_2O_3) decreased to 292 m^2/g and pore volume to 0.66 cc/g . When reducible oxide was also present (4Pt-8 MO_x / Al_2O_3), this value decreased still further ($S_{BET} = 187 - 269 m^2/g$; pore volume = 0.16 - 0.23 cc/g and average pore size = 1.4 - 1.9 nm; Table 6.1). Partial blockage of pores by Pt and reducible oxide (MO_x) particles is the possible cause for reduction in the textural property values.

6.3.1.2. CO-chemisorption

Chemisorption studies pointed out that the monolayer uptake of CO by 4Pt/ Al_2O_3 was 100 $\mu mol/g$. This value for 4Pt-8 MO_x / Al_2O_3 catalysts decreased to 36 - 76 $\mu mol/g$. Active specific surface area, percentage dispersion and average crystallite size of supported Pt were determined from the monolayer CO uptake values assuming the stoichiometric molar ratio of CO/Pt as unity (Table 6.1). In the presence of reducible oxide, the average crystallite size of Pt had increased from 1.2 to 3.0-6.4 nm and percentage metal dispersion decreased from 49 to 18-37. Metal surface area and metal dispersion for different supported Pt catalysts decreased in the order: 4Pt/ Al_2O_3 > 4Pt-8 WO_x / Al_2O_3 > 4Pt-8 SnO_x / Al_2O_3 > 4Pt-8 MoO_x / Al_2O_3 > 4Pt-8 ReO_x / Al_2O_3 . Average Pt crystallite size followed the reverse order. Such variations in CO uptake and Pt dispersion were reported also by Ro et al. [26] for Pt- MoO_x / SiO_2 catalysts used in reverse water gas shift reaction and Yang et al. [25] for Pd- FeO_x / SiO_2 catalysts used in hydrodeoxygenation of furans under atmospheric pressure. Thus, the study reveals that the type of reducible oxide (MO_x) affects differently the structural and textural properties of Pt.

6.3.1.3. X-ray diffraction

XRD showed characteristic peaks at 39.7, 45.2, 67.3, 81.3 and 85.6° arising from (111), (200), (220), (311) and (322) crystal planes of metallic Pt with a cubic closed-pack structure (having a space group of Fm-3m; JCPDS No. 65-2868) (Fig. 6.1). These peaks (mainly the reflection from (111) and (200) of Pt) overlapped with the broad diffused peaks of support γ - Al_2O_3 and hence, couldn't permit us to determine, precisely, Pt

Table 6.1. Physicochemical characteristics of promoted supported Pt catalysts.

Sample	N ₂ -physisorption			CO-chemisorption				Pt metal particle size (TEM, nm)
	S _{BET} (m ² /g)	Pore volume (cc/g)	Average pore size (nm)	Monolayer uptake (μmol/g)	Pt metal surface area (m ² /g)	Pt metal dispersion (%)	Pt metal crystallite size (nm)	
γ-Al ₂ O ₃	352	0.68	3.9	-	-	-	-	-
4Pt/Al ₂ O ₃	292	0.66	4.5	100	121	49	1.2	2.5
4Pt-8WO _x /Al ₂ O ₃	240	0.23	1.9	76	92	37	3.0	4.1
4Pt-8MoO _x /Al ₂ O ₃	269	0.19	1.4	43	52	21	5.4	5.3
4Pt-8ReO _x /Al ₂ O ₃	242	0.21	1.8	36	44	18	6.4	6.7
4Pt-8SnO _x /Al ₂ O ₃	187	0.16	1.7	49	58	24	4.8	4.0
4Pt-8WO _x /Al ₂ O ₃ (Spent)	-	-	-	15	19	7.5	15.0	5.3
4Pt-8MoO _x /Al ₂ O ₃ (Spent)	-	-	-	17	21	8.4	13.5	7.6
4Pt-8ReO _x /Al ₂ O ₃ (Spent)	-	-	-	21	25	10.1	11.2	7.6

crystallite size from the XRD patterns. No separate peaks due to reducible oxides were found inferring that these oxides are in a highly dispersed state. According to Zhu et al. [23], no diffraction peaks related to tungsten oxide were detected with WO_x loading of ≤ 10 wt%. At these loadings, tungsten oxide was in sub-monolayer coverage and hydrogenolysis of glycerol to 1,3-propanediol was higher. In our study, irrespective of the type of reducible oxide, its content in the catalyst was kept at 8 wt%. Although by mole percentage, tin and molybdenum oxides (in the present series of catalysts) are in much higher content than tungsten and rhenium oxides, absence of crystalline SnO_2 and MoO_3 peaks in the XRD patterns reveals that all these reducible oxides (at 8 wt% loading) are in highly dispersed monolayer coverage regime and Pt is in contact with those mono-layer, two-dimensional polyoxide species. The intense peaks of Pt observed in the case of $4\text{Pt-8ReO}_x/\text{Al}_2\text{O}_3$ are due to larger crystallite size of Pt in that sample (CO chemisorption) than in other promoted supported Pt catalysts (Fig. 6.1).

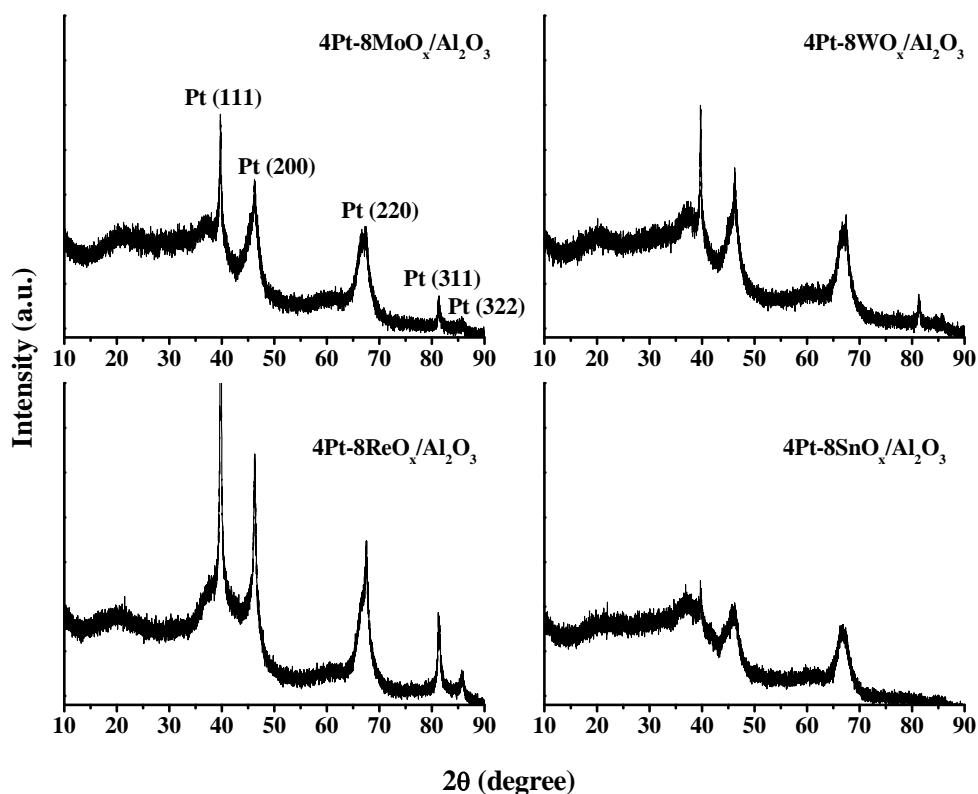


Fig. 6.1. XRD profiles of $\text{Pt-MO}_x/\text{Al}_2\text{O}_3$ catalysts.

6.3.1.4. TEM

Representative TEM images of 4Pt-8MO_x/Al₂O₃ catalysts are shown in Fig. 6.2. About 100 random Pt particles were chosen, particle size histograms were drawn and statistical average particle size of Pt was determined (Fig. 6.3). The particle size of Pt in 4Pt-8MO_x/Al₂O₃ was found larger (4.0 - 6.7 nm) than in 4Pt/Al₂O₃ (2.5 nm). With different reducible oxides, Pt particle size increased in the following order: 4Pt-8SnO_x/Al₂O₃ (4.0 nm) < 4Pt-8WO_x/Al₂O₃ (4.1 nm) < 4Pt-8MoO_x/Al₂O₃ (5.3 nm) < 4Pt-8ReO_x/Al₂O₃ (6.7 nm). The comparable values of crystallite size (CO chemisorption) and particle size (TEM analysis) of Pt confirm that Pt is highly dispersed (even at 4 wt%) in these catalysts and each particle is composed mostly of one Pt crystallite only. The increased crystallite size of Pt when deposited on 8MO_x/Al₂O₃ (instead on "neat" Al₂O₃) suggests direct contact of most of the Pt particles with supported, dispersed reducible oxide (MoO_x, ReO_x, WO_x or SnO_x) than with "bare" Al₂O₃. In other words, in these modified catalysts, Pt is preferentially located on the reducible oxide.

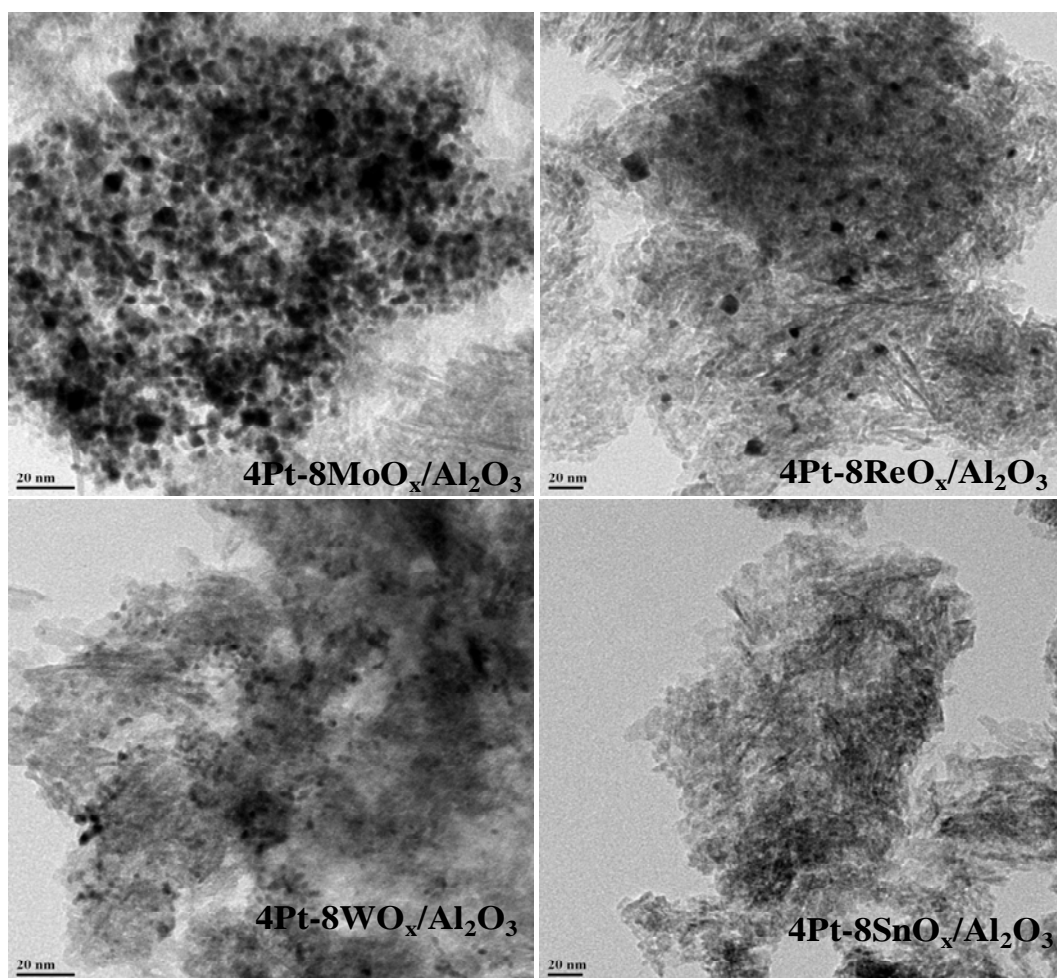


Fig. 6.2. TEM images of Pt-MO_x/Al₂O₃ (MO_x = MoO_x, WO_x, ReO_x or SnO_x) catalysts.

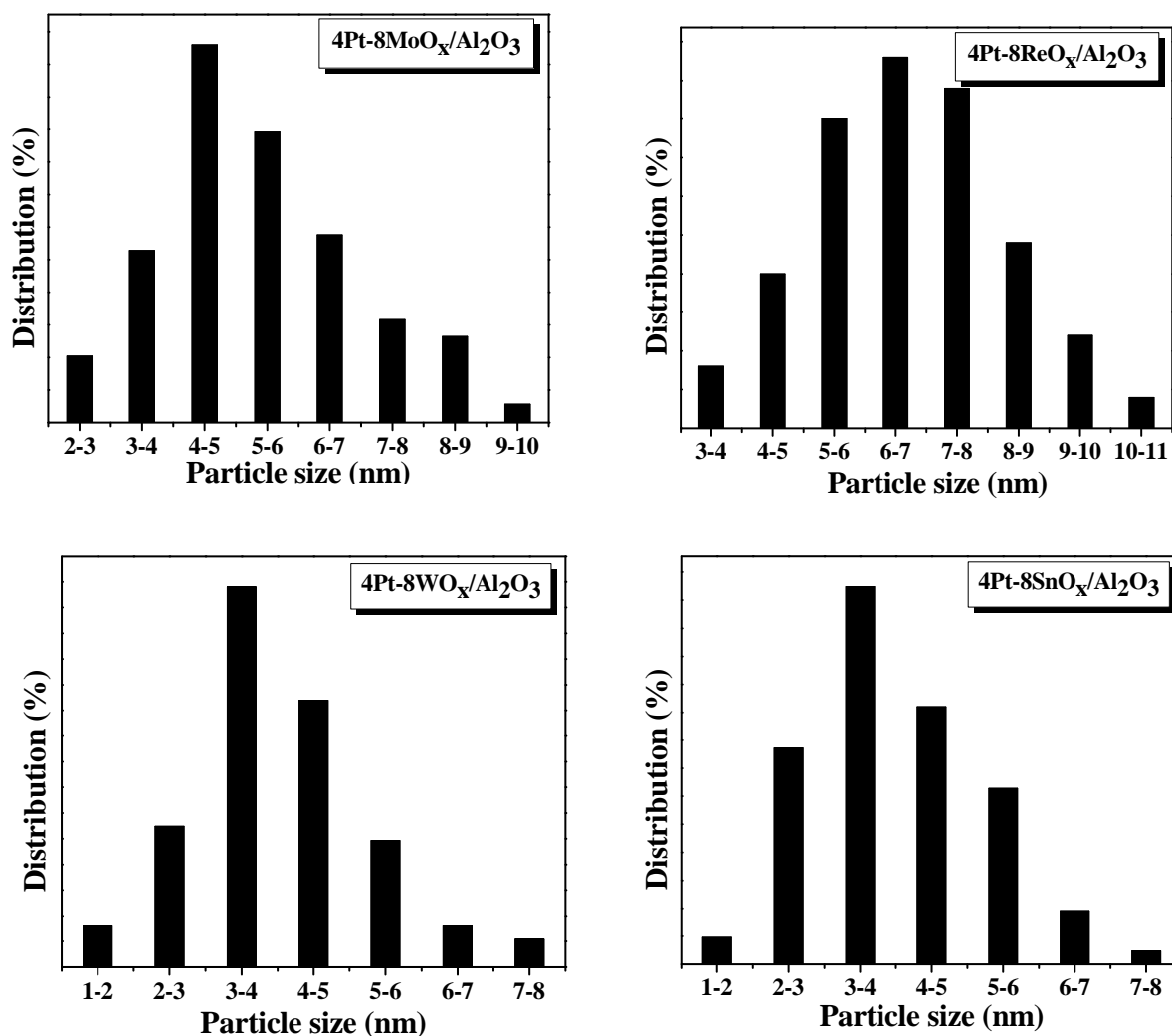


Fig. 6.3. Pt particle size distribution histograms of Pt-MO_x/Al₂O₃ (MO_x = MoO_x, WO_x, ReO_x or SnO_x) catalysts.

6.3.1.5. NH₃-TPD

NH₃-TPD profiles showed a broad desorption in the temperature range of 75 to 550 °C (Fig. 6.4). These profiles could be deconvoluted into four to five peaks attributable to acid sites of different strength located on γ -Al₂O₃ and reducible oxide. They are categorized into weak (desorption maximum: 100 - 200 °C), moderate (200 - 350 °C) and strong (> 350 °C) acid sites. Neat γ -Al₂O₃ had an overall acidity of 0.99 mmol/g with weak, moderate and strong acid sites distribution being 0.40, 0.21 and 0.37 mmol/g, respectively (Table 6.2). The total acidity of the catalyst increased (to 1.27 mmol/g) when Pt was loaded on Al₂O₃. It enhanced still further (to 1.26 - 1.70 mmol/g) for 4Pt-8MO_x/Al₂O₃. In other words, the reducible oxides promoted the overall acidity of Pt/Al₂O₃ catalyst. This promotional effect increased with oxides in the order: 4Pt-8SnO_x/Al₂O₃ (total acidity: 1.26 mmol/g) < 4Pt-8WO_x/Al₂O₃ (1.39 mmol/g) < 4Pt-8ReO_x/Al₂O₃ (1.40 mmol/g) < 4Pt-8MoO_x/Al₂O₃ (1.70 mmol/g). Reducible

oxide created additional moderate acid sites (Table 6.2). 4Pt-8MoO_x/Al₂O₃ had weak, moderate and strong acid sites distribution of 0.64, 0.80 and 0.25 mmol/g, respectively.

Table 6.2. NH₃-TPD data of promoted supported Pt catalysts.

Catalyst	Total acidity (mmol/g)	Acid sites distribution (mmol/g)		
		Weak (100-200 °C)	Moderate (200-350 °C)	Strong (>350 °C)
γ-Al ₂ O ₃	0.99	0.40	0.21	0.37
4Pt/Al ₂ O ₃	1.27	0.56	0.63	0.07
4Pt-8WO _x /Al ₂ O ₃	1.39	0.55	0.47	0.37
4Pt-8MoO _x /Al ₂ O ₃	1.70	0.64	0.80	0.25
4Pt-8ReO _x /Al ₂ O ₃	1.40	0.68	0.64	0.07
4Pt-8SnO _x /Al ₂ O ₃	1.26	0.35	0.63	0.27

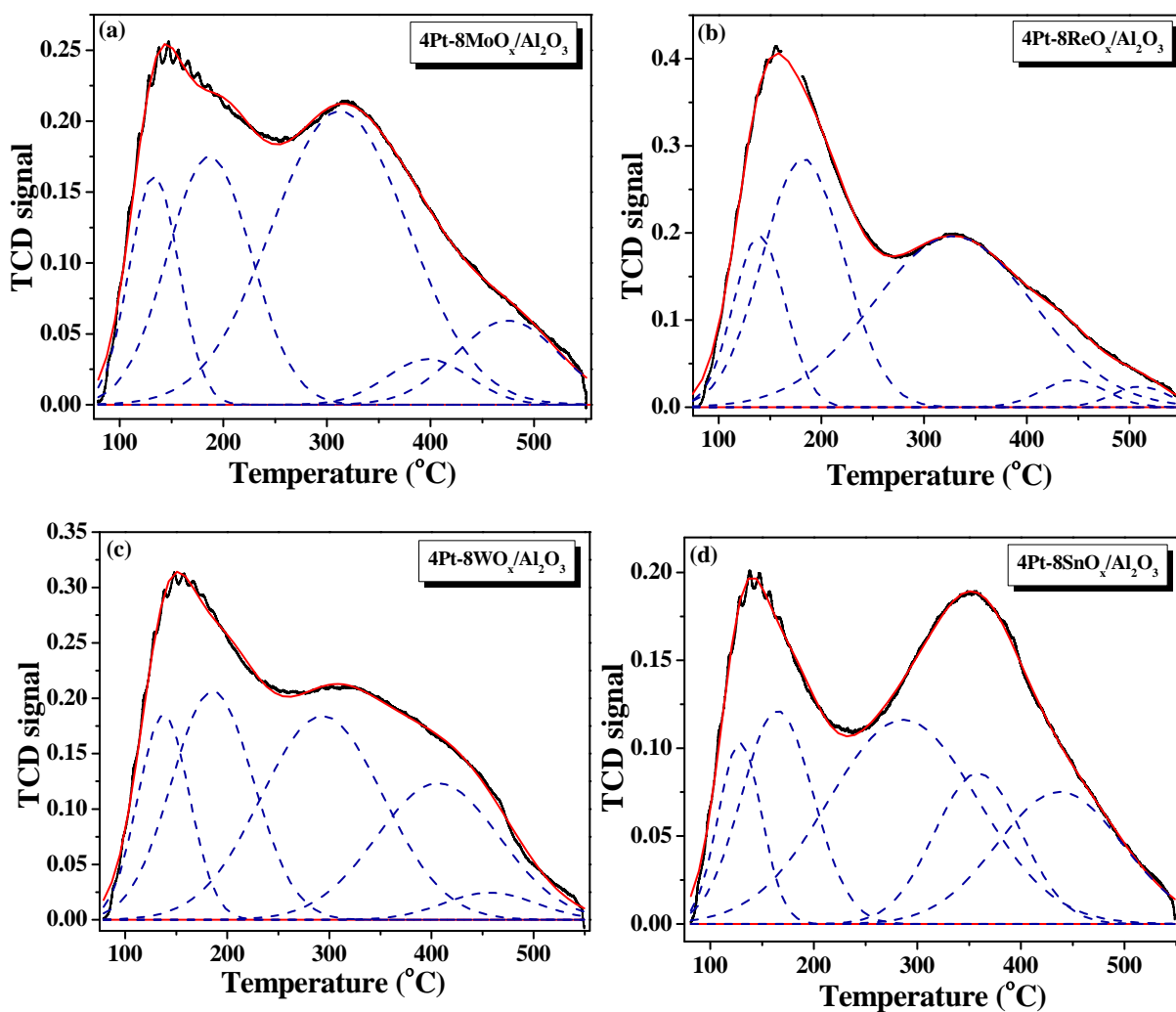


Fig. 6.4. NH₃-TPD profiles of (a) 4Pt-8MoO_x/Al₂O₃, (b) 4Pt-8ReO_x/Al₂O₃, (c) 4Pt-8WO_x/Al₂O₃ and (d) 4Pt-8SnO_x/Al₂O₃ catalysts.

6.3.1.6. H_2 -TPR

H_2 -TPR profile of 4Pt/ Al_2O_3 showed reduction peak of Pt^{2+} to Pt^0 at 74 °C. For 4Pt-8 MO_x / Al_2O_3 , this peak occurred at lower temperatures ca., 69 - 73 °C (Fig. 6.5) confirming electronic contact between Pt and reducible oxide (MoO_x , ReO_x , WO_x or SnO_x). The crystallite size of Pt was larger in reducible oxide promoted catalysts (TEM and CO-chemisorption; Table 6.1). The oxide promoter facilitated the reducibility of Pt and hence, H_2 -TPR peak was observed at lower temperature. ReO_x depicted prominent reduction peaks at 83, 243 and 357 °C (Fig. 6.5). The peak at 83 °C overlaps partly with that of the Pt peak. These peaks for other oxides were relatively weak and occurred at 173 °C (for MoO_x), 350 °C (for WO_x) and 71 and 420 °C (for SnO_x) in presence of Pt. Unsupported rhenium oxides show reduction peak at 400-500 °C [27-29]. Depending on calcination temperature (prior to reduction), rhenium supported on Al_2O_3 can be present as Re_2O_7 and as strongly interacting Re^{4+} . The former type rhenium species on Al_2O_3 is easily reduced in presence of hydrogen at 300-350 °C, while the latter type (dispersed Re^{4+} species) is more difficult to reduce (reduction peak for this occurs at around 550 °C). In presence of platinum, the reduction of rhenium starts at much lower temperatures ca., 160 - 180 °C instead of 300 - 350 °C [27-29]. Thus, the reduction peaks for 4Pt-8 ReO_x / Al_2O_3 observed at 83 and 243 °C (in the present study) may be attributed to rhenium in the form of Re_2O_7 closely associated with Pt and the reduction peak at 357 °C may be corresponded to isolated Re_2O_7 clusters on Al_2O_3 (Fig. 6.5).

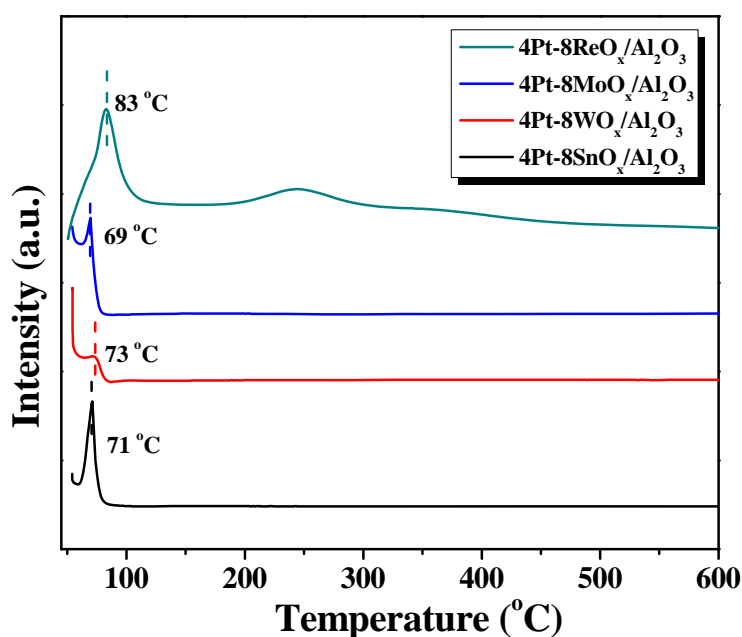


Fig. 6.5. H_2 -TPR profiles of reducible oxide-promoted Pt/ Al_2O_3 catalysts.

Reduction of pure MoO_3 occurs at 767 (corresponding to $\text{MoO}_3 \rightarrow \text{MoO}_2$) and 997 °C ($\text{MoO}_2 \rightarrow \text{Mo}$). A minor shoulder to the first peak at 797 °C (corresponding to Mo_4O_{11} formed by the reduction of MoO_3) was also reported [30, 31]. In the case of Mo/ZrO_2 , the two reduction peaks observed at 400 - 420 °C and 800 - 940 °C were assigned to octahedral and tetrahedral molybdenum oxide species, respectively [32, 33]. In the present study (for $4\text{Pt}-8\text{MoO}_x/\text{Al}_2\text{O}_3$) the reduction peak of octahedral molybdenum oxide had shifted to 173 °C due to its intimate contact with platinum. Zhu et al [23] reported for $\text{Pt}-5\text{WO}_x/\text{Al}_2\text{O}_3$ a low temperature reduction peak at 320 °C and a high temperature peak above 800 °C attributable to reduction of WO_3 to $\text{WO}_{2.9}$ and WO_2 , respectively. Presence of a reduction peak at 350 °C in the present system ($4\text{Pt}-8\text{WO}_x/\text{Al}_2\text{O}_3$) is in line with that report for a similar system. $\text{SnO}_x/\text{Al}_2\text{O}_3$ shows reduction peak at 450-544 °C [34]. However, in the presence of Pt, the reduction of SnO_x shifted to lower temperature (200-400 °C) depending on Sn/Pt content [35]. The weak peak at 420 °C observed in the present study (for $4\text{Pt}-8\text{SnO}_x/\text{Al}_2\text{O}_3$) is in conformity with this report. Thus, observation of reduction peaks for Pt and reducible oxide at lower temperatures substantiate the synergy and mutual electronic contact between them.

6.3.1.7. X-ray photoelectron spectroscopy

XPS provided evidence for complete reduction of ionic platinum to its metallic state. Peaks due to Pt^{4+} or Pt^{2+} were absent. The Pt 4d lines were followed instead of the most intense Pt 4f lines due to their overlap of the latter lines with the strong Al 2p lines [35]. The peaks due to Pt $4d_{5/2}$ and Pt $4d_{3/2}$ occurred at 314.5 and 331.1 eV for $4\text{Pt}-8\text{MoO}_x/\text{Al}_2\text{O}_3$, 314.6 and 331.4 eV for $4\text{Pt}-8\text{ReO}_x/\text{Al}_2\text{O}_3$, 314.7 and 331.3 eV for $4\text{Pt}-8\text{WO}_x/\text{Al}_2\text{O}_3$ and 314.8 and 331.7 eV for $4\text{Pt}-8\text{SnO}_x/\text{Al}_2\text{O}_3$ (Fig. 6.6). Thus, reducible oxide has an effect on the electronic structure of Pt.

Furthermore, the binding energy values of Pt 4d suggest that the metallic nature of Pt in different catalysts increases in the order: $4\text{Pt}-8\text{SnO}_x/\text{Al}_2\text{O}_3 < 4\text{Pt}-8\text{WO}_x/\text{Al}_2\text{O}_3 < 4\text{Pt}-8\text{ReO}_x/\text{Al}_2\text{O}_3 < 4\text{Pt}-\text{MoO}_x/\text{Al}_2\text{O}_3$. The MoO_x and ReO_x promoted catalysts have electron rich Pt (4d peaks occurs at lower binding energy values). More facile spillover of hydrogen is, therefore, expected on MoO_x and ReO_x -promoted Pt than on WO_x and SnO_x -promoted Pt catalysts. The crystallite size of Pt in WO_x and SnO_x promoted catalysts is smaller than in MoO_x and ReO_x promoted catalysts. Thus, one would expect lower binding energy values for $4\text{Pt}-8\text{WO}_x/\text{Al}_2\text{O}_3$ and $4\text{Pt}-8\text{SnO}_x/\text{Al}_2\text{O}_3$ than for $4\text{Pt}-\text{MoO}_x/\text{Al}_2\text{O}_3$ and $4\text{Pt}-\text{ReO}_x/\text{Al}_2\text{O}_3$ [36, 37]. The reverse trend observed in binding energy values suggests that in these catalysts, the electronic factors are dominating the particle size effects.

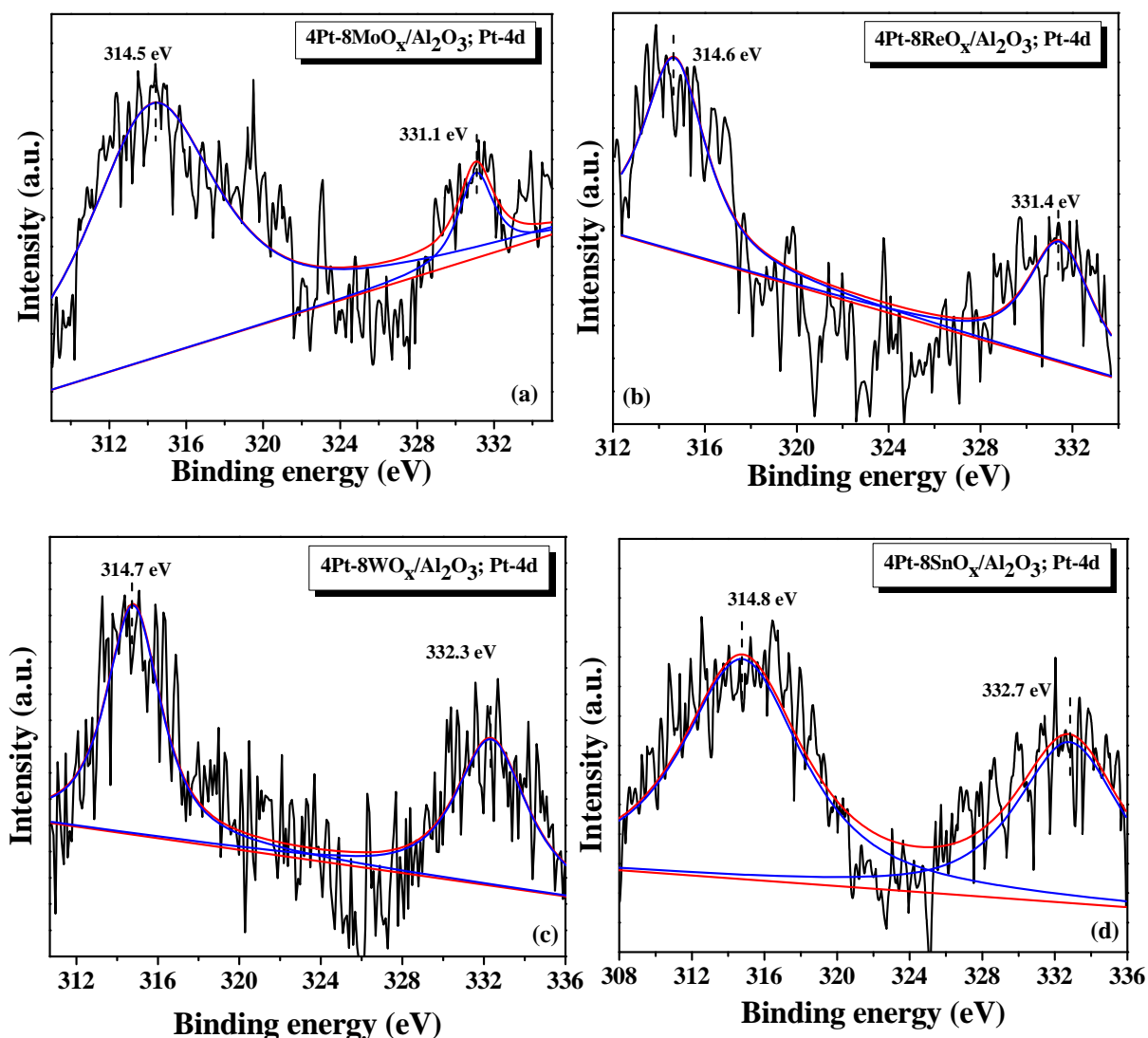


Fig. 6.6. XPS of (a) 4Pt-8MoO_x/Al₂O₃, (b) 4Pt-8ReO_x/Al₂O₃, (c) 4Pt-8WO_x/Al₂O₃ and (d) 4Pt-8SnO_x/Al₂O₃ catalysts in Pt 4d region.

On the other hand, in Mo 3d region, 4Pt-8MoO_x/Al₂O₃ showed peaks corresponding to both +6 and +5 oxidation state of molybdenum (Fig. 6.7). Mo⁶⁺ showed peaks at 235.3 and 241.8 eV due to Mo 3d_{5/2} and Mo 3d_{3/2} transitions. These spin-orbit doublets for Mo⁵⁺ appeared at 232.1 and 238.8 eV, respectively [38]. The ratio of the concentration of surface Mo⁵⁺/Mo⁶⁺ species is 1.23. For 4Pt-8WO_x/Al₂O₃, in the W 4f region, peaks corresponding to both +6 and +5 states of tungsten were observed at 35.5 & 37.6 eV and 34.8 & 36.5 eV (due to W 4f_{7/2} & W 4f_{5/2} transitions, respectively) [23, 39]. The concentration of surface W⁵⁺/W⁶⁺ species is in the ratio of 0.86. For 4Pt-8ReO_x/Al₂O₃, in the Re 4f region, peaks corresponding to +7, +6 and +4 oxidation state of rhenium were observed at 50.9 & 53.9 eV, 48.9 & 52.1 eV and 41.5 & 46.2 eV (due to Re 4f_{7/2} & Re 4f_{5/2} transitions, respectively). The concentration of surface Re⁶⁺/Re⁷⁺ species is in the ratio of 0.7. For 4Pt-8SnO_x/Al₂O₃, in the Sn 3d region,

peaks corresponding to +4 oxidation state only were observed. Sn^{4+} showed peaks at 486.1 and 493.0 eV due to Sn 3d_{5/2} and Sn 3d_{3/2} transitions. Reduced tin species (Sn^{2+}) were not detected. In other words, in presence of Pt, the reducibility of promoter oxides decreased in the order: $\text{MoO}_x > \text{ReO}_x > \text{WO}_x > \text{SnO}_x$. Higher the reducibility of these oxides higher would be the spillover efficiency of Pt. The hydrogen atoms from dissociatively adsorbed hydrogen molecule on Pt surface would spillover onto promoter oxide surface and lead to its reduction [40, 41]. Accordingly, electron donor-acceptor interaction between Pt^0 and MO_x takes place on Al_2O_3 surface. In 4Pt-8 $\text{MoO}_x/\text{Al}_2\text{O}_3$, platinum is in highly metallic state and hence, hydrogen adsorption and its spillover efficiency are higher and the promoter oxide is reduced to a larger extent to its lower oxidation state.

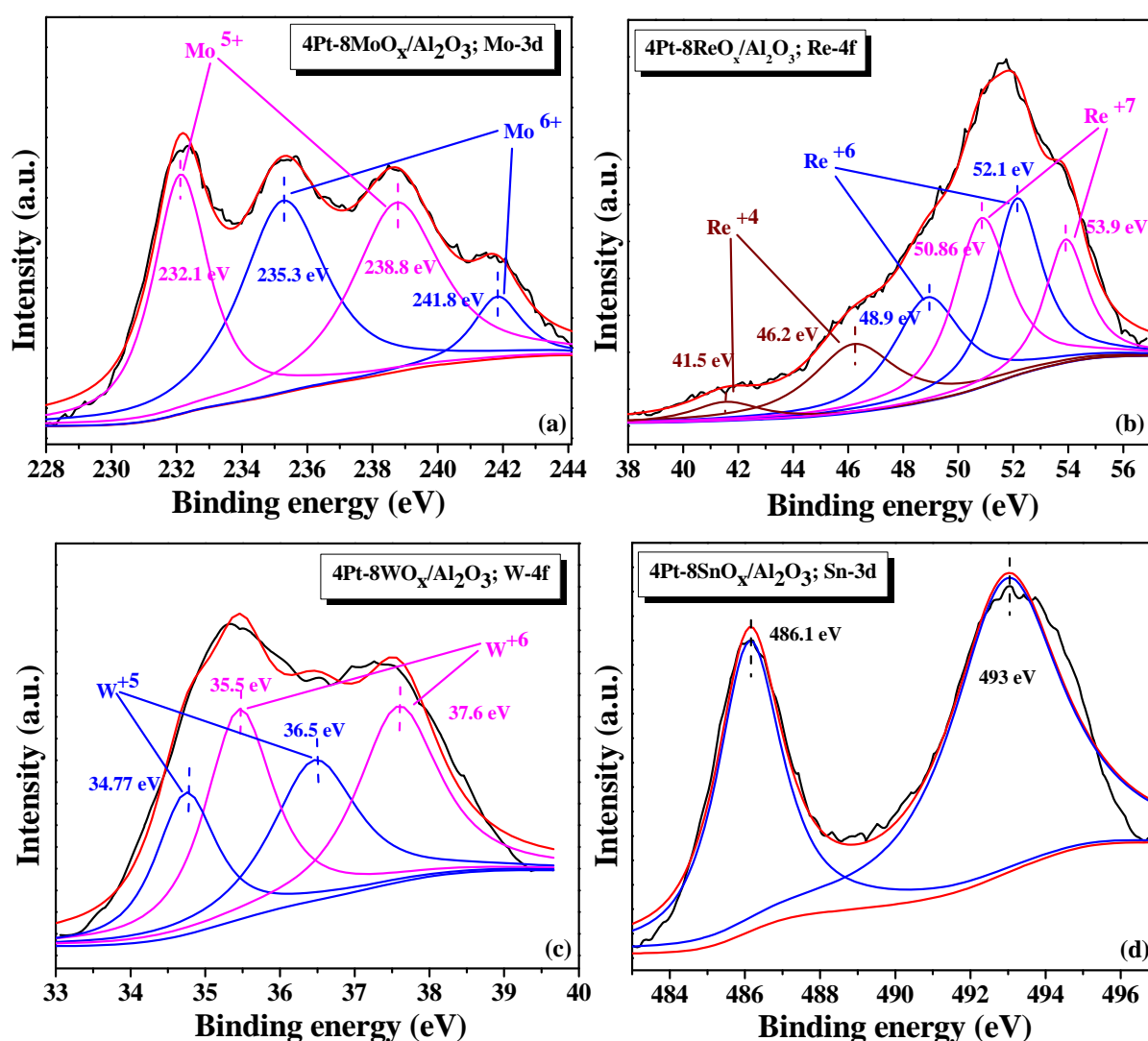
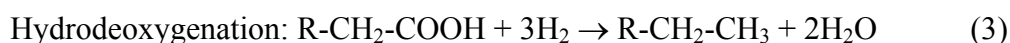
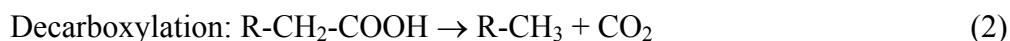
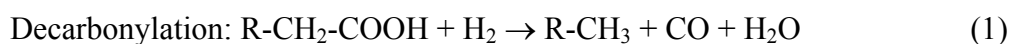


Fig. 6.7. XPS of (a) Mo 3d, (b) Re 4f, (c) W 4f and (d) Sn 3d of reducible oxide-promoted Pt/Al₂O₃ catalysts.

6.3.2. Catalytic activity

6.3.2.1. Effect of promoters

Deoxygenation of fatty acids proceeds by two different mechanisms: (i) decarbonylation/decarboxylation (DCO) and (ii) hydrodeoxygenation/hydrodehydrogenation (HDO). In the former approach, oxygen atom in the fatty acid is removed as CO and CO₂, respectively forming a hydrocarbon having one carbon lower than the original fatty acid (i.e., oleic acid (C_{18.1}; OA) is converted into heptadecane (C₁₇); Eqs. (1) and (2)). In the latter mechanism, the oxygen atom in fatty acid is removed in presence of hydrogen as H₂O while forming a hydrocarbon with same carbon number as that of the original fatty acid (i.e., OA is converted into octadecane (C₁₈); Eq. (3)). The extent of DCO and HDO reactions depends on the nature of catalyst and reaction conditions. Supported noble metal catalysts, often, follow the DCO pathway [10-15]. Cracking of C₁₈ and C₁₇ hydrocarbons formed through deoxygenation reactions would result in shorter chain hydrocarbons.



Control experiments (OA = 2 g, n-heptane (solvent) = 30 g), in the absence of a catalyst, at 220 °C and 20 bar H₂ for 5 h revealed a little conversion of OA (1 mol%). Thus, under these conditions, contribution of thermal (non-catalytic) reaction is negligible. 4Pt/Al₂O₃ resulted in OA conversion of 6 - 10 mol% only (Table 6.3; Run Nos. 1 and 6). Interestingly, the promoted Pt/Al₂O₃ catalysts exhibited high deoxygenation activity even with smaller amount of Pt (0.006 mol% of OA) (Table 6.3; Run Nos. 2-5). Reducible oxide had a marked influence on catalytic activity of Pt with OA conversion decreasing in the order: 4Pt-8MoO_x/Al₂O₃ (97.0 mol%) > 4Pt-8ReO_x/Al₂O₃ (60.0 mol%) > 4Pt-8WO_x/Al₂O₃ (40.0 mol%) > 4Pt-8SnO_x/Al₂O₃ (16.0 mol%). Except for 4Pt-8SnO_x/Al₂O₃ where others (octadecanal, octadecanol and their esters) were the major products (selectivity = 97.0 wt%), on rest of the catalysts, octadecane (C₁₈) (formed through HDO route) had higher selectivity (60.4 to 92.1 wt%) than heptadecane (C₁₇) (formed through DCO route; selectivity 5.8 - 27.8 wt%) (Table 6.3). As demonstrated in the earlier chapters, the unpromoted supported Pt catalysts yielded higher amount of heptadecane than octadecane. In other words, DCO was the prominent mechanism over unpromoted Pt catalysts. This change in catalytic activity and product selectivity (by alteration of reaction pathway) is a consequence of promotional effect of reducible oxides.

Table 6.3. Deoxygenation of oleic acid over reducible oxide promoted supported Pt catalysts.^a

Run No.	Catalyst	OA conversion (mol%) ^b	Product selectivity (wt%) ^c			
			C ₁₈	C ₁₇	C ₁₀₋₁₆	Others ^d
<i>A: Hydrogen pressure = 20 bar</i>						
1	4Pt/Al ₂ O ₃	6.0	46.0	37.0	1.0	16.0
2	4Pt-8WO _x /Al ₂ O ₃	40.0	88.0	9.2	0.3	3.0
3	4Pt-8MoO _x /Al ₂ O ₃	97.0	92.1	5.8	0.5	1.5
4	4Pt-8ReO _x /Al ₂ O ₃	60.0	60.4	27.8	0.5	11.3
5	4Pt-8SnO _x /Al ₂ O ₃	16.0	3.0	0.6	0	97.0
<i>B: Hydrogen pressure = 40 bar</i>						
6	4Pt/Al ₂ O ₃	10.0	35.0	54.0	0.0	10.3
7	4Pt-8WO _x /Al ₂ O ₃	51.0	83.0	8.5	0.5	8.0
8	4Pt-8MoO _x /Al ₂ O ₃	100	93.5	5.3	0.6	0.5
9	4Pt-8ReO _x /Al ₂ O ₃	91.0	73.0	18.3	0.7	8.3
10	4Pt-8SnO _x /Al ₂ O ₃	19.0	18.5	1.5	0	80.0

^aReaction conditions: Catalyst = 0.2 g (0.006 mol% of Pt with respect to OA), oleic acid (OA) = 2 g, n-heptane (solvent) = 30 g, reaction temperature = 220 °C, reaction time = 5 h, pressure = 20 bar H₂. Reactions were conducted in 300 ml Parr stainless steel batch autoclave with stirring speed of 600 rpm. ^bDetermined from titration with NaOH. ^cDetermined from GC analysis. ^dOthers include octadecanal, octadecanol and their esters.

6.3.2.2. Effect of reaction parameters

Fig. 6.8 presents plots of OA conversion versus reaction time and reaction temperature. Initial activity (OA conversion at 0.25 h at 260 °C, 20 bar H₂) of Pt catalysts decreased in the order: 4Pt-8MoO_x/Al₂O₃ > 4Pt-8ReO_x/Al₂O₃ > 4Pt-8WO_x/Al₂O₃ > 4Pt-8SnO_x/Al₂O₃. However, at longer reaction times (5 h), Mo and ReO_x-promoted Pt catalysts showed similar OA conversion (100 and 99.0 mol%, respectively; Fig. 6.8(a)) possibly due to metal structural changes during the reaction. Selectivity for octadecane followed the order: 4Pt-8MoO_x/Al₂O₃ (81.6 - 89.1%) > 4Pt-8WO_x/Al₂O₃ (59.3 - 76.0%) > 4Pt-8ReO_x/Al₂O₃ (50.6 - 60.3%) > 4Pt-8SnO_x/Al₂O₃ (41.1 - 49.0) (Table 6.4).

Temperature had a positive effect on deoxygenation (Fig. 6.8(b) and Table 6.5). 4Pt-8MoO_x/Al₂O₃ exhibited higher catalytic activity than the other catalysts. With increasing temperature a marginal loss in C₁₈ selectivity (from 92.5 to 87.2%) and gain in C₁₇ selectivity (from 4.7 to 11.7%) was observed over 4Pt-8MoO_x/Al₂O₃. Others were the main products for 4Pt-8SnO_x/Al₂O₃ at lower temperature (200-240 °C).

Table 6.4. Deoxygenation of oleic acid over reducible oxide-promoted Pt/Al₂O₃ catalysts as a function reaction time.

Run No.	Reaction time (h)	OA conversion (mol%) ^a	Product selectivity (wt%) ^b			
			C ₁₈	C ₁₇	C ₁₀₋₁₆	Others ^c
<i>Catalyst: 4Pt-8WO_x/Al₂O₃:^d</i>						
1	0.25	34.0	76.0	19.6	0.6	2.9
2	0.5	38.0	60.0	36.2	0.8	3.0
3	1	40.0	59.3	38.5	0	2.1
4	3	49.0	60.0	39.1	0	1.0
5	5	67.0	67.5	31.5	0	1.0
<i>Catalyst: 4Pt-8MoO_x/Al₂O₃:^d</i>						
1	0.25	75.0	81.6	13.8	0.6	4.0
2	0.5	79.0	86.3	12.8	0.4	0.5
3	1	84.0	87.0	11.8	0.6	0.6
4	3	97.0	89.1	9.8	0.5	0.5
5	5	100.0	87.2	11.7	0.5	0.5
<i>Catalyst: 4Pt-8ReO_x/Al₂O₃:^d</i>						
1	0.25	43.0	50.6	45.5	0	3.8
2	0.5	61.0	50.9	45.8	0.8	2.4
3	1	89.0	57.2	40.9	1.2	0.7
4	3	94.0	55.0	39.9	0.7	4.4
5	5	99.0	60.3	36.8	0.9	2.0
<i>Catalyst: 4Pt-8SnO_x/Al₂O₃:^d</i>						
1	0.25	17.0	49.0	20.4	0	30.6
2	0.5	21.0	41.1	29.5	0	29.3
3	1	60.0	49.2	27.0	0	23.8
4	3	80.0	47.0	20.0	0	33.3
5	5	85.0	47.5	10.2	0	42.3

^aDetermined from titration with NaOH. ^bDetermined from GC analysis. ^cOthers include octadecanal, octadecanol and their esters. ^dReaction conditions: Catalyst = 0.2 g, oleic acid (OA) = 2 g, n-heptane (solvent) = 30 g, pressure = 20 bar H₂, reaction temperature = 260 °C. Reactions were conducted in 300 ml Parr stainless steel batch autoclave with stirring speed of 600 rpm.

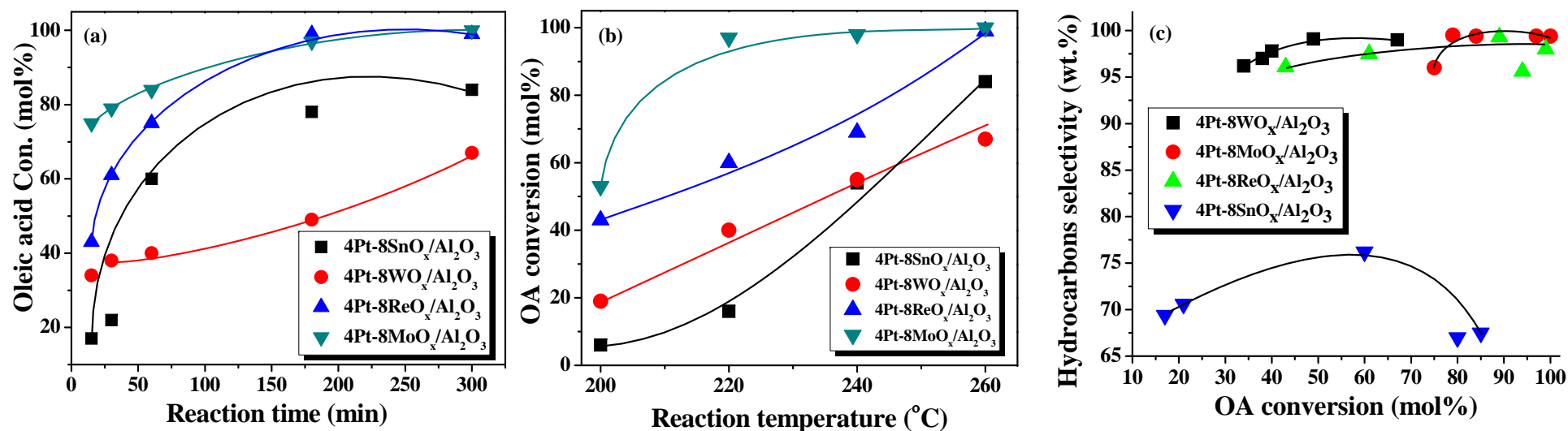


Fig. 6.8. Deoxygenation of oleic acid (OA) over reducible oxide-promoted Pt/Al₂O₃ catalysts. (a) Influence of reaction time on OA conversion. *Reaction conditions*: catalyst = 0.2 g, oleic acid (OA) = 2 g, n-heptane (solvent) = 30 g, reaction temperature = 260 °C, reaction time = 0.25 to 5 h, pressure = 20 bar H₂. (b) Influence of reaction temperature on OA conversion. *Reaction conditions*: same as in (a) except for reaction temperature = 200 to 260 °C, reaction time = 5 h. (c) Plot showing the variation of hydrocarbons selectivity with OA conversion. *Reaction conditions*: same as in (a) except for reaction temperature = 200 to 260 °C, reaction time = 0.25 to 5 h. Reactions were conducted in 300 ml Parr stainless steel batch autoclave with stirring speed of 600 rpm.

Table 6.5. Deoxygenation of oleic acid over reducible oxide-promoted Pt/Al₂O₃ catalysts as a function reaction temperature.^a

Run No.	Reaction time (h)	OA conversion (mol%) ^b	Product selectivity (wt%) ^c			
			C ₁₈	C ₁₇	C ₁₀₋₁₆	Others ^d
<i>Catalyst: 4Pt-8WO_x/Al₂O₃:</i>						
1	200	19.0	89.0	7.0	0	4.0
2	220	40.0	88.0	9.2	0.3	3.0
3	240	55.0	86.4	12.8	0.5	0.3
4	260	67.0	67.5	31.5	0	1.0
<i>Catalyst: 4Pt-8MoO_x/Al₂O₃:</i>						
1	200	53.0	92.5	4.7	0.4	2.4
2	220	97.0	92.1	5.8	0.5	1.5
3	240	98.0	92.4	6.6	0.6	0.5
4	260	100.0	87.2	11.7	0.5	0.5
<i>Catalyst: 4Pt-8ReO_x/Al₂O₃:</i>						
1	200	43.0	56.4	21.2	0.4	22.0
2	220	60.0	60.4	27.8	0.5	11.3
3	240	69.0	54.0	39.2	0.5	6.3
4	260	99.0	60.3	36.8	0.9	2.0
<i>Catalyst: 4Pt-8SnO_x/Al₂O₃:</i>						
1	200	6.0	1.2	0.3	0	98.5
2	220	16.0	3.0	0.6	0	97.0
3	240	54.0	9.6	3.2	0	87.1
4	260	85.0	47.5	10.2	0	42.3

^aReaction conditions: Catalyst = 0.2 g, oleic acid (OA) = 2 g, n-heptane (solvent) = 30 g, pressure = 20 bar H₂, reaction time = 5 h. Reactions were conducted in 300 ml Parr stainless steel batch autoclave with stirring speed of 600 rpm. ^bDetermined from titration with NaOH. ^cDetermined from GC analysis. ^dOthers include octadecanal, octadecanol and their esters.

Hydrogen pressure had an affirmative effect on OA conversion and C₁₈ selectivity (Table 6.6). OA conversion over 4Pt-8MoO_x/Al₂O₃ (at 220 °C and 5 h) increased from 10.0 (at zero hydrogen) to 100 mol% (at 40 bar H₂). At these conditions, selectivity for octadecane increased from 40.0 to 93.5%. Observation of 40% C₁₈ even at zero hydrogen infers that a part of n-heptane solvent is reformed over these promoted Pt catalysts forming *in situ* hydrogen and thereby, facilitating the HDO activity. Bimetallic Pt-Re/Al₂O₃ are known reforming catalysts [27]. In the presence of hydrogen, HDO is more predominant than DCO over these

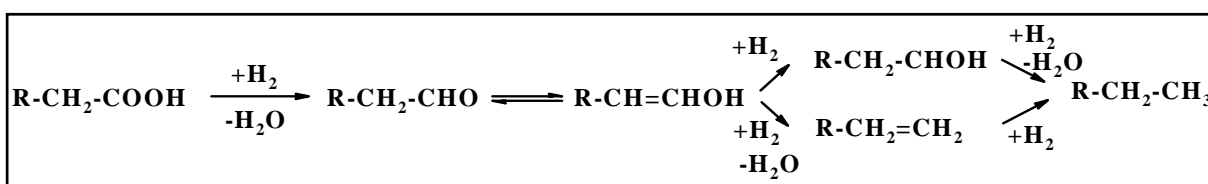
promoted catalysts (compare Run Nos. 5 and 6-10). Catalytic activity increased with increasing amount of catalyst (0 to 10 wt% of OA). A reaction condition with 10 wt% catalyst with respect to OA exhibited complete conversion to mainly C₁₈ product (Table 6.6; Run No. 4).

Table 6.6. Effect of catalyst amount and hydrogen pressure on deoxygenation of oleic acid over 4Pt-8MoO_x/Al₂O₃.

Run No.	Reaction parameter	OA conversion (mol%) ^a	Product selectivity (wt%) ^b			
			C ₁₈	C ₁₇	C ₁₀₋₁₆	Others ^c
<i>A: Effect catalyst amount in g (wt% with respect to OA)^d</i>						
1	0 (0)	1.0	Trace	Trace	0	Trace
2	0.1 (5)	48.0	68.0	12.5	0.5	19.2
3	0.15 (7.5)	62.0	88.0	10.0	0.5	1.6
4	0.2 (10)	97.0	92.1	5.8	0.5	1.5
<i>B: Effect of hydrogen pressure (bar)^e</i>						
5	0	10.0	40.0	0	0	60.0
6	5	45.0	56.0	40.0	0.8	3.2
7	10	58.0	77.8	19.6	0.5	2.1
8	15	70.0	83.0	15.0	0.3	1.7
9	20	97.0	92.1	5.8	0.5	1.5
10	40	100	93.5	5.3	0.6	0.5

^aDetermined from titration with NaOH. ^bDetermined from GC analysis. ^cOthers include octadecanal, octadecanol and their esters. ^dReaction conditions: catalyst = 0 - 0.2 g, oleic acid (OA) = 2 g, n-heptane (solvent) = 30 g, pressure = 20 bar H₂, reaction temperature = 220 °C, reaction time = 5 h. ^eReaction conditions: catalyst = 0.2 g, oleic acid (OA) = 2 g, n-heptane (solvent) = 30 g, pressure = 0 - 40 bar H₂ (note! run no. 5, was conducted in presence of 20 bar nitrogen), reaction temperature = 220 °C, reaction time = 5 h.

Fig. 6.8(c) shows a plot of OA conversion versus hydrocarbon (C₁₀ to C₁₈) selectivity (deoxygenation activity) over different promoted Pt/Al₂O₃ catalysts. Within 2% difference, overall hydrocarbon selectivity was the same at all OA conversions over MoO_x, WO_x and ReO_x-promoted Pt/Al₂O₃ catalysts indicating their efficient performance at all reduction steps in hydrodeoxygenation (Scheme 6.1). SnO_x-promoted Pt is least active for green diesel production.



Scheme 6.1. Reduction steps and some intermediates in hydrodeoxygenation of fatty acids.

Table 6.7. Deoxygenation of fatty compounds over 4Pt-8MoO_x/Al₂O₃.^a

Run No.	Substrate	Conversion (mol%)	Product selectivity (wt%)										
			C ₁₈	C ₁₇	C ₁₆	C ₁₅	C ₁₄	C ₁₃	C ₁₂	C ₁₁	C ₁₀	Others	
<i>A: Reaction time = 1 h</i>													
1	Capric acid (C _{10.0})	34.0	0	0	0	0	0	0	0	0	0	9.1	90.9
2	Lauric acid (C _{12.0})	34.0	0	0	0	0	0	0	0	26.6	4.2	0	69.3
3	Myristic acid (C _{14.0})	35.0	0	0	0	0	27.6	3.1	0.2	0	0	0	69.0
4	Palmitic acid (C _{16.0})	39.0	0	0	43.6	4.2	0.3	0	0	0	0	0	52.0
5	Stearic acid (C _{18.0})	58.0	90.8	6.9	0	0	0	0	0	0	0	0	2.2
6	Oleic acid (C _{18.1})	47.0	83.0	13.8	1.0	0	0	0	0	0	0	0	2.5
<i>B: Reaction time = 5 h</i>													
7	Capric acid (C _{10.0})	82.0	0	0	0	0	0	0	0	0	0	13.6	86.4
8	Lauric acid (C _{12.0})	90.0	0	0	0	0	0	0	0	31.2	4.8	0	64.0
9	Myristic acid (C _{14.0})	94.0	0	0	0	0	41.0	5.4	0.2	0	0	0	53.4
10	Palmitic acid (C _{16.0})	90.0	0	0	50.1	6.3	0.2	0	0	0	0	0	42.5
11	Oleic acid (C _{18.1})	97.0	92.1	5.8	0.5	0.04	0	0	0	0	0	0	1.5
12	Methyl oleate	95.0	51.6	27.4	12.2	1.9	3.7	0.34	0.9	0	0	0	19.0
13	Soyabean oil	96.0	69.2	12.0	11.8	1.4	0	0	0	0	0	0	5.5

^aReaction conditions: Catalyst = 0.2 g, substrate = 2 g, n-heptane (solvent) = 30 g, pressure = 20 bar H₂, reaction temperature = 220 °C, reaction time = 1 h. Reactions were conducted in 100 ml Parr stainless steel batch autoclave with stirring speed of 600 rpm.

To demonstrate the scope of reaction, different fatty acids [capric acid (C_{10.0}), lauric acid (C_{12.0}), myristic acid (C_{14.0}), palmitic acid (C_{16.0}), stearic acid (C_{18.0}) and oleic acid (C_{18.1})], biodiesel (methyl oleate) and vegetable oil (soybean oil) were subjected for hydrodeoxygenation over the best performing 4Pt-8MoO_x/Al₂O₃ catalyst at 220 °C and 20 bar H₂ for 1 & 5 h (Table 6.7). Conversion and hydrocarbon yield increased with increasing chain length of fatty acid. While longer chain acids were deoxygenated fast, shorter ones underwent dimerization and esters/anhydrides formation. It is likely that higher temperatures are needed to break the ester/anhydride bonds and to deoxygenate short chain length fatty acids (C_{10.0}). It is gratifying to note that OA, methyl oleate and soybean oil were converted with near equal efficiency over this catalyst (Table 6.7; Run Nos. 11 to 13).

6.3.2.3. Catalyst reusability study

With a view to understand catalyst stability during reactions, the MoO_x, WO_x and ReO_x-promoted Pt/Al₂O₃ catalysts were reused in several recycling experiments conducted at 260 & 320 °C and 25 bar H₂ for 1 & 5 h, respectively, using OA as substrate (Tables 6.8 and 6.9). At the end of each recycle run, the catalyst was separated, washed with acetone and dried in an oven at 110 °C for 12 h. It was reduced in hydrogen (at 350 °C for 150 min) prior to use in the next recycle experiment. At 320 °C, 4Pt-8MoO_x/Al₂O₃ and 4Pt-8WO_x/Al₂O₃ showed nearly stable catalytic activity (Table 6.8). In fact, upon reuse of the catalyst, OA conversion and C₁₈ selectivity had marginally improved. However, at lower temperature (260 °C), in recycle experiments, the catalysts showed loss in catalytic activity and octadecane product selectivity (Table 6.9).

To understand the causes for loss in catalytic performance at lower temperature, the spent (260 °C, after three reuses) promoted Pt catalysts were analyzed. Chemisorption studies (Table 6.1) revealed a significant decrease in monolayer CO uptake from 43 to 17 μmol/g for 4Pt-8MoO_x/Al₂O₃, 76 to 15 μmol/g for 4Pt-8WO_x/Al₂O₃, and 36 to 21 μmol/g for 4Pt-8ReO_x/Al₂O₃. As a consequence of that, Pt dispersion decreased from 21 to 8.4% for 4Pt-8MoO_x/Al₂O₃, 37 to 7.5% for 4Pt-8WO_x/Al₂O₃ and 18 to 10.1% for 4Pt-8ReO_x/Al₂O₃. A growth in Pt crystallite (CO chemisorption) and particle size (TEM; Fig. 6.9) on reuse was noted. A similar decrease in monolayer CO uptake (18 μmol/g) & Pt dispersion (8.8%) and increase in Pt crystallite (13 nm) & particle size (6 nm) were observed even for the 4Pt-8MoO_x/Al₂O₃ catalyst reused at 320 °C. SEM-EDAX analysis revealed that the chemical compositions of Pt and promoter oxide were unchanged on reuse (Table 6.10). XRD of the spent catalyst was comparable to that of the fresh catalyst (Fig. 6.10) and confirmed structural integrity. High reusability of the catalyst at higher

temperature (320 °C) than at lower temperature (260 °C) could perhaps be due to strong sticking of reactant polar molecules at lower temperature on catalyst surface than at higher temperature.

Table 6.8. Catalyst recyclability study in deoxygenation of oleic acid at 320 °C.^a

Catalyst	Number of recycles	OA conversion (mol%)	Product selectivity (wt%)			
			C ₁₈	C ₁₇	C ₁₀₋₁₆	Others
	Fresh	97.0	41.0	58.0	0.7	0.3
4Pt-8MoO _x /Al ₂ O ₃	1	100	45.3	54.0	0.7	0.0
	2	100	49.8	49.4	0.8	0.0
	Fresh	100	67.1	31.6	1.3	0.0
	1	100	64.5	34.6	0.9	0.0
	2	100	75.7	23.5	0.8	0.0
4Pt-8WO _x /Al ₂ O ₃	3	100	75.8	23.0	0.2	0.0
	4	100	76.7	22.6	0.7	0.0
	5	100	78.8	20.4	0.8	0.0
	6	100	80.8	18.5	0.7	0.0

^aReaction conditions: Catalyst = 0.4 g, oleic acid (OA) = 4 g, n-heptane (solvent) = 40 g, pressure = 25 bar H₂, reaction temperature = 320 °C, reaction time = 5 h. Reactions were conducted in 100 ml Parr stainless steel batch autoclave with stirring speed of 600 rpm.

Table 6.9. Catalyst recyclability study in deoxygenation of oleic acid at 260 °C.^a

Catalyst	Number of recycles	OA conversion (mol%)	Product selectivity (wt%)			
			C ₁₈	C ₁₇	C ₁₀₋₁₆	Others
	Fresh	69.0	76.0	23.0	0.7	0.5
4Pt-8MoO _x /Al ₂ O ₃	1	51.0	69.1	28.3	0.5	2.1
	2	33.0	61.3	33.5	0	4.6
	3	31.0	50.8	39.6	0	9.6
	Fresh	24.0	69.4	28.6	0.7	1.3
4Pt-8WO _x /Al ₂ O ₃	1	23.0	65.1	30.2	0.5	4.2
	2	15.0	62.7	31.3	0.0	6.0
	3	14.0	58.6	32.0	0.1	9.3
	Fresh	48.0	52.7	35.5	0.9	10.9
4Pt-8ReO _x /Al ₂ O ₃	1	27.0	37.3	53.7	0.0	9.0
	2	25.0	33.0	65.4	0.1	1.5
	3	22.0	28.3	48.3	0.0	23.4

^aReaction conditions: Catalyst = 0.4 g, oleic acid (OA) = 4 g, n-heptane (solvent) = 40 g, reaction temperature = 260 °C, pressure = 25 bar H₂ and reaction time = 1 h. Reactions were conducted in a 100 ml Parr stainless steel batch autoclave with stirring speed of 600 rpm.

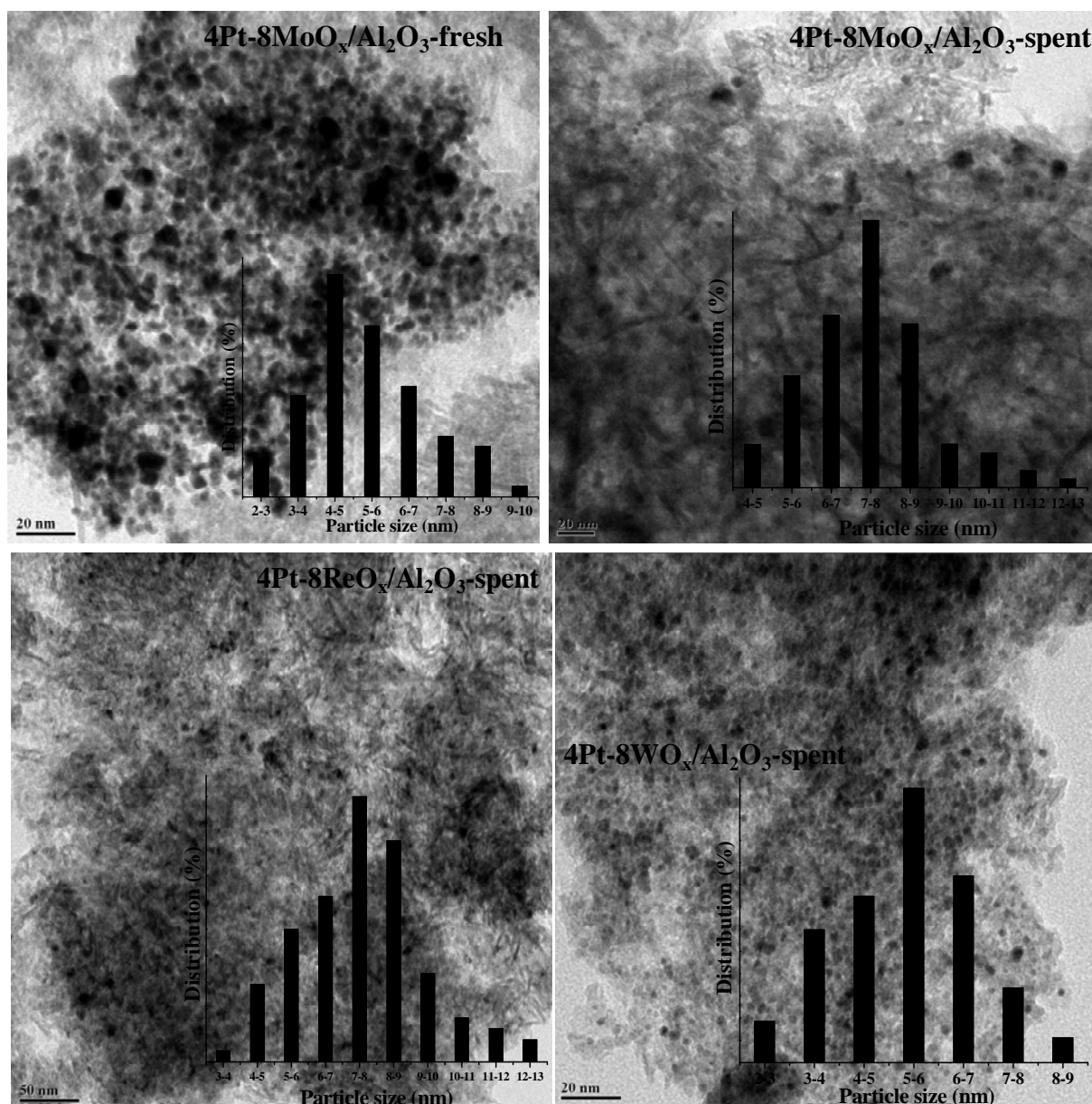


Fig. 6.9. TEM images of spent (at 260 °C; after three reuses) reducible oxide-promoted Pt/Al₂O₃ catalysts

Table 6.10. SEM-EDAX analysis of chemical composition of fresh and spent catalysts (at 260 °C; after three reuses)

Catalyst		Chemical composition (wt%)			
		Pt	Mo/W	Al	O
4Pt-8MoO _x /Al ₂ O ₃	Fresh	3.4	7.6	43.2	45.8
	Spent	3.5	6.8	41	48.5
4Pt-8WO _x /Al ₂ O ₃	Fresh	2.4	10.3	42.7	44.4
	Spent	2.5	10.2	42.7	44.5

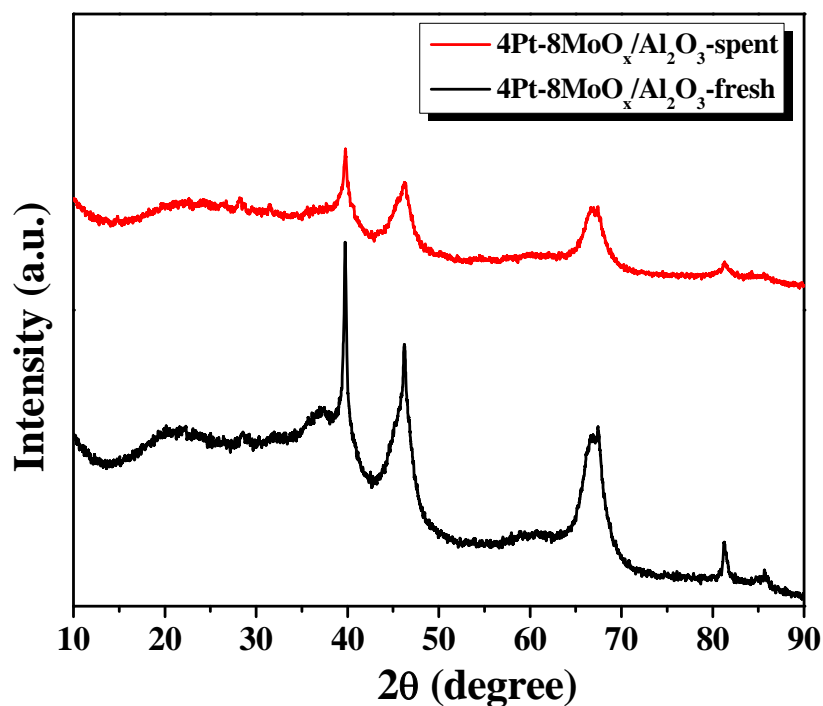


Fig. 6.10. XRD of fresh and spent (at 260 °C; after three reuses) 4Pt-8MoO_x/Al₂O₃ catalysts.

6.3.2.4. Structure-activity correlation

A linear correlation between binding energy (of Pt 4d_{3/2} line) and catalytic activity (OA conversion) was found (Fig. 6.11(a)). OA conversion increased with lowering of binding energy of Pt suggesting that higher the metallic nature of Pt (i.e., electron rich Pt), the higher the catalytic activity. 4Pt-8MoO_x/Al₂O₃ having lower binding energy value exhibited higher deoxygenation activity (OA conversion) and 4Pt-8SnO_x/Al₂O₃ having higher binding energy value showed lower OA conversion. It is known that higher the metallic nature higher will be the dissociative splitting and spillover of adsorbed hydrogen. Thus, higher will be the catalytic activity.

Although no direct correlation of OA conversion with dispersion was found. It appeared that OA conversion is higher at an optimum dispersion value. Below and above that, the catalytic activity was lower. Too high a dispersion was found no good. Thus, the relation between Pt dispersion (Pt size) and OA conversion suggests that metal dispersion is important but plays a secondary role to metallicity on the deoxygenation activity. SnO_x and WO_x-promoted Pt/Al₂O₃ catalysts had higher dispersion but their metallic natures were lower and thereby, exhibited poorer deoxygenation activity. 4Pt-8MoO_x/Al₂O₃ had the lowest Pt 4d_{3/2} binding energy value and optimal metal dispersion and so exhibited the highest deoxygenation activity.

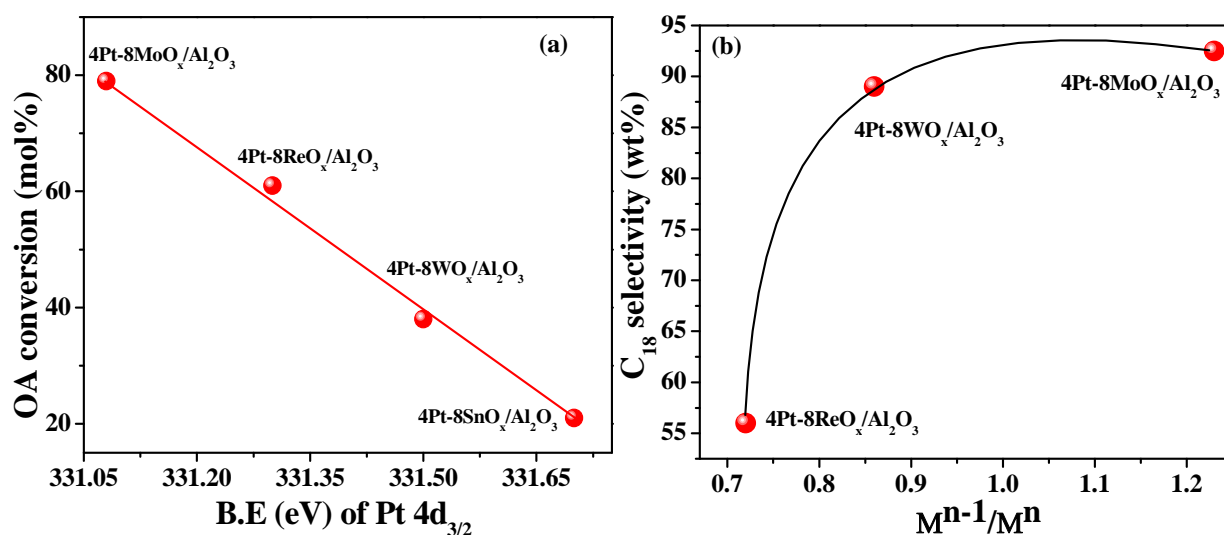


Fig. 6.11. Correlation of (a) OA conversion with binding energy values of Pt 4d_{3/2} line and (b) octadecane (C₁₈) selectivity with the ratio of concentration of Mⁿ⁻¹ to Mⁿ ions of promoter metal. *Reaction conditions* for (a): catalyst = 0.2 g, oleic acid (OA) = 2 g, n-heptane (solvent) = 30 g, pressure = 20 bar H₂, reaction temperature = 260 °C. reaction time = 0.5 h. Reactions were conducted in 300 ml Parr stainless steel batch autoclave with stirring speed of 600 rpm. *Reaction conditions* for (b): same as in (a) except for reaction time = 0.25 to 5 h.

Partial reduction of promoter oxides generates surface –OH groups which activate OA and change the reaction pathway. The extent of reduction of promoter oxide i.e. the ratio of Mⁿ⁻¹/Mⁿ correlates with C₁₈ (octadecane) selectivity (Fig. 6.11(b)). MoO_x and WO_x are more susceptible for reduction (from +6 to +5 states) in the presence of Pt and hence, exhibited higher HDO product (C₁₈) selectivity. Re with multiple oxidation states (XPS: +4, +6, +7) showed lesser C₁₈ selectivity. In other words, the type of oxophilic, reducible promoter oxide does play a crucial role on hydrodeoxygenation performance of supported Pt. The reducible oxide alters the textural (crystallite/particle size and dispersion) and electronic properties (reducibility and metallic nature) of Pt and Pt in turn modifies the reducibility of promoter oxide. These two together determine the deoxygenation activity and selectivity.

Similar correlations between reaction rate constant for hydrodesulfurization (HDS) of thiophene over sulfided MoO₃ and WO₃/γ-Al₂O₃ and the average reduction temperature were reported by Thomas et al. [42]. HDS activity increased with decreasing reduction temperature suggesting that reduction of the transition metal compound is a crucial step in the transformation of the oxidic precursor catalyst into the sulfided catalyst. They also found that hydrogenation of butene increases with decreasing reduction temperature consistent with the fact that in hydrogenation reaction, oxidation state of metal is an important parameter; generally

better hydrogenation properties are related to low oxidation state [42]. Also in methanol oxidation to formaldehyde, Hu and Wachs [43] found correlation of turnover frequency (TOF) with reducibility of the support. It is interesting to note that such correlations do exist even between deoxygenation activity/selectivity and the electronic properties (metallicity and reducibility).

6.4. Conclusions

4Pt-8MO_x/Al₂O₃ catalysts (where M = Mo, Re, W and Sn) were prepared by wet-impregnation method and studied for deoxygenation of fatty acids producing hydrocarbon-based biofuels (green diesel). The Pt deposited on reducible oxide (MO_x) modified Al₂O₃ showed higher catalytic activity and HDO selectivity than the unmodified Pt/Al₂O₃ catalysts. Among the catalysts investigated, 4Pt-8MoO_x/Al₂O₃ enabled complete conversion of oleic acid with 93.5% selectivity for octadecane at a temperature as low as 220 °C in 5 h. Fatty acids, methyl oleate (biodiesel) and vegetable oil were deoxygenated with near equal efficiency. Reducible oxide altered the textural and electronic properties of Pt and Pt, in turn, modified the reducibility of the promoter oxide. These two, together determined the deoxygenation performance of reducible oxide-promoted Pt catalyst. 4Pt-8MoO_x/Al₂O₃ having a right amount of metal dispersion and high metallic nature and reduced Mo⁵⁺ species exhibited high deoxygenation activity and HDO selectivity. Superior low temperature deoxygenation performance and high HDO selectivity (low carbon loss) of MoO_x-promoted Pt/Al₂O₃ may lead to greener catalytic biofuels technologies.

6.5. References

- [1] B. Iama, in R. Luque, J. Campelo, J. Clark (Eds.), *Hand Book of Biofuels: Process and Technologies*, Woodhead Publishing Ltd., 2011.
- [2] E. Furimsky, *Appl. Catal. A: Gen.* 199 (2000) 147-190.
- [3] T.V. Choudhary, C.B. Phillips, *Appl. Catal. A: Gen.* 397 (2011) 1-12.
- [4] B. Peng, C. Zhao, S. Kasakov, S. Foraita, J.A. Lercher, *Chem. Eur. J.* 19 (2013) 4732-4741.
- [5] <http://www.uop.com/pr/release/PR.EniEcofiningFacility.pdf>.
- [6] T. Kalnes, T. Marker, D.R. Shonnard, *Int. J. Chem. React. Eng.* 5 (2007) Article A48, 1-9.
- [7] <http://www.tyson.com/RenewableEnergy/Initiative/Conoco/Default.aspx>.
- [8] B. Donnis, R.G. Egeberg, P. Blom, K.G. Knudsen, *Top. Catal.* 52 (2009) 229-240.
- [9] M. Gousi, C. Andriopoulou, K. Bourikas, S. Ladas, M. Sotiriou, C. Kordulis, A. Lycourghiotis, *Appl. Catal. A: Gen.* 536 (2017) 45-56.

- [10] S. Lestari, P. Mäki-Arvela, H. Bernas, O. Simakova, R. Sjöholm, J. Beltramini, G.Q. Max Lu, J. Myllyoja, I. Simakova, D.Y. Murzin, *Energy Fuels* 23 (2009) 3842-3845.
- [11] I. Simakova, O. Simakova, P. Mäki-Arvela, A. Simakova, M. Estrada, D.Y. Murzin, *Appl. Catal. A: Gen.* 355 (2009) 100-108.
- [12] M. Ahmadi, A. Nambo, J.B. Jasinski, P. Ratnasamy, M.A. Carreon, *Catal. Sci. Tech.* 5 (2015) 380-388.
- [13] P.T. Do, M. Chiappero, L.L. Lobban, D.E. Resasco, *Catal. Lett.* 130 (2009) 9-18.
- [14] M. Rabaev, M.V. Landau, R. Vidruk-Nehemya, A. Goldbourt, M. Herskowitz, *J. Catal.* 332 (2015) 164-176.
- [15] R. Raut, V.V. Bankar, S. Darbha, *J. Mol. Catal. A: Chem.* 417 (2016) 126 - 134.
- [16] Leifeng Gong, Yuan Lu, Yunjie Ding, Ronghe Lin, Jingwei Li, Wenda Dong, Tao Wang, Weimiao Chen, *Applied Catalysis A: Gen.* 390 (2010) 119–126.
- [17] Yoshinao Nakagawa, Yasunori Shinmura, Shuichi Koso, Keiichi Tomishige, *J. Catal.* 272 (2010) 191–194.
- [18] Ryan Loe, Eduardo Santillan-Jimenez, Tonya Morgan, Lilia Sewell, Yaying Ji, Samantha Jones, Mark A. Isaacs, Adam F. Lee, Mark Crocker, *Appl. Catal. B: Environ.* 191 (2016) 147–156.
- [19] M.V. Tsodikov, A.V. Chistyakov, M.A. Gubanov, P.A. Zharova, S.S. Shapovalov, A.A. Pasyanskii, V.V. Kriventsov, I.I. Moiseev, *Rus. Chem. Bull. Int. Ed.* 64 (2015) 2062-2068.
- [20] I.-H. Choi, J.-S. Lee, C.-U. Kim, T.-W. Kim, K.-Y. Lee, K.-R. Hwang, *Fuel* 215 (2018) 675-685.
- [21] K. Kon, T. Toyao, W. Onodera, S.M.A.H. Siddiki and K.-i. Shimizu, *ChemCatChem* 9 (2017) 2822-2827.
- [22] S. García-Fernández, I. Gandarias, J. Requies, M.B. Güemez, S. Bennici, A. Auroux, P. L. Arias, *J. Catal.* 323 (2015) 65-75.
- [23] S. Zhu, X. Gao, Y. Zhu, Y. Li, *J. Mol. Catal. A: Chem.* 398 (2015) 391-398.
- [24] A. Robinson, G.A. Ferguson, J.R. Gallagher, S. Cheah, G.T. Beckham, J.A. Schaidle, J.E. Hensley, J.W. Medlin, *ACS Catal.* 6 (2016) 4356-4368.
- [25] J. Yang, S. Li, L. Zhang, X. Liu, J. Wang, X. Pan, N. Li, A. Wang, Y. Cong, X. Wang, T. Zhang, *Appl. Catal. B: Environ.*, 201 (2017) 266-277.
- [26] I. Ro, C. Sener, T.M. Stadelmen, M. R. Bal, J.M. Venegas, S.P. Burt, I. Hermans, J.A. Dumesic, G.W. Huber, *J. Catal.* 344 (2016) 784-794.
- [27] R. Burch, *Platinum Metals Rev.*, 22 (1978) 57-60.
-

- [28] B. Mitra, X. Gao, I.E. Wachs, A.M. Hirt, G. Deo, *Phys. Chem. Chem. Phys.* 3 (2001) 1144-1152.
- [29] M. Stoyanova, U. Rodemerck, U. Bentrup, U. Dingerdissen, D. Linke, R.-W. Mayer, H. G. J. Lansink rotgerink, T. Tacke, *Appl. Catal. A: Gen.*, 340 (2008) 242-249.
- [30] P. Arnoldy, J.C.M. de Jonge, J.A. Moulijn, *J. Phys. Chem.* 89 (1985) 4517-4526.
- [31] K.V.R. Chary, T. Bhaskar, G. Kishan, K. Rajender Reddy, *J. Phys. Chem. B* 105 (2001) 4392-4399.
- [32] K.V.R. Chary, K. Rajender Reddy, G. Kishan, J.W. Niemantsverdriet, G. Mestl, *J. Catal.* 226 (2004) 283-291.
- [33] D. Meng, B. Wang, W. Yu, W. Wang, Z. Li, X. Ma, *Catalysts* 7 (2017) 151-160.
- [34] H. Cheng, W. Lin, X. Li, C. Zhang, F. Zhao, *Catalysts*, 4 (2014) 276-288.
- [35] T. Deng, H. Liu, *Green Chem.*, 15 (2013) 116-124.
- [36] M. Dömök, A. Oszkó, K. Baán, I. Sarusi, A. Erdöhelyi, *Appl. Catal. A: Gen.* 383 (2010) 33-42.
- [37] Z.-T. Liu, C.-X. Wang, Z.-W. Liu, J. Lu, *Appl. Catal. A: Gen.* 344 (2008) 114-123.
- [38] M. Shetty, K. Murugappan, W.H. Green, Y. Román-Leshkov, *ACS Sus. Chem. Eng.*, 5 (2017) 5293-5301.
- [39] T.Y. Kim, D.S. Park, Y. Choi, J. Baek, J.R. Park, J. Yi, *J. Mater. Chem.* 22 (2012) 10021-10028.
- [40] S. Kuba, M. Che, R.K. Grasselli, H. Knözinger, *J. Phys. Chem. B* 107 (2003) 3459-3463.
- [41] K. Zhang, H. Zhang, H. Ma, W. Ying, D. Fang, *Catal. Lett.*, 144 (2014) 691-701.
- [42] R. Thomas, E.M. van Oers, V.H.J. de Beer, J. Medema, J.A. Moulijn, *J. Catal.* 76 (1982) 241-253.
- [43] H. Hu, I.E. Wachs, *J. Phys. Chem.* 99 (1995) 10911-10922.

Chapter-7
**Highly Efficient Pt-MoO_x/ZrO₂ Catalyst for Green Diesel
Production**

6.1. Introduction

Green diesel produced by deoxygenation of inedible oils is the most appropriate renewable fuel for application in transport sector as it addresses some of the issues related to the conventional petro-diesel *viz.*, non-renewability and global warming [1-3]. Supported noble metals were found more efficient in green diesel production than Ni-Mo(W) and Co-Mo(W)-based hydrotreating catalysts [4-7]. However, catalyst durability and process economics are issues for the use of known noble metal catalysts [8, 9]. To make the process economical, catalyst should be active at moderate temperatures and hydrogen pressures and handle a variety of vegetable oil feedstocks. In addition to catalyst durability, minimum carbon loss and high yield of green diesel are essential. With a view to develop such an efficient catalyst, Pt deposited on reducible oxide modified supports has been explored in this thesis. It was found (in Chapters-3 and 4) that the reducible oxide promotes the catalytic activity and hydrodeoxygenation (HDO) selectivity of Pt. Among different reducible oxides, MoO_x showed superior enhancement effect (Chapter-6). The electronic interaction amongst the support, reducible oxide and Pt plays critical role on the reaction. Amongst different supports (Chapter-5), zirconia (ZrO₂) enabled higher catalytic activity/selectivity. Thus, having established that ZrO₂ is the best support and MoO_x is the superior reducing oxide, a catalyst composition of 4Pt-8MoO_x/ZrO₂ has been synthesized and investigated in this chapter. For comparison, 4Pt-8WO_x/ZrO₂ has also been prepared and its catalytic activity has been evaluated. In line with the expectations, 4Pt-8MoO_x/ZrO₂ showed remarkably high catalytic activity. This catalyst was found active even at 200 °C and more efficient than most of the known hydrodeoxygenation catalysts for green diesel production.

Due to high thermal stability, chemical resistance, surface redox properties, polymorphism and amphoteric nature, ZrO₂ has been investigated as a catalyst component or support in various chemical transformations including VOC oxidation, methane combustion, HCHO oxidation and hydrodeoxygenation of phenol [10-13]. It exists in three crystal phases *viz.*, monoclinic (m-ZrO₂), tetragonal (t-ZrO₂) and cubic (c-ZrO₂) [14,15]. The monoclinic phase is stable below 1000 °C and the tetragonal and cubic phases are formed at high temperature or can be stabilized at room temperature by doping with elements like Y, La, Ce, etc in the zirconia lattice [16]. Compared to pure phases, a mixed phase zirconia (t + m-ZrO₂) was found superior in certain reactions, as the mixed phase at the interfacial structure stabilizes the supported metal [10, 17-19]. ZrO₂ with mixed phase structure was prepared, modified with reducible oxide. Pt was deposited on it and used in this study.

7.2. Experimental

7.2.1. Catalyst preparation

ZrO₂ support used in this study was prepared as reported in Chapter-2. A known quantity of MoO_x or WO_x (8 wt%) and Pt (4 wt%) were deposited on to it by sequential wet-impregnation method (Chapter-2).

7.2.2. Catalyst characterization and reaction procedure

Fresh and spent catalysts were characterized by X-ray powder diffraction (XRD), N₂-physisorption, CO-chemisorption, NH₃-temperature-programmed desorption (NH₃-TPD), H₂-temperature-programmed reduction (H₂-TPR), X-ray photoelectron spectroscopy (XPS), transmission electron microscopy (TEM) and scanning electron microscopy-energy dispersive X-ray analysis (SEM-EDAX) techniques. Details of characterization techniques, reaction procedure and product analysis are presented in Chapter-2.

7.3. Results and discussion

7.3.1. Catalyst characterization

7.3.1.1. X-ray diffraction

XRD pattern of ZrO₂ used in this study (Fig. 7.1) revealed co-existence of monoclinic (m) and tetragonal (t) crystal phases. The monoclinic phase showed characteristic XRD peaks at 17.6, 24.3, 28.2, 31.5, 34.4, 35.4, 38.6, 41.1, 45.0, 45.6, 49.3, 50.3, 54.2, 55.6, 57.2, 58.0, 60.1, 65.87, 71.38, 75.1 and 81.8° (JCPDS 37-1484) and the tetragonal phase showed peaks at 30.3, 34.4, 35.4, 43.1, 50.4, 54.1, 60.07, 63.03 and 81.5° (JCPDS 80-0965). From peak areas, the composition of monoclinic and tetragonal crystal phases was determined to be 73 and 27%, respectively. 4Pt/ZrO₂ showed additional peaks at 39.7, 46.2, 67.3, 81.3 and 85.6° arising from (111), (200), (220), (311) and (322) planes of metallic Pt with a cubic closed-pack structure having a space group of Fm-3m (JCPDS No. 65-2868). These peaks were weak and overlapped with those of the support and hence, no attempts to determine the crystallite size of Pt from XRD were made. When MoO_x or WO_x was also present a considerable reduction in tetragonal phase and increase in monoclinic phase of ZrO₂ was observed. The monoclinic and tetragonal phase compositions were 92 and 8%, respectively for 4Pt-8MoO_x/ZrO₂ and 93 and 7%, respectively for 4Pt-8WO_x/ZrO₂ (Fig. 7.1). Catalysts containing 2 wt% Pt along with 4 to 16 wt% MoO_x were prepared. The tetragonal phase of ZrO₂ decreased systematically with increasing loading of MoO_x (Fig. 7.2). Absence of peaks at 12.8, 23.1, 23.6, 25.8, 27.4, 29.1, 33.6, 39.1, 45.9, 49.3, 55.4, 59.1° due to crystalline MoO₃ even at 16 wt% molybdenum loading (JCPDS 85-2405) and at 23.3 and 33.4° due to

crystalline WO₃ at 8 wt% tungsten loading (JCPDS 75-2072) confirm that the reducible oxide is in a highly dispersed state and in the monolayer coverage regime at chosen concentrations.

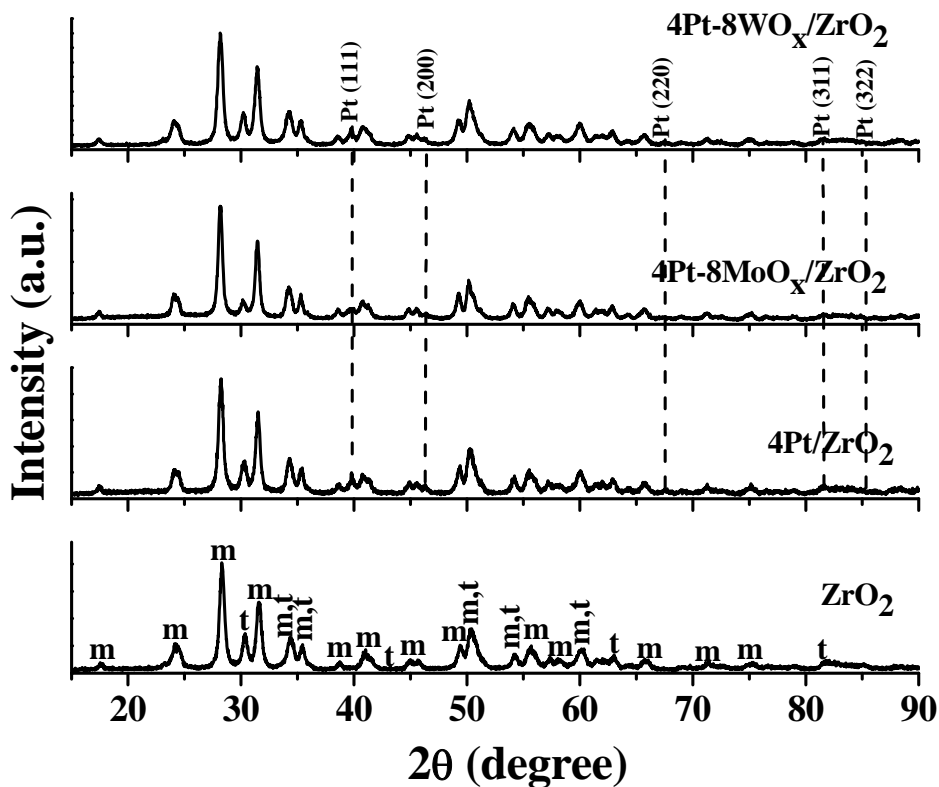


Fig. 7.1. XRD patterns of ZrO₂ and ZrO₂-supported Pt catalysts.

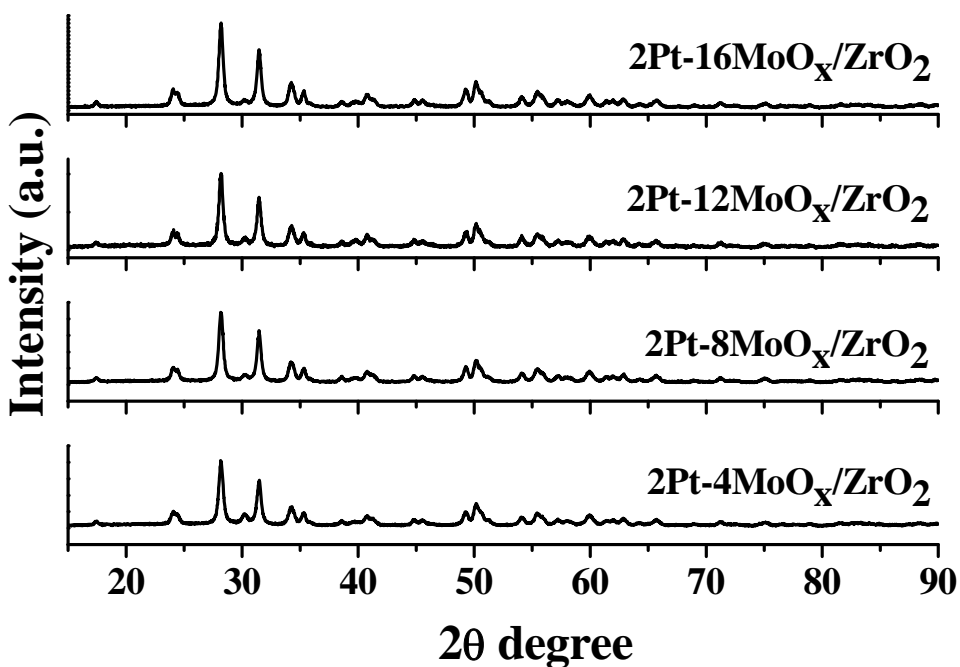


Fig. 7.2. XRD profiles of 2 wt% Pt deposited on varying amounts of MoO_x modified ZrO₂.

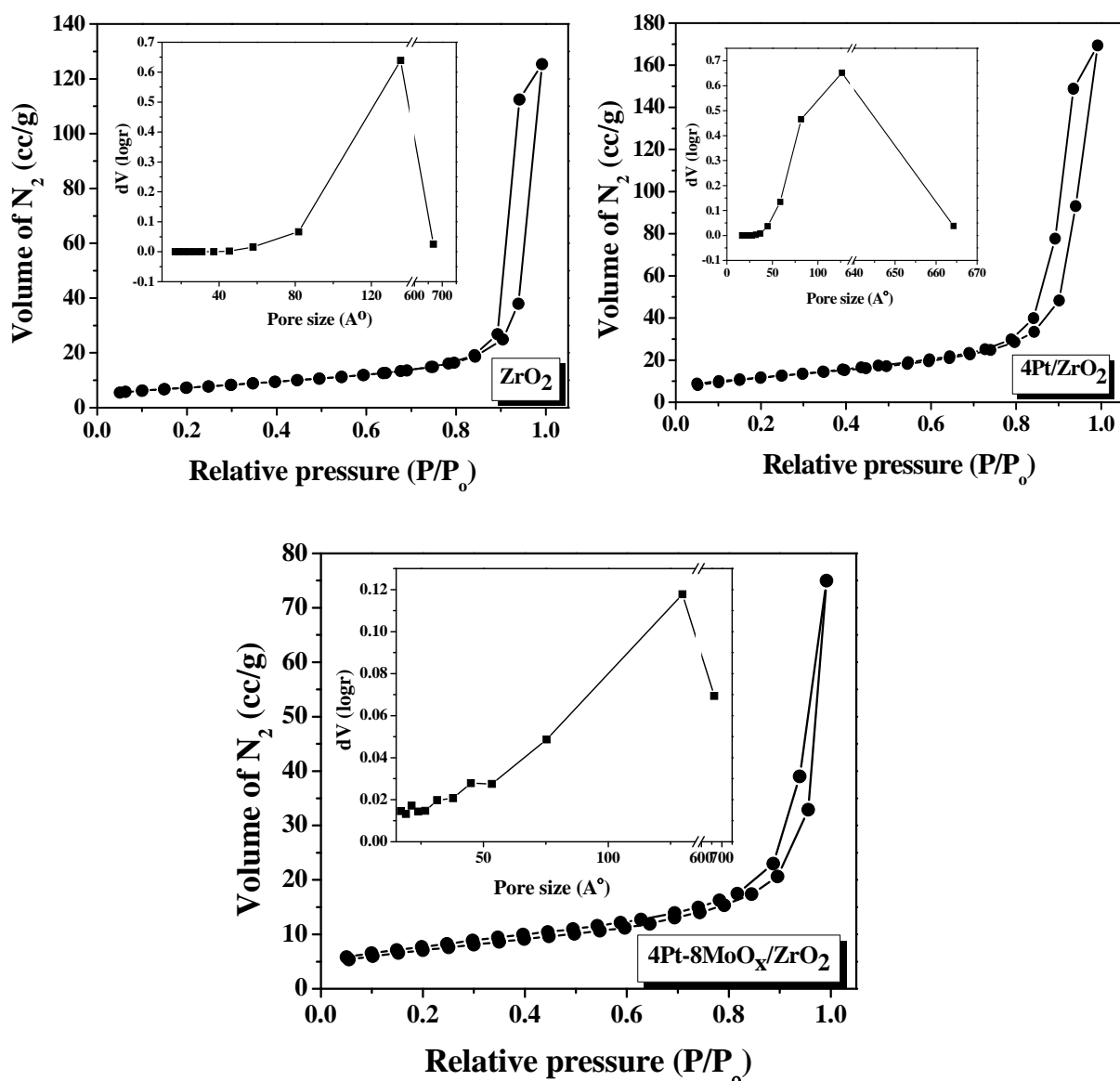


Fig. 7.3. Nitrogen adsorption-desorption isotherms of ZrO₂ and ZrO₂-supported Pt catalysts.

7.3.1.2. N₂-Physisorption

ZrO₂, 4Pt/ZrO₂, 4Pt-8MoO_x/ZrO₂ and 4Pt-8WO_x/ZrO₂ showed Type IV nitrogen adsorption-desorption isotherms typical of mesoporous materials (Fig. 7.3). Neat ZrO₂ had a surface area of 38 m²/g, pore volume of 0.194 cc/g and average pore size of 14.9 nm. On loading Pt and reducible oxide these values have decreased substantially (Table 7.1) suggesting their deposition at the pore mouth and pore walls of mesopores.

Table 7.1. Physicochemical characteristics of ZrO₂-supported Pt catalysts

Catalyst	N ₂ physisorption			CO chemisorption			Pt particle size (nm; TEM)
	S _{BET} (m ² /g)	Total pore volume (cc/g)	Av. pore size (nm)	Mono-layer CO uptake (μmol/g)	Active Pt surface area (m ² /g)	Pt dispersion (%)	
ZrO ₂	38	0.194	14.9	-	-	-	-
4Pt/ZrO ₂	34	0.165	12.5	44.0	53	22	5.3
4Pt-8MoO _x /ZrO ₂	25	0.116	9.2	24.4	29	12	9.5
4Pt-8WO _x /ZrO ₂	28	0.110	9.0	30.5	37	15	7.6

7.3.1.3. CO-chemisorption

Chemisorption studies revealed that the monolayer uptake of CO by 4Pt/ZrO₂ was 44.0 μmol/g. This value had decreased to 24.4 and 30.5 μmol/g for 4Pt-8MoO_x/ZrO₂ and 4Pt-8WO_x/ZrO₂ catalysts, respectively (Table 7.1). Active specific surface area, percentage dispersion and average crystallite size of supported Pt were determined from the monolayer CO uptake values assuming the stoichiometric molar ratio of CO/Pt as unity (Table 7.1). In the presence of reducible oxide, the average crystallite size of Pt had increased from 5.3 to 9.5 for 4Pt-8MoO_x/ZrO₂ and 7.3 nm for 4Pt-8WO_x/ZrO₂ and percentage metal dispersion decreased from 22% (for 4Pt/ZrO₂) to 12% for 4Pt-8MoO_x/ZrO₂ and 15% for 4Pt-8WO_x/ZrO₂. Such variations in CO uptake and Pt dispersion in presence of reducible oxide were found also in Chapters 3 to 6.

Table 7.2. CO-chemisorption data of 2Pt-MoO_x/ZrO₂ catalysts

Catalyst	Monolayer CO uptake (μmol/g)	Active Pt surface area (m ² /g)	Pt dispersion (%)	Av. Pt crystallite size (nm)
2Pt-4MoO _x /ZrO ₂	9.3	23	9	12.4
2Pt-8MoO _x /ZrO ₂	22.4	54	22	5.2
2Pt-12MoO _x /ZrO ₂	27.7	67	27	4.2
2Pt-16MoO _x /ZrO ₂	37.3	90	36	3.1

Table 7.2 summarizes CO chemisorption data of 2 wt% Pt deposited on varying amounts of MoO_x modified ZrO₂. With increasing MoO_x content, monolayer CO coverage had increased from 9.3 to 37.7 μmol/g, active Pt surface area had increased from 23 to 90 m²/g, Pt had dispersion increased from 9 to 36% and average Pt crystallite size had decreased from 12.4 to 3.1 nm. In other words, higher the Mo/Pt weight ratio higher was the dispersion of Pt. Thus, by varying reducible oxide content, one could change Pt dispersion and its crystallite size.

7.3.1.4. TEM

Electron microscopic images of 4Pt/ZrO₂, 4Pt-8MoO_x/ZrO₂ and 4Pt-8WO_x/ZrO₂ are shown in Fig. 7.4. Platinum particles in 4Pt/ZrO₂ are distributed on the crystallites of zirconia. However, in the case of reducible oxide modified supports, the reducible oxide formed an uniform layer on ZrO₂ and Pt particles were supported on the reducible oxide. Particle size histograms plotted considering 100 random Pt particle revealed heterogeneous distribution of particles with varying size. The average particle size of Pt increased from 4 nm (on unmodified supports - 4Pt/ZrO₂) to 6 nm (on modified supports - 4Pt-8MoO_x/ZrO₂) and 4.5 nm (4Pt-8WO_x/ZrO₂). Such an increase in Pt particle size in presence of reducible oxide was found also on other supports (Chapter 5).

7.3.1.5. NH₃-TPD

Temperature-programmed desorption studies using NH₃ as probe molecule revealed a broad distribution of acid sites in the temperature range 100 to 500 °C. Upon loading Pt and reducible oxide, acid sites distribution in a narrow temperature range was observed (Fig. 7.5). Especially, the content of strong acid sites has decreased and those of weak and medium type increased (Table 7.3). Overall acidity decreased marginally on modifying with reducible oxides.

Table 7.3. Acidity data of ZrO₂-supported Pt catalysts

Catalyst	Total acidity (mmol/g)	Acidity distribution (mmol/g)		
		Weak (100-200 °C)	Medium (200-300 °C)	Strong (>300 °C)
ZrO ₂	0.23	0.071	0.064	0.095
4Pt/ZrO ₂	0.26	0.131	0.103	0.025
8MoO _x /ZrO ₂	0.19	0.083	0.102	0.006
4Pt-8MoO _x /ZrO ₂	0.21	0.136	0.058	0.015
4Pt-8WO _x /ZrO ₂	0.24	0.179	0.037	0.024
2Pt-4MoO _x /ZrO ₂	0.19	0.102	0.075	0.013
2Pt-8MoO _x /ZrO ₂	0.15	0.090	0.050	0.010
2Pt-12MoO _x /ZrO ₂	0.14	0.057	0.076	0.006
2Pt-16MoO _x /ZrO ₂	0.11	0.063	0.040	0.007

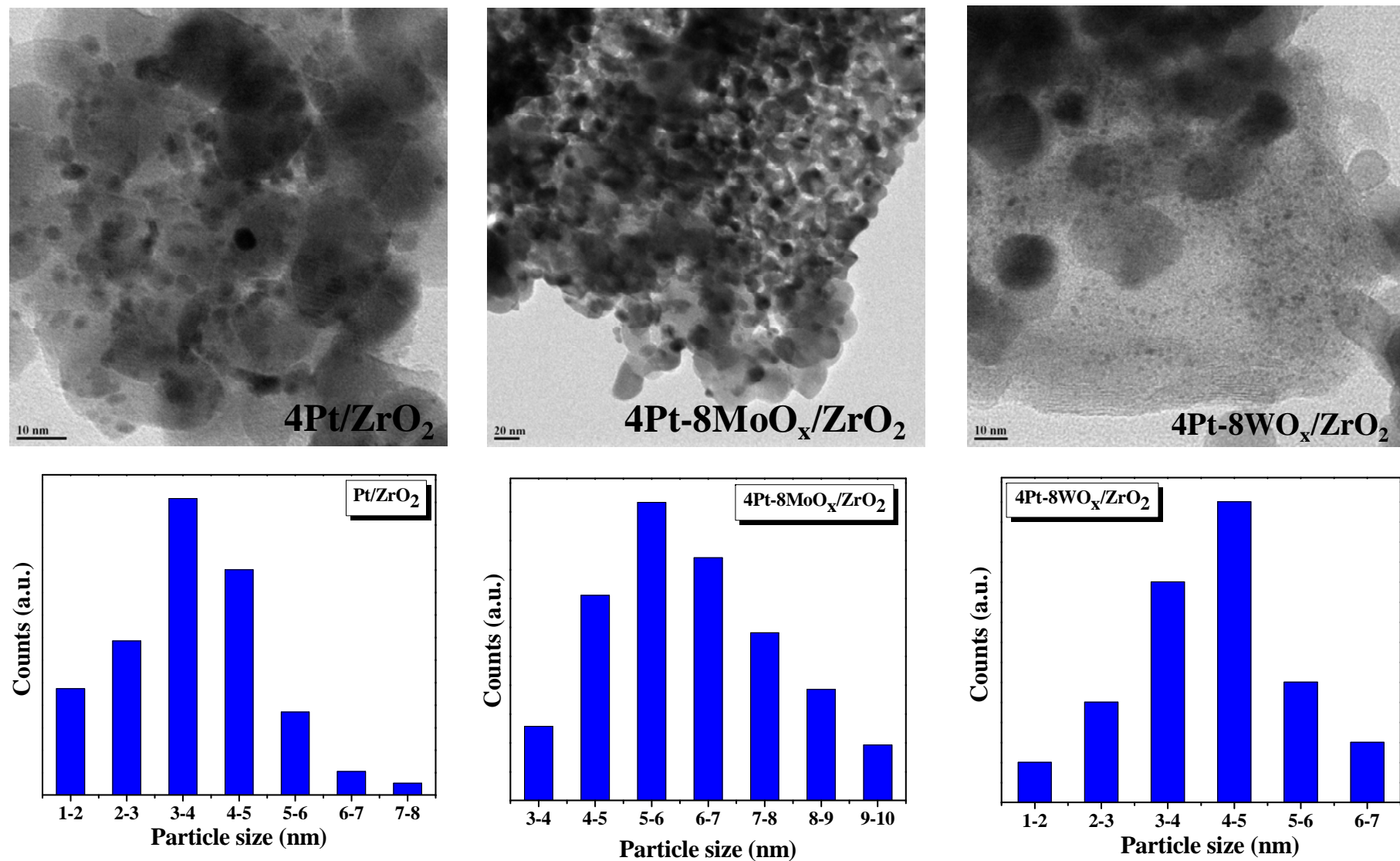


Fig. 7.4. TEM images and particle size histograms of ZrO₂-supported Pt catalysts.

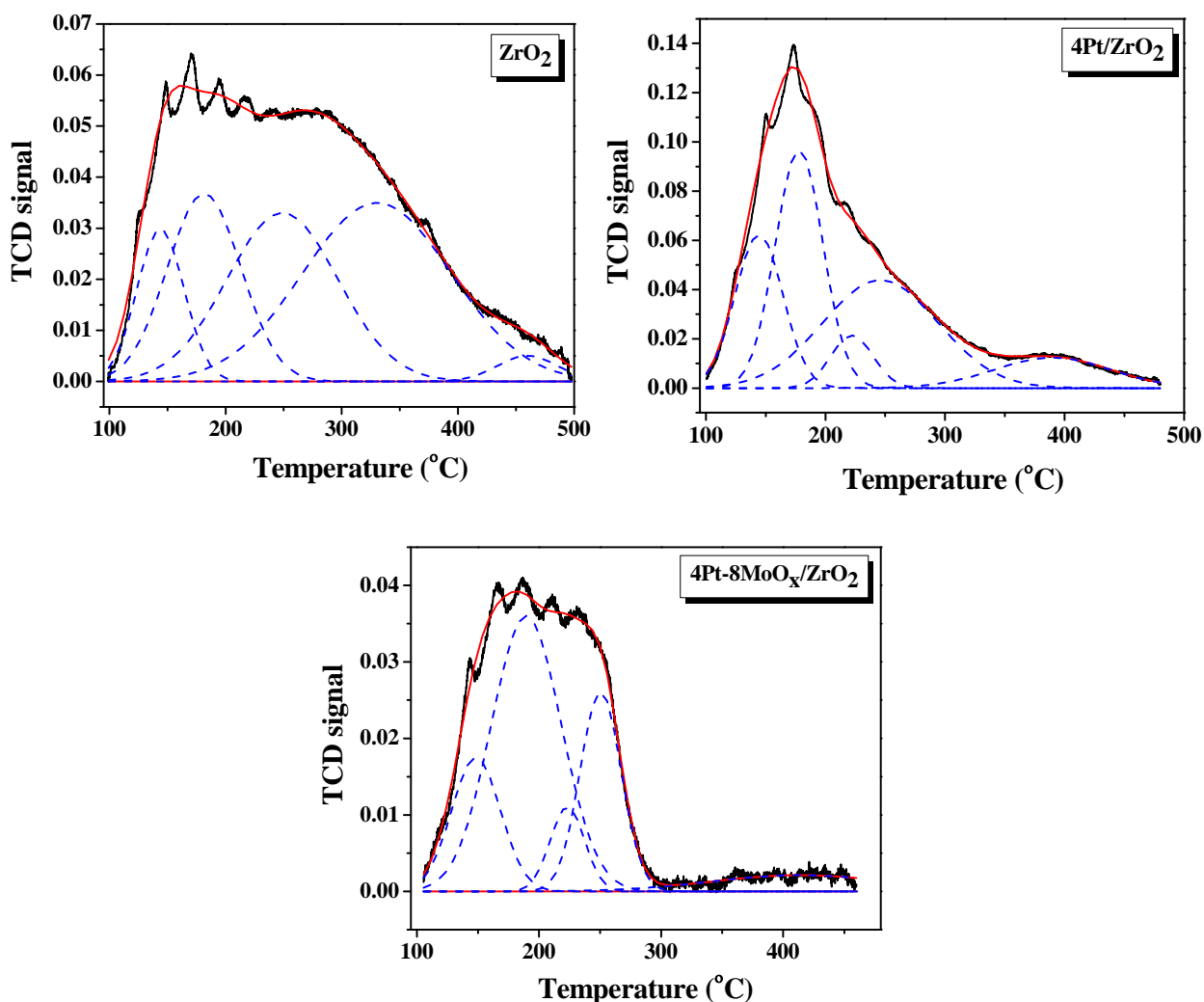


Fig. 7.5. NH₃-TPD profiles of ZrO₂ and ZrO₂-supported Pt catalysts.

7.3.1.6. H₂-TPR

H₂-TPR profiles of neat ZrO₂, 4Pt/ZrO₂, 8MoO_x/ZrO₂ and 4Pt-8MoO_x/ZrO₂ are shown in Fig. 7.6. Neat ZrO₂ did not show any reduction peaks in the temperature range 100 to 900 °C. Also no reduction peaks were observed for 4Pt/ZrO₂. Broad reduction peaks in the range 279-443 °C (with T_{max} at 357 °C) and 619-856 °C (with T_{max} at 774 °C) were detected for 8MoO_x/ZrO₂ due to bulk octahedral and dispersed tetrahedral molybdenum oxide species [10, 20-22]. The multi-step desorption peak behavior indicates a step-wise reduction of +6 to lower oxidation state molybdenum. In the case of 4Pt-8MoO_x/ZrO₂, a sharp reduction peak with T_{max} at 697 °C was observed. This decrease in reduction temperature is due to the presence of Pt. It also indicates that molybdenum oxide is in a highly dispersed state when Pt is present and there exists electronic contact between Pt and Mo located on the zirconia surface.

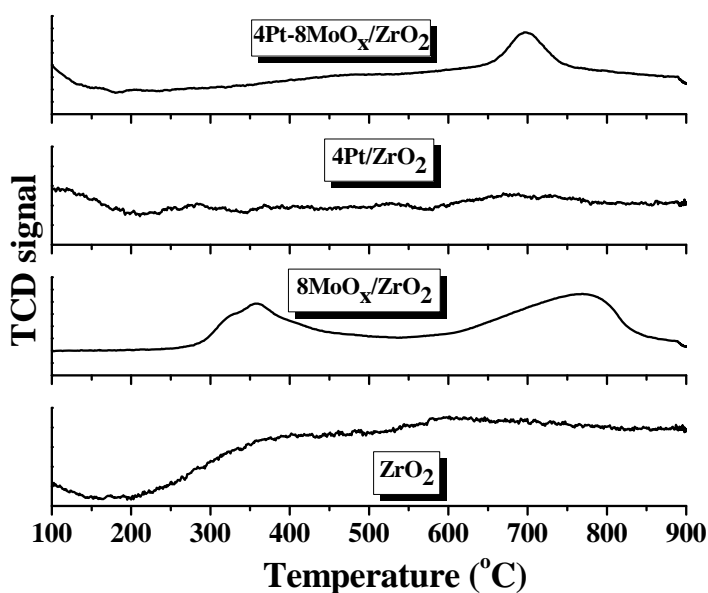


Fig. 7.6. H₂-TPR profiles of ZrO₂-supported Pt catalysts.

7.3.1.7. X-ray photoelectron spectroscopy

XPS showed intense Pt 4f lines which could be deconvoluted into spin-orbit coupling lines of Pt⁰ and Pt²⁺ species. The 4f lines of Pt⁰ for 4Pt/ZrO₂ occurred at 71.0 and 74.4 eV and those of Pt²⁺ occurred at 72.5 and 75.9 eV. These spin-orbit doublets for Pt supported on MoO_x and WO_x modified ZrO₂ occurred at lower binding energy values suggesting that Pt on modified ZrO₂ is richer in electron density than on unmodified ZrO₂. The 4f lines of Pt⁰ occurred at 70.8 & 74.0 eV (for both the modified catalysts) and those of Pt²⁺ occurred at 72.3 and 75.3 eV for 4Pt-8MoO_x/ZrO₂ and at 72.4 and 75.7 eV for 4Pt-WO_x/ZrO₂ (Fig. 7.7). In the case of 4Pt-8MoO_x/ZrO₂ an additional overlapping line due to Mo 4s occurred at 69.5 eV. Bulk MoO₃ shows this 4s line at 66.8 eV [23]. Occurrence of this peak at higher binding energy in the present system suggests that the Mo species in the present catalysts is different from crystalline MoO₃. The relative intensity of Pt⁰/Pt²⁺ for 4Pt/ZrO₂, 4Pt-8MoO_x/ZrO₂ and 4Pt-8WO_x/ZrO₂ is 3.2, 3.3 and 2.6, respectively. Thus, MoO_x enables more amount of Pt in reduced Pt⁰ state.

XPS of 4Pt-8MoO_x/ZrO₂ in Mo 3d region and 4Pt-8WO_x/ZrO₂ in W 4f region are shown in Fig. 7.8. In presence of Pt and after reduction with hydrogen, a part of Mo and W content on the catalyst got reduced to +5 oxidation state and hence, XPS lines corresponding to both +6 and +5 oxidation states of Mo and W were observed. The relative ratio of +5/+6 species for 4Pt-8MoO_x/ZrO₂ and 4Pt-8WO_x/ZrO₂ were found to be 0.56 and 1.55, respectively. In other words, tungsten oxide is more easily reduced than molybdenum oxide in the present catalysts.

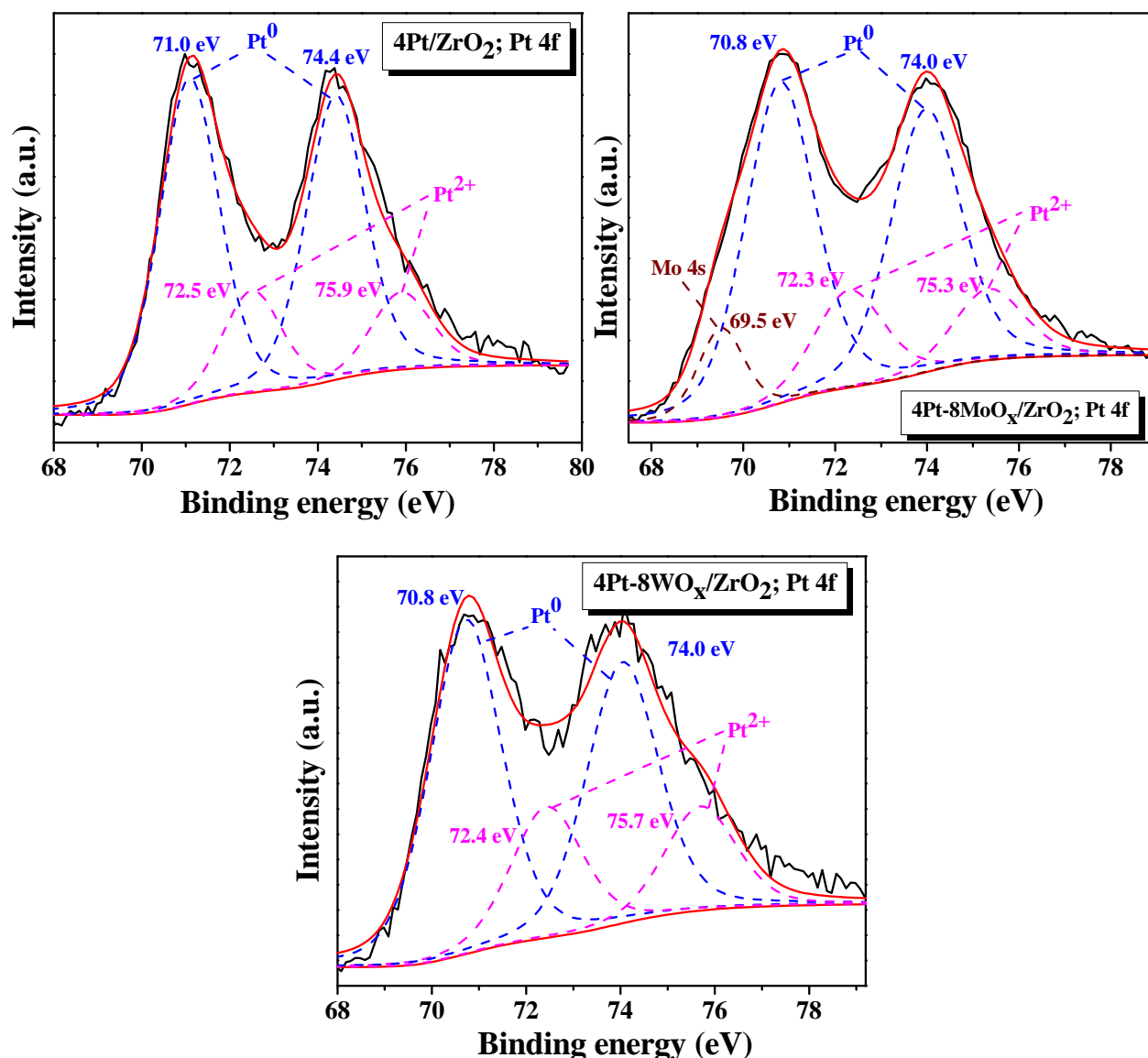


Fig. 7.7. XPS of 4Pt/ZrO₂, 4Pt-8MoO_x/ZrO₂ and 4Pt-8WO_x/ZrO₂ in Pt 4f region. Peaks due to Pt⁰ and Pt²⁺ are deconvoluted and indexed. Peak due to Mo 4s is also indexed.

4Pt/ZrO₂ in Zr 3d region showed characteristic spin-orbit doublet at 182.1 and 184.5 eV due to 3d_{5/2} and 3d_{3/2} lines, respectively of zirconium in +4 oxidation state (Fig. 7.9). An additional spin-orbit doublet in the lower binding energy at 180.9 & 183.1 eV for 4Pt-8MoO_x/ZrO₂ and 181.1 & 183.6 eV for 4Pt-8WO_x/ZrO₂ was observed suggesting that in the presence of reducible oxide a portion of support zirconia is reduced into lower oxidation state forming a sub-oxide [24-26]. The intensity ratio of sub-oxide to stoichiometric ZrO₂ is 0.38 and 2.17 for 4Pt-8MoO_x/ZrO₂ and 4Pt-8WO_x/ZrO₂, respectively. Thus, the XPS study reveals that

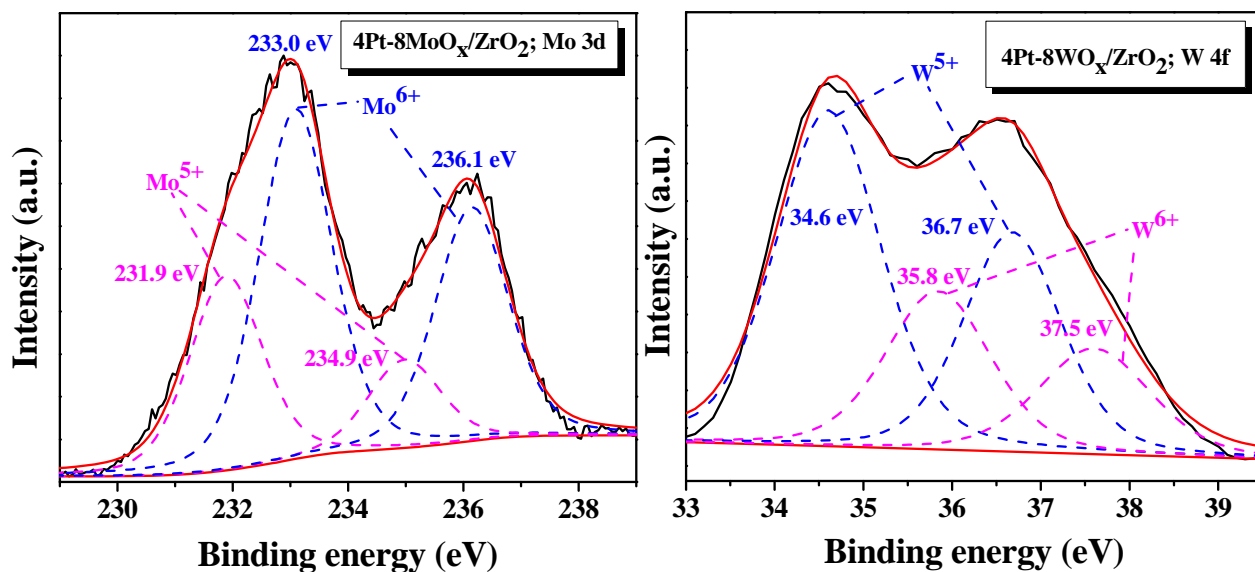


Fig. 7.8. XPS of 4Pt-8MoO_x/ZrO₂ and 4Pt-8WO_x/ZrO₂ in Mo 3d and W 4f regions.

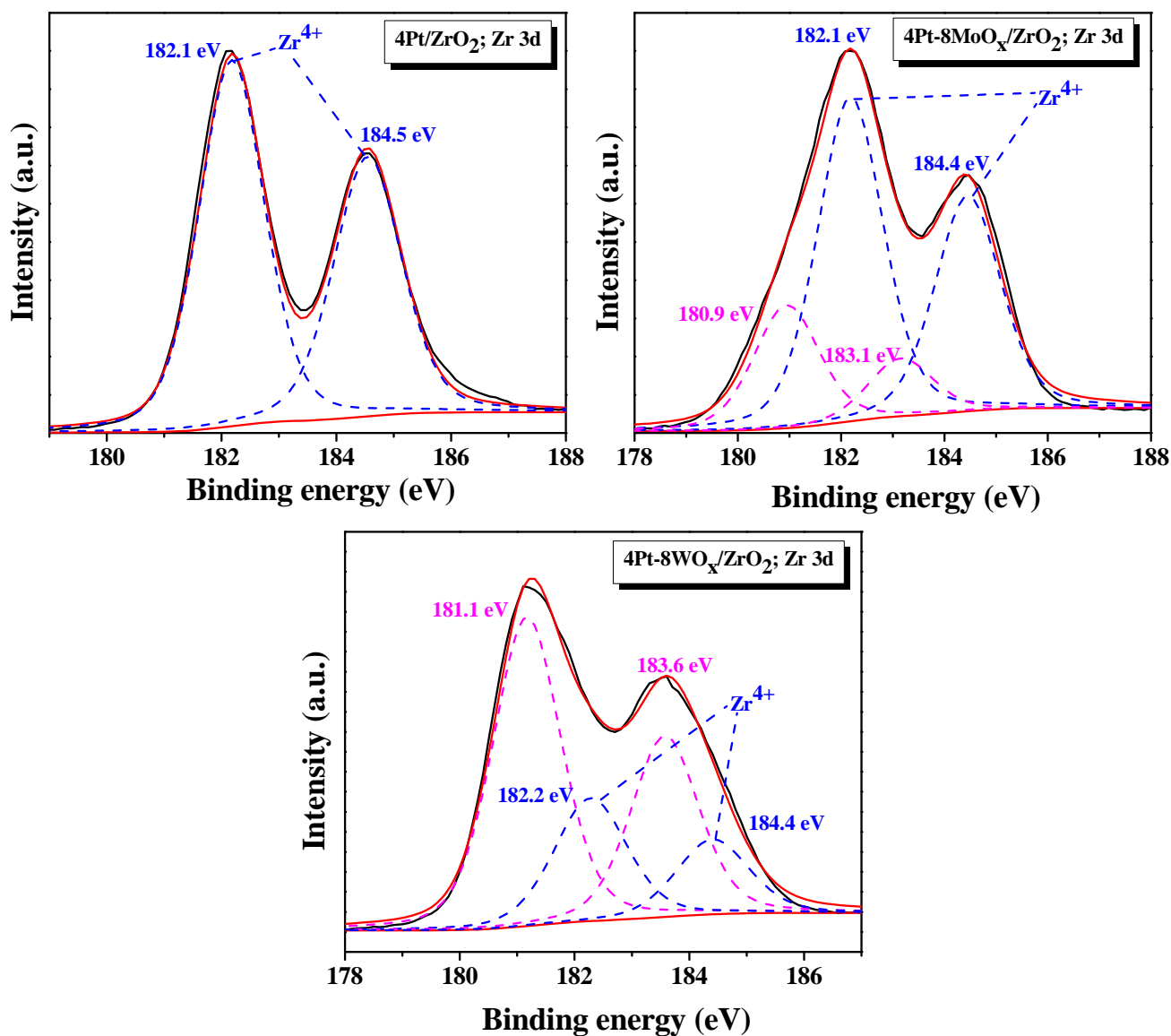


Fig. 7.9. XPS of ZrO₂-supported Pt catalysts in Zr 3d region.

there exists electronic connectivity between Pt, reducible oxide and ZrO₂. The reduction of these elements depended on the chemical composition of the catalyst. Table 7.4 presents surface chemical composition of the catalysts determined from the intensity of spectral lines of XPS.

Table 7.4. Surface chemical composition (atomic ratio) of ZrO₂-supported Pt catalysts

Catalyst	Pt ⁰ /Pt ²⁺	Mo ⁵⁺ /Mo ⁶⁺ or W ⁵⁺ /W ⁶⁺	Zr ^{4-δ} /Zr ⁴⁺	Pt/O	Mo/O or W/O	Zr/O
4Pt/ZrO ₂	3.20	-	0	0.02	-	1.5
4Pt-8MoO _x /ZrO ₂	3.30	0.56	0.38	0.04	0.6	1.2
4Pt-8WO _x /ZrO ₂	2.55	1.55	2.17	0.02	0.2	1.4
4Pt-8MoO _x /ZrO ₂ -Spent	4.35	0.67	0.31	0.03	0.4	1.2
4Pt-8WO _x /ZrO ₂ -Spent	3.6	0.74	0.51	0.02	0.3	1.3

7.3.2. Catalytic activity

Control experiments in the absence of a catalyst conducted at 220 °C and 20 bar H₂ for 5 h revealed no conversion of oleic acid (OA) and thereby, confirm absence of any thermal cracking contribution to the results reported hereafter. 8MoO_x/ZrO₂ under these conditions exhibited OA conversion of 6 mol% with the product selectivity for octadecane (C₁₈) being 4.9 wt% and alcohols + aldehydes + ester products (hereafter referred as others) being 95.1%. Thus, ZrO₂-dispersed reducible oxide itself is not a good deoxygenation catalyst. 4Pt/ZrO₂ under these conditions (OA = 2 g; solvent (n-heptane) = 30 g, catalyst = 10 wt% of OA) enabled OA conversion of 23.0 mol% with the selectivity for octadecane (C₁₈), heptadecane (C₁₇) and others being 27.4, 58.9 and 13.7 wt%, respectively. A significant enhancement in OA conversion and hydrodeoxygenation product (C₁₈) selectivity was observed when Pt supported on MoO_x or

Table 7.5. Deoxygenation of oleic acid over 4Pt-8MoO_x/ZrO₂ and 4Pt-8WO_x/ZrO₂ catalysts at varying reaction temperature^a

Run No.	Reaction Parameter	Reaction time = 1 h					Reaction time = 5 h					
		OA conv. (mol%) ^b	Product selectivity (wt.%) ^c				OA conv. (mol%) ^b	Product selectivity (wt.%) ^c				
		C ₁₈	C ₁₇	C ₁₀₋₁₆	Others ^d	C ₁₈	C ₁₇	C ₁₀₋₁₆	Others ^d			
Catalyst: 4Pt-8MoO _x /ZrO ₂												
1	180	13.0	79.3	5.5	2.2	13.0	18.0	88.0	10	1.3	0.7	
2	200	16.0	69.7	5.5	0.6	24.2	75.0	94.6	4.7	0.4	0.3	
3	220	29.0	62.4	14.3	0	23.3	94.0	92.0	6.3	0.5	1.1	
4	240	30.0	85.3	10.2	0	4.5	100.0	91.4	7.3	0.5	0.8	
5	260	83.0	85.6	12.3	0.6	1.5						
Catalyst: 4Pt-8WO _x /ZrO ₂												
6	180	5.0	86.0	12.2	0	1.8						
7	220	24.0	93.5	4.73	0.5	1.3						
8	260	69.0	83.5	15.0	0.3	1.2						

^aReaction conditions: Oleic acid (OA) = 2 g, solvent (n-heptane) = 30 g, catalyst = 10 wt.% of OA, H₂ pressure = 20 bar, reaction time = 1 or 5 h, reactor = 100 ml Parr batch autoclave, stirring speed = 600 RPM.

^bDetermined from titration against NaOH. ^cDetermined from GC analysis. ^dOthers include alcohol, aldehyde and esters.

WO_x modified ZrO₂ were used as catalysts (Table 7.5). Under the above conditions, 4Pt-8MoO_x/ZrO₂ led to OA conversion of 94 mol% with 92.0 wt% selectivity for C₁₈, 6.3 wt% for C₁₇, 0.5 wt% for C₁₀₋₁₆ alkanes and 1.1 wt% for others. As observed in other chapters, even with these set of catalysts, the reaction path had changed from decarboxylation/decarbonylation (DCO) route (in unpromoted catalysts; 4Pt/ZrO₂) to hydrodeoxygenation (HDO) path (in reducible oxide-promoted Pt catalysts; 4Pt-8MoO_x/ZrO₂ and 4Pt-8WO_x/ZrO₂).

Reactions were conducted in the temperature range of 180 to 260 °C for 1 to 5 h (Table 7.5). Interestingly, 4Pt-8MoO_x/ZrO₂ showed high catalytic activity (OA conversion = 75.0 mol%; C₁₈ selectivity = 94.6 wt%) even at 200 °C in the reaction extended for 5 h. Catalytic activity increased with increasing reaction temperature. While the product selectivity was more or less the same (irrespective of reaction temperature) in the runs conducted for 5 h (as the system attains the equilibrium condition), differences were noticed in the runs conducted for 1 h (Table 7.5). This is expected as the deoxygenation rate increases with temperature more and more amount of C₁₈ would be formed. In general, octadecane was the major product. 4Pt-8MoO_x/ZrO₂ was catalytically more active than 4Pt-8WO_x/ZrO₂. Product selectivity for hydrocarbons was higher on the latter than on the former at 1 h of reaction time. The catalytic activity of 4Pt-8MoO_x/ZrO₂ is much higher than the catalysts investigated so far in this thesis and reported by others [27-30].

Table 7.6. Effect of hydrogen pressure on deoxygenation of oleic acid^a

Run No.	H ₂ pressure (bar)	OA conv. (mol%) ^b	Product selectivity (wt.%) ^c			
			C ₁₈	C ₁₇	C ₁₀₋₁₆	Others ^d
<i>Reactions conducted @ 260 °C for 1 h</i>						
1	3	5.0	trace	trace	-	trace
2	5	15.0	27.3	36.4	6.0	30.3
3	10	34.0	50.5	45.5	0.5	3.5
4	15	77.0	82.6	16.0	0.5	0.9
5	20	83.0	85.6	12.3	0.6	1.5
<i>Reactions conducted @ 200 °C for 5 h</i>						
6	5	14.0	68.0	29.0	0.3	2.7
7	10	52.0	91.5	6.8	0.6	1.1
8	20	75.0	94.6	4.7	0.4	0.3

^aReaction conditions: Oleic acid (OA) = 2 g, solvent (n-heptane) = 30 g, catalyst (4Pt-8MoO_x/ZrO₂) = 10 wt% of OA, reactor = 100 ml Parr batch autoclave, stirring speed = 600 RPM. ^bDetermined from titration against NaOH. ^cDetermined from GC analysis. ^dOthers include alcohol, aldehyde and esters.

Hydrogen pressure had a marked effect on the catalytic hydrodeoxygenation activity of 4Pt-8MoO_x/ZrO₂ (Table 7.6). In the experiments conducted at 200 °C (for 5 h) and 260 °C (for 1 h), OA conversion and C₁₈ selectivity increased with increasing hydrogen pressure. In other words, hydrogen has a positive effect on the reaction and facilitated the HDO path.

Table 7.7 presents the catalytic activity data at 200 °C as a function of reaction time over 4Pt-8MoO_x/ZrO₂. OA conversion and C₁₈ product selectivity increased with increasing reaction time.

Table 7.7. Influence of reaction time on deoxygenation of OA over 4Pt-8MoO_x/ZrO₂ catalyst^a

Run No.	Reaction time (h)	OA conv. (mol%)	Product selectivity (wt.%)			
			C ₁₈	C ₁₇	C ₁₀₋₁₆	Others
1	0.5	8	67.7	16.0	0	16.3
2	1	16	69.7	5.5	0.6	24.2
3	3	40	95.5	3.5	0.4	0.6
4	5	75	94.6	4.7	0.4	0.3

^aReaction conditions: Oleic acid (OA) = 2 g, solvent (n-heptane) = 30 g, catalyst (4Pt-8MoO_x/ZrO₂) = 10 wt% of OA, reaction temperature = 200 °C, reactor = 100 ml Parr batch autoclave, stirring speed = 600 RPM.

Catalyst amount taken in the reaction was varied from 5 to 10 wt% of OA (Table 7.8). With increasing catalyst amount, OA conversion increased. C₁₈ selectivity was in the range of 83.0 to 96.0 wt%.

Table 7.8. Influence of catalyst amount on deoxygenation of oleic acid^a

Run No.	Catalyst amount (wt% of OA)	OA conversion (mol%)	Product selectivity (wt%)			
			C ₁₈	C ₁₇	C ₁₀₋₁₆	Others
1	5	12.0	83.0	5.5	0	11.7
2	7.5	38.0	96.0	2.0	0.2	1.8
3	10	75.0	95.0	4.5	0.44	0.3

^aReaction conditions: Oleic acid (OA) = 2 g, solvent (n-heptane) = 30 g, catalyst = 4Pt-8MoO_x/ZrO₂, reaction temperature = 200 °C, reaction time = 5 h, pressure = 20 bar H₂, reactor = 100 ml Parr batch autoclave, stirring speed = 600 RPM.

The composition of the catalyst (Pt-Mo composition) had a marked effect. Keeping Pt content at 2 wt%, Mo content in the catalyst was varied from 4 to 8, 12 and 16 wt%. OA conversion and C₁₈ selectivity increased with increasing Mo content up to 8 wt% and then onwards showed a decreasing trend (Table 7.9). With increasing Mo content, the dispersion of

Pt had increased and acidity of the catalyst decreased. Hence, too high a dispersion and low acidity are not good for hydrodeoxygenation activity.

Table 7.9. Effect of Mo content on the deoxygenation of OA over 2Pt-xMoO_x/ZrO₂ (x = 4-16)^a

Run No.	Mo content (wt%)	OA conversion (mol%) ^b	Product selectivity (wt %) ^c			
			C ₁₈	C ₁₇	C ₁₀₋₁₆	Others ^d
1	4	31.0	81.0	12.0	6.0	1.0
2	8	53.0	93.6	4.5	0.6	1.3
3	12	25.0	90.0	6.8	0.6	2.6
4	16	8.0	68.0	10.1	1.6	20.3

^aReaction conditions: Oleic acid (OA) = 2 g, solvent (n-heptane) = 30 g, catalyst (2Pt-xMoO_x/ZrO₂) = 10 wt% of OA, reaction temperature = 200 °C, reaction time = 5 h, pressure = 20 bar H₂, reactor = 100 ml Parr batch autoclave, stirring speed = 600 RPM. ^bDetermined from titration against NaOH. ^cDetermined from GC analysis. ^dOthers include alcohol, aldehyde and esters.

With a view to understand the effect of gaseous environment on deoxygenation, in different experiments, reactor was filled with 20 bar CO₂, N₂ and H₂. The reaction was negligible in CO₂ environment. OA conversion was 2.0 mol% only. Catalytic activity increased to 15.0 mol% in presence of nitrogen gas (Table 7.10). Higher selectivity for the hydrodeoxygenation product (C₁₈) in presence of both CO₂ and nitrogen, indicate that a part of n-heptane is getting reforming into hydrogen, which in turn, drove the hydrodeoxygenation reaction. Supported Pt catalysts are known for reforming of hydrocarbons [31, 32].

Table 7.10. Effect of gaseous atmosphere on deoxygenation of oleic acid^a

Run No.	Pressurized gas	OA conversion (mol%) ^b	Product selectivity (wt %) ^c			
			C ₁₈	C ₁₇	C ₁₀₋₁₆	Others ^d
1	CO ₂	2	73.3	26.7	0	0
2	N ₂	15	85.7	14.3	0	0
3	H ₂	100	91.4	7.3	0.54	0.8

^aReaction conditions: Oleic acid (OA) = 2 g, solvent (n-heptane) = 30 g, catalyst (4Pt-8MoO_x/ZrO₂) = 10 wt.% of OA, temperature = 240 °C, reaction time = 5 h, pressure = 20 bar H₂, reactor = 100 ml Parr batch autoclave, stirring speed = 600 RPM. ^bDetermined from titration against NaOH. ^cDetermined from GC analysis. ^dOthers include alcohol, aldehyde and esters.

Table 7.11. Substrate study over 4Pt-8MoO_x/ZrO₂^a

Run No.	Substrate	Conversion (mol%)	Product selectivity (wt %)										
			C ₁₈	C ₁₇	C ₁₆	C ₁₅	C ₁₄	C ₁₃	C ₁₂	C ₁₁	C ₁₀	Others	
1	Oleic acid (C _{18,1})	75	94.6	4.7	0.44	0	0	0	0	0	0	0	0.28
2	Stearic acid (C ₁₈)	99	92.4	2.5	0.5	0.1	0	0	0	0	0	0	4.5
3	Palmitic acid (C ₁₆)	85	-	-	85.14	1.74	0.25	0	0	0	0	0	12.9
4	Myristic acid (C ₁₄)	95	-	-	-	-	83.0	2.3	0.3	0	0	0	14.4
5	Lauric acid (C ₁₂)	98	-	-	-	-	-	-	84.6	1.6	0	0	13.8
6	Capric acid (C ₁₀)	84	-	-	-	-	-	-	-	-	-	23.6	76.4

^aReaction conditions: Fatty acid = 0.007 mol, solvent (n-heptane) = 30 g, catalyst = 0.2 g, temperature = 200 °C, reaction time = 5 h, pressure = 20 bar H₂, reactor = 100 ml Parr batch autoclave, stirring speed = 600 RPM.

The scope of the reaction was examined by deoxygenating a range of fatty acids (Table 7.11). Irrespective of the chain length of fatty acid, its conversion was high (75 - 99 mol%). Major component was the hydrodeoxygenation product.

In catalyst recyclability study at 320 °C, at the end of each run catalyst was separated from the liquid product, washed with acetone and dried at 110 °C for 12 h, reduced in hydrogen at 350 °C for 2.5 h and reused in the next recycle. As seen from Table 7.12, both 4Pt-8MoO_x/ZrO₂ and 4Pt-8WO_x/ZrO₂ were highly activity with no loss in catalytic activity and selectivity even after several recycles.

Table 7.12. Recyclability study of Pt supported on MoO_x/WO_x modified ZrO₂ catalysts^a

Recycle No.	OA conversion (mol%)	Product selectivity (wt %)			
		C ₁₈	C ₁₇	C ₁₀₋₁₆	Others
<i>Catalyst A: 4Pt-8MoO_x/ZrO₂</i>					
0 (Fresh)	100	89.88	9.56	0.57	0
1	100	81.29	18.05	0.59	0
2	100	81.69	17.55	0.76	0
3	100	80.1	17.48	0.80	0
4	100	82.53	14.71	0.80	1.95
<i>Catalyst B: 4Pt-8WO_x/ZrO₂</i>					
0 (Fresh)	100	83.33	15.85	0.72	0.1
1	100	88.1	11.1	0.69	0.1
2	100	87.5	12.1	0.3	0.1

^aReaction conditions: Oleic acid (OA) = 6 g, solvent (n-heptane) = 40 g, catalyst = 10 wt.% of OA, temperature = 320 °C, reaction time = 5 h, pressure = 25 bar H₂, reactor = 300 ml Parr batch autoclave, stirring speed = 600 RPM.

The spent catalysts were characterized by XRD, CO-chemisorption, TEM, SEM-EDAX and XPS. XRD revealed reduced peak intensity in spent catalyst as compared to the fresh catalyst (compare Fig. 7.10 with Fig. 7.1). Tetragonal/monoclinic phase composition ratio was found to increase from 0.08 for fresh to 0.23 for spent 4Pt-8MoO_x/ZrO₂ and from 0.07 for fresh to 0.11 for spent 4Pt-8WO_x/ZrO₂ catalysts. In other words, there seems to be some structural change on reuse of the catalyst. CO-chemisorption studies of spent 4Pt-8MoO_x/ZrO₂ revealed that the CO monolayer uptake decreased from 24.2 μmol/g for fresh catalyst to 6.2 μmol/g for spent catalyst, active metal surface area decreased from 29 to 8 m²/g, average crystallite size of Pt increased from 9.5 to 37.0 nm and Pt dispersion decreased from 12 to 3%.

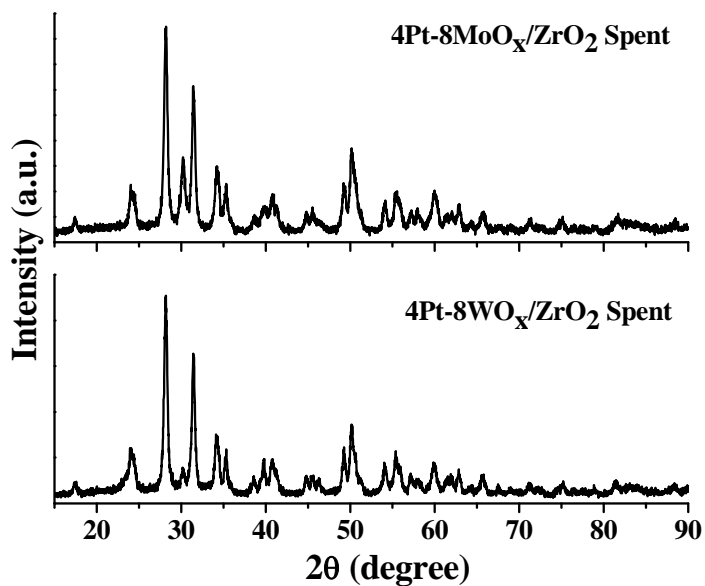


Fig. 7.10. XRD of spent catalysts.

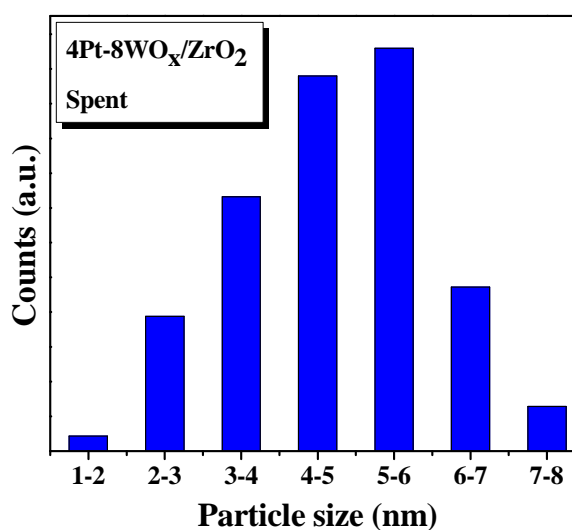
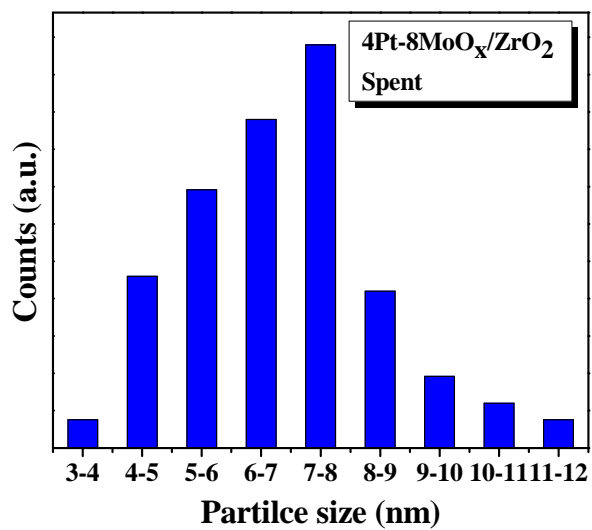
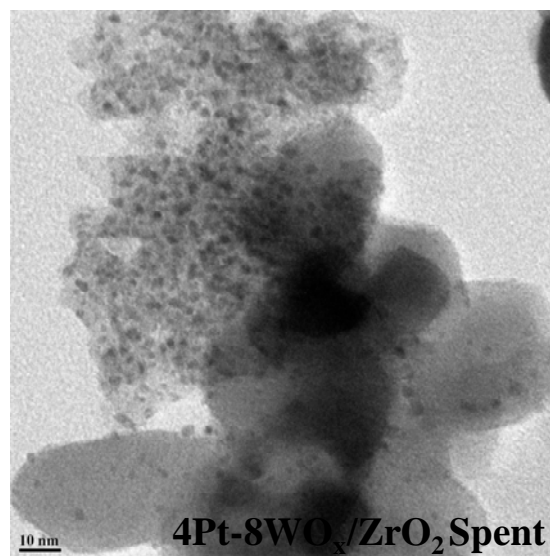
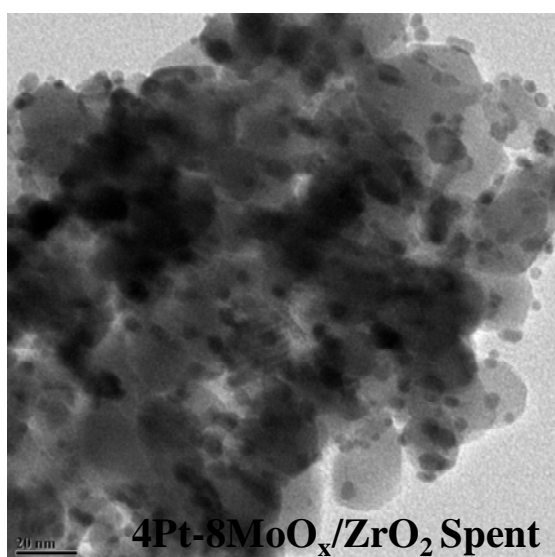


Fig. 7.11. TEM images and particle size histograms of spent catalysts.

Table 7.13. Chemical composition (SEM-EDAX) of fresh and spent catalysts

Catalyst	Composition (wt%)			
	Pt	M	Zr	O
4Pt-8MoO _x /ZrO ₂ Fresh	3.1	8.6	45.2	43.0
4Pt-8MoO _x /ZrO ₂ Spent	3.4	7.2	47.2	42.2
4Pt-8WO _x /ZrO ₂ Fresh	4.1	8.0	43.1	44.8
4Pt-8WO _x /ZrO ₂ Spent	3.9	11.0	39.0	56.1

Chemical composition by SEM-EDAX analysis (Table 7.13) revealed that the chemical composition of the catalyst is intact even after its use in several recycling experiments. No appreciable leaching of Pt and reducible oxide was noted.

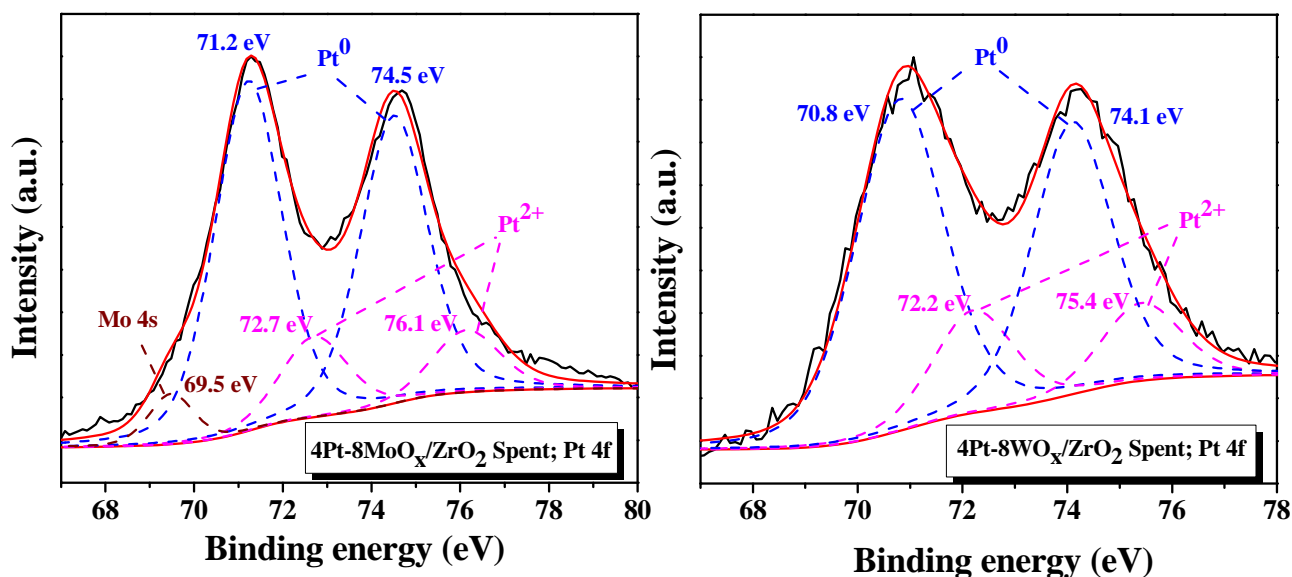


Fig. 7.12. XPS of spent catalysts in Pt 4f region.

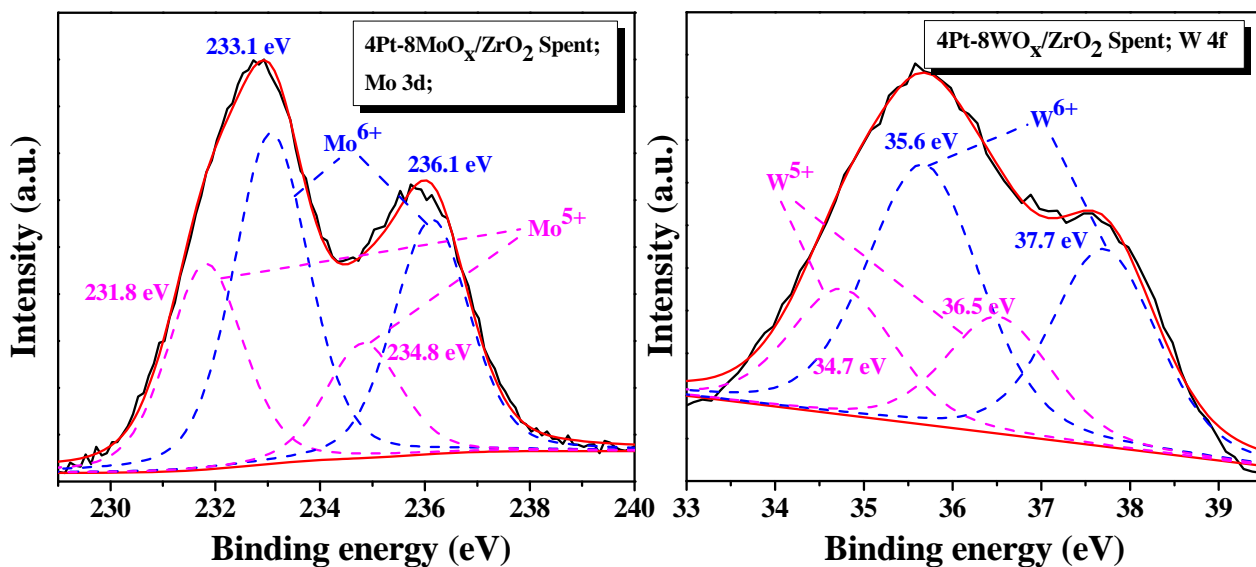


Fig. 7.13. XPS of spent catalyst in Mo 3d and W 4f regions.

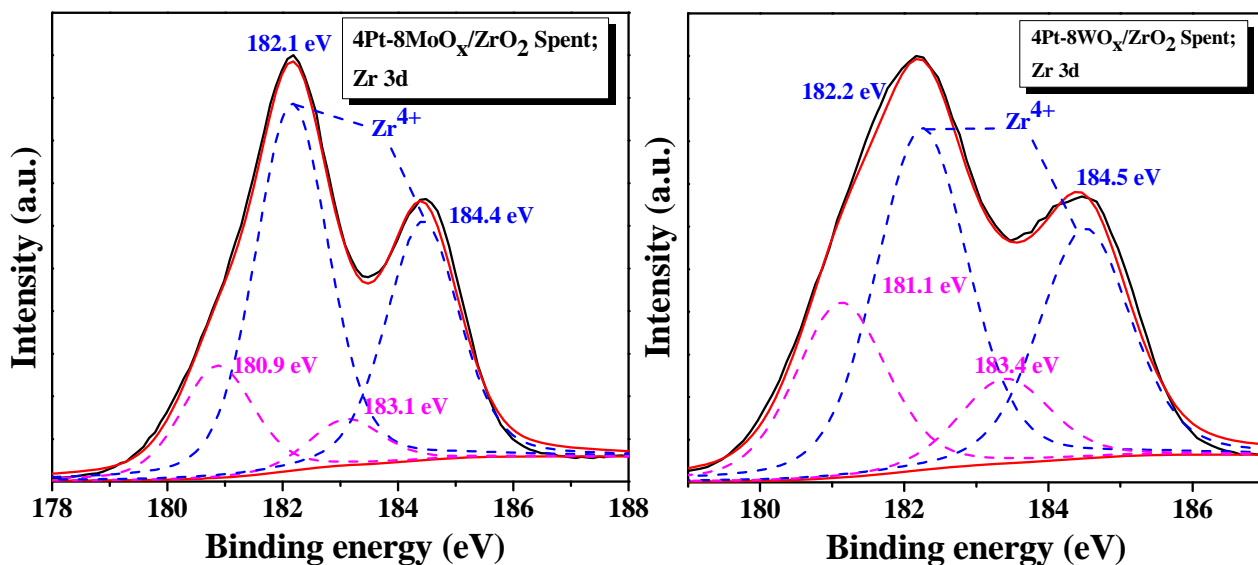


Fig. 7.14. XPS of spent catalyst in Zr 3d region.

A marginal increase in Pt particle size on reuse of the catalyst was observed (Fig. 7.11). TEM images of spent 4Pt-8MoO_x/ZrO₂ revealed that the particle size of Pt increased from 6 (Table 7.1) to 7.5 nm and that of 4Pt-8WO_x/ZrO₂ pointed out an increase in Pt particle size from 4.5 (Table 7.1) to 5 nm. X-ray photoelectron spectra of spent 4Pt-8MoO_x/ZrO₂ and 4Pt-8WO_x/ZrO₂ are shown in Figs. 7.12 - 7.14. The spectra are nearly the same as of fresh catalyst (Figs. 7.7 - 7.9). However, on reuse the ratio of Pt⁰/Pt²⁺ increased from 3.3 to 4.3 for 4Pt-8MoO_x/ZrO₂ and from 2.6 to 3.6 for 4Pt-8WO_x/ZrO₂. The ratio of Mo⁵⁺/Mo⁶⁺ increased from 0.6 to 0.7 and W⁵⁺/W⁶⁺ decreased from 1.6 to 0.7. The ratio of reduced zirconium species/Zr⁴⁺ decreased in spent catalysts from 0.4 to 0.3 and 2.2 to 0.5 for 4Pt-8MoO_x/ZrO₂ and 4Pt-8WO_x/ZrO₂, respectively. In other words, these characterizations of spent catalysts infer that the chemical composition is intact but the structural changes have happened on reuse of the catalyst. However, these structural changes are within limit and did not bring in any change in the activity/selectivity of these bimetallic catalysts.

7.3.3. Tentative reaction mechanism

Based on the results obtained from different chapters a tentative mechanism (Fig. 7.15) for deoxygenation of OA was proposed. Accordingly, H₂ dissociates on platinum surface and spills over on promoter oxide (MO_x; M = W and Mo), reducing and forming surface -OH species [33] responsible for OA activation through dehydration and ester-bond formation [34]. Then, the olefinic group (of OA) is hydrogenated followed by removal of oxygen (of C=O group) through hydrogenation and dehydration forming C₁₈ paraffin and regenerating Pt-MO_xH catalyst active site. In the absence of promoter (MO_x), OA is activated through C=O group over Lewis sites of the support. The hydride ions (H⁻) generated over Pt surface (by reaction with H₂)

facilitate deprotonation of carboxylic group, C-C bond cleavage, decarboxylation and formation of C₁₇ and then, catalyst is regenerated. Thus, activation of fatty acid on reducible oxide (MO_xH) species leads to HDO (C₁₈) while its activation on Lewis acid sites of support (ZrO₂, for example) leads to DCO (C₁₇) product.

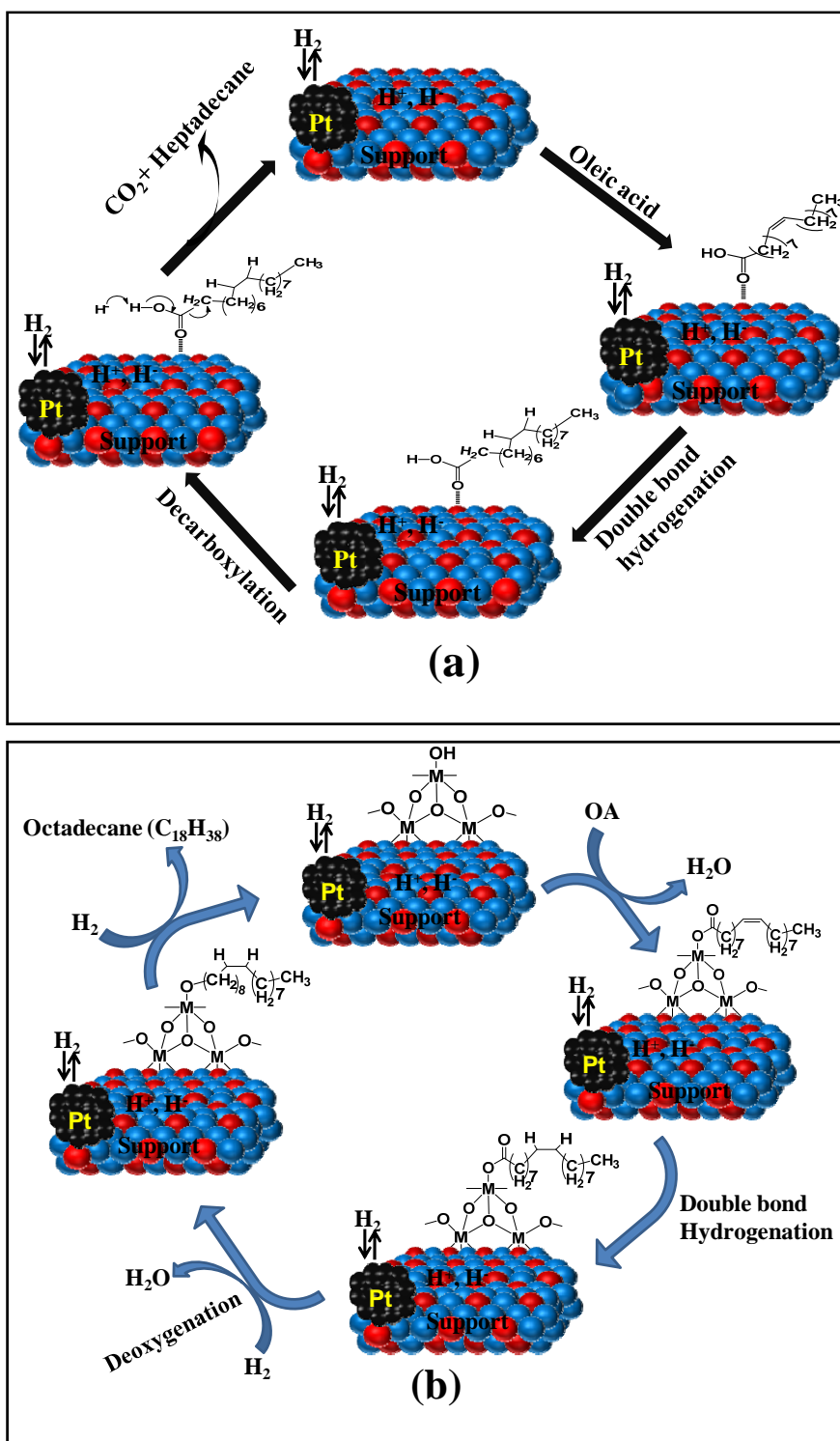


Fig. 7.15. A tentative deoxygenation mechanism of fatty acids over (a) Pt on ZrO₂ support and (b) Pt on reducible oxide modified ZrO₂ support.

7.4. Conclusions

4Pt-8MoO_x/ZrO₂ and 4Pt-8WO_x/ZrO₂ catalysts prepared by wet impregnation method showed high catalytic activity for hydrodeoxygenation of fatty acids converting into diesel-range hydrocarbons (green diesel). High conversion of OA was observed even at 200 °C. The former showed higher activity than the latter and most of the known deoxygenation catalysts. The catalyst was reusable in recycling experiments conducted at 320 °C. Although the chemical composition was unchanged, structural changes were noted on reusing the catalyst. Higher amount of Pt in metallic state is the cause for high catalytic activity and HDO selectivity of 4Pt-8MoO_x/ZrO₂. Pt to Mo weight ratio of 1:2 to 1:4 is optimum resulting in most effective catalyst.

7.5. References

- [1] M. V. Domínguez-Barroso, C. Herrera, M. A. Larrubia, L. J. Alemany, *Fuel Processing Technology*, 2016, 48, 110–116.
- [2] Chen Zhao, Thomas Brück, Johannes A. Lercher, *Green Chem.*, 2013, 15, 1720-1739.
- [3] Kyung-Ran Hwang, Il-Ho Choi, Hye-Young Choi, Jeong-Sik Han, Kyong-Hwan Lee, Jin-Suk Lee, *Fuel*, 2016, 174, 107–113.
- [4] Nicolás A. Grosso-Giordano, Todd R. Eaton, Zhenyu Bo, Sara Yacob, Chieh-Chao Yang, Justin M. Notestein, *Applied Catalysis B: Environmental*, 2016, 192, 93–100.
- [5] Liqiu Yang, Kirby L. Tate, Jacek B. Jasinski, and Moises A. Carreon, *ACS Catal.* 2015, 5, 6497–6502.
- [6] Konstantin Hengst, Matthias Arend, Rebecca Pfützenreuter, Wolfgang F. Hoelderich, *Applied Catalysis B: Environmental*, 2015, 174–175, 383–394.
- [7] Jie Fu, Xiuyang Lu, Phillip E. Savage, *ChemSusChem*, 2011, 4, 481–486.
- [8] Elvan Sari, Manhoe Kim, Steven O. Salley, K.Y. Simon Ng, *Applied Catalysis A: General*, 2013, 467. 261–269.
- [9] Moti Herskowitz, Miron V. Landau, Yehudit Reizner, Dov Berger, *Fuel*, 2013, 111, 157–164.
- [10] Xueqin Yang, Xiaolin Yu, Mengya Lin, Maofa Ge, Yao Zhao, Fuyi Wang, *J. Mater. Chem. A*, 2017, 5, 13799-13806.
- [11] Tsutomu Yamaguchi, *Catalysis Today*, 1994, 20, 199-218.
- [12] Jamal Ftouni Ara Muñoz-Murillo, Andrey Goryachev, Jan P. Hofmann, Emiel J. M. Hensen, Li Lu, Christopher J. Kiely, Pieter C. A. Bruijninx, Bert M. Weckhuysen, *ACS Catalysis*, 2016, 6, 5462–5472.
- [13] Xin Zhang, Hai Wang, Bo-Qing Xu, *J. Phys. Chem. B*, 2005, 109, 9678–9683.

- [14] Sulaiman. N. Basahel, Tarek. T. Ali, Mohamed. Mokhtar, Katabathini Narasimharao, *Nanoscale Research Letters*, 2015, 10:73.
- [15] Sreethawong. T, Ngamsinlapasathian. S, Yoshikawa. S, *Chem. Eng. J.* 2013, 228, 256–262.
- [16] Elisabeth W. Leib , Robert M. Pasquarelli , Malte Blankenburg , Martin Müller , Andreas Schreyer , Rolf Janssen , Horst Weller , Tobias Vossmeier, *Part. Part. Syst. Charact.* 2016, 33, 645–665.
- [17] Yiqiu Fan, Shijie Cheng, Hao Wang, Jing Tian, Songhai Xie, Yan Pei, Minghua Qiao, Baoning Zong, *Applied Catalysis B: Environmental*, 2017, 217, 331-341.
- [18] Juan Li, Junli Chen, Wei Song, Junlong Liu ,Wenjie Shen, *Applied Catalysis A: General*, 2008, 334, 321-329.
- [19] Javier Grau, J. C. Yori, C. R. Vera, J. A. Parera, *Applied Catalysis A: General*, 2004, 265, 141-152.
- [20] Polina A. Zosimova, Andrey V. Smirnov, Sergey N. Nesterenko,Valentina V. Yuschenko, Wharton Sinkler, Joseph Kocal, Jeniffer Holmgren, Irina I. Ivanova, *J. Phys. Chem. C*, 2007, 111, 14790-14798.
- [21] Dajun Meng, Baowei Wang, Wenxia Yu, Weihang Wang, Zhenhua Li, Xinbin Ma, *Catalysts*, 2017, 7, 151-162.
- [22] Komandur. V. R. Chary, Kondakindi Rajender Reddy, Gurram Kishan, J. W. Niemantsverdriet, Gerhard Mestl, *Journal of Catalysis*, 2004, 226, 283–291.
- [23] Sarma D.D., Rao C.N.R., *J. Electron Spectrosc. Relat. Phenom.* 1980, 20, 25-45.
- [24] I. Bepalov, M. Datler, S. Buhr, W. Drachsel, G. Rupprechter, Y. Suchorski, *Ultramicroscopy*, 2015, 159, 147–151.
- [25] Chiara Gionco, Maria Cristina Paganini, Elio Giamello, Robertson Burgess, Cristiana Di Valentin, Gianfranco Pacchioni, *Chem. Mater.* 2013, 25, 2243–2253.
- [26] Wen Ma, F. William Herbert, Sanjaya D. Senanayake, Bilge Yildiz, *Applied Physics Letters*, 2015, 106, 101603-101608.

- [27] Sujan Mondal, Ramana Singuru, Subhash Chandra Shit, Taku Hayashi, Stephan Irle, Yuh Hijikata, John Mondal, Asim Bhaumik, *ACS Sustainable Chem. Eng.* 2018, 6, 1610–1619.
- [28] Zhengyi Pan, Rijie Wang, Jixiang Chen, *Applied Catalysis B: Environmental*, 2018, 224 88–100.
- [29] Ning Chen, Yuxiong Ren, Eika W. Qian, *Journal of Catalysis*, 2016, 334, 79–88.
- [30] Jingjing Zhang, Chen Zhao, *ACS Catalysis*, 2016, 6, 4512–4525.
- [31] Yazhong Chen, Zongping Shao, Nanping Xu, *Energy Fuels*, 2008, 1873–1879.
- [32] Muhammad Bilal S. David Jackson, *Catal. Sci. Technol.*, 2013, 3, 754-766.
- [33] S. García-Fernández, I. Gandarias, J. Requies, M. B. Güemez, S. Bennici, A. Auroux, P. L. Arias, *Journal of Catalysis*, 2015, 323, 65–75.
- [34] Yoshinao Nakagawa, Yasunori Shinmi, Shuichi Koso, Keiichi Tomishige, *Journal of Catalysis*, 2010, 272, 191–194.

Chapter-8
Summary and Conclusions

Catalysis plays an important role in providing suitable solutions for societal problems. Energy security and environment pollution are the issues gaining world attention. This ignited the zeal to develop solutions for sustainable energy production. Catalytic conversion of biomass to renewable, transport fuels surmounts the shortage of fossil fuel resources and provides future energy assurance. Non-edible vegetable oils and their constituent fatty acids are the right choice of biomass having a vast scope of research to produce renewable fuels. Since this biogenous feedstock is rich in oxygen content, it must be deoxygenated and hydroisomerized (if needed) to exploit its feasible application as hydrocarbon fuel (green diesel or jet fuel). Thus, the catalytic deoxygenation is considered as heart of 'biorefinery.' The green diesel produced by deoxygenation of inedible vegetable oils or fatty acids is advantageous over the ester-based biodiesel in terms of its oxidation stability, viscosity, cold-flow property and compatibility for mixing with the conventional diesel. Moreover, the green diesel process could be integrated with the conventional refining process.

The commercial green diesel processes using sulfided NiMo/Al₂O₃ or CoMo/Al₂O₃ hydrotreating catalysts operates at severe conditions and suffer from sulphur leaching issues. There have been efforts to develop non-sulfided catalysts. But the activities of those catalysts were lower than the sulfided ones. Noble metals (Pt, Pd, Rh etc.) supported on mesoporous C, Al₂O₃, SiO₂ and zeolites operate at moderate conditions but proved futile due to their poor stability during the operation. Thus, the challenge in this area is to develop efficient and stable catalyst and an atom-efficient, economic process that operates at mild conditions *ca.*, below 280 °C and 20 bar H₂.

The objective of this work is to understand the parameters dictating catalytic deoxygenation activity and selectivity and to design an efficient and stable catalyst for green diesel production. Here, Pt was chosen as active metal. Its activity and selectivity were altered by varying the support and employing reducible oxides as promoters. The supports used in this work include: AlPO₄₋₅, γ -Al₂O₃, ZrO₂ and SiO₂-Al₂O₃. The reducible oxide promoters used include: WO_x, MoO_x, SnO_x and ReO_x. Catalysts with varying textural, electronic and acidic properties were designed with the choice of above metal, reducible oxide and support. Firstly, the promoter oxides were deposited on the supports by wet impregnation method, dried and calcined at 450 °C. In the second step, platinum precursor was deposited on the modified supports, dried, calcined at 450 °C and reduced in a flow of hydrogen. For comparative studies, unpromoted supported Pt catalysts were also prepared. Catalysts were characterized by X-ray powder diffraction (XRD), N₂-physisorption, CO-chemisorption, H₂-temperature-programmed reduction (H₂-TPR), NH₃-temperature-programmed desorption

(NH₃-TPD), X-ray photoelectron spectroscopy (XPS), scanning electron microscopy (SEM), transmission electron microscopy (TEM) and energy dispersive X-ray analysis (EDAX) techniques. Catalytic activity tests were performed in a stainless-steel Parr batch reactor (100 and 300 ml). Prior to reaction, the catalysts were reduced in a flow of hydrogen (20 ml/min) at 350 °C for 150 min. The overall summary and conclusion of results (obtained in different chapters) are presented below.

Chapter 3 reported catalytic deoxygenation activity studies of Pt supported on AlPO₄₋₅ and WO_x modified AlPO₄₋₅. Pt content was varied from 1 to 4 wt% and W content was varied from 0 to 16 wt%. Below 8 wt%, WO₃ was in a highly dispersed form on AlPO₄₋₅ surface. Above that content, presence of crystalline WO₃ phase was detected. Modification of AlPO₄₋₅ with WO_x led to changes in structural and electronic properties of Pt. The particle and crystallite sizes of Pt were bigger in 4Pt-8WO_x/AlPO₄₋₅ than in 4Pt/AlPO₄₋₅ (TEM, XRD and CO-chemisorption). Enhancement in acidity and in particular, strong acid sites were noted when WO_x was present in the catalyst composition (NH₃-TPD). There existed synergy and electronic connectivity between Pt and WO_x resulting in facile reduction of these species under hydrogen environment (H₂-TPR). WO_x in presence of Pt reduced at 345 °C instead at 700 °C and above. Pt in presence of WO_x reduced at 69 °C instead at 74 °C. Hydrogen spillover occurs from Pt to WO_x partly reducing its surface to WO_xH species. These changes in structural and electronic properties led to changes in deoxygenation activity and selectivity. In deoxygenation of oleic acid (OA), 4Pt-8WO_x/AlPO₄₋₅ showed higher catalytic activity than 4Pt/AlPO₄₋₅. While the latter formed heptadecane (C₁₇) as major product (through decarboxylation/decarbonylation (DCO) path), the former catalyst resulted mainly octadecane (C₁₈) product (through hydrodeoxygenation (HDO) path). Catalyst with Pt:W weight ratio of 1:2 showed better performance. Unlike other related catalysts, 4Pt-8WO_x/AlPO₄₋₅ exhibited quantitative conversion of OA with 80 wt% selectivity for C₁₈ at 260 - 280 °C. Reaction occurred even at short contact times (0.5 h) and in the absence of hydrogen. However, this catalyst was unstable in reusability studies. Structural instability of AlPO₄₋₅ was found the cause for catalyst deactivation. No hydroisomerized products were detected.

With a view to develop stable catalyst, studies were then made on 4Pt-8WO_x/Al₂O₃ (Chapter-4). Promoted Pt/Al₂O₃ are well known catalysts in commercial refining operations. Pt content was varied from 1 to 4 wt% and W content was varied from 0 to 16 wt%. Unlike on AlPO₄₋₅, WO_x on γ -Al₂O₃ was in the monolayer coverage limit even at 16 wt% W loading. A marginal increase in crystallite and particle sizes of Pt was detected when supported on WO_x modified Al₂O₃. An increase in strong acid sites was detected. For 4Pt-8WO_x/Al₂O₃, the

electronic lines corresponding to Pt 4d_{5/2} and 4d_{3/2} shifted to lower binding energy (312.6 and 330.4 eV, respectively) indicating that Pt on WO_x-modified Al₂O₃ is richer in e⁻ density than that supported on unmodified Al₂O₃. XPS in W 4f region pointed out that a portion of WO_x is reduced and W was present in +5 oxidation state. Surface W⁶⁺ and W⁵⁺ species are in the proportion of 56% and 44%, respectively. WO_x enhanced the reducibility of Pt making it e⁻ rich due to enduring synergistic effect between Pt and WO_x. This, in turn enhanced the H₂ splitting and facilitated deoxygenation activity. In a similar manner, presence of nascent H species (H⁺ and H[•]) generated by H₂ splitting over Pt particles led to partial reduction of WO_x forming surface hydroxyl groups. In conformity with characterization studies, the WO_x-promoted Pt catalysts showed higher catalytic deoxygenation activity and HDO selectivity than Pt supported on "neat" Al₂O₃. Palmitic acid, oleic acid and methyl oleate were deoxygenated with equal efficiency. Catalytic activity and HDO selectivity of 4Pt-8WO_x/Al₂O₃ was lower than 4Pt-8WO_x/AlPO₄₋₅. But then, 4Pt-8WO_x/Al₂O₃ was reusable (at 320 °C) with little loss in catalytic activity. HDO selectivity increased on reusing of the catalyst.

The effect of support on catalytic activity was probed in Chapter-5. Pt to W composition was kept at 1:2 weight ratio and deposited on γ -Al₂O₃, ZrO₂, AlPO₄₋₅ and SiO₂-Al₂O₃ (SA) mixed oxide. These oxide supports differed in their surface acidity and textural properties and thereby, influenced Pt structure. Even in this chapter, it was found that there exists electronic synergy between Pt and WO_x. Metallic nature of Pt (e⁻ rich Pt) in different promoted catalysts decreased (as the Pt 4d_{3/2} line shifted to lower B.E.) as follows: 4Pt-8WO_x/ZrO₂ (331.2 eV) > 4Pt-8WO_x/AlPO₄₋₅ (331.3 eV) > 4Pt-8WO_x/Al₂O₃ (331.5 eV) > 4Pt-8WO_x/SA (331.8 eV). Surface concentrations of W⁵⁺/W⁶⁺ were found as follows: 4Pt-8WO_x/Al₂O₃ (65.9/34.1), 4Pt-8WO_x/ZrO₂ (55.1/44.9), 4Pt-8WO_x/AlPO₄₋₅ (48.4/51.6) and 4Pt-8WO_x/SA (38.7/61.3). Thus the efficiency of hydrogen spillover is higher on more metallic 4Pt-8WO_x/ZrO₂ than on 4Pt-8WO_x/AlPO₄₋₅, 4Pt-8WO_x/Al₂O₃, 4Pt-8WO_x/SA. A parallel variation of catalytic activity with hydrogen spillover efficiency was observed. 4Pt-8WO_x supported on ZrO₂ showed 100 mol% OA conversion and 89.4% C₁₈ selectivity at a temperature as low as 260 °C. Structure-activity correlations revealed that *adequate metal dispersion, high electron density at metal (enhancing hydrogen dissociation activity), high amount of W⁵⁺ species in the composition (enhancing OA activation) and less amount of strong acid sites (enabling hydrocracking) are the important parameters dictate the performance of a hydrodeoxygenation catalyst. The choice of support is crucial in designing an efficient deoxygenation catalyst.* Among the supports investigated, ZrO₂ was found the best.

In Chapter-6, Al₂O₃ was modified with different reducible oxides (WO_x, MoO_x, ReO_x and SnO_x) and then Pt was deposited on it. Structural, textural, electron and redox properties of Pt changed as a consequence of altering reducible oxides. Binding energy values of Pt 4d suggested that the metallic nature of Pt increases in the order: 4Pt-8SnO_x/Al₂O₃ < 4Pt-8WO_x/Al₂O₃ < 4Pt-8ReO_x/Al₂O₃ < 4Pt-MoO_x/Al₂O₃. More facile spillover of hydrogen is, therefore, expected on MoO_x and ReO_x-promoted Pt than on WO_x and SnO_x-promoted Pt catalysts. The reducibility of promoter oxides in presence of Pt decreased in the order: MoO_x > ReO_x > WO_x > SnO_x. *Catalytic activity followed the variation in Pt metallicity and extent of promoter oxide reducibility.* MoO_x was found the best reducible oxide promoter. 4Pt-8MoO_x/Al₂O₃ exhibited highest catalytic activity even at 220 °C with 97 mol% conversion of OA and 92.1% C₁₈ selectivity. The catalyst was recyclable at 320 °C with no loss in catalytic activity. A range of fatty acids were deoxygenated to corresponding alkanes.

Table 8.1. Comparative catalytic activity of Pt supported on reducible oxide modified supports^a

Catalyst	Reaction temperature (°C)	OA conversion (mol%)	Product selectivity (wt%)			
			C ₁₈	C ₁₇	C ₁₀₋₁₆	Others
4Pt-8WO _x /AlPO ₄₋₅	260	93.0	80.8	18.3	0.9	0
	280	100	81.7	17.6	0.7	0
4Pt-8WO _x /Al ₂ O ₃	260	86.0	75.3	21.8	1.7	1.3
	280	98.0	69.2	30.1	0.7	0
4Pt-8WO _x /SiO ₂ -Al ₂ O ₃	260	82.0	88.0	11.3	0.4	0.4
	280	90.0	84.0	15.0	0.6	0.4
4Pt-8WO _x /ZrO ₂	260	100	89.4	10.0	0.6	0
	280	100	85.1	14.3	0.6	0
4Pt-8MoO _x /Al ₂ O ₃	200	53.0	92.5	4.7	0.4	2.4
	220	97.0	92.1	5.8	0.5	1.5
	240	98.0	92.4	6.6	0.6	0.5
	260	100	87.2	11.7	0.5	0
4Pt-8MoO _x /ZrO ₂	200	75.0	94.6	4.7	0.4	0.3
	220	94.0	92.0	6.3	0.5	1.1
	240	100	91.4	7.3	0.5	0.8

^a*Reaction conditions:* Oleic acid (OA) = 2 g, solvent (n-heptane) = 30 g, catalyst = 10 wt.% of OA, H₂ pressure = 20 bar, reaction time = 5 h.

Having found that ZrO₂ is superior support (Chapter-5) and MoO_x is superior reducible oxide promoter (Chapter-6), a catalyst composition of 4Pt-8MoO_x/ZrO₂ was prepared and evaluated for deoxygenation of oleic acid (Chapter-7). ZrO₂ prepared in this study had a mixed monoclinic (m) and tetragonal (t) crystal phase. On depositing Pt and MoO_x, the composition of the m-phase had increased. MoO_x was highly dispersed on ZrO₂ even at 16 wt% loading. Acidity of 4Pt-8MoO_x/ZrO₂ was lower than those investigated in other chapters. Pt was present in both zero and +2 states with the former being more in content. Reduced molybdenum oxide species was also in high content. *4Pt-8MoO_x/ZrO₂ showed high catalytic activity and selectivity even at 200 °C. OA conversion was 75.0 mol% and C₁₈ selectivity was 94.6%, the highest achieved so far in this work.* The catalyst was reusable. Chemical integrity was present but structural variations were noted in the spent catalyst. A tentative mechanism was proposed. Table 8.1 presents comparative activity of different catalysts investigated in this study.

By and large, a careful design enabled highly active and selective catalyst for deoxygenation of fatty acids producing green diesel. The catalyst was found reusable under certain conditions. Parameters controlling catalytic activity and selectivity were established. The study revealed that by a suitable choice of support and reducible oxide the structure and electronic properties of Pt could be tuned to result in a highly efficient, selective and stable deoxygenation catalyst. This work contributes to the area of catalysis for renewable fuels.

List of Publications

1. Promotional effect of WO_x in Pt- $\text{WO}_x/\text{AlPO}_4\text{-5}$ catalyzed deoxygenation of fatty acids
Sagar Janampelli and D. Srinivas
ChemistrySelect., 2017, 2, 1895 – 1901.
2. Selective and reusable Pt- $\text{WO}_x/\text{Al}_2\text{O}_3$ catalyst for deoxygenation of fatty acids and their esters to diesel-range hydrocarbons
Sagar Janampelli and D. Srinivas
Catalysis Today, 2018, 309, 219–226.
3. Effect of support on the catalytic activity of WO_x promoted Pt in green diesel production.
Sagar Janampelli and D. Srinivas
Molecular Catalysis, 2018, 451, 125–134.
4. Reducible oxide promoted hydrodeoxygenation activity of Pt- $\text{MO}_x/\text{Al}_2\text{O}_3$ in biofuels production
Sagar Janampelli and D. Srinivas
Manuscript communicated.
5. Highly efficient Pt- $\text{MoO}_x/\text{ZrO}_2$ catalyst for green diesel production
Sagar Janampelli and D. Srinivas
Manuscript communicated.